Dissertation zur Erlangung des Doktorgrades
der Fakultät für Chemie und Pharmazie
der Ludwig-Maximilians-Universität München

Reaction Kinetics and Cure Monitoring of Highly Reactive Epoxy Resins for Carbon Fiber Reinforced Plastics

von

Manuel Boehm

aus

München

2015

Erklärung

Diese Dissertation wurde im Sinne von §7 der Promotionsordnung vom 28. November 2011 von Herrn Prof. Dr. Konstantin Karaghiosoff betreut.

Eidesstattliche Versicherung

Diese Dissertation wurde eigenständig und ohne unerlaubte Hilfe erarbeitet.

München, den 28.04.2015

_____

Manuel Boehm

Dissertation eingereicht am: 28.04.2015

1. Gutachter: Prof. Dr. Konstantin Karaghiosoff
2. Gutachter: Prof. Dr. Thomas M. Klapötke

Mündliche Prüfung am: 29.05.2015

Vertraulichkeitsverpflichtung

Die vorliegende Dissertation,

Reaction Kinetics and Cure Monitoring of Highly Reactive Epoxy Resins for Carbon Fiber Reinforced Plastics

ist im Rahmen der Tätigkeit in der Abteilung MT-40 Technologieentwicklung CFK der *BMW AG* entstanden.

Die Arbeit umfasst oder berührt Entwicklungen, die außerhalb der BMW AG nicht bekannt sind und daher vertraulich behandelt werden müssen. Die in diesem Zusammenhang erlangten Erkenntnisse und Einblicke dürfen deshalb ohne vorherige schriftliche Genehmigung der BMW AG nicht veröffentlicht, vorgetragen oder Dritten zugänglich gemacht werden. Lassen sich die vertraulich zu behandelnden Inhalte des Berichtes nicht vom übrigen Inhalt trennen, so gelten die Einschränkungen für die gesamte Arbeit.

Ausgenommen von dieser Verpflichtung ist die Weitergabe der Kenntnisse im Rahmen der Prüfungsordnung, soweit damit keine Veröffentlichung verbunden ist. Nach Ablauf von 4 Jahren, gerechnet ab dem Abgabedatum der schriftlichen Arbeit, unterliegt diese nicht mehr der Geheimhaltung.

To Lena with Love

– Thanks for Everything

Abstract

The first mass production of carbon fiber reinforces plastic parts (CFRP) produced in the high pressure resin transfer moulding process (HP-RTM) for implementation in the vehicle body was realized by BMW with the launch of the *BMW i-series*. The key for an economic and efficient HP-RTM production process for high volume CFRP part production is to characterize the cure behavior of the fast thermosetting epoxy resin matrix in detail.

The objective of this work is to provide a new methodology for a comprehensive understanding of the curing behavior of fast curing epoxy resin systems applicable in high volume CFRP part production not only by laboratory analysis but also by direct investigation of the curing progress in the HP-RTM production process. In addition, a reaction kinetic model is derived to provide cure simulations. On this basis, a detailed examination of current processes is allowed to identify potential process optimizations. This also provides a benchmark method to compare the curing performance of future potential thermosetting matrix resins with prior art matrix systems.

For this purpose, two fast curing epoxy resin systems, suitable for high volume CFRP part production in the HP-RTM process, were investigated exemplarily. Laboratory analysis was conducted by using differential scanning calorimetry (DSC), near-infrared (NIR) spectroscopy, rheometry and ultrasound technique. For online-cure-monitoring of the epoxy resin directly in the HP-RTM process also the ultrasound technique was applied. Furthermore a reaction kinetic model was developed to provide the prediction of the curing process and complement the comparison of laboratory and process investigations. This approach allows a comparison between theory and practice, which is absolutely necessary for a successful and efficient high volume CFRP manufacturing process.

It could be demonstrated that a comprehensive understanding of the curing behavior of fast curing epoxy resins used in the HP-RTM process was achieved by both laboratory analysis and online-cure-monitoring in the HP-RTM process. Also confident cure simulations could be achieved by the developed reaction kinetic models based on laboratory analytical data. The correlation of laboratory analysis, investigations of the curing progress in the HP-RTM process and the prediction of the curing progress was in good agreement.

The developed methodology provides a comprehensive and consistent characterization strategy of the curing behavior of fast curing epoxy resin systems both in the laboratory and in the HP-RTM production process and a well-founded prediction of the curing progress depending on the applied cure temperatures is possible.

Acknowledgements

First of all, I would like to thank my supervisor, Prof. Dr. Konstantin Karaghiosoff at the Ludwig-Maximilians-University Munich for his dedicated support and advice.

I am very thankful to Prof. Dr. Thomas M. Klapötke for agreeing to be the second reviewer of this thesis as well as Prof. Dr. Jun Takahashi, Prof. Dr. Heinz Sturm, Prof. Dr. Dina Fattakhova-Rohlfing and Prof. Dr. Hans-Christian Böttcher for accepting to be co-reviewers.

I am very grateful to *BMW AG* for funding my Ph.D. project and giving me the opportunity to work on a very exciting and challenging topic at the cutting edge research in the field of new lightweight design in the automotive industry.

Especially, I am very grateful to my professional supervisors Dr. Jarlath McHugh and Manfred Schmiedel at BMW AG for their invaluable support, guidance, encouragement and mentorship throughout the entire time.

I am also very thankful to my mentor Hans-Peter Lang for his support, his trust and deep personal and professional discussions.

My deep thanks go to Dr. rer. nat. habil. Wolfgang Stark for detailed and enthusiastic discussions and his professional advice especially in the field of mechanical analysis.

My special thanks go to Prof. Dr. Jun Takahashi who accepted me as research Ph.D. student at his laboratory in the Department of Systems Innovation at the University of Tokyo and gave me the opportunity to expand my professional knowledge in all facets of advanced material science and also to expand my personal horizon. In this context, I would also like to thank Dr. Thomas Wolff and Masashi Yoshino who made this research trip possible by their financial and organizational support.

I would like to thank Ulrike Braun and Erik Dümichen of the Federal Institute for Materials Research and Testing for their professional collaboration and their expertise in all issues concerning IR spectroscopy.

I thank my former students Ulrike Roth, Daniela Horvat, Christian Will and Mark Keane for their hard work and input.

I want to thank the entire CFRP technology development team for a great time and good working atmosphere and I am especially grateful to Franz Maidl, Christoph Jagoda and Ramona Franke for their expertise and support.

Finally, I am deeply thankful to Lena, my mother and my family who have accompanied me throughout the way and who gave me tremendous and never-ending support.

Table of Contents

List of Abbreviations

A	Pre-exponential factor
α	Degree of conversion
α_{exp}	Experimentally determined degree of conversion
α_{pred}	Predicted degree of conversion
BAM	Federal Institute for Materials Research and Testing
c	Sound velocity
CFRP	Carbon fiber reinforced plastics
ch	Channel
d	Thickness, Shear gap
δ	Phase angle
DGEBA	Diglycidyl ether of bisphenol A
DGEBF	Diglycidyl ether of bisphenol F
DSC	Differential scanning calorimetry
E_a	Activation energy
η	Shear viscosity
η', η''	Real and imaginary parts of the complex viscosity
η^*	Complex viscosity
f	Functionality of epoxy monomer
F_τ	Shear stress factor
g	Functionality of amine monomer
G'	Storage modulus
G''	Loss modulus
γ	Shear strain
γ_0	Strain amplitude
$\dot{\gamma}$	Shear rate
ΔH_{loss}	Non-detectable enthalpy of reaction
ΔH_R	Enthalpy of reaction
ΔH_{res}	Residual enthalpy of reaction
ΔH_{tot}	Total enthalpy of reaction
HP-RTM	High-pressure resin transfer moulding
HV	High Voltage
IMR	Internal mould release agent
K'	Compression modulus
k	Reaction rate
k_{chem}	Chemically controlled reaction rate

k_{diff}	Diffusion controlled reaction rate
L'	Longitudinal modulus
Mult-NLR	Multivariate non-linear regression technique
NIR	Near infrared
$\tilde{\nu}$	Wavenumber
ω	Angular frequency
p	Concentration of product
p	Conversion of the chemical reaction
p_c	Critical point of conversion for gelation
PT	Plate tool
r	Concentration of reactant
R	Universal gas constant
r_a	Ratio of amine reactivity
ρ	Density
T	Temperature
t	Time
Δt_{trans}	Transmission time
τ	Shear stress
τ_0	Stress amplitude
TTT	Time-Temperature-Transformation
T_{cure}	Cure temperature
T_g	Glass transition temperature
T_{g0}	Glass transition temperature of the uncured polymer
$T_{g\infty}$	Glass transition temperature of the fully cured polymer
${}_{gel}T_g$	Glass transition temperature at gel point
T_m	Melting temperature
V	Fluid velocity

A. INTRODUCTION

1 Overview

1.1 Political Trends and Effects for Automotive Industry

In these times of serious debate about climatic change, global warming and its effects to the environment, sustainability and environmental protection plays an increasingly important role in global politics. As it is a global matter, it is the responsibility of every country to change the way of thinking about environmental protection fundamentally. A mile stone in international climate policy was the passage of the "Kyoto Protocol", which was ratified by 191 countries and took effect in 2005. The listed greenhouse gases in the Kyoto Protocol are carbon dioxide (CO_2), methane (CH_4), nitrous oxide (N_2O), hydrofluorocarbons (HFCs), perfluorocarbons (PFCs) and sulphur hexafluoride (SF_6), whereas CO_2 plays the most important role according to the amount emitted.[1]
Industry and traffic are the major contributors to CO_2 emission in the EU, whereas traffic is responsible for approx. 26 % of the emission. Approx. 16 % thereof is attributed to car traffic.[2]
As a result, the European Union enacted a regulation which stipulates a reduction of the maximum CO_2 emission of new vehicles from an average of 140 g CO_2/km to 95 g CO_2/km until 2020.[3,4]

This leads to a fundamental change in the automotive industry regarding product strategies and development of new efficient vehicle technologies. There are three major approaches to reduce CO_2 emission of the vehicles of the next generation. First the development of combustion engines with higher efficient, providing lower fuel consumption and thereby lower CO_2 emission per kilometer. Second the development and implementation of alternative drive systems, like hydrogen combustion engines or electric/hybrid motors to completely reduce the direct CO_2 emission to zero. Finally the reduction of the total vehicle weight also leads to lower fuel consumption and thereby lower CO_2 emission per kilometer.

1.2 CFRP for Automotive Lightweight Production – *BMW i-Series*

For several years, CFRP parts have been implemented in cars. However, the field of application was limited to high performance cars with low production numbers. An example is the CFRP roof of the *BMW M-Series*.
To meet the challenge of CO_2 emission reduction, BMW pursued a revolutionary approach. With the *BMW i-Series*, *BMW* combines fully-/hybrid-electrical vehicles with radical and innovative lightweight design. This was realized by the so called BMW LifeDrive Concept, shown in Figure 1, and implemented for the first time in the *BMW i3* and *BMW i8* which was designed specifically for electric vehicles.

Figure 1: *BMW* LifeDrive-Concept realized *in BMW i3* with Life-Module (top) and Drive-Module (bottom).[5]

The LifeDrive Concept provides completely new vehicle architecture, and comprises two independent vehicle units. The Life-Module represents the passenger compartment and is fully made out of Carbon Fiber Reinforced Plastics (CFRP) and the Drive-Module which comprises the chassis and powertrain components including the electric motor and the high voltage (HV) battery. The lightweight design of the Life-Module compensates for most of the additional weight of the HV battery and thereby increases efficiency and vehicle range.

The advantages of CFRP parts are apparent from material characteristics. Carbon fibers have very good mechanical properties combined with a very low density of 1.5 g/cm^3. In fiber direction they have higher tensile strength and a greater elastic modulus than steel or aluminum. However, carbon fibers alone are not dimensionally stable. Therefore a resin matrix is required as both shaping component and as energy transfer medium. Only after connection of the fibers with the matrix, the mechanical stability of the entire component is given. In addition the resin matrix usually has very good chemical resistance and provides high durability. In the case of the *BMW i3*, the additional weight of the HV battery is compensated by the weight savings of the CFRP body structure compared to a conventional steel body. Due to the weight saving, the range of the vehicle significantly increases.

Though Fiber Reinforced Plastics (FRP) have had a wide field of application for several decades, especially in civil and military aerospace industries, the development of completely new materials and process techniques was necessary to meet the requirements of an application in the automotive

industry.[6,7] High mechanical requirements of the CFRP parts combined with automated high volume production processes under economically reasonable expenses had to be realized.[8–10]

BMW is the first to meet the challenge and realizes the mass production of CFRP parts for the implementation in the vehicle body structure. The basis is an efficient manufacturing process. A key point for a successful and effective implementation is the detailed knowledge and characterization of the cure behavior of the polymer matrix used for CFRP. The processing of the polymer matrix dominates the cycle times and the understanding of the relationship between filling times and curing times are crucial for an efficient process. In addition, a deep understanding of the processing characteristics of the matrix leads to improved material development in the future. This thesis presents a methodology for understanding the nature of these materials.

2 Fundamentals

2.1 Epoxy Resin Systems

2.1.1 Epoxy Resins and Hardeners

A major type of epoxy resins is derived by the reaction product of *4,4'*-(propane-*2,2*-diyl)diphenol commonly known as bisphenol A and (±)-*2*-(chloromethyl)oxirane commonly known as epichlorohydrin which leads to the most popular epoxy resins diglycidyl ether of bisphenol A (DGEBA). The reaction principle of epichlorohydrin with bisphenol A is shown in Scheme 1.

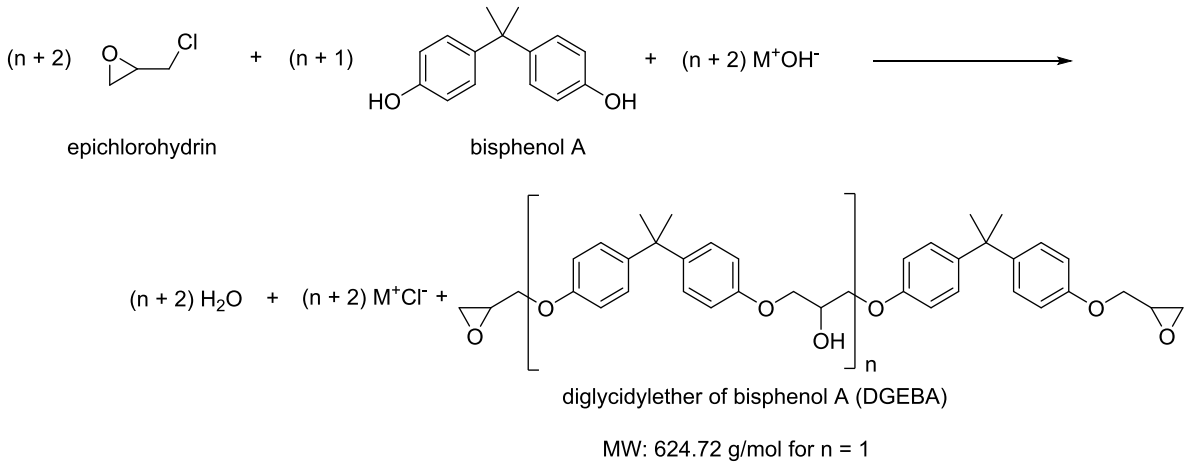

Scheme 1: Principle reaction of epichlorohydrin and bisphenol A.[11]

Depending on the phenol component used in the reaction with epichlorohydrin, several derivatives of DGEBA can be obtained. These are commonly diglycidyl ether of bisphenol F (DGEBF), epoxy novolac (EN) and tris(4-hydroxyphenyl)methane triglycidyl ether, shown in Figure 2 (a) – (d). Another type of epoxy resins is derived by the reaction of aromatic amines with epichlorohydrin, such as aniline (DGA), *p*-aminophenol (TGpAP) and methylene dianiline (TGMDA) Figure 2 (e) – (g).[12]

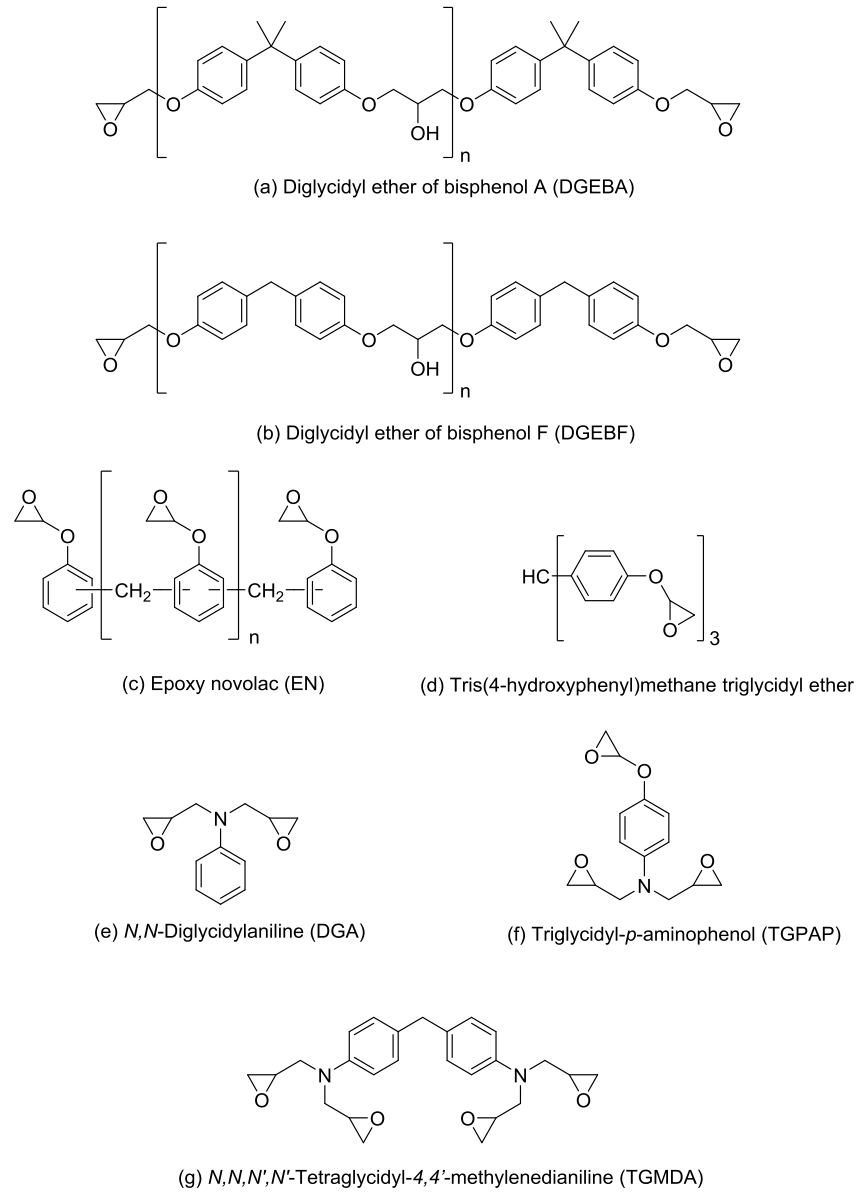

Figure 2: Overview of main commercially available epoxy resins.

The state of DGEBA and DGEBF epoxy resins depend on the *n* value. At room temperature these resins are crystalline solids for *n* value close to 0, liquids for *n* values around 0.5 and amorphous solids (glass transition temperature T_g ~ 40 – 90°C) for higher *n* values. For DGEBA and DGEBF typical *n* values are in a range from 0.03 up to 10.[12]

Many different types of hardeners can be used for epoxy resin curing. Besides the homopolymerization of epoxy components initiated by lewis bases like tertiary amines or imidazoles, amines, anhydrides, phenols and thiols can be used as curing agents.

Bifunctional epoxy resins and bifunctional curing agents lead to a linear polymerization. Three-dimensional networks are obtained when one component is at least trifunctional.

Amine hardeners are the most versatile curing agents used for epoxy resins. The curing performance depends on the composition of the amine hardener, the use of catalysts, the stoichiometry of reactive epoxy and amino groups and the curing temperature.

The curing reaction of epoxides with amines is a polyaddition, driven by the nucleophilic attack of the amine on the epoxy group. Therefore, the reactivity of the amine increases with its nucleophilic character which is influenced by its substituents as follows: aliphatic > cycloaliphatic > aromatic.[12]

Commonly used aliphatic amine hardeners are diethylenetriamine (DETA), triethylenetetraamine (TETA), tetraethylenepentaamine (TEPA) and *N*-aminoethylpiperazine, shown in Figure 3 (a) – (d).

Cycloaliphatic amine curing agents are for example isophoronediamine (IPD), *4,4'*-diaminodicyclohexylmethane (PACM) and *4,4'*-Diamino-*3,3'*-dimethyldicyclohexyl-methan (DMDC), shown in Figure 3 (e) – (g).

Typical aromatic amine hardeners are for example *m*-xylylenediamine (mXDA) *m*-phenylenediamine (mPDA) *4,4'*-diaminodiphenylmethane (DDM) *4,4'*-diaminodiphenyl-sulfone (DDS), shown in Figure 3 (g) – (k).

Tertiary amines cannot undergo the polyaddition reaction with epoxy groups as they lack the required hydrogen atom. Therefore they are often referred to as ‘catalysts’ in the literature. However, they are no real catalysts but initiators for an anionic chain polymerization of epoxy groups. The mechanism of the initiation is explained in the next section. Also boron trifluoride complexes are used as curing additives. Like tertiary amines boron trifluoride complexes do also not serve as direct crosslinking agents but as initiators which promote a cationic chain polymerization of epoxy groups.[13] Typical substances of this class are dicyandiamide (Dicy) 2-Methylimidazole, *N*-benzyldimethylamine (BDMA), *2,4,6*-tris(dimethylaminomethyl)phenol and boron trifluoride ethylamine (BF_3 MEA), shown in Figure 3 (l) – (p).

• Aliphatic Amine Hardeners

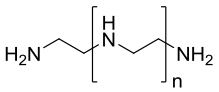

(a) n = 1 Diethylenetriamine (DETA)
(b) n = 2 Triethylenetetraamine (TETA)
(c) n = 3 Tetraethylenepentaamine (TEPA)

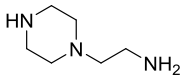

(d) *N*-Aminoethylpiperazine

• Cycloaliphatic Amine Hardeners

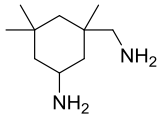

(e) Isophoronediamine (IPD)

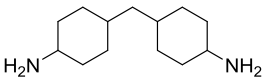

(f) *4,4'*-Diaminodicyclohexylmethane (PACM)

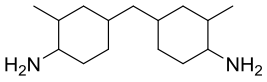

(g) *4,4'*-Diamino-*3,3'*-dimethyldicyclohexylmethane (DMDC)

• Aromatic Amine Hardeners

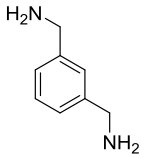

(g) *m*-Xylylenediamine (mXDA)

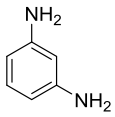

(i) *m*-Phenylenediamine (mPDA)

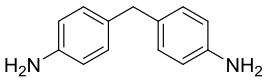

(j) *4,4'*-Diaminodiphenylmethane (DDM)

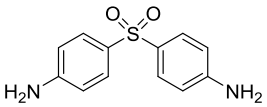

(k) *4,4'*-Diaminodiphenyl sulfone (DDS)

• Latent Amine Hardeners and 'Catalysts'

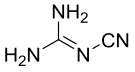

(l) Dicyandiamide (Dicy)

(m) *2*-Methylimidazole

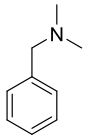

(n) *N*-Benzyldimethylamine (BDMA)

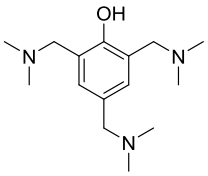

(o) *2,4,6*-Tris(dimethylaminomethyl)phenol

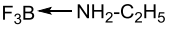

(p) BF_3 Monoethylamine (BF_3 MEA)

Figure 3: Overview of main commercially available amine hardeners and catalysts.

2.1.2 Principle reaction mechanism of epoxy resins with amine hardeners

The principle reaction mechanism of epoxy resins and amine hardeners, shown in Scheme 2, is a step growth polyaddition reaction.[12]

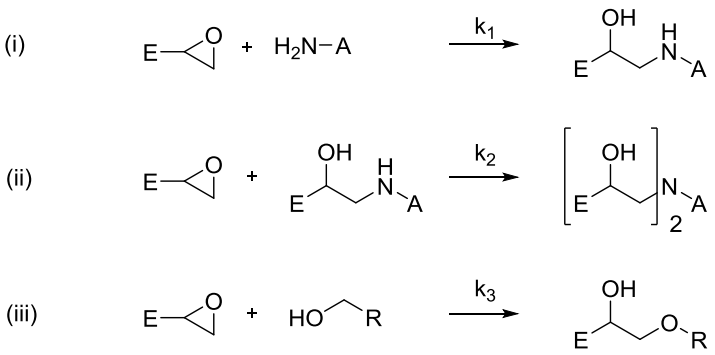

Scheme 2: Principle polyaddition reaction of epoxy resins with primary amines (i), with secondary amines (ii) and with hydroxy groups (iii).[12]

The epoxy group can react with primary amines to yield a *β*-hydroxy amine generating a secondary amine. Secondary amines react in the same way and yield tertiary amine. The newly formed hydroxy groups can also undergo an addition reaction with an epoxy group to yield a *2*-hydroxy ether.

Several studies towards the reactivity of primary amines with epoxides (k_1) and secondary amines with epoxides (k_2) were conducted. The ratio of the amine reactivity r_a is given as

$$r_a = \frac{k_2}{k_1} \qquad (1)$$

where k_1 is the rate constant of the reaction of a primary amine with an epoxide and k_2 is the rate constant of the reaction of a secondary amine with an epoxide.

The reactivity of the amine is influenced by both substitution and steric effects.[14] Electron donating substituents lead to a higher reactivity due to an *+I* effect which increases the nucleophilic character of the amine.[15] A set of reactivity ratios r_a for different amine hardener components is shown in Table 1.

Table 1: Reaction rate constant ratios of primary and secondary amines with epoxides.

Compound	$r_a = k_2/k_1$
Hexamethylendiamine (HMDA)	0.6-0.7[16]
4,4'-Diaminodiphenylmethane (DDM)	0.35-0.45[16]
4,4'-Diamino-3,3'-dimethyldicyclohexylmethane (DMDC)	0.40[17]
Aniline	0.40[15]
p-Anisidine	0.55[15]
p-Nitroaniline	0.09[15]
4,4'-Diaminodiphenyl sulfone (DDS)	0.22[15,18]

The hydroxy group is usually less reactive than a secondary amine towards the polyaddition reaction with an epoxy group. Therefore the etherification reaction plays a minor role in the crosslinking reaction, as long as the concentration of the amine groups is higher. For an epoxy resin with DDS as hardener the reaction rate constant ratio of the secondary amine k_2 and the hydroxy group k_3 equals $4.14 \cdot 10^{-4}$.[18]

The reaction mechanism of the polyaddition reaction of epoxy groups with amine hardeners during network formation of epoxy resins was investigated in detail. Studies have shown, that proton donors like alcohols and water have an accelerating effect on the crosslinking reaction.[19]
As hydroxy groups are formed in the polyaddition reaction of epoxy resins with amine hardeners, an autocatalytic reaction is assumed. T. Smith proposed an autocatalytic reaction mechanism of the polyaddition reaction, which is shown in Scheme 3.[20]

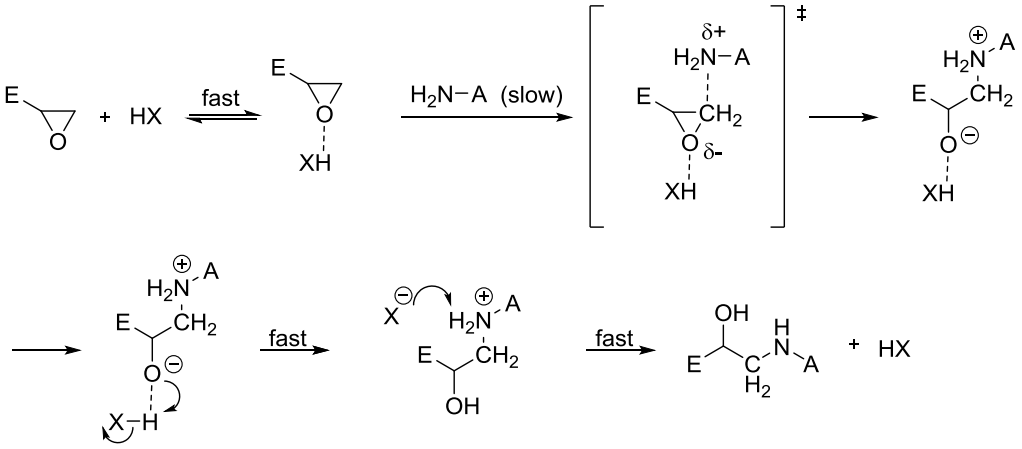

Scheme 3: Autocatalytic reaction mechanism of epoxy-amine-polyaddition proposed by T. Smith, with epoxy component E, amine component A and catalyst HX.[20]

The proton donating catalyst, i.e. the formed hydroxy groups in an autocatalytic reaction, form a hydrogen bridge bond with the oxygen of the epoxy group. By accumulation of a primary or secondary amine, a cyclic trimolecular transition state is formed. The addition reaction of the amine

and the ring opening reaction of the epoxide are enhanced by the activation of the proton donor. After subsequent proton transition, a new hydroxy group is formed, the catalyst is restored and the polyaddition is completed.

In addition to proton donating groups which catalyze the epoxy amine polyaddition, tertiary amines can also accelerate the polymerization. They act as initiators for an anionic chain polymerization. The acceleration of crosslinking reaction of epoxy resins by tertiary amines is very complex and the proposed mechanisms are controversially discussed.[21–23] In principle, the reaction of tertiary amines with epoxides is shown in Scheme 4.

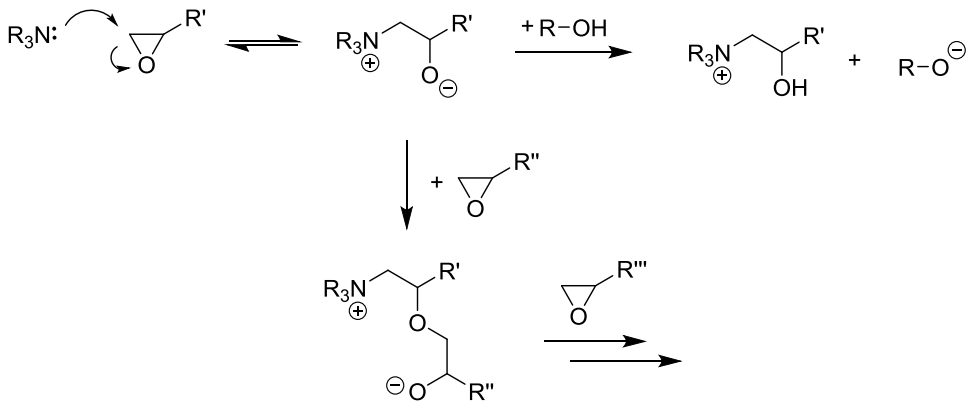

Scheme 4: Initiation of anionic homopolymerization of epoxides by tertiary amines.

The tertiary amine opens the oxirane ring in form of a nucleophilic attack of the nitrogen atom to form a zwitterion. This zwitterion can then deprotonate an alcohol to generate a new nucleophile, or undergoes homopolymerization with another epoxy group.

Depending on the formulation of the epoxy resin hardener, a combination of reactions, the step-growth polyaddition with amines and the anionic chain polymerization can take place. This leads to a very complex crosslinking mechanism and a competition of both pathways, depending on the cure temperature.[23,24]

A very prominent amine hardener, which realizes both features in one molecule, the crosslinking amine groups and a tertiary amine for initiation of anionic homopolymerization, is dicyandiamide (Dicy), shown in Figure 3 (m). Dicy is widely used as latent hardener in epoxy resins systems and fields of application are prepregs, laminates and powder coatings. Its latency originates from the high melting point (T_m = 207°C) and the low solubility in epoxy monomers.[23]

2.1.3 Properties of Epoxy Resin Systems

During network formation of epoxy resins, molecules with an epoxy group are covalently linked with amine molecules to form three-dimensional branched molecules with a wide size distribution and their molecular weight increases with increasing conversion.[25] During the crosslinking reaction, two characteristic and macroscopic transformations can occur, depending on the cure temperature. The first one is gelation which leads to a rapid transformation from a liquid-like to a rubber-like behavior. Much research has been conducted about the phenomenon of gelation, its characterization and the molecular basis. The basics were established by the research of Flory and Stockmayer in 1941/42, who described the network formation due to covalent bond formation of molecules, which lead to what is today known as percolation theory, which has been further developed ever since.[26–29] The percolation theory states, that at the gel point the molecular weight of the largest molecule becomes infinite or one molecule is spanning the entire network. This infinite macromolecule, also called gel fraction, is insoluble and the finite and still soluble molecules, called sol fraction, are trapped inside.[30,31] The conversion of the chemical reaction p assumes values of $0 \leq p \leq 1$ and the point at which gelation occurs is referred to as critical point p_c. [25,31]

The value of the gel point p_c can be estimated for particular polymers reacting in an ideal polymerization by using following equation,

$$p_c = \frac{1}{\sqrt{(f-1)\cdot(g-1)}} \qquad (2)$$

where f and g are the functionalities of the monomers.[23]

The assumptions for an ideal polymerization are: (i) a stoichiometric mixture of the functionalities of the monomers; (ii) an equal reactivity of the functional groups of the same type; (iii) the absence of substitution effects of partially reacted functional groups or monomers; (iv) the absence of intramolecular reactions; (v) all functional groups do react.[12,26]

For an ideal polymerization of an epoxy resin system with a stoichiometric mixture of resin component DGEBA (f = 2) with a diamine hardener (g = 4) the gelation occurs at p_c =0.58 or 58% of conversion. Experimental values of p_c for the stoichiometric reaction of DGEBA and diamines are in a range of 0.58 – 0.60.[12]

The second characteristic and macroscopic transformation is vitrification which is the transformation from an either liquid-like or a rubber-like behavior to a solid glass-like state. Vitrification occurs, when the temperature is below the glass transition temperature T_g of the respective polymer. During the polymerization reaction of epoxy resins, the glass transition temperature increases with progressing degree of conversion α. When the glass transition temperature exceeds the cure temperature, the polymerization vitrifies. In the vitrified state, the speed of the polymerization reaction

is no longer driven by the chemical reactivity of the functional groups, but due to the immobility of the molecules the reaction becomes diffusion controlled. Vitrification is independent of gelation and can either occur before or after the gel point.

A Time-Temperature-Transformation (TTT) diagram, which shows all state transitions, which can occur during curing of a thermosetting polymer, depending on curing time and curing temperature is shown in Figure 4. Three critical temperatures are identified for the curing of a thermosetting polymer. First the glass transition temperature of the uncured polymer T_{g0}, second the temperature ${}_{gel}T_g$ at which gelation and vitrification occurs simultaneously and third the glass transition temperature of the fully cured polymer $T_{g\infty}$. Depending on the cure temperature, the polymer adopts different states. For temperatures below T_{g0}, the polymer is a vitrified sol. Cure temperatures between T_{g0} and ${}_{gel}T_g$ lead to a liquid state first and end in a vitrified sol with progressing degree of conversion. For cure temperatures between ${}_{gel}T_g$ and $T_{g\infty}$ the transformation of the polymer from liquid over sol/gel rubber to sol/gel glass can be observed. When T_{cure} is above $T_{g\infty}$ the fully cured polymer ends in a gel rubber state and does not vitrify.

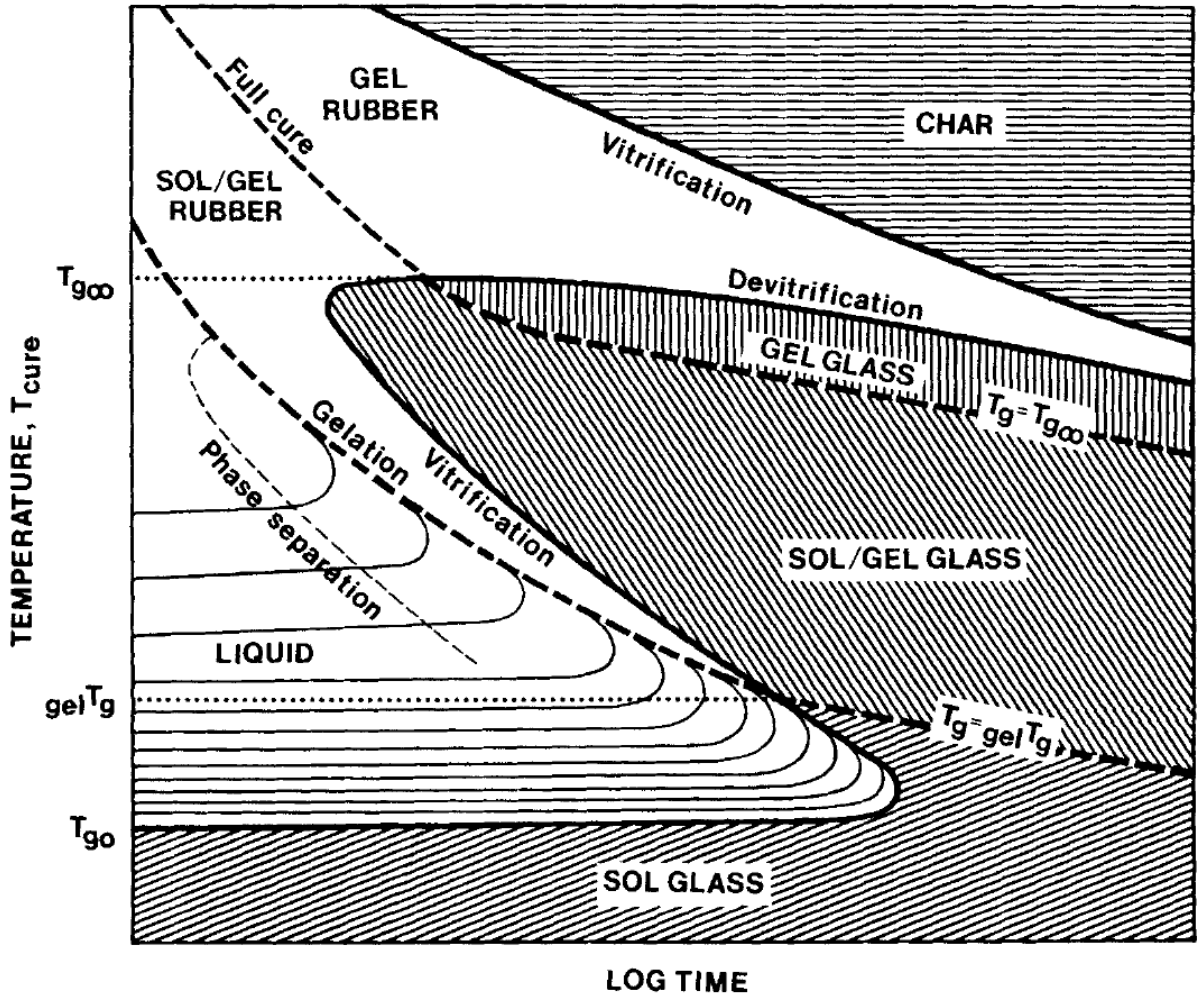

Figure 4: Time-Temperature-Transformation (TTT) diagram of a thermosetting polymer.[32]

2.1.4 Investigated Epoxy Resin Systems

2.1.4.1 Epoxy Resin System A supplied by Huntsman Corp.

The resin component of epoxy resin system A supplied by the *Huntsman Corporation* consists of the reaction product of epichlorohydrin and bisphenol A, which yields diglycidyl ether of bisphenol A (DGEBA), shown in Figure 5. The supplied DGEBA has a molar weight ≤ 700 g/mol.

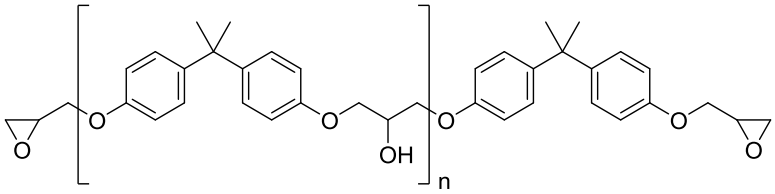

Diglycidyl ether of bisphenol A (DGEBA)

Figure 5: Resin component of epoxy resin system A.

The amine hardener of epoxy resins system A consists of a mixture of diethylenetriamine and bisphenol A, shown in Figure 6.

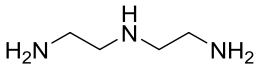

diethylenetriamine

approx. 60 wt.%

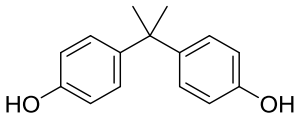

bisphenol A

approx. 40 wt.%

Figure 6: Hardener composition of epoxy resin system A.

The bisphenol A in the hardener serves both as a catalyst in the early stages of the crosslinking reaction, where the concentration of newly formed hydroxy groups as autocatalyst is very low, and as crosslinking agent to form *2*-hydroxy ethers with epoxy groups according to reaction (iii) in Scheme 1.

The third component of epoxy resins system A is an internal mould release agent (IMR). It is based on refined oils, based on natural products. The ingredients are not further specified, though it is known that the main component is an unsaturated C_{18} fatty acid and its mono- and diglycerides.

The mixing ratio for the manufacturing process for epoxy resins system A is 100 resin, 19 hardener and 2 internal mould release agent by weight equivalent.

The gel point p_c for this resin system is calculated according to equation (2) with the following functionality parameters: the resin component DGEBA is bifunctional and therefore $f = 2$; the hardener component diethylenetriamine has a functionality of 5 and bisphenol A has a functionality of 2

resulting in a mixed functionality *g* for the hardener according to the concentrations of (0.6 · 5) + (0.4 · 2) = 3.8. This results in a calculated gel point p_c = 0.60 or at 60% of conversion.

2.1.4.2 Epoxy Resin System B supplied by Hexion Corp.

The resin component of epoxy resin system B supplied by the *Hexion Corporation* consists of a mixture of diglycidyl ether of bisphenol A (DGEBA) and diglycidyl ether of bisphenol F (DGEBF), shown in Figure 7. Both components have a molar weight ≤ 700 g/mol.

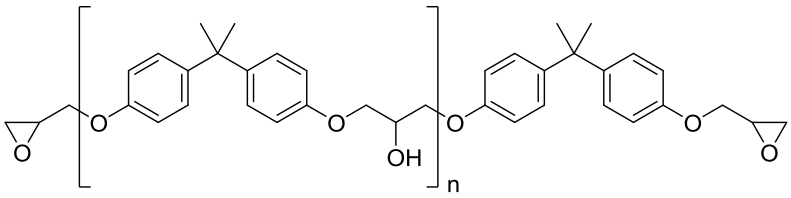

Diglycidyl ether of bisphenol A (DGEBA)

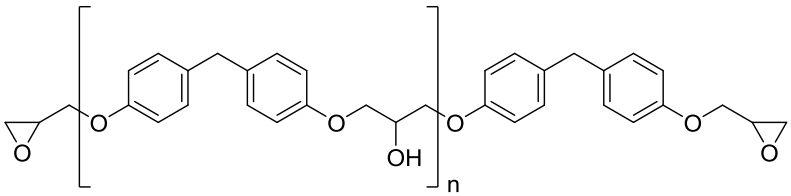

Diglycidyl ether of bisphenol F (DGEBF)

Figure 7: Components of resin component of epoxy resins system B.

The hardener of epoxy resins system B completely consists of amine components. The crosslinking agents are triethylenetetraamine, *1*,*3*-cyclohexanebis(methylamine) and *1*-(*2*-Aminoethyl)piperazine in unspecified concentrations. *1*,*8*-Diazabicyclo[5.4.0]undec-*7*-ene (DBU) contains only tertiary amines and is therefore believed to initiate the anionic chain polymerization of the epoxide.

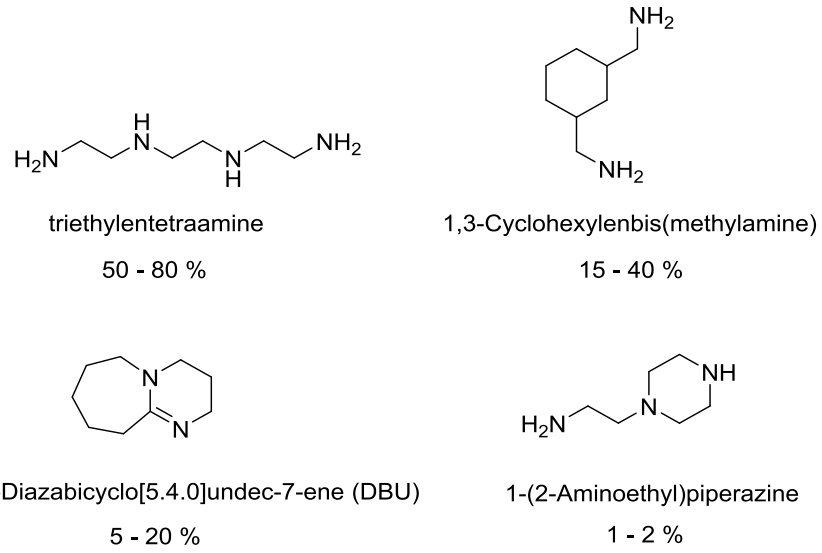

Figure 8: Hardener composition of epoxy resin system B.

The third component of epoxy resins system B is an internal mould release agent (IMR) which is similar to that of epoxy resins system A.

Due to the unknown concentrations of the amines in the components, a calculation of the degree of conversions at gel point p_c is not possible. However, the gel point for this epoxy resin system is also assumed in the range of the literature values for epoxy resins $p_c = 0.58 – 0.60$.

2.2 Resin Transfer Moulding for CFRP-Production

Many process technologies for composite production were developed in the last decades to meet the different requirements of the industry, e. g. complexity of parts, part size, quantities, production speed and costs. To achieve the goal of high volume CFRP part production for application in the automotive body structure, one of the production methods implemented at *BMW* is high-pressure resin transfer moulding (HP-RTM). The main advantages of the HP-RTM process are the high degree of automation, reasonably short cycle times and the possibility to manufacture components with complex geometries. These advantages are needed to realize the mass production of CFRP parts for the vehicle body structure.

The HP-RTM process is divided into several process steps, which are illustrated in Figure 9. In the first step the dry carbon fiber fabric, which is preformed to the final geometry in previous processes and thus referred as ‘preform’, is transferred into the heated mould. The mould is closed and vacuum is applied to support the following infusion process. During this process step, the dry preform is heated up in the mould and assumes the same temperature. After the evacuation step, the components of the epoxy resin system are injected with high pressure via a high pressure mixing head into the mould. The time of injection depends on the part size and geometry, whereby for big and complex shaped parts a longer injection time is needed to impregnate the whole preform due to longer flow paths. Subsequently to the injection step, the epoxy resin cures in the mould and the finished part can be removed from the mould afterwards. The biggest challenge of the RTM process regarding the realization of short cycle times is the critical interdependence of injection time and curing time. The main control parameter of the speed of curing is the cure temperature of the mould. The higher the cure temperature the shorter the curing time, but also the injection time and vice versa. Too short injection times cause dry spots and voids as a proper impregnation of the dry preform is not given. Too long injection times result in unnecessary high cycle times. To realize a high volume CFRP part production at reasonable costs, the specified curing time is < 5 min. For this reason a low resin viscosity is required to provide optimal injection and impregnation properties.

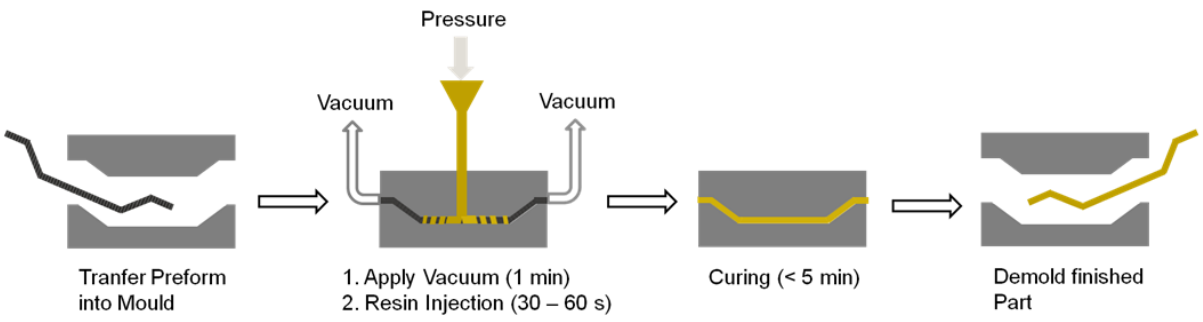

Figure 9: Schematic representation of the process steps in the HP-RTM process.

3 Objectives

The key to realize an economic and efficient HP-RTM production process for high volume CFRP part production is to characterize the cure behavior of the thermosetting epoxy resin matrix in detail.

Within the scope of this work, a new methodology is developed to provide a comprehensive understanding of the curing behavior of fast setting epoxy resin systems for high volume CFRP part production not only by laboratory analysis but also by direct investigation of the curing progress in the HP-RTM production process. Furthermore a reaction kinetic model is developed to allow prediction of the curing process and complement the comparison of laboratory and process investigations. This approach allows a comparison between theory and practice which is absolutely necessary for a successful and efficient high volume CFRP manufacturing process.

Previously, it was not necessary to analyze the curing behavior of fast curing epoxy resins for mass production in the RTM process in depth, because such kind of CFRP production did not exist. The required short cycle times, to provide an economical mass production of CFTP parts for the automotive body structure, leaves less space for errors. The extremely short curing times represent a major challenge, because the analysis of the epoxy resins with existing analytical methods is pushed to its limits due to difficult sample handling or errors accompanied by inadequate acquisition times. In addition, the sample and measurement conditions of the laboratory investigations are fundamentally different from those of CFRP production in the HP-RTM process, such as carbon fibers or high-pressure mixing of the epoxy resin system.

Differential scanning calorimetry (DSC) is an established laboratory analytic method at *BMW* and is used and evaluated with respect to its suitability for the analysis of fast curing epoxy resins.
Rheometry was also used to investigate the rheological behavior of the epoxy resin during curing and is also present at the *BMW* laboratories. However, a completely new test specification had to be developed to allow reliable measurements of fast curing epoxy resins.
Another analytical method used was IR spectroscopy. Since the laboratories at *BMW* are not equipped with a suitable IR spectroscopy measuring device, these investigations were conducted in collaboration with the Federal Institute for Materials Research and Testing. A newly developed IR spectroscopy measuring cell is used, which allows the investigation of the curing behavior of fast curing epoxy resins.
Ultrasound technique is used for laboratory investigations of the curing behavior of epoxy resins and is implemented as well as an online-cure-monitoring technique to provide the cure characterization of the epoxy resins directly in the HP-RTM process. The implementation of the ultrasound technique in the HP-RTM process is completely new at *BMW* and was built from the ground up.

Based on experimental data, a reaction kinetic model is developed. The prediction according to the kinetic model is used on the one hand to compare laboratory and process analysis. On the other hand the simulation is a tool to provide an overview and a quick answer to all questions regarding the impact of curing time and curing temperature. This is valuable for the practitioner who wants to optimize his process as well as for the development engineer who can derive his optimal process by virtual experimental series instead of real large-scale test series.

In the following a stepwise cure characterization of the two epoxy resin systems introduced above is conducted. To provide a correlation of theory and practice, the results of the cure simulation according to the reaction kinetic model, the results of the laboratory analysis and the measurements in the HP-RTM process are gradually compared. It will be demonstrated that the combination of analytical methods, cure simulation and online-cure-monitoring by ultrasound allows the tracking of the curing state of the epoxy resin directly in the HP-RTM process.

The investigation according to this methodology is conducted for two fast curing epoxy matrix resin systems suitable for the application in CFRP parts for the body structure. On the basis of this methodology, the curing properties of future potential thermosetting matrix resins can be characterized methodically and a fast assessment of the curing performance compared to the prior art matrix systems should be possible. With the provided methods, the current processes can be analyzed to identify potential process optimizations. Especially component-specific adaptations of the curing processes with the help of the provided methods can reduce the cycle times further. Due to the comprehensive knowledge of cause-effect relationships and easy and fast assessments of cure behavior by cure simulation, new process strategies can be identified.

B. DEVELOPMENT OF A KINETIC MODEL AND SIMULATION OF EPOXY RESIN SYSTEM A

4 Analytical Methods to derive a Kinetic Model

4.1 Differential Scanning Calorimetry DSC

4.1.1 Basic Working Principle of Differential Scanning Calorimetry DSC

The principle of differential scanning calorimetry (DSC) is to measure the exchange of heat of a sample in relation to a reference with both sample holders in a temperature controlled measuring chamber. Chemical reactions and physical change of states are related with either heat absorption (endothermic processes) or heat release (exothermic processes). Depending on the design of the differential scanning calorimeter, the exchange of heat can be detected in two ways. One way is the measurement of the heat flow of the sample during isothermal conditions or with a defined heating- or cooling-rate in relation to a reference (heat flux DSC). The other way is to keep the thermal condition of sample and reference identical during an experiment under isothermal conditions or with a defined heating- or cooling-rate by adjusting the electrical power of the measurement chambers (power compensation DSC).
Since only a heat flux DSC was used for the following experiments, the power compensation DSC will not be further discussed.

The schematic design of a sample chamber and working principle of a heat flow DSC is shown in Figure 10. The sample, usually placed in a crucible and the reference, usually an empty crucible, are heated symmetrically in the sample chamber via a disc of medium thermal conductivity.[33] A change in the heat flow of the sample, due to endothermic and exothermic processes or the change of the heat capacity of the sample, is detected by thermal resistors in the form of a temperature gradient ΔT which is recorded by sensitive temperature sensors (thermocouples). When sample and reference are ideally identical, the heat flow of the two is identical and $\Delta T = 0$. When this equilibrium is disturbed by an endothermic process, for example melting or glass transition, or an exothermic process, for example combustion reactions or the polymerization reaction of an epoxy resin, a differential signal of the heat flux is detected.

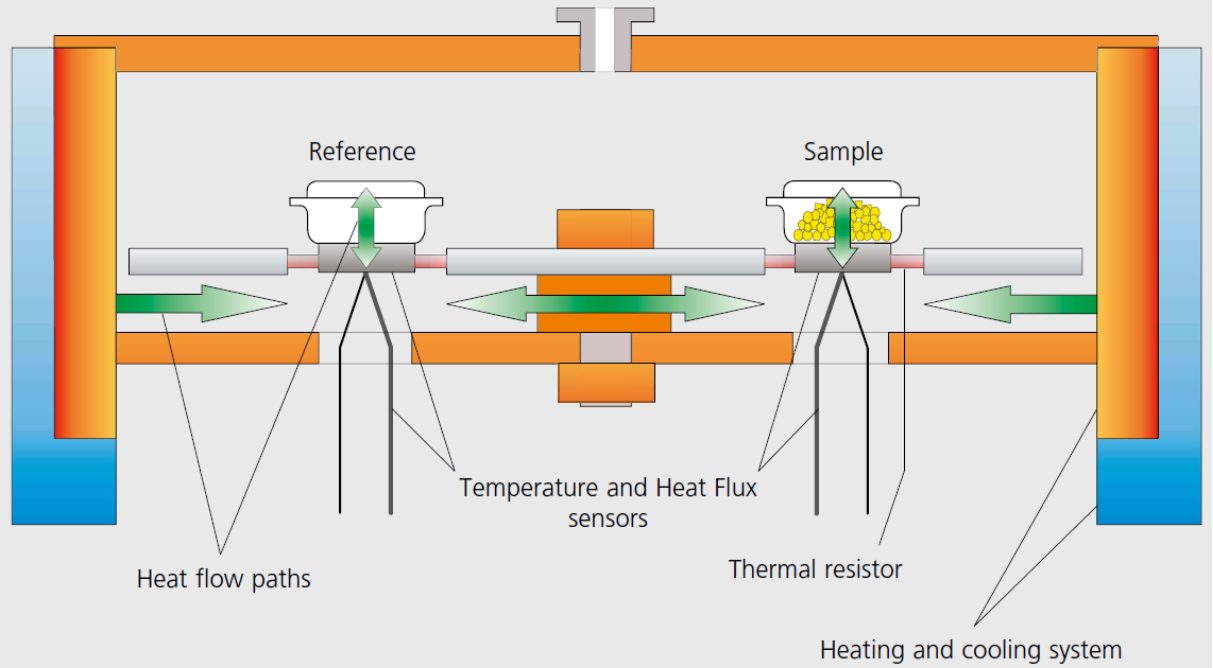

Figure 10: Schematic design of the sample chamber and working principle of a heat flow DSC (DSC 204 F1 Phoenix by *NETZSCH-Gerätebau GmbH*).

4.1.2 DSC Measurement Assembly

All experiments were conducted on a DSC 204 F1 Phoenix by *NETZSCH-Gerätebau GmbH*.

The heating rate experiments were conducted in a temperature range from 10 up to 200°C with sample masses of 10 – 11 mg in perforated aluminum pans.

The isothermal DSC experiments were conducted with sample masses of 19 – 28 mg in perforated aluminum pans. The sample chamber was preheated to the respective isothermal cure temperature and the curable is inserted requiring about 1 minute for thermal equilibrium. The following analytical runs to determine the state of cure were conducted with a heating rate of 10 K/min.

For all experiments the components were weighed separately according to the respective mixing ratio 100 : 19 : 2 epoxy resin : hardener : IMR calculated for 5 g batch and subsequently mixed with a spatula for 30 s to provide a homogeneous mixture.

4.1.3 Interpretation of DSC Data

A dynamic DSC measurement of the curing reaction of epoxy resin system A at a heating rate of 10 K/min in a temperature range from –50°C to 200°C is shown in Figure 11. After the transient response due to the adjustment of the thermal equilibrium an endothermic process can be observed beginning at –30°C and is assigned to the glass transition of the uncured epoxy resin system, which vitrifies at temperatures < –30°C. For all experiments the temperature at the half step height of the

glass transition, called $T_{g(mid)}$ midpoint, is taken as the glass transition temperature and herein after referred to as T_g.

An exothermic process can be observed starting at 25°C, which is assigned to the polymerization of the epoxy resins system. The area of the exothermic peak yields the total enthalpy of reaction ΔH_{tot} of the crosslinking reaction, for epoxy resin system A ΔH_{tot} = –515.16 J/g.

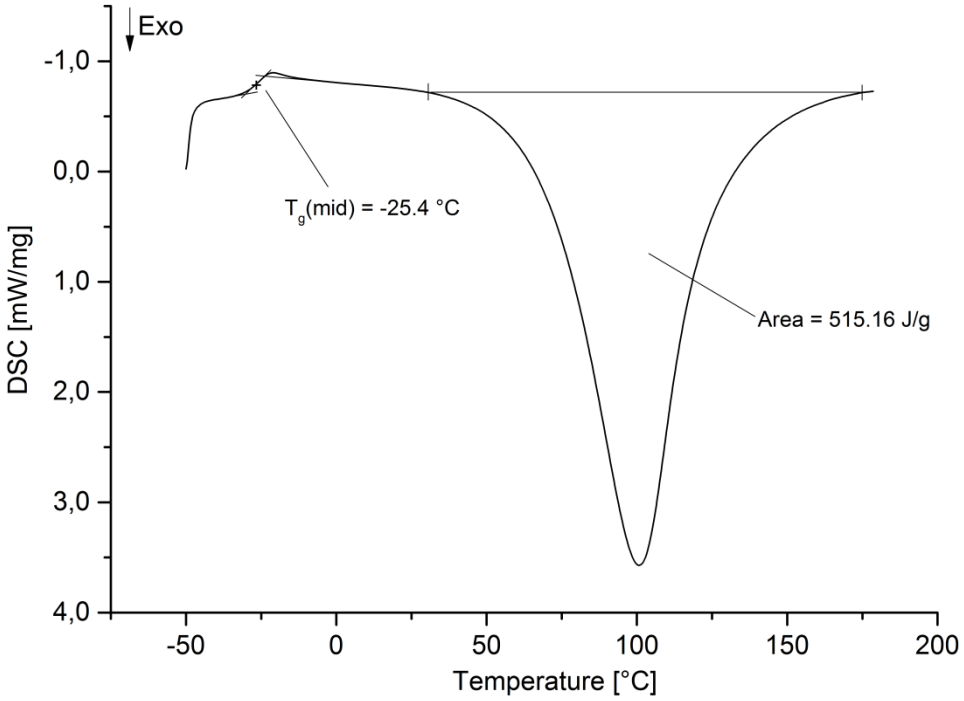

Figure 11: Dynamic DSC measurement of the curing reaction of epoxy resin system A with a heating rate of 10 K/min to determine T_{g0} and the total enthalpy of reaction ΔH_{tot}.

A combined DSC experiment with a mixed temperature profile containing both isothermal conditions, segments 1 and 3, and dynamic heating and cooling conditions, segments 2 and 4, is shown in Figure 12.

In the first isothermal segment, the uncured epoxy resin system cures to a certain extent, depending on curing time and temperature. After insertion of the sample crucible into the preheated sample chamber, the polymerization starts immediately. Because of the transient response due to the adjustment of the thermal equilibrium at the beginning of the measurement, the first part of the exothermic reaction is not detectable.

After the first isothermal curing segment a cooling segment follows to stop the crosslinking reaction and to provide a starting point at low temperatures for the dynamic heating segment 4. The short isothermal segment 3 ensures an equilibrium adjustment between segment 2 and segment 4. The dynamic heating segment 4 serves as analytical run to determine the curing state of the epoxy resin system.

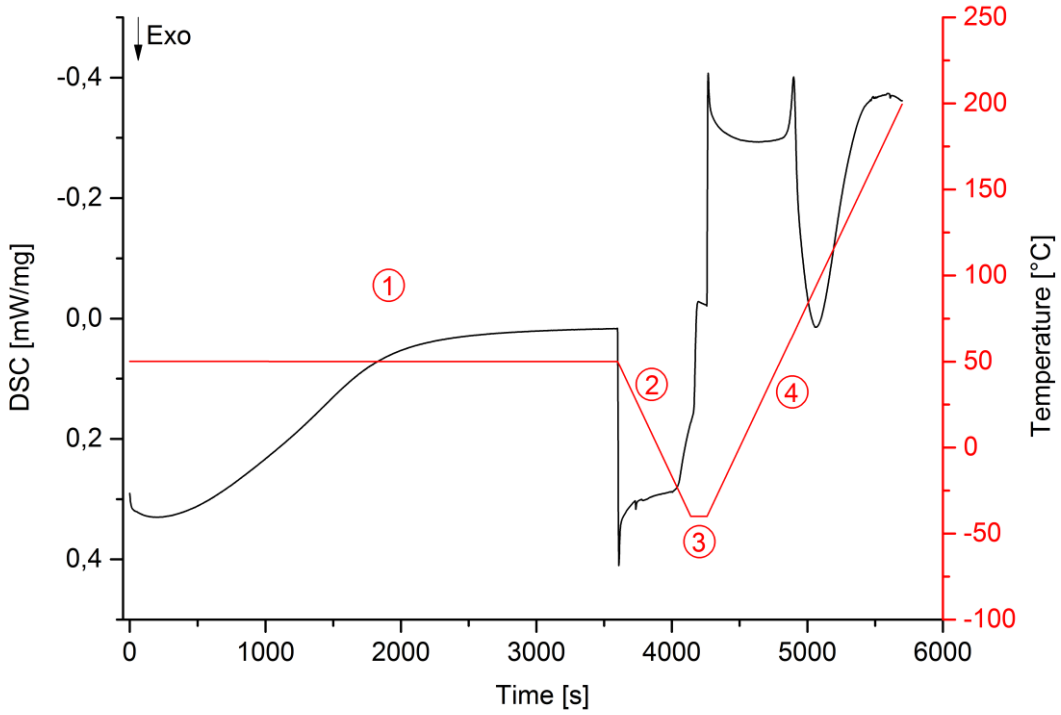

Figure 12: Combined DSC experiment of an epoxy resin with isothermal segments 1 and 3 and dynamic segments 2 and 4.

The interpretation of the analytical run at heating segment 4, shown in Figure 13, is used to determine the attained glass transition temperature T_g and the residual enthalpy of reaction ΔH_{res} after the first isothermal segment 1. It can be observed, that for the partially cured epoxy resin system A, the endothermic peak of the glass transition interferes with the beginning of the residual exothermic polymerization reaction. The baseline to determine the residual enthalpy of reaction ΔH_{res} was therefore constructed by horizontal linear extension of the right end of the signal to the glass transition temperature peak.

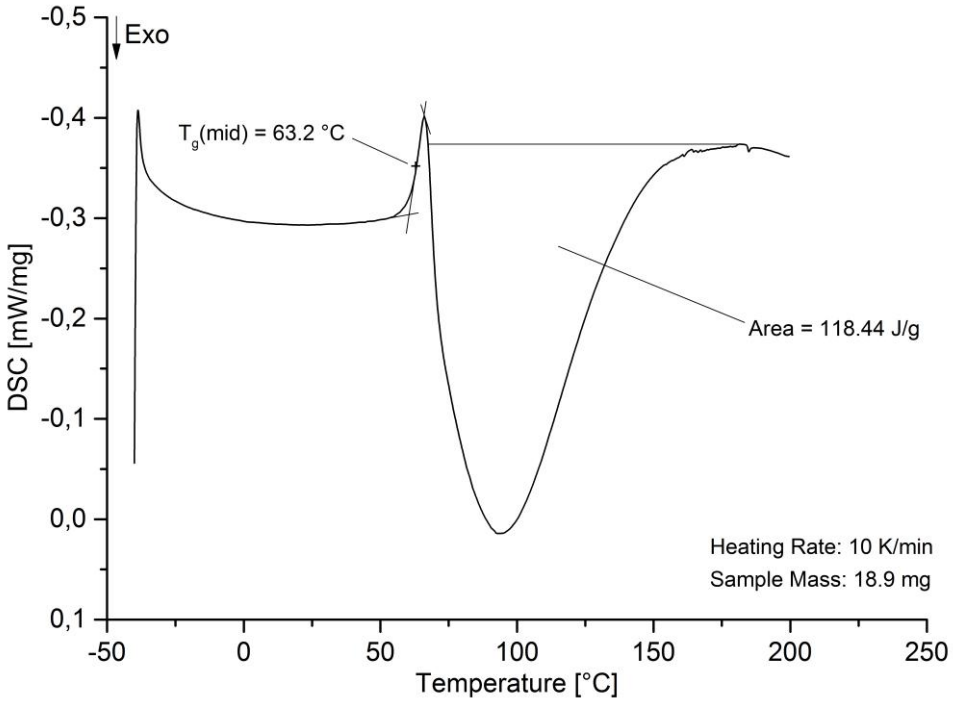

Figure 13: Interpretation of analytical of segment 4 of a partially cured epoxy resin sample with a heating rate of 10 K/min to determine T_g and the residual enthalpy of reaction ΔH_{res}.

The degree of conversion α, i. e. the extent of the crosslinking reaction which is directly related to the enthalpy of reaction, can be calculated according to equation (3),

$$\alpha = \frac{\Delta H_{tot} - \Delta H_{res}}{\Delta H_{tot}} \qquad (3)$$

where α ($0 \leq \alpha \leq 1$) is the degree of conversion, ΔH_{tot} is the total enthalpy of reaction and ΔH_{res} is the residual enthalpy of reaction of a partially cured sample. A correlation of the progress of the glass transition temperature T_g and the advancing degree of conversion α can then be obtained.

4.1.4 Results and Discussion of Heating Rate DSC Experiments

Distinct degrees of conversion α were achieved by different isothermal curing conditions shown in Table 2. The correlation to the corresponding glass transition temperature T_g and the residual enthalpy of reaction ΔH_{res} are evaluated in a second dynamic DSC run with a 10 K/min heating rate shown in Figure 14.

Table 2: Isothermal curing conditions of the first segment of combined DSC experiments.

Curing Temp. [°C]	10	25	50	70	80	90	100	110	120
Curing Time [min]	500	400	60	30	30	30	20	20	20

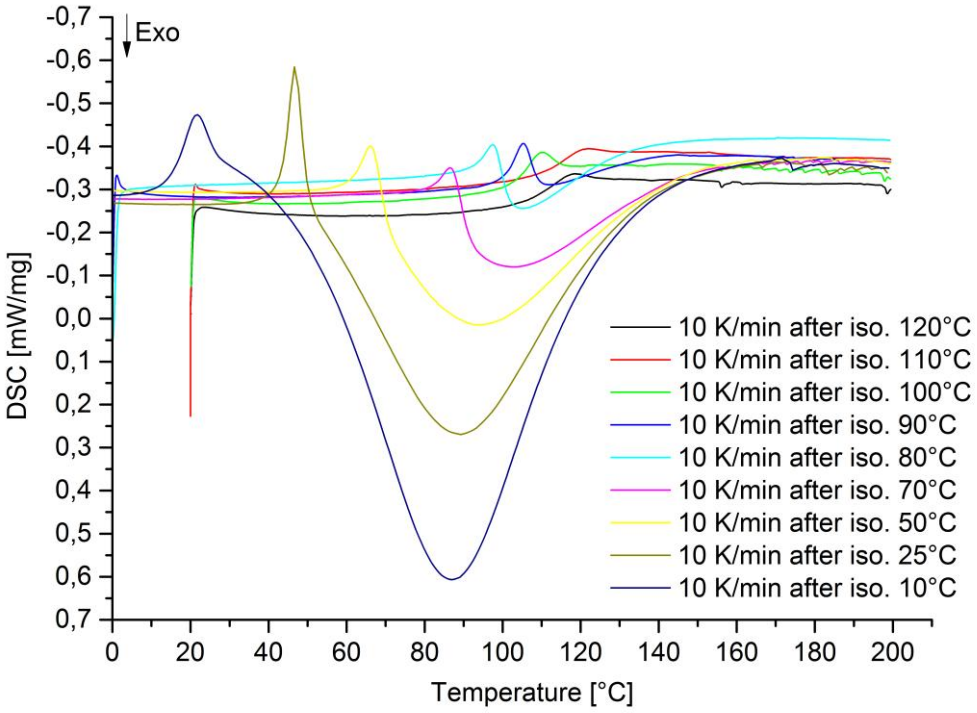

Figure 14: Analytical dynamic run with 10 K/min heating rate to determine the degree of conversion α and the respective glass transition temperature T_g after isothermal curing conditions form 10°C up to 120°C.

Table 3 shows the initial state of the uncured epoxy resin and the states after isothermal curing conditions at different temperatures from 10°C up to 120°C. The degree of conversion α was calculated according to equation (3) with reference to a total enthalpy of reaction $\Delta H_{tot} = -515.16$ J/g which was determined according to Figure 11.

Table 3: States of the uncured, partially and fully cured epoxy resin system A.

Isothermal Cure Temp [°C]	Residual enthalpy ΔH_{res} [J/g]	Degree of Conv. α	Glass Transition Temp. T_g [°C]
--	–515.16	0	-25.4
10	–305.72	0.41	18.5
25	–169.40	0.67	45.7
50	–118.44	0.77	63.2
70	–52.21	0.90	84.9
80	–19.57	0.96	94.7
90	–0.70	0.98	103.1
100	–0.59	1.00	106.5
110	0	1.00	112.3
120	0	1.00	113.1

To provide a continuous correlation of degree of conversion α and the glass transition temperature T_g based on a limited set of experimentally determined values, a suitable fit equation was proposed by Hesekamp,[34]

$$T_g(\alpha) = T_g(0) \cdot e^{\left(\frac{g_1 \cdot \alpha}{g_2 - \alpha}\right)} \qquad (4)$$

where $T_g(0)$ is the glass transition temperature of the uncured epoxy resin, which is adjusted by the best fit and g_1 and g_2 are free fit parameters. For epoxy resin system A the following parameters were determined for the best fit:

$T_g(0)$ = –23.4°C
g_1 = 0.9685
g_2 = 3.2565

In addition to the fit equation proposed by Hesekamp, another well known fit equation was proposed by DiBenedetto and has the following form, [35,36]

$$T_g = T_{g0} + \frac{\left(T_{g\infty} - T_{g0}\right) \cdot \lambda \cdot \alpha}{1 - \left(1 - \lambda\right) \cdot \alpha} \qquad (5)$$

where T_{g0} is the experimentally determined glass transition temperature of the uncured epoxy resin, $T_{g\infty}$ is the experimentally determined glass transition temperature of the fully cured epoxy resin and λ

is a free fit parameter with values between 0 and 1. For epoxy resin system A the best fit is found at $\lambda = 0.51$.

The correlation of the degree of conversion α and the glass transition temperature T_g and the comparison of fit equation (4) by Hesekamp and fit equation (5) by DiBenedetto is shown in Figure 15.

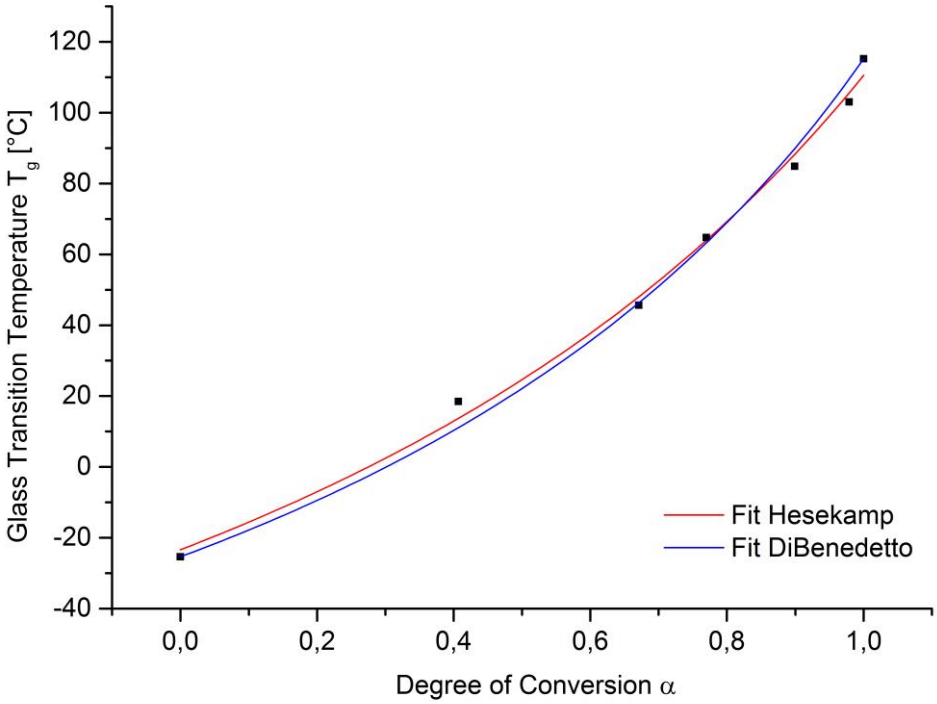

Figure 15: Correlation of glass transition temperature T_g and degree of conversion α of epoxy resin system A.

Both equations provide a very good fit to the experimentally determined values. It can be observed, that the glass transition temperature strongly increases for the last 10% of curing from 85°C to 113°C which is about 20% of the total increase of glass transition temperature ΔT_g. This finding indicates that the formation of the final covalent bonds is responsible for strong increase of the network stability due to the formation of a higher density of the entire network.

The difficulty of investigating the curing behavior of fast curing epoxy resins is that they start to react immediately when they are exposed to higher temperatures, which are usually required for curing to provide a short cycle time and to meet the required glass transition temperature which is responsible for the mechanical stability. Thus, the cure characterization at isothermal process temperatures is very complex since the beginning of the curing progress cannot be detected due to sample preparation, insertion of the sample in the measuring cell and start of the measurement including initialization time.

To determine the complete curing progress by DSC, dynamic experiments with different heating rates were conducted. The curing behavior of epoxy resin system A at heating rates of 1, 2, 5, 10 and

20 K/min plotted over time is shown in Figure 16. It can be observed that the total area of the signal is equal for each heating rate. At small heating rates the cure temperature rises only slowly and therefore the polymerization reaction proceeds slowly and takes more time. At high heating rates, the reaction proceeds faster and more heat is released in shorter time, which results in a more pronounced DSC signal.

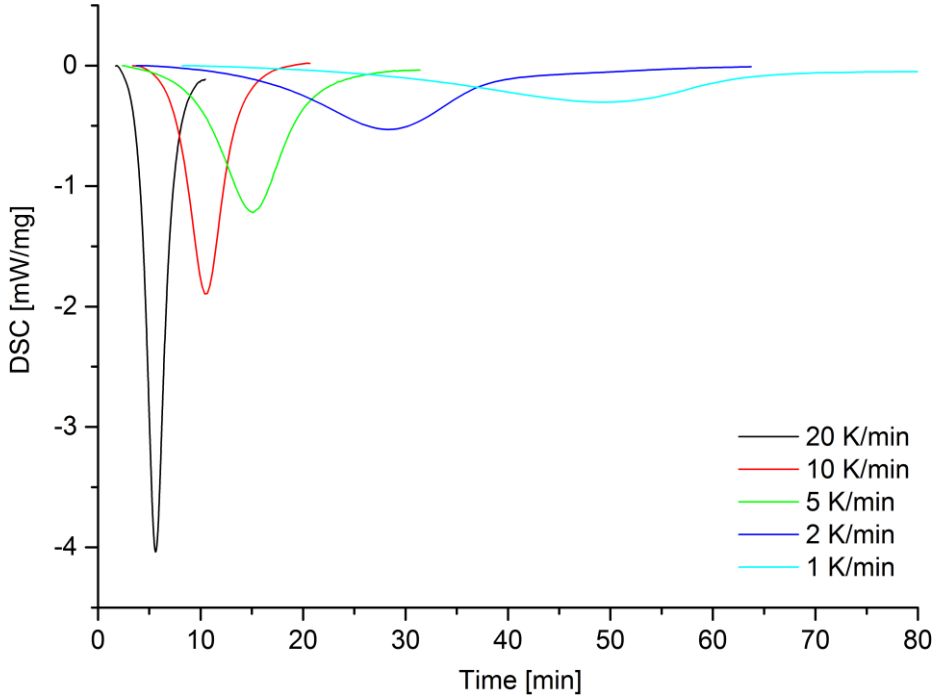

Figure 16: DSC signal of the curing reaction of epoxy resin system A at 1 K/min, 2 K/min, 5 K/min, 10 K/min and 20 K/min plotted over time.

Figure 17 shows the same DSC measurements of epoxy resin system A at heating rates of 1, 2, 5, 10 and 20 K/min plotted over temperature. As the polymerization reaction depends on time and temperature, the maximum of the DSC signal is observed at lower temperatures as the reaction has more time to proceed. At higher heating rates a shift of the maximum of the DSC signals to higher temperatures is observed. However, the signal area of the DSC measurements plotted over the temperature does not represent the total heat of reaction.

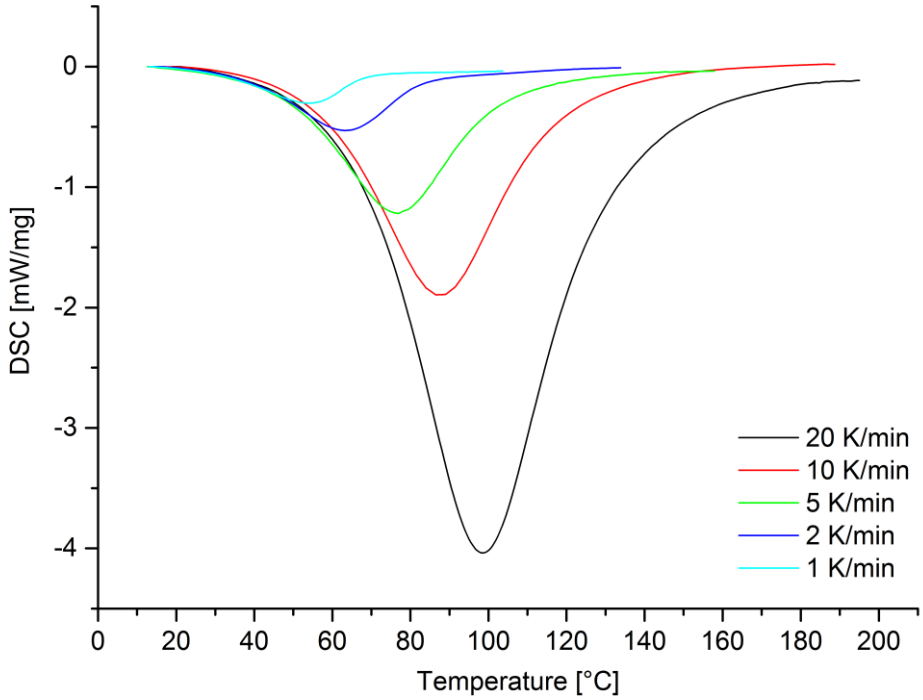

Figure 17: DSC experiments with heating rates of, 1 K/min, 2 K/min, 5 K/min, 10 K/min and 20 K/min

4.1.5 Investigation of Pressure Dependence on Epoxy Resin Curing Reaction

As described in section 2.2 in the HP-RTM process pressures up to 100 bars can be observed. To investigate the influence of pressure on the speed of the curing reaction, high-pressure DSC measurements were conducted using a DSC 204 HP Phoenix by *NETZSCH-Gerätebau GmbH*. The curing of epoxy resin system A at 1, 25, 50 and 100 bar and a heating rate of 1 K/min is shown in Figure 18. As described above, the peak of the DSC signal displays the highest release of heat and therefore the highest turnover rate of the polymerization reaction. Therefore the peak of the DSC signal is used as indicator of the speed of the curing reaction. The observed peak maxima are in a range of 64.6 – 67.3°C at all pressures. The small deviation is related to measurement inaccuracy of the DSC signal due to the pressures applied. This finding shows that there is no pressure dependence of the curing reaction speed of an epoxy resin system with amine hardener.

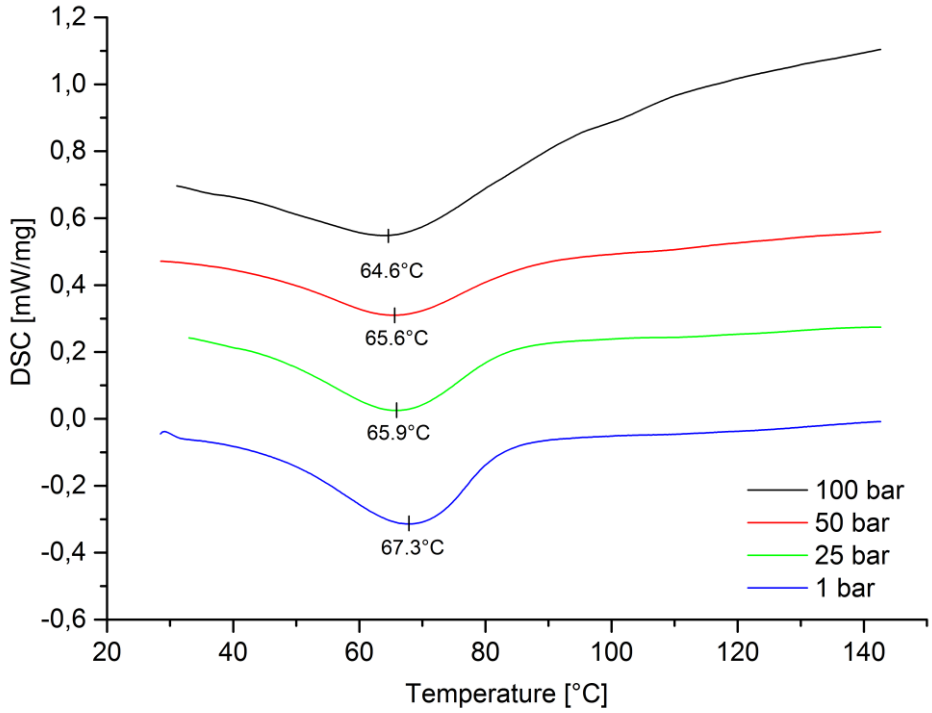

Figure 18: DSC signal of the curing reaction of epoxy resin system A at applied pressures of 1, 25, 50 and 100 bar at a heating rate of 1 K/min.

4.2 IR Spectroscopy

A commonly and often used analytical method in chemistry is IR spectroscopy, particularly in mid-infrared spectroscopy with wave lengths from 3 – 50 µm or wavenumbers $\tilde{\nu}$ = 4000 – 200 cm^{-1}.
Mid-infrared spectroscopy was also used for the analysis of the curing progress and curing mechanism of epoxy resins.[37–41]
At the laboratories of *BMW*, no IR spectrometer suitable for the investigation of the curing behavior of epoxy resins is available. A highly competent research partner in the field of IR spectroscopy and polymer science was found with the Federal Institute for Materials Research and Testing (BAM). The following investigations of epoxy resins with IR spectroscopy were conducted in form of a research collaboration of *BMW* and *BAM*.

4.2.1 Basic Working Principle of IR Spectroscopy

For the mid-infrared investigation a Nexus 470 FT-IR spectrometer by *Thermo Nicolet* equipped with a Linkam cell 600 by *Linkam Scientific Instruments* with a Nernst glower as radiation source and a mercury cadmium telluride (MCT) detector in transmission mode. A 2 g batch of the epoxy resin system in the mixing ration 100 (epoxy resin) : 19 (hardener) : 2 (IMR) weight equivalents was prepared and a thin film was applied on a potassium bromide substrate.

As a reference of the extent of the curing reaction, the amount of converted epoxy groups due to the polyaddition reaction with amines is used. A spectrum of epoxy resin system A with the relevant peaks assigned is shown in Figure 19. The peak for the epoxy group is found at $\tilde{\nu}$ = 915 cm^{-1} and the integral of the peak yields the concentration.[42] Additionally an increase of the signal at $\tilde{\nu}$ = 3600 – 3200 cm^{-1} can be observed through the epoxy ring-opening and formation of hydroxy groups, partially superimposed by the decrease of primary and secondary amines during the network formation and which can be observed at $\tilde{\nu}$ = 3470 – 3230 cm^{-1}.[40]

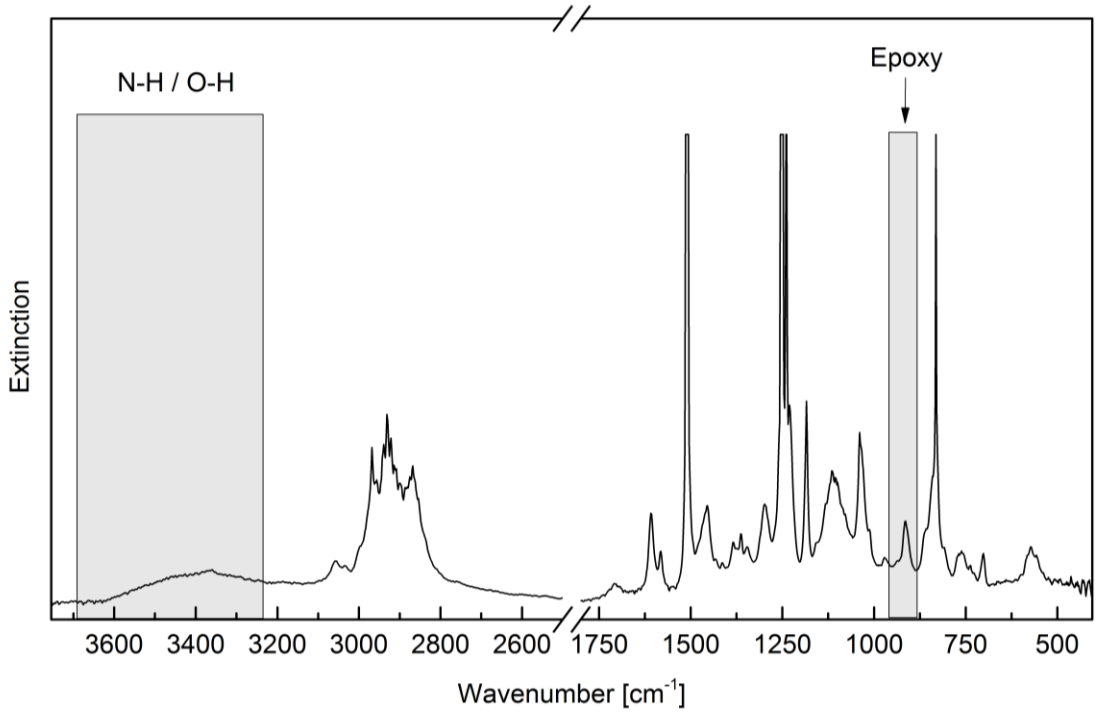

Figure 19: Mid-infrared spectrum of epoxy resin system A with relevant peaks assigned.

A better resolution of the absorption bands of the reacting functional groups is provided by IR spectroscopy in a near-infrared region with wave lengths from 0.78 – 3 µm or wavenumbers $\tilde{\nu}$ = 12800 – 4000 cm^{-1}.[43–45] In the near-infrared region, molecular overlapped overtone vibrations and combination bands are observed.[46,47] Through shorter wavelength and thus higher energy of near-IR (NIR) spectroscopy compared to mid-infrared spectroscopy, the analysis of a wide range of samples in addition with a higher penetration depth is possible. This advantage is often used for analysis and quality control in industry, such as agricultural industry, fine chemicals, polymer chemistry and in pharmaceuticals.[47]

The peaks in a NIR spectroscopy spectrum of an epoxy resin with amine hardener are shown in Figure 20 and assigned as follows. The peak $\tilde{\nu}$ = 6970 cm^{-1} is assigned as an –OH overtone vibration.[18,48] The peak at $\tilde{\nu}$ = 6678 cm^{-1} is assigned to a combination of –NH and –NH_2 overtones.[18,44] The peak at $\tilde{\nu}$ = 6060 cm^{-1} is assigned to the overtone of the CH stretching vibration of the epoxy group.[49] The peak at $\tilde{\nu}$ = 5067 cm^{-1} is combination band of stretching and bending vibrations of –NH_2.[18] The peak at $\tilde{\nu}$ = 4530 cm^{-1} is assigned to a conjugated epoxy –CH_2 deformation band. [44]

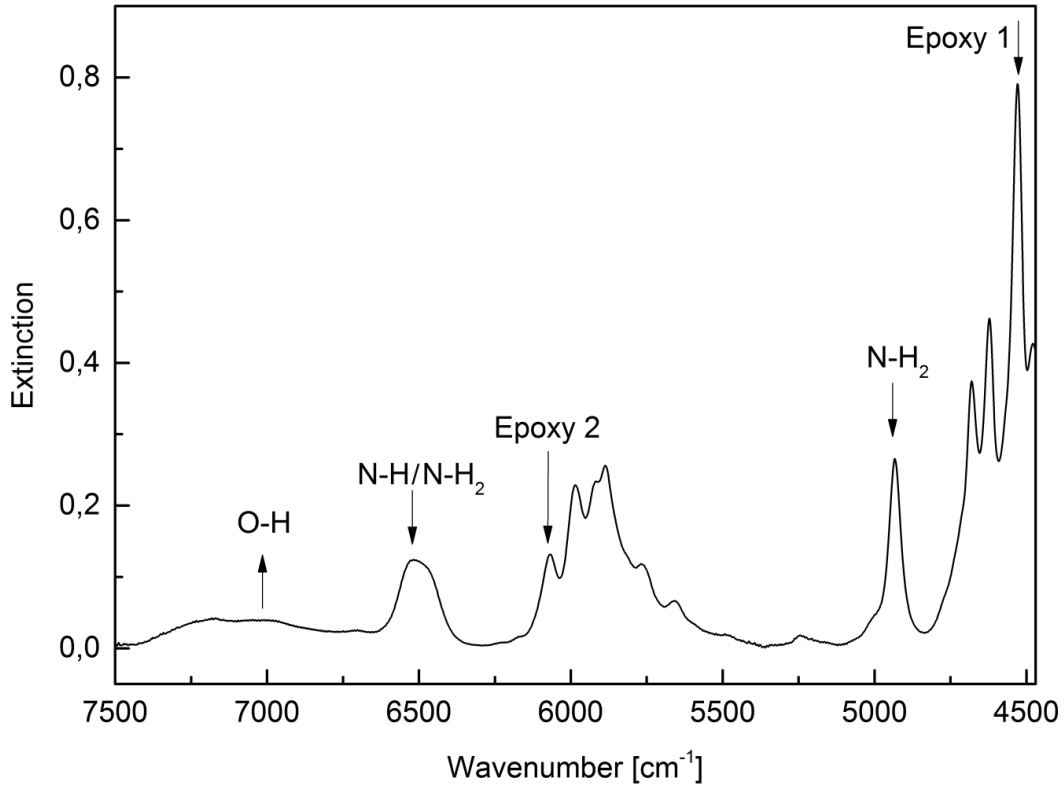

Figure 20: NIR spectrum of epoxy resin system A with relevant peaks assigned.

4.2.2 NIR Spectroscopy Measurement Assembly

All NIR spectroscopy experiments were conducted on a Nexus 600 FT-IR spectrometer by *Thermo Nicolet*, with a tungsten filament lamp as radiation source and a MCT detector in transmission mode. As sample vessel a glass cuvette (Starna, Type: 1/G/1) with a sample compartment thickness of 1 mm. The NIR measuring cell is a programmable, heatable cell for temperatures up to 300°C with a maximum heating rate of 10 K/min. A schematic representation of the NIR measuring cell displaying the basic mode of operation and a picture of the actual experimental setup is shown in Figure 21. For each measurement 16 scans were taken with a resolution of 4 cm^{-1}. The first measurement point is obtained 8 seconds after placing the cuvette into the NIR cell.

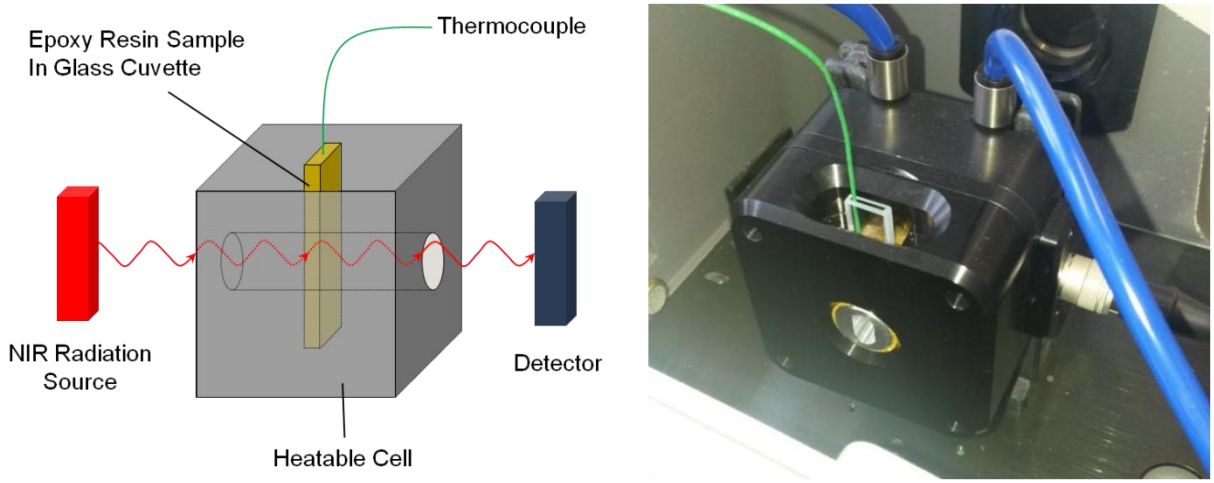

Figure 21: Schematic representation of the heatable NIR measuring cell (left) and actual experimental setup (right).

For all experiments the components were weighed separately according to the respective mixing ration 100 (epoxy resin) : 19 (hardener) : 2 (IMR) weight equivalents calculated for 2 g batch and subsequently mixed with a spatula for 30 s to provide a homogeneous mixture.
Approx. 0.4 g of the mixed epoxy resin system was filled in the glass cuvette immediately afterwards. The glass cuvette was then placed into the NIR measuring cell. For isothermal experiments, a thermocouple sensor was placed into the sample to determine the temperature profile during curing additionally to the temperature measurement of the NIR cell.

4.2.3 Interpretation of NIR Spectra

The measurements of the curing progress of epoxy resin system A at a heating rate of 5 K/min in a temperature range from 30 – 205°C are shown in Figure 22. It can be observed that the signals of the epoxy group at $\tilde{\nu}$ = 4520 cm^{-1} and $\tilde{\nu}$ = 6090 cm^{-1} and the signals of the amine group at $\tilde{\nu}$ = 4920 cm^{-1} and $\tilde{\nu}$ = 6500 cm^{-1} are decreasing over time. This is related to progression of the polyaddition reaction of epoxy- and amine group to form β-hydroxy amines. On the other hand the signal of the hydroxy group at $\tilde{\nu}$ = 7050 cm^{-1} is increasing due to the newly formed hydroxy groups in the polyaddition reaction.

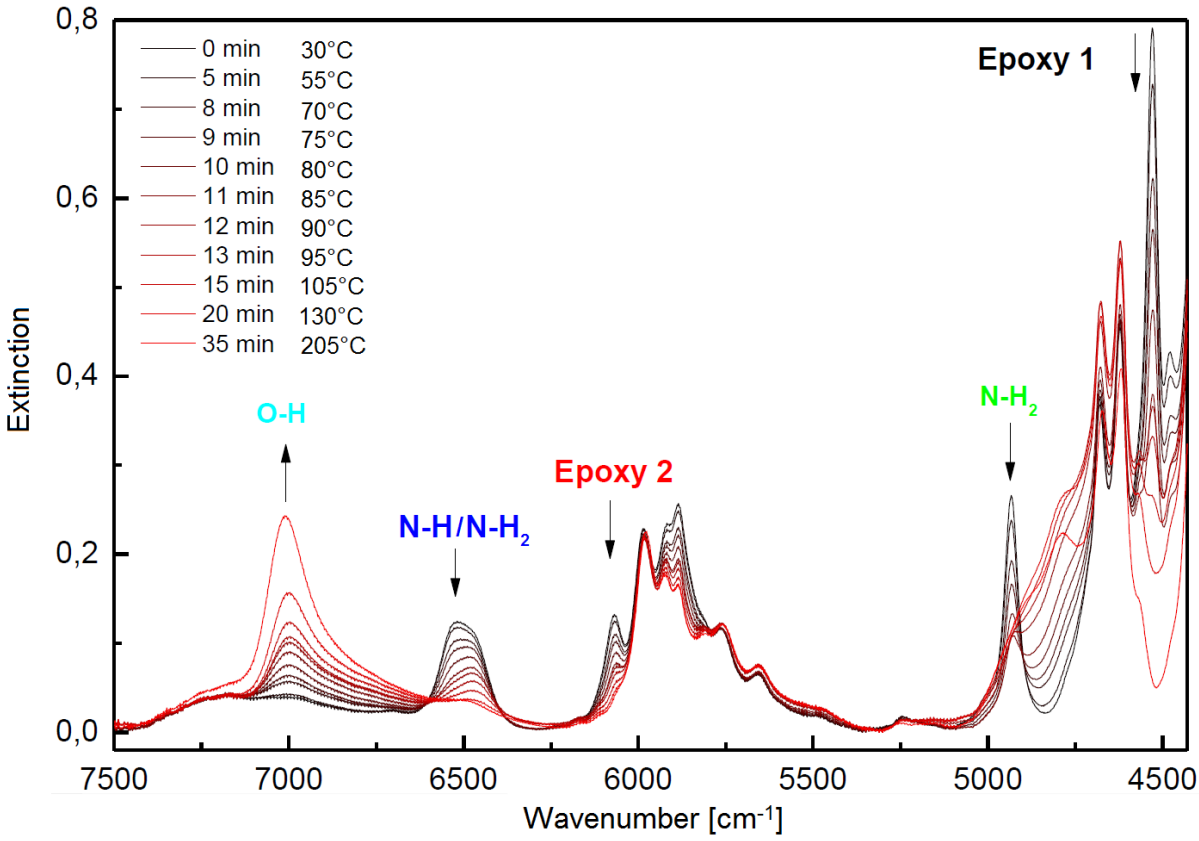

Figure 22: Superimposed NIR spectra of the curing progress of epoxy resin system A at a heating rate of 5 K/min in a temperature range from 30 – 205°C.

For a quantitative assessment of the turnover of the polyaddition reaction and thus the network formation, the signal area was evaluated. The respective integration limits of the single signals are shown in Table 4.

Table 4: Integration limits for quantitative NIR spectra interpretation.

	Integration limits $\tilde{\nu}$ [cm^{-1}]	
Epoxy 1	4552	4497
Phenol 2	4651	4593
NH_2	5090	4863
Epoxy 2	6149	6027
N-H / NH_2	6647	6366
OH	7153	6719

For a proper quantitative assessment of the turnover of the reaction by using the signal areas, the temperature dependence of signal area has to be clarified. To assess the temperature dependence of the integrated absorption band of Epoxy 1, a NIR measurement of the pure epoxy component of the resin system was conducted. The first part of the measurement consists of a heating segment of 10 K/min for 6 min to increase the temperature from 30°C to 90°C, followed by a cooling phase down to 33°C. As an internal reference, the signals of the phenol ring of DGEBA, at $\tilde{\nu}$ = 4070 cm^{-1} (Phenol 1) and

$\tilde{\nu}$ = 4610 cm^{-1} (Phenol 2) are used. The respective integration limits are $\tilde{\nu}$ = 4109 – 4023 cm^{-1} (Phenol 1) and $\tilde{\nu}$ = 4651 – 4593 cm^{-1} (Phenol 2). The area of the signals of Epoxy 1, Phenol 1 and Phenol 2 over time with the applied temperature profile is shown in Figure 23. It can be observed, that the area of the signals for all components decreases with rising temperature and vice versa. A good correlation of the temperature dependence is displayed for the peaks of Phenol 2 and Epoxy 1. Therefore a correction of the areas of all integrated signals shown in Figure 22 with Phenol 2 was conducted.

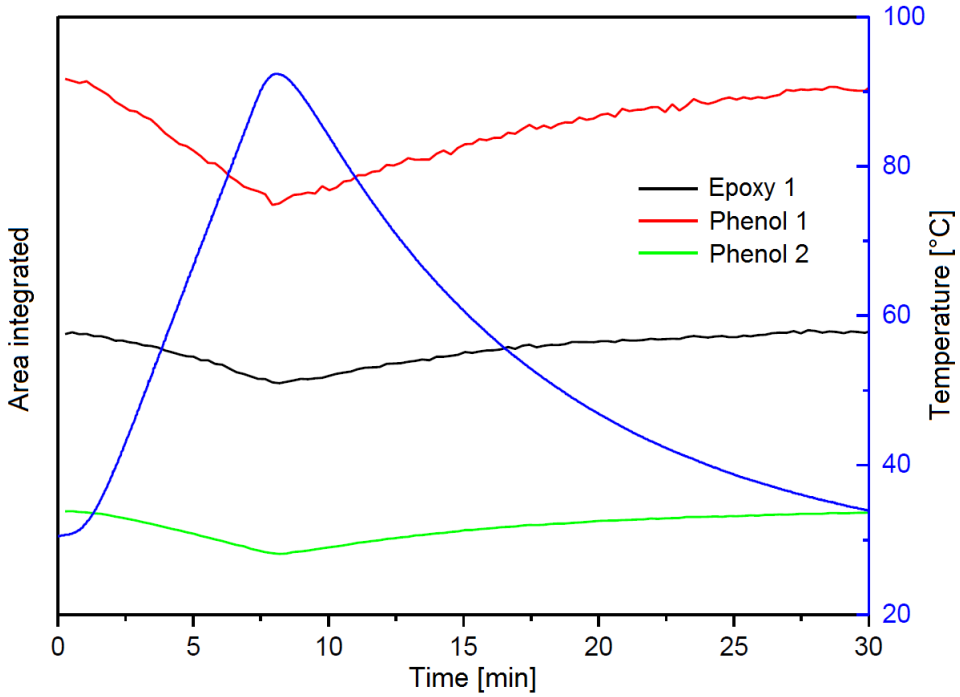

Figure 23: Heating and cooling of the neat epoxy resin to determine the temperature dependence of the Epoxy 1 signal and the internal reference signal Phenol 1 and Phenol 2.

The decrease and increase of the integrated signals of the measurements shown in Figure 22 is shown in Figure 24. The areas of all peaks were corrected with Phenol 2 as reference and were normalized to provide a good comparability.

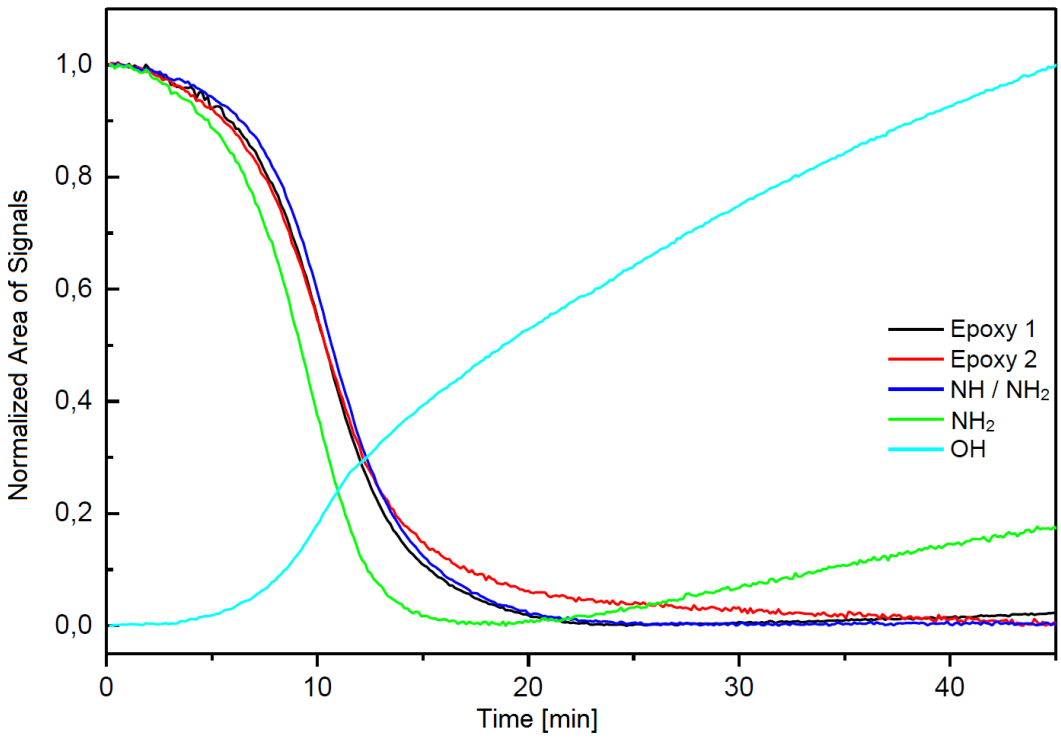

Figure 24: Normalized integrated areas of NIR peaks of relevant functional groups participating in the network formation.

As explained above, the concentration of the epoxy group and the amine group is decreasing with progressing polymerization, whereas the concentration of the hydroxy group increases due to the epoxy ring opening. The concentration gradient of the epoxy group according to the Epoxy 1 signal and the concentration gradient of the amine according to the NH/NH_2 signal are in very good agreement. The epoxy group concentration according to the Epoxy 2 signal is also in good agreement for the first 14 minutes and differs afterwards. The slower decrease afterwards can be attributed to the superposition with the adjacent signal at lower wavenumbers which disturbs the signal analysis.

The concentration of primary amines, according to the NH_2 signal, decreases faster and after a minimum at 17 min rises again. The faster decrease of the primary amine can be explained by the higher reactivity towards the polyaddition reaction to an epoxy group compared to secondary amines and hydroxy groups. The increase of the primary amine concentration at the end of the reaction can be attributed to the superposition with the adjacent signal at lower wavenumbers, which leads to an increase of the signal area. The evaluation of hydroxy concentration is shown for illustrative purposes but quantitative assessment has to be neglected because of the unknown initial -OH concentration from bisphenol A as one of the hardener components in epoxy resins system A and the unknown concentration of newly formed hydroxy groups which remain and which take part in further crosslinking reactions.

Because the concentration of the epoxy group gives an ultimate indicator for the progress of the crosslinking reaction and can be reliably evaluated by the Epoxy 1 signal, the further analysis and the

determination of the degree of conversion α is conducted using the Epoxy 1 signal. A correction of the Epoxy 1 signal area with the Phenol 2 signal was carried out for each measurement.

4.2.4 Results and Discussion of Heating Rate NIR-Spectroscopy Experiments

The curing progress of the epoxy resin system A at heating rates of 1, 3, 5 and 10 K/min in a temperature range of 30 – 180°C was measured. The normalized and temperature corrected NIR signal areas of Epoxy 1 at respective heating rates are shown in Figure 25. The normalized signal area of Epoxy 1 is considered equal to the opposed degree of conversion α.

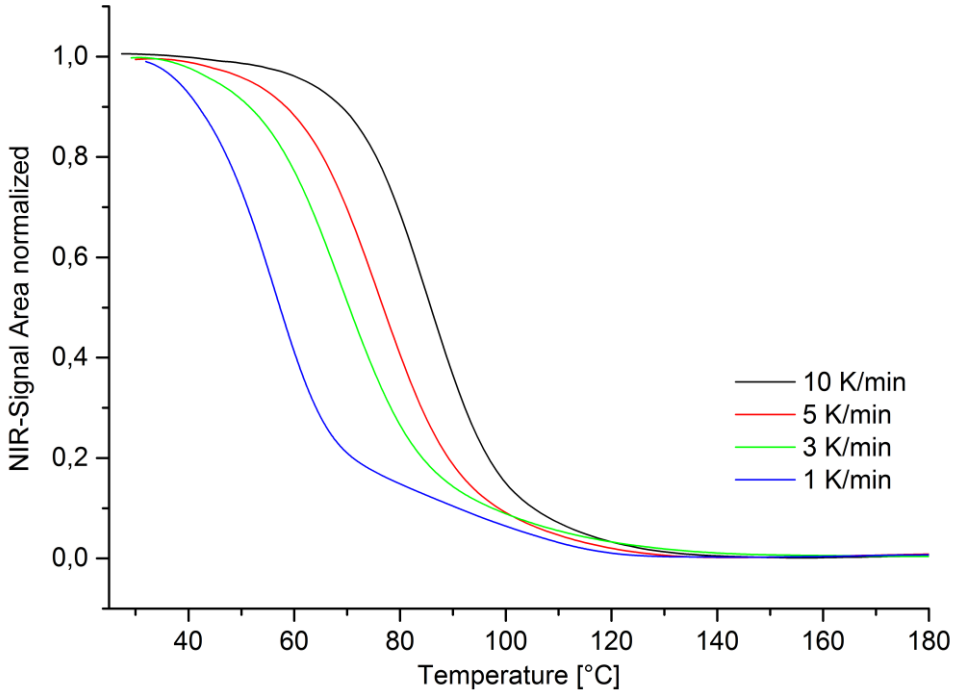

Figure 25: Curing progress of epoxy resin system A according to normalized and temperature corrected Epoxy 1 signal at heating rates of 1, 3, 5 and 10 K/min.

It can be observed that the decrease of the epoxy group concentration according to Epoxy 1 is shifted to lower temperatures for smaller heating rates. The lower the heating rate the more time for reaction is available and higher curing degrees are reached at lower temperatures already. At 1 K/min heating rate the conversion of epoxy groups slows down at 70°C and a degree of conversion α = 0.8. This can be attributed to the increasing glass transition temperature of the epoxy resin during curing, which leads to a deceleration of the polymerization reaction when it reaches the cure temperature because of vitrification. This is in total agreement with the findings of the DSC measurements shown in Figure 15, where the correlation of the progress of the glass transition temperature with increasing degree of conversion α has been pointed out and predicts a T_g = 69°C for α = 0.8. Due to the small heating rate

of 1 K/min the cure temperature rises slowly and does not overcome the glass transition temperature of the epoxy resin. Thus the residual crosslinking reaction proceeds in a nearly vitrified state and the reaction progresses gradually.

The cure temperature for heating rates 3, 5 and 10 K/min rises faster than the glass transition temperature of the epoxy resin system and no deceleration of the polymerization reaction due to vitrification takes place.

For better comparison with the dynamic DSC experiments and for reaction kinetic modeling, the normalized NIR peak areas were converted to DSC like curves. Therefore, the normalized value 1.0 was assigned to the total enthalpy of reaction ΔH_{tot} = –515.16 J/g. The differentiations of the curves yield the DSC like signals $d\alpha/dt$ shown in Figure 26 over the temperature.

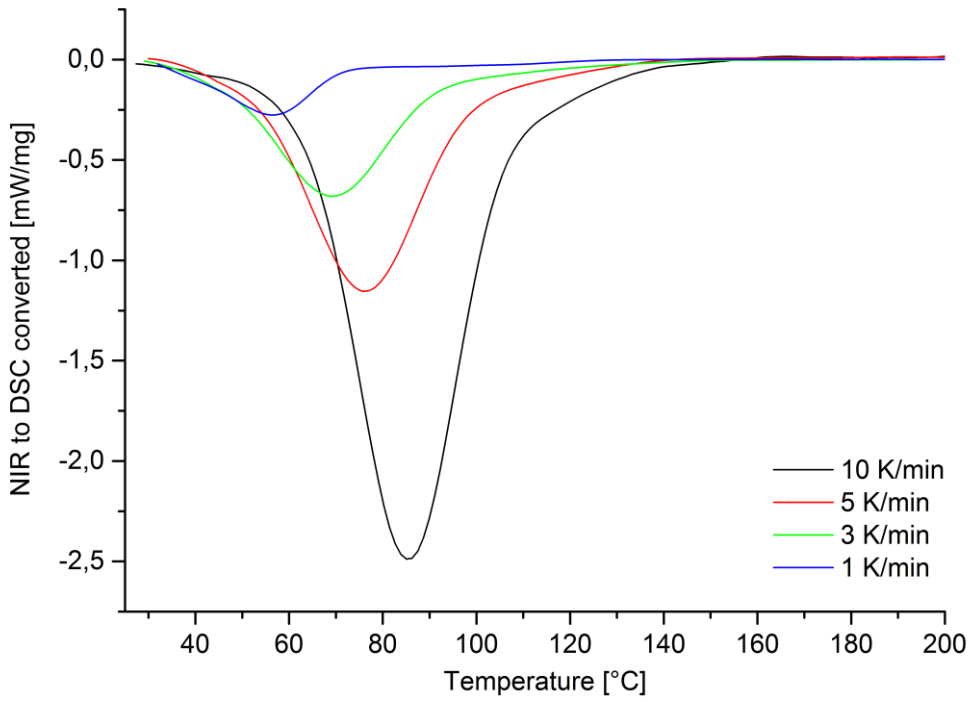

Figure 26: Converted $d\alpha/dt$ signals derived from the normalized decrease of Epoxy 1 signal assigned to the total enthalpy of reaction ΔH_{tot} = –515.16 J/g.

The comparison of heating rate experiments at 1, 3, 5 and 10 K/min of DSC and NIR spectroscopy is shown in Figure 27. The curing progress at a heating rate of 1 K/min and 5 K/min show a good correlation. The maximum reaction rate at 10 K/min, indicated by the peak maximum where the released enthalpy of reaction has its maximum, is shifted to lower temperatures in the NIR spectroscopy measurement compared to the DSC measurement. Also the release of the total enthalpy of reaction ΔH_{tot} is more intense and the reaction is done earlier. A reason for this diverging progress

can be the different sample weight. For the DSC experiment the sample weight is only 9 mg whereas the sample weight of the NIR spectroscopy experiment is 400 mg. The higher amount of epoxy resin can lead to a self-heating of the sample due to the exothermic polymerization reaction.

The self-heating of the sample due to the exothermic polymerization reaction is minor for small sample volumes and the generated heat is directly absorbed by the crucible. The higher sample volume in the glass cuvette in NIR spectroscopy compared with the low thermal conductivity of the glass cuvette and the epoxy resin itself, lead to a self-heating of the sample and therefore an acceleration of the polymerization reaction.

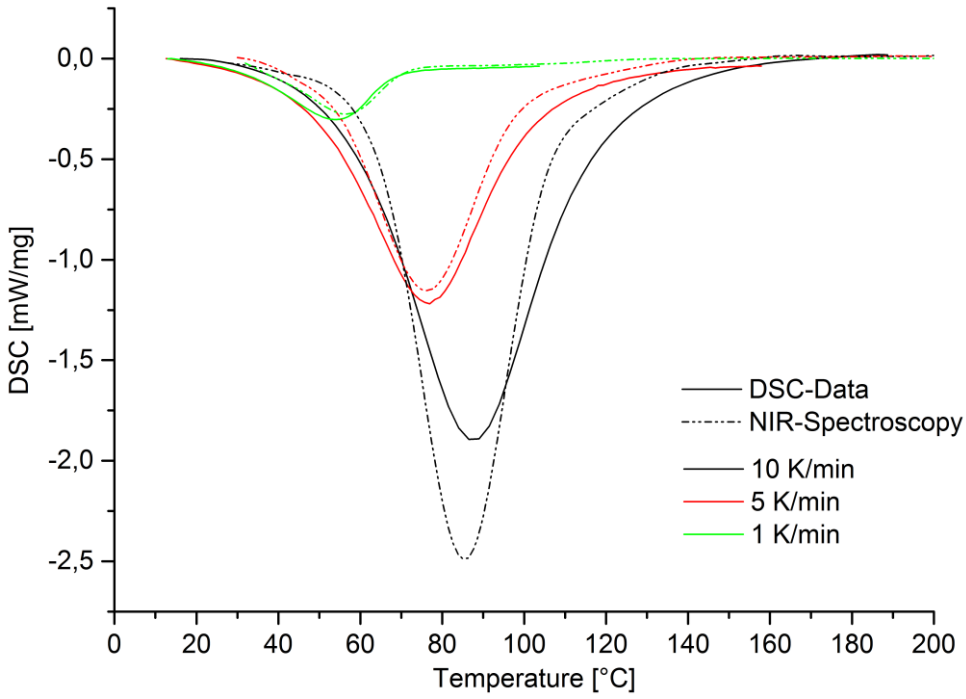

Figure 27: Comparison of DSC and NIR spectroscopy heating rate experiments at 1, 5 and 10 K/min.

5 Kinetic Modeling and Simulation

5.1 Assessment of Reaction Kinetics of Polymerization Reactions

There are multiple ways to describe the reaction kinetics of a chemical reaction. One approach is based on the analysis of the reaction mechanism of a chemical reaction. Therefore the reaction rate constants of all reactions taking place have to be determined, whereby the slowest step is the overall rate-determining step. This method can become very complex, especially for multistep reactions as it gets difficult to break down the reaction sequence to the elementary steps based on a detailed reaction mechanism. In addition, the experimental determination of the reaction rate constants can be hard to achieve, depending on the speed and state of aggregation of the reaction.
The above mentioned hurdles are faced when it comes to the reaction kinetic analysis of polymerization reaction, e.g. epoxy polymers for composite applications. A detailed reaction mechanism is hard to provide due to complex parallel reactions with often more than two functional groups reacting, additives which retard the polymerization (retardants) or promote the polymerization (catalysts) and unknown detailed stoichiometry. Furthermore the change of the aggregation state from liquid to solid has a significant effect to the reaction rate, as the polymerization slows down dramatically when the evolving glass transition temperature reaches the cure temperature. Besides, the solidification complicates the determination of residual reactive groups and thus state of cure and a correlation to an overall rate constant.

A more practical approach to determine the reaction kinetics of a polymerization process is the investigation of the reaction by thermal analysis. The temperature rise during the polymerization due to an exothermic reaction can be measured by DSC and taken as reference for the conversion depending on curing time and temperature, provided that the total enthalpy of reaction ΔH_{tot} is known. The degree of conversion can then be determined according to equation (3).

However, when it comes to the optimization of the curing process and therefore the evaluation of the ideal process temperature, depending on the specific process requirements, an empirical study is very cost-intensive and time-consuming. To minimize the number of trials and therefore reduce the valuation effort significantly, the capability of simulating the curing process at any desired temperatures or temperature profiles to assess the curing parameters is of great importance.
Following, an approach to a simulation model of the curing behavior of two epoxy resins with amine hardeners is provided.

5.2 Approach to Kinetic Model

5.2.1 Fundamentals

One of the most fundamental equations stating the temperature dependence of chemical reactions is the Arrhenius Equation (6) proposed by Svante Arrhenius in 1889,

$$k = A \cdot e^{\frac{-Ea}{RT}} \qquad (6)$$

where k is the Arrhenius rate constant, A is the pre-exponential factor, E_a is the activation energy, R is the universal gas constant and T is the temperature.[50]

The kinetics of a one step-reaction of thermal transformation processes can be in principle described by

$$\frac{d\alpha}{dt} = k(T) \cdot f(\alpha) \qquad (7)$$

where α is the degree of conversion, t is the time, $k(T)$ is the Arrhenius type function, and $f(\alpha)$ is the function of the reaction model.[51]

For non-isothermal conditions with a constant heating rate following equation can be derived from (7),

$$\frac{d\alpha}{dt} = \frac{A}{\beta} \cdot e^{\frac{-Ea}{RT}} \cdot f(\alpha) \qquad (8)$$

where, $\beta = dT/dt$ is the heating rate.[51]

In the past, equation (9) was developed by Kamal and Sourour, based on empirical data, to mathematically describe the progress of the degree of conversion in polymerization reactions and fitted to experimental data for several epoxy resin systems with good approximation,

$$\frac{d\alpha}{dt} = (k_1 + k_2 \alpha^{m(T)}) \cdot (1-\alpha)^{n(T)} \qquad (9)$$

where α ($0 \leq \alpha \leq 1$) is the degree of conversion, k is the reaction rate constant and m and n are reaction order coefficients.[33,52–55]

Kamal's model describes a parallel reaction pathway with the according reaction rate constants for an uncatalyzed reaction k_1 and an autocatalyzed reaction k_2.[56] Based on the phenomenological assumption of the reaction mechanism of the epoxy-amine-polymerization by Smith, which takes a trimolecular cyclic transition state as basis, the reaction order coefficients *m* and *n* are 1 and 2. Thus the cross-linking mechanism is considered, but these reaction order values provide an insufficient correlation to experimental data. The accordance to experimental data can be improved by empirical fitting of reaction order coefficients *m* and *n* admitting non-integer numbers, however the connection with the chemical cross-linking mechanism is lost.[56]

In general, the conversion function of a chemical reaction can be described as

$$\frac{dr}{dt} = U(t, T, r, p) \qquad (10)$$

where *U(t,T,r,p)* is the conversion function, *r* is the concentration of the reactant, *p* is the concentration of the product.
The conversion function *U(t,T,r,p)* can be divided into two separate functions and has following form

$$U(t, T, r, p) = k(T) \cdot f(r, p) \qquad (11)$$

where *k(T)* is the Arrhenius type function and *f(r,p)* is the reaction type function. For single step processes *f(r,p)* reduces to *f(x)*, where $r = 1 - \alpha$ and $p = \alpha$ with α as the degree of conversion. For multi-step reaction however, equation (11) becomes a set of differential equations, for which a separation of variables is not possible and which is therefore analytically unsolvable.[57]

During the polymerization reaction of epoxy resins, a change of the state of aggregation from liquid to solid takes place, due to progressing network formation and decreasing movement possibilities of the molecules up to vitrification. In the liquid stage the reaction rate of the polymerization is determined by the reactivity of the crosslinking functional groups (chemically controlled), whereas in the vitrified state the mobility of the molecules is heavily limited and the reaction rate is only determined by the diffusion rate (diffusion controlled). When investigating the cure kinetics of epoxy resins, the change of chemically to diffusion controlled reaction stages has to be taken into account. The most frequently used equation to describe the relation of chemical and diffusion control was proposed by Rabinowitch,[58]

$$\frac{1}{k} = \frac{1}{k_{diff}} + \frac{1}{k_{chem}} \qquad (12)$$

where k is the overall reaction rate constant, k_{diff} is the reaction rate constant for the diffusion controlled reaction stage and k_{chem} is the reaction rate constant for the chemically controlled reaction stage, which is described by the Arrhenius equation (6).

A well known approximation of the rate constant in the diffusion controlled reaction stage, i. e. when vitrification occurs, is a modified Williams-Landel-Ferry (WLF) equation (13) proposed by Wise,[59]

$$k_{diff} = k_{diff(T_g)} \cdot e^{\left(\frac{C_1 \cdot (T - T_g)}{C_2 + T - T_g}\right)} \qquad (13)$$

where $k_{diff(Tg)}$ is the diffusion rate constant at glass transition temperature T_g, T is the cure temperature and C_1 and C_2 are adjustable parameters.

When the increasing glass transition temperature T_g is near or equal the reaction temperature the reaction vitrifies and $k_{chem} >> k_{diff}$ which leads to diffusion controlled domination of reaction rate k according to equation (13).

5.2.2 Determination of Kinetic Parameters

As shown in the equations (6) – (9), a fundamental parameter to characterize the reaction kinetics of polymerizations is the activation energy E_a. In the last decades, several research groups implemented methods to estimate the activation energy by thermal analysis.[60]
One method was implemented by Friedman, who first published his approach in 1964.[61] This a model-free analysis allows the estimation of a conversion-dependent activation energy as differential isoconversional method, by using experimental data of thermal analysis with different heating rates. The advantage of this method is, as the term model-free indicates, that the activation energy can be obtained without knowing the exact form of the kinetic equation. The approach takes the proportionality between the degree of conversion and the rate constant at given conversions as a basis, to obtain the temperature dependence of the rate constant.[60] Equation (14) can be derived from (8) by linearizing.[62]

$$\ln\left(\frac{d\alpha}{dt}\right) = \ln\left(\frac{A}{\beta}\right) - \frac{Ea}{R} \cdot \frac{1}{T} + \ln(f(\alpha)) \qquad (14)$$

Arrhenius plot like, the logarithmic conversion rate *ln(dα/dt)* can be plotted against the inverse temperature *1/T*, like shown in Figure 28, whereas the conversion rate is directly derived from the experimental data. The activation energy is proportional to the slope *m* = *-E/R* of the isoconversional lines, i.e. for a constant *α,* and can be calculated for each degree of conversion.

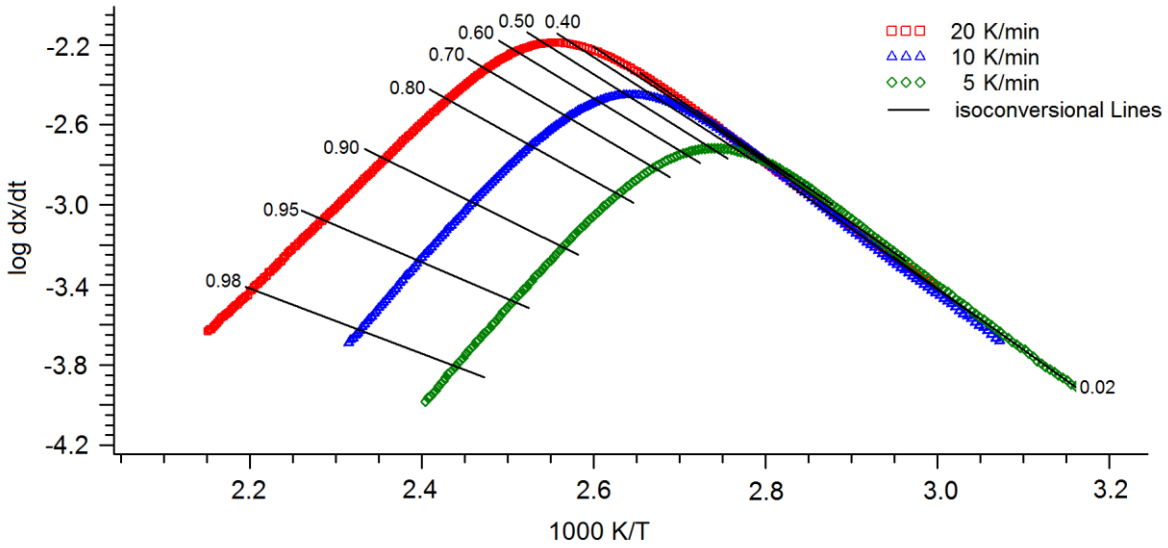

Figure 28: Friedman plot of the conversion rate as a function of inverse temperature with isoconversional lines of experimental DSC data of an epoxy resin cured with amine hardener at three heating rates (red: 20 K/min, blue: 10 K/min, green: 5 K/min).

The pre-exponential factor *A* can be calculated by equation (15) derived from (14), by assuming a first order reaction with *f(α) = (1- α)*.[62]

$$\ln\left(\frac{A}{\beta}\right) = \ln\left(\frac{d\alpha}{dt}\right) + \frac{Ea}{R}\cdot\frac{1}{T} + \ln(1-\alpha) \qquad (15)$$

Additionally the Friedman gives an indication of the reaction type, i. e. whether the reaction is a single-step or a multi-step reaction and whether it is an autocatalytic reaction or not. For constant slopes of the isoconversional lines and therefore constant activation energy, a single-step reaction can be assumed. Varying slopes of the isoconversional lines and therefore varying activation energies indicates a multi-step reaction.[57] The course of the slopes of the isoconversional lines compared to the slopes of the experimental curves at the beginning of the reaction, i. e. at lower temperatures 1000 K/3.2 – 2.8, gives an indication whether the reaction is autocatalytic or not. Is the slope of the isoconversional lines and the experimental curves identical then the reaction is not catalyzed. However, if the slope of the experimental curves is steeper than that of the isoconversional lines, the reaction is then autocatalytic.[63]

Another well known concept was derived by the results of Ozawa, Flynn and Wall.[64,65] Similar to the method of Friedman, this concept provides a conversion-dependent activation energy based on a model-free analysis, based on the same experimental data mention above. Therefore equation (16) can be derived by (8) by integration.[62] Underlying is the approximately linear relation between the logarithm of the heating rate and the reciprocal absolute temperature at given conversions.

$$G(\alpha) = \int_0^1 \frac{d\alpha}{f(\alpha)} = \frac{A}{\beta} \int_{T_0}^{T} e^{\frac{-Ea}{RT}} \cdot dt \qquad (16)$$

Subsequently, equation (17) can be derived from (16), assuming that the temperature T_0 is below the temperature where the reaction starts noticeably,[62]

$$\ln G(\alpha) = \ln\left(\frac{A \cdot Ea}{R}\right) - \ln \beta + \ln p(z) \qquad (17)$$

where the term *p(z)* is expressed by equation (18)

$$p(z) = \frac{e^{-z}}{z} - \int_{-\infty}^{z} \frac{e^{-z}}{z} dz \qquad (18)$$

with $z = E_a/RT$.[62]

As the analytical calculation of equation (18) is not possible, the Doyle approximation is used, with *p(z)* = -5.3305 + 1.052z, to reduce equation (17) to[62,65]

$$\ln \beta = \ln\left(\frac{A \cdot Ea}{R}\right) - \ln G(\alpha) - 5.3305 + 1.052 \frac{Ea}{R} \cdot \frac{1}{T} \qquad (19)$$

From experimental thermal analysis data with different heating rates at fixed degree of conversion $\alpha = \alpha_k$ the logarithmic heating rate *ln(β) = dT/dt* can be plotted against the inverse temperature *1/T* in the following form derived from (19),

$$\ln \beta_i = f\left(\frac{1}{T_{ik}}\right) \qquad (20)$$

where T_{ik} is the temperature at which the degree of conversion α_k is obtained at heating rate β_i giving the slope $m = -1.052E/R$ as a straight line. This yields the activation energy, which is proportional to the slopes of the isoconversional lines as shown in Figure 29. The course of the slopes of

isoconversional lines is indicating whether it is a single-step or multi-step reaction according to the Friedman plot.

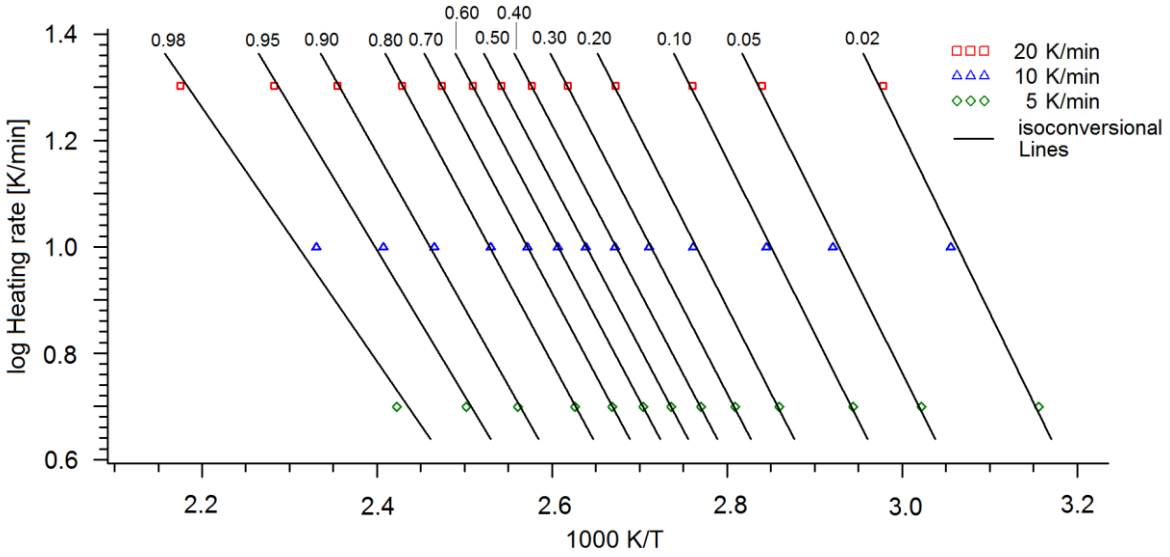

Figure 29: Ozawa-Flynn-Wall plot of the conversion rate as a function of inverse temperature with isoconversional lines of experimental DSC data of an epoxy resin cured with amine hardener at three heating rates (red squares: 20 K/min, blue triangles: 10 K/min, green checks: 5 K/min).

The pre-exponential factor *A* can be calculated by equation (21) derived from (17) by assuming a first order reaction with $G(\alpha) = (1-\alpha)$.[62]

$$\ln A = \ln G(\alpha) - \ln\left(\frac{Ea}{R}\right) + \ln\beta - \ln p(z) \qquad (21)$$

5.2.3 Thermokinetics Software

A complex software module, called Thermokinetics, was developed by NETZSCH-Gerätebau GmbH. This comprehensive software provides a sophisticated and a fast fitting method of experimental reaction curves to a wide set of reaction kinetic models. This yields a formal-kinetic description of the substance under investigation, from simple single-step reactions up to highly complex multi-step reaction-patterns including independent, consecutive, parallel and competitive reactions. For each single reaction step, separate constant activation energies and constant pre-exponential factors can be set. The basic principle of the software is the so-called Multivariate Non-linear Regression technique (Mult-NLR), where one kinetic model is obtained to describe a set of experimental measurements carried out under different conditions, e.g. different heating rates. The underlying assumption is made, that all kinetic parameters of the model are independent of the measurement conditions and therefore

identical.[57] As it is a formal kinetic model and not based on a sophisticated reaction mechanism, an interpretation of the single steps and their reaction parameters is permissible.

This software module combines all fundamental equations which are relevant for the kinetc description of epoxy polymer curing, shown in Table 5, and methods to derive the essential reaction-kinetic parameters and find an appropriate kinetic model.[33,57]

Table 5: Relevant reaction types of Thermokinetics Software with the according reaction function *f(r)*, where *r* is the initial concentration of the reactant.[57]

Code	*f(r)*	Reaction type
F1	r	first-order reaction
F2	r^2	second-order reaction
Fn	r^n	n^{th}-order reaction
C1-X	$r \cdot (1+k_{cat}X)$	first-order reaction with autocatalysis through catalyst X
Cn-X	$r^n \cdot (1+k_{cat}X)$	n^{th}-order reaction with autocatalysis through catalyst X

In addition, predictions of the reaction behavior depending on temperature and time of the system under investigation can be calculated. The calculation of time-temperature-transformation diagrams (TTT) is also possible. This graphic presentation was proposed by Gillham in 1983 and gives a clear overview of the progress of degree of cure and glass transition temperature at different temperatures over time.[66] The TTT diagram also displays physical effects like vitrification in a suitable way.

5.3 Formal Kinetic Analysis

For the formal kinetic Analysis the software module NETZSCH Thermokinetics 3.1 (Version 072010) was used.

5.3.1 Reaction Kinetic Model based on Experimental DSC Data

5.3.1.1 Development of Reaction Kinetic Model

Prior to kinetic modeling, the correlation of the progress of the glass transition temperature T_g with increasing degree of conversion α, according to Figure 15 is taken as basis to consider the chemically and diffusion controlled reaction stages depending on the cure temperature. The fit equation (4) according to Hesekamp with the respective determined parameters was used for the correlation.

The dynamic DSC measurements of epoxy resin system A at heating rates of 1, 2, 5, 10 and 20 K/min in temperature ranges from 10°C up to 200°C shown in section 4.1.4 are used as input data for the reaction kinetic model are shown in Figure 30.

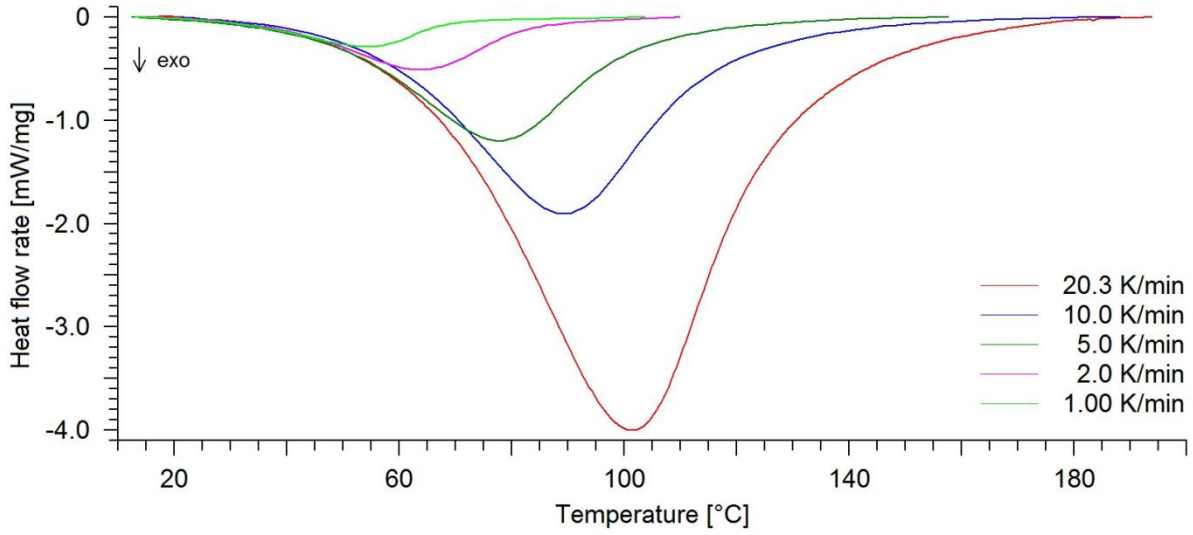

Figure 30: Dynamic DSC heating rate experiments at 1, 2, 5, 10 and 20 K/min.

The Friedman plot with isoconversional lines for all heating rates of DSC input data is shown in Figure 31. The slopes of the isoconversional lines and experimental data are identical in the low temperature range which indicates a non-catalytic reaction. The change of the slopes of the isoconversional lines towards higher degrees of conversion α indicates a multi-step reaction.

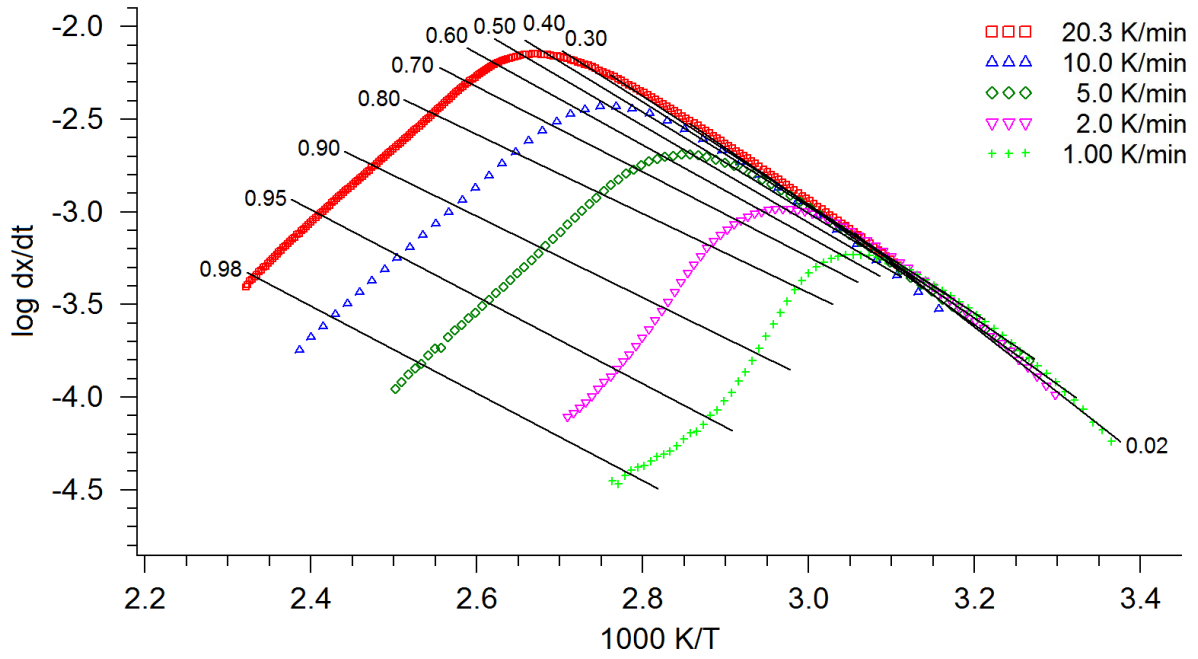

Figure 31: Friedman plot of the dynamic DSC heating rate experiments at 1, 2, 5, 10 and 20 K/min with isoconversional lines.

The estimated activation energy E_a and pre-exponential factor A derived from the Friedman analysis depending on the degree of conversion α is shown in Figure 32. The activation energy decreases from 65 kJ/mol to 40 kJ/mol for a degree of conversion $\alpha < 0.8$. For $\alpha > 0.8$ the activation energy seems to increase, but also the error bars spread which is an indication for vitrification. The same can be observed for the pre-exponential factor A which decreases from 7.0 s^{-1} to 3.5 s^{-1} for a degree of conversion $\alpha < 0.8$ and slightly increases for $\alpha > 0.8$. Because the determination of the pre-exponential factor A derived by the activation energy, the increase of A at $\alpha > 0.8$ can therefore be attributed to the uncertain E_a values. The change of the activation energy with progressing degree of conversion also indicates a multi-step reaction.

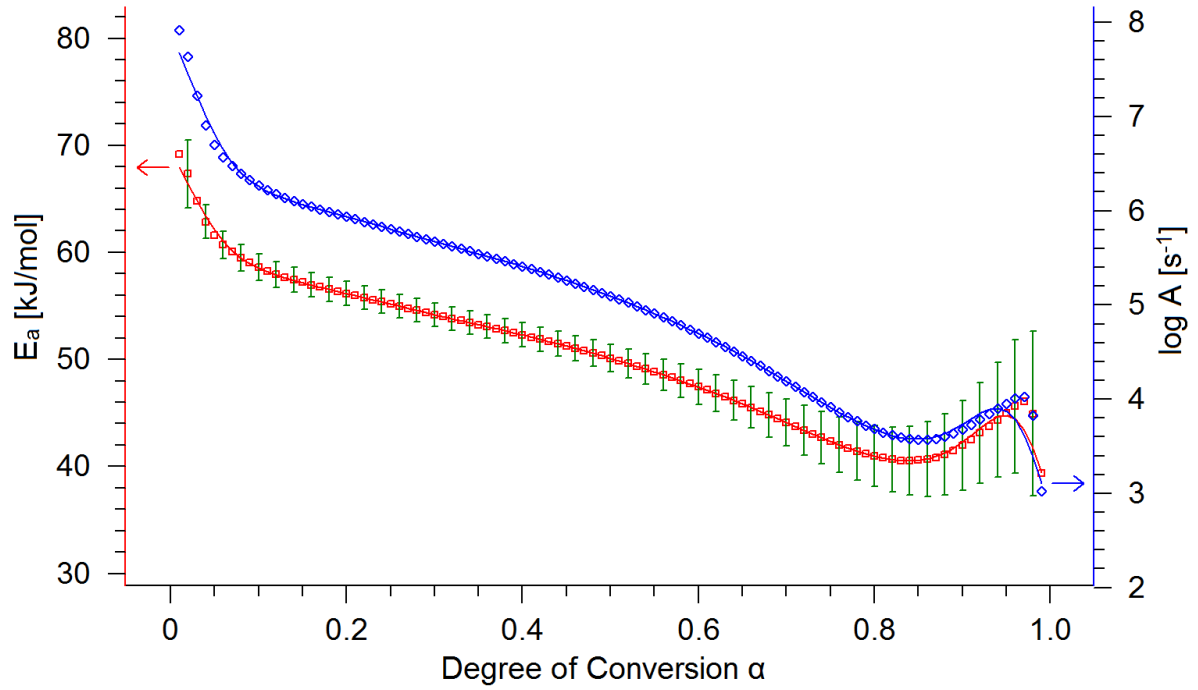

Figure 32: Estimated activation energy E_a and pre-exponential factor A according to the Friedman analysis.

The Ozawa-Flynn-Wall plot with isoconversional lines for all heating rates of DSC input data is shown in Figure 33. Similar to the Friedman plot, the change of the slopes of the isoconversional lines towards higher degrees of conversion α is also observed and indicates a multi-step reaction.

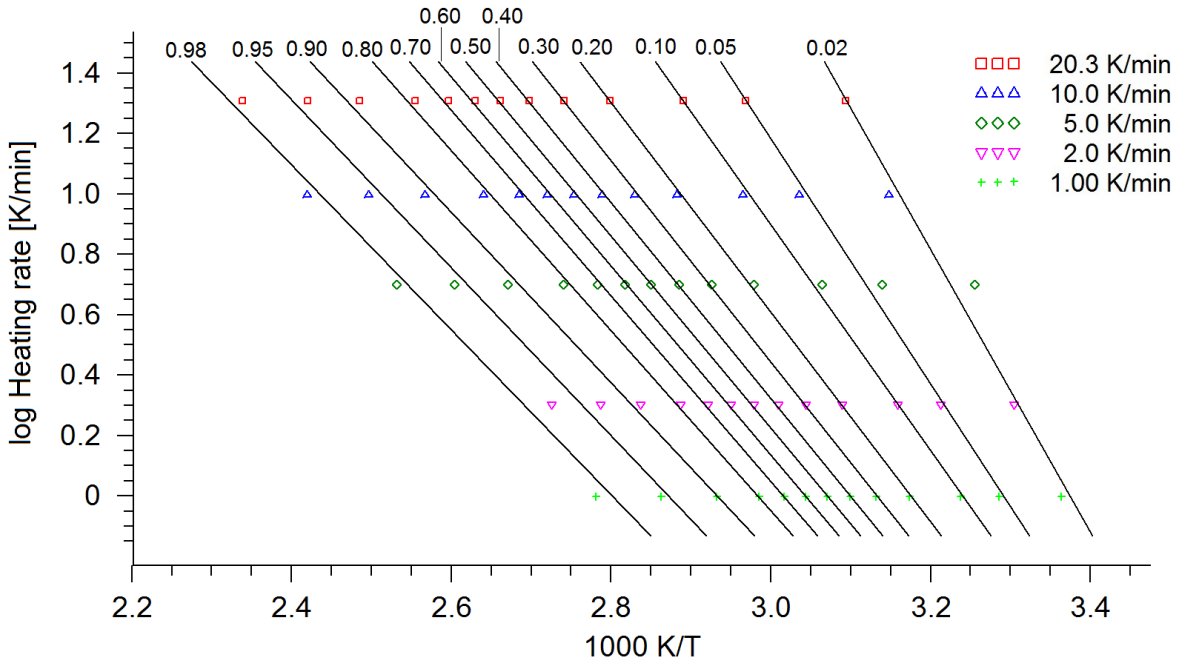

Figure 33: Ozawa-Flynn-Wall plot of the dynamic DSC heating rate experiments at 1, 2, 5, 10 and 20 K/min with isoconversional lines.

The Ozawa-Flynn-Wall plot of estimated activation energy E_a and pre-exponential factor A depending on the degree of conversion α is shown in Figure 34. The activation energy continuously decreases from 65 kJ/mol to 47 kJ/mol and a higher scattering can also be observed at $\alpha > 0.8$. The pre-exponential factor equally decreases from 6.7 s^{-1} to 4.5 s^{-1}. The values are in the same range as the estimated activation energy E_a and pre-exponential factor A according to the Friedman analysis. The change of the activation energy with progressing degree of conversion also indicates a multi-step reaction.

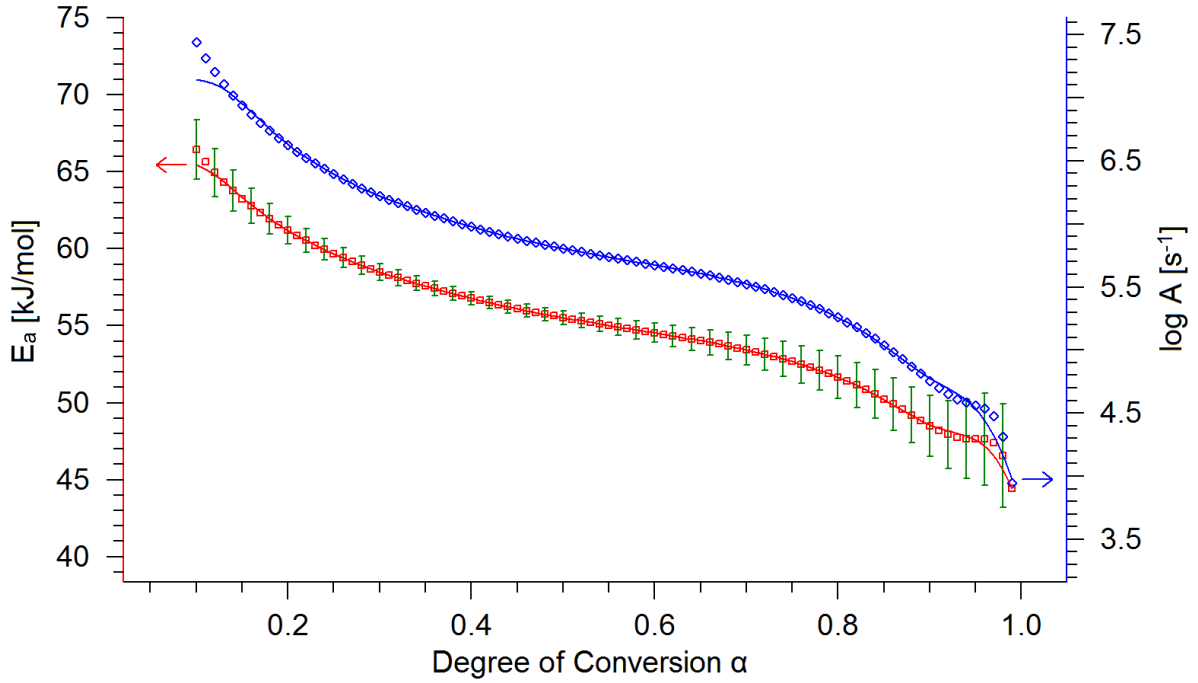

Figure 34: Estimated activation energy E_a and pre-exponential factor A according to the Ozawa-Flynn-Wall analysis.

After the estimation of the energy E_a and pre-exponential factor A, which are needed as initial parameters, the best fitting model was determined. A single-step reaction model of n^{th} order, which was used as a starting point and rough estimation, only yielded an unsatisfying fit model, which was previously indicated by the Friedman and Ozawa-Flynn-Wall analysis. The best fit provided a kinetic model with two following steps of n^{th} order of reaction and diffusion control, which is shown in Figure 35. This is in total agreement with the indication of Friedman and Ozawa-Flynn-Wall analysis. According to Table 5 the reaction model consists of two following Fn,d Fn,d reactions with diffusion control indicated by index d. The correlation coefficient, which indicates the fit quality of the model to the experimental data, is 0.9999. Though, the reaction kinetic model is only a formal kinetic model and does not necessarily describe reactions according to their reaction mechanism, a two-step reaction model is in agreement with the crosslinking reaction of an epoxy resin with amine hardener. The first reaction step can be attributed to the reaction of an epoxy group with a primary amine, yielding intermediate B in form of a secondary amine, according to reaction (i) of Scheme 2. The second

reaction step displays the reaction of an epoxy group with a secondary amine, yielding a non-reactive tertiary amine, according to reaction (ii) of Scheme 2. Though the reactivity of a hydroxy group towards an epoxy group is lower than a secondary amine, the resulting crosslinking connection is also a dead end in terms of further crosslinking possibilities and can therefore also be seen as product C.

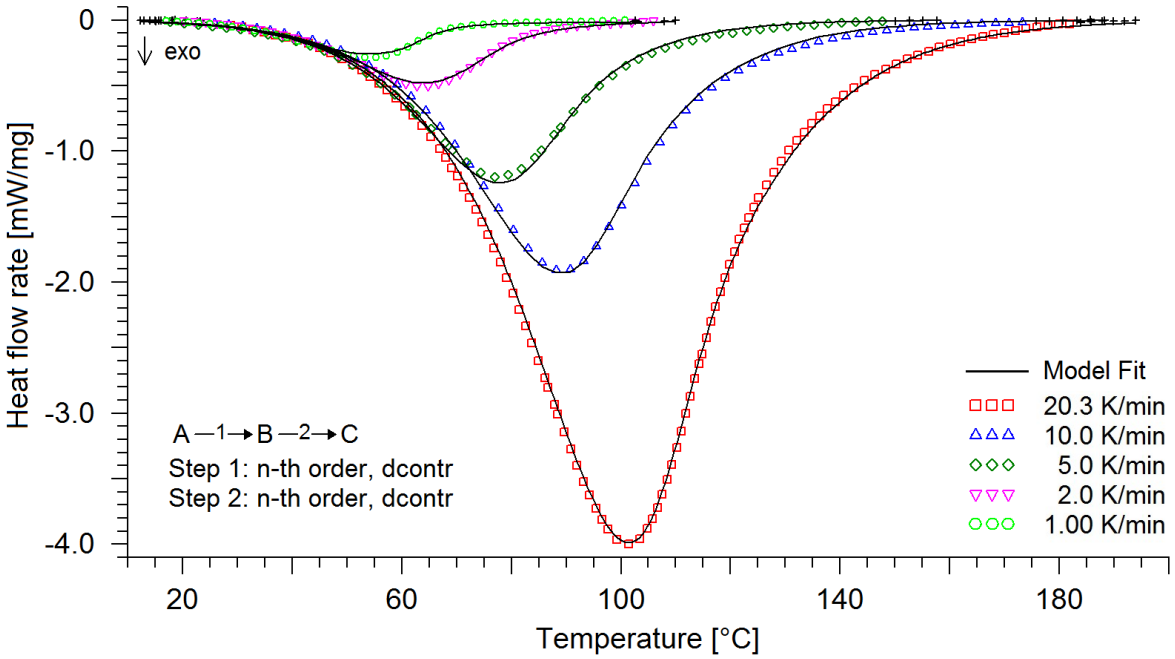

Figure 35: Model fit of a 2-step model, n^{th} order and diffusion control superimposed by experimental DSC input data.

The optimum values of the kinetic parameters and the respective standard deviation of the Fn,d Fn,d model are shown in Table 6. The values of the activation energy E_{a1} and the pre-exponential A_1 of the first step are in good agreement with the Friedman and Ozawa-Flynn-Wall analysis. The decrease of activation energy E_{a2} and the pre-exponential A_2 do also match with the Friedman and Ozawa-Flynn-Wall analysis. The decrease of the activation energy during the crosslinking reaction can be explained by the increase of the hydroxy group concentration, which facilitate the polyaddition of epoxy and amine groups like shown in Scheme 3. The values of E_{a1} and E_{a2} reported in literature for the epoxy amine crosslinking reaction, 64.4 kJ/mol and 45.6 kJ/mol,[67] 63.2 kJ/mol and 48.8 kJ/mol,[68] 71.2 kJ/mol and 49.3 kJ/mol,[69] are also in very good agreement to those found in the kinetic model. The first reaction step is describe by a reaction order $n = 1$, the second reaction step by $n = 1.5$. To obtain the diffusion rate constant according to equation (13), $k_{diff1} = -5.1294\ s^{-1}$ for the first reaction step and $k_{diff2} = -1.0745\ s^{-1}$ for the second reaction step with adjustable parameters $C_1 = 1220.5341$ and $C_2 = 2055.73$ K. The value of Foll. React. 1 gives a weighting of the two following reactions and is described by the following equation,

$$\Delta_{sum} = \text{Foll.React.1} \cdot \frac{dB}{dt} + (1 - \text{Foll.React.1}) \cdot \frac{dC}{dt} \qquad (22)$$

where Δ_{sum}·Area = DSC-signal, *dB/dt* is the differential equation for the first reaction step and *dB/dt* is the differential equation for the second reaction step.

Table 6: Kinetic parameters and standard deviation of the best fit model Fn,d Fn,d based on DSC data.

#	Parameter	Optimum Value	std. Deviation
1	log A_1 [s^{-1}]	7.8780	$2.5971 \cdot 10^{-2}$
2	E_{a1} [kJ/mol]	65.9237	0.1703
3	React. Order 1	1.0673	$1.9050 \cdot 10^{-2}$
4	log k_{diff1} [s^{-1}]	–5.1294	1.1147
5	log A_2 [s^{-1}]	4.7012	$5.8556 \cdot 10^{-2}$
6	E_{a2} [kJ/mol]	46.2689	0.4218
7	React. Order 2	1.5482	$2.6367 \cdot 10^{-2}$
8	log k_{diff2} [s^{-1}]	–1.0745	0.3368
9	C_1	1220.5341	8682.5463
10	C_2 [K]	2055.7368	14517.1737
11	Foll. React. 1	0.3285	$8.2396 \cdot 10^{-3}$
12	Area 1 [J/g]	–566.7299	1.8358
13	Area 2 [J/g]	–507.9225	2.0812
14	Area 3 [J/g]	–581.6113	2.8438
15	Area 4 [J/g]	–536.5718	3.8361
16	Area 5 [J/g]	–551.4445	5.8512

5.3.1.2 Temperature Dependent Cure Simulation

The prediction of the progress of the degree of conversion α and the glass transition temperature T_g over the time at a heating rate of 1 K/min is shown in Figure 36. It can be observed that at 1 K/min heating rate the increasing glass transition T_g reaches the cure temperature and the reaction is dramatically slowed down by vitrification at which the crosslinking reaction gets diffusion controlled. This finding shows the importance of the implementation of correlation of the progress of the glass transition temperature T_g and increasing degree of conversion α to enable diffusion control considerations.

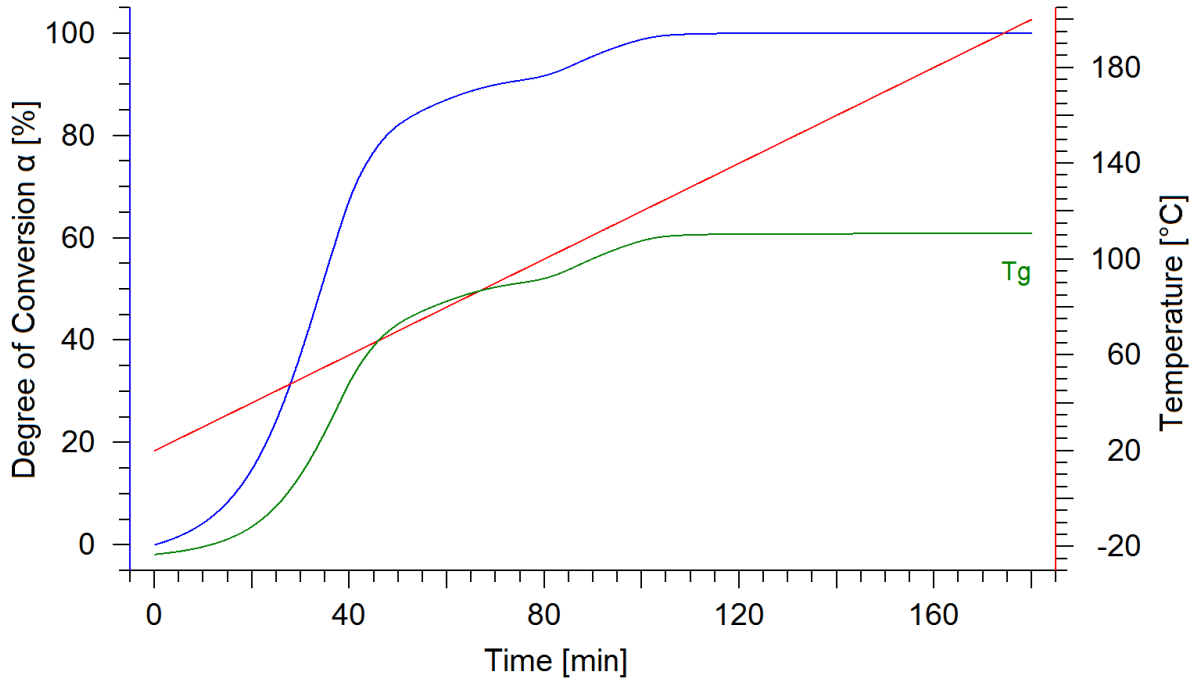

Figure 36: Prediction of degree of conversion α and the progress of the glass transition temperature T_g at 1 K/min heating rate from 20 – 200°C.

The prediction of the progress of the degree of conversion α and the glass transition temperature T_g at a heating rate of 10 K/min, shown in Figure 37, shows that the cure temperature is increasing faster than the glass transition temperature T_g and the reaction does not vitrify.

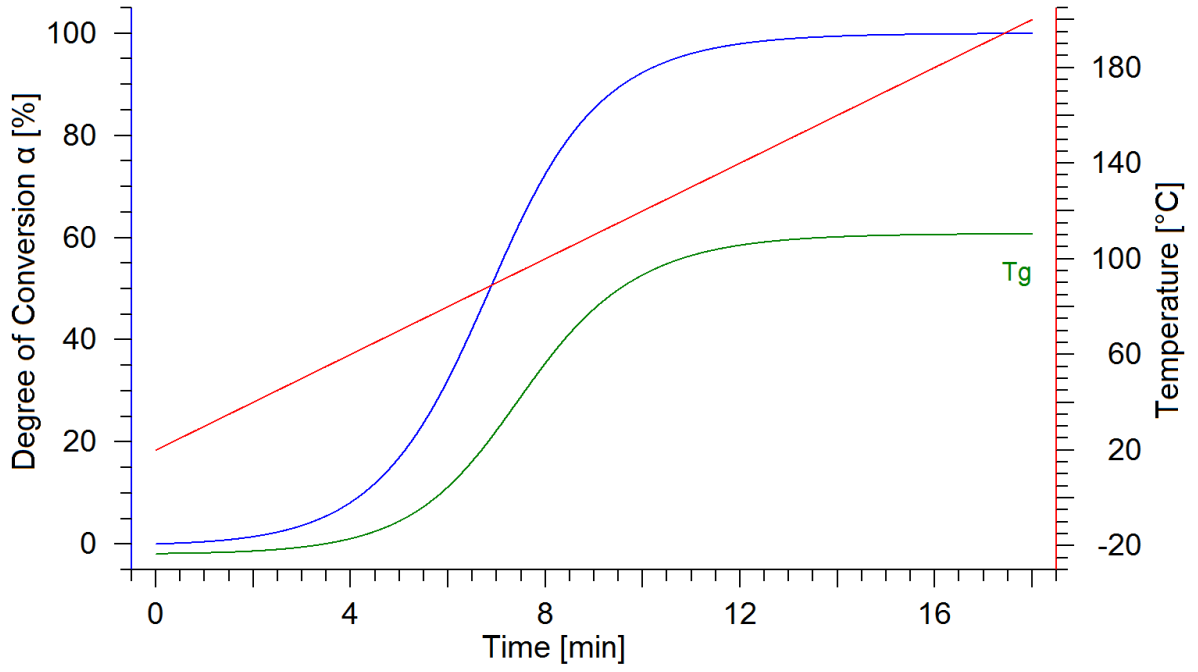

Figure 37: Prediction of degree of conversion α and the progress of the glass transition temperature T_g at 10 K/min heating rate from 20 – 200°C.

The prediction of the progress of the degree of conversion α and the increase of the corresponding glass transition temperature T_g over the time at isothermal cure temperatures 70, 80, 90, 100, 110 and 120°C is shown in Figure 38. The curing reaction is faster at higher temperatures as expected. At cure temperatures from 70 – 100°C the curing reaction is not completed due to vitrification. For these temperatures the final T_g after 35 min curing time is predicted approx. 10°C above the cure temperature.

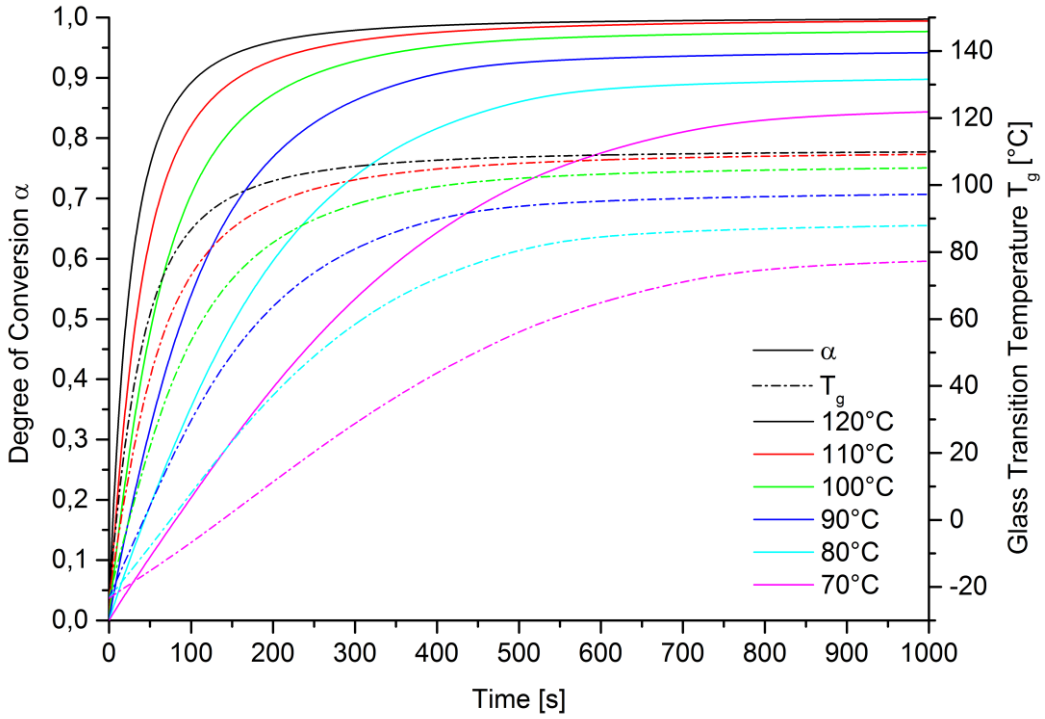

Figure 38: Prediction of degree of conversion α and the progress of the glass transition temperature T_g at isothermal cure temperatures from 70 – 120°C.

The predicted values of the degree of conversion α and the glass transition temperature T_g after 5 min and 35 min are shown in Table 7.

Table 7: Predicted values of degree of conversion α and glass transition temperature T_g after 5 min and 35 min for the respective isothermal cure temperature.

Curing Temp. [°C]	α (5 min)	T_g (5 min)	α (35 min)	T_g (35 min)
70	0.53	28.8	0.86	80.2
80	0.74	58.5	0.91	89.9
90	0.86	81.0	0.95	98.9
100	0.93	94.2	0.98	106.5
110	0.96	101.6	1.00	110.1
120	0.98	105.6	1.00	110.4

5.3.1.3 Time-Temperature-Transformation Analysis

A comprehensive representation of the curing performance of an epoxy resin is give by the TTT analysis as shown previously in Figure 4. This kind of graphical representation provides a good understanding of the curing performance, i. e. the progress of the glass transition temperature over the time at isothermal cure temperatures in addition with isoconversional lines. This allows a quick overview of the development important curing parameters and a corresponding planning of the curing process. Figure 39 shows the predicted TTT diagram of epoxy resin system A at isothermal cure temperatures from 70 – 120°C. A deceleration of the curing reaction due to vitrification can be observed for cure temperatures from 70 – 100°C.

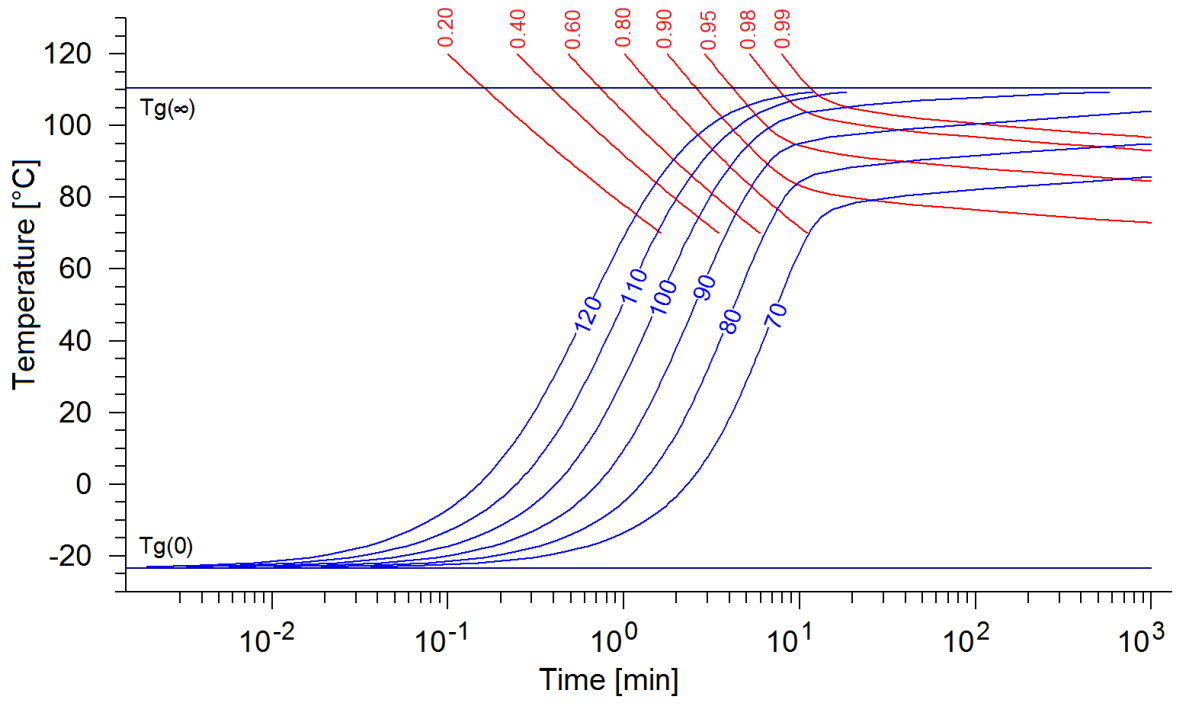

Figure 39: Predicted TTT diagram at isothermal cure temperatures from 70 – 120°C with T_{g0} and $T_{g\infty}$ the progress of the glass transition temperature (blue) and isoconversional lines (red).

5.3.2 Reaction Kinetic Model based on Experimental NIR-Spectroscopy Data

5.3.2.1 Development of Reaction Kinetic Model

A reaction kinetic model based on experimental NIR spectroscopy data is developed in the following according to the model based on DSC data.

Figure 40 shows the input data of dynamic heating NIR spectroscopy experiments at heating rates 2, 5 and 10 K/min from section 4.2.4. As shown in Figure 25, the curing reaction at a heating rate of 1 K/min is dominated by retardation of the reaction due to vitrification for $\alpha > 0.8$. This has a negative effect on model fitting because the curve does not describe the actual crosslinking reaction but physical effects. As diffusion controlled reactions and vitrification effects are considered in the prediction by the implementation of correlation of the degree of conversion α and glass transition temperature T_g anyway, the heating rate at 1 K/min is not taken into account for reaction kinetic modeling.

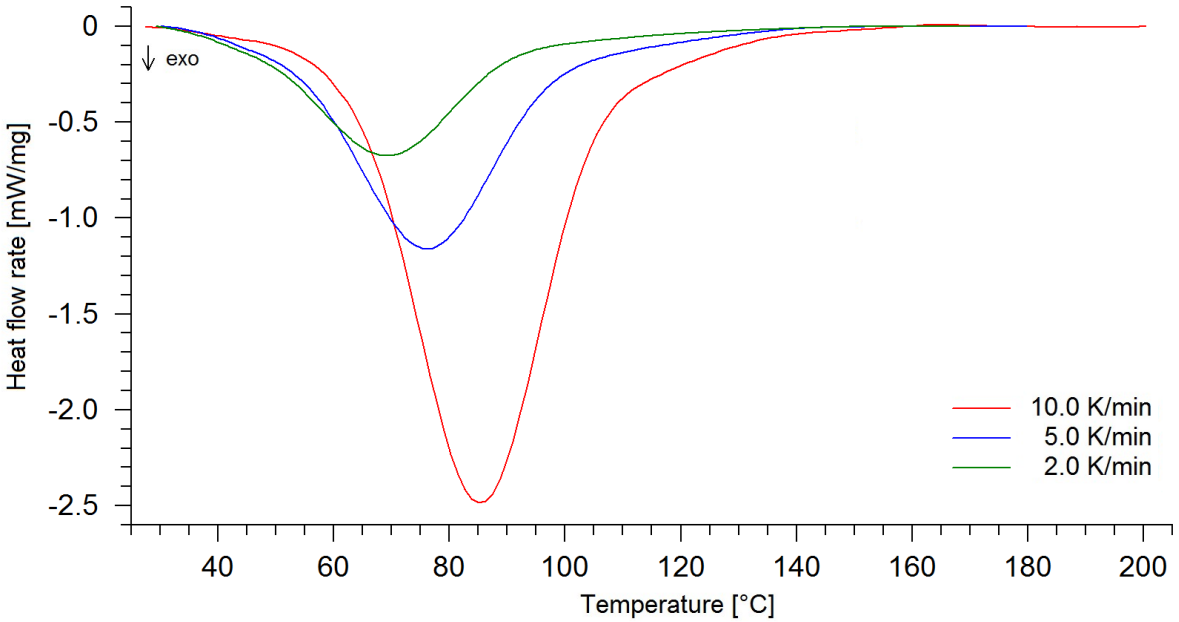

Figure 40: Dynamic NIR spectroscopy heating rate experiments at 2, 5 and 10 K/min.

Figure 41 shows the Friedman plot of the dynamic NIR spectroscopy experiments at heating rates of 2, 5 and 10 K/min and the respective isoconversional lines. The slope of the isoconversional lines changes with rising temperatures, which indicates a multi-step reaction. The slope of the experimental curves is steeper than the slope of the isoconversional lines at lower temperatures from 1000 K/3.2 – 2.9, which indicates an autocatalytic reaction. This is in contrast to the Friedman plot of the DSC data and is probably connected with the higher sample weight and the self-heating of the sample described in section 4.2.4.

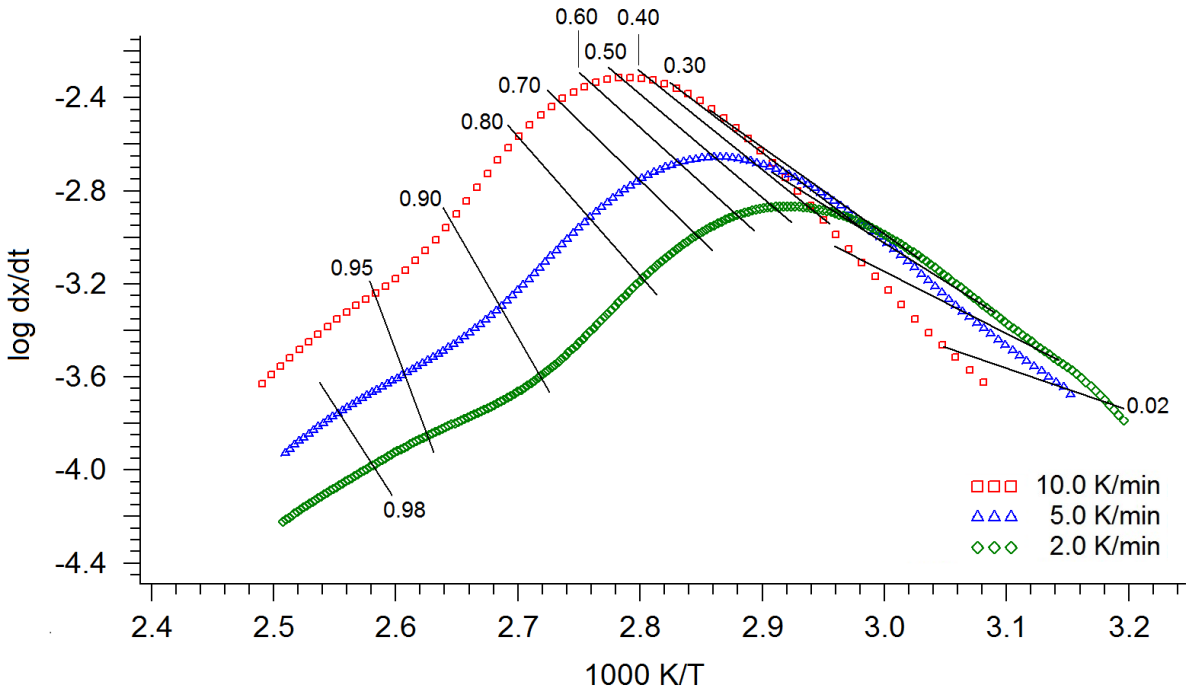

Figure 41: Friedman plot of the dynamic NIR spectroscopy heating rate experiments at 2, 5 and 10 K/min with isoconversional lines.

The estimated activation energy E_a and the pre-exponential factor A derived from the Friedman analysis is shown in Figure 42. E_a and A increase from 65 – 90 kJ/mol and 7 – 13 s^{-1} respectively up to a degree of conversion α = 0.8. For α > 0.8 a very strong increase of both activation energy and pre-exponential factor occurs in addition with very large error bars. This uncertainty originates from vitrification effects of the reaction at high degrees of conversion and high glass transition temperatures respectively and shall not be taken into account as reference for further kinetic modeling.

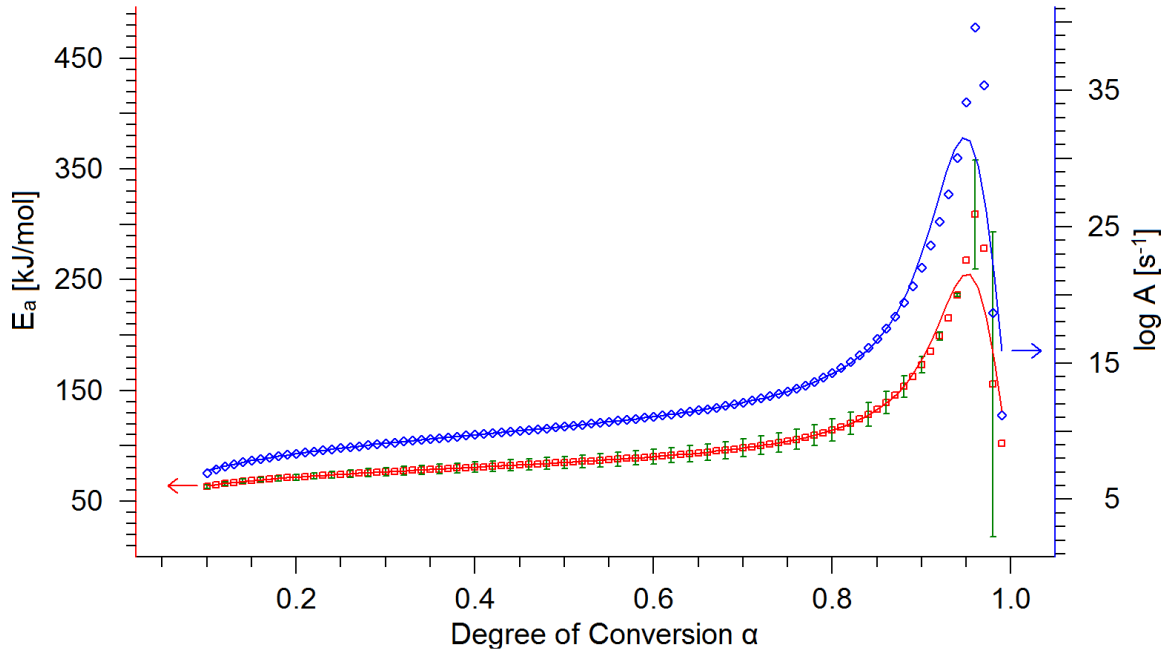

Figure 42: Estimated activation energy E_a and pre-exponential factor *A* according to the Friedman analysis.

Figure 43 shows the Friedman plot of the dynamic NIR spectroscopy experiments at heating rates of 2, 5 and 10 K/min. The change of the slopes of the isoconversional lines also indicate a multi-step reaction, which is in agreement with the Friedman plot.

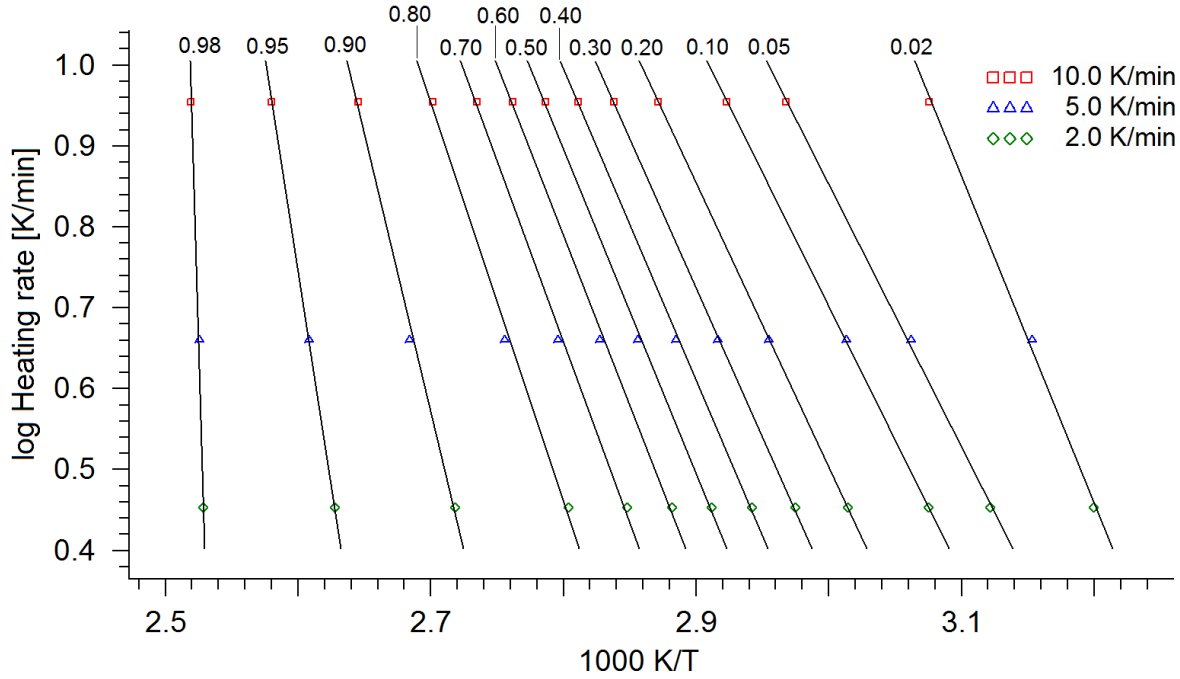

Figure 43: Ozawa-Flynn-Wall plot of the dynamic NIR spectroscopy heating rate experiments at 2, 5 and 10 K/min with isoconversional lines.

The estimated activation energy E_a and the pre-exponential factor A derived from the Ozawa-Flynn-Wall analysis, shown in Figure 44, show the same behavior as for the Friedman analysis. The activation energy E_a increases from 60 – 85 kJ/mol up to a degree of conversion α = 0.8 and the pre-exponential factor A from 7 – 11 s^{-1} respectively. The strong increase of both values for α > 0.8 is also observed and can be attributed to vitrification effects.

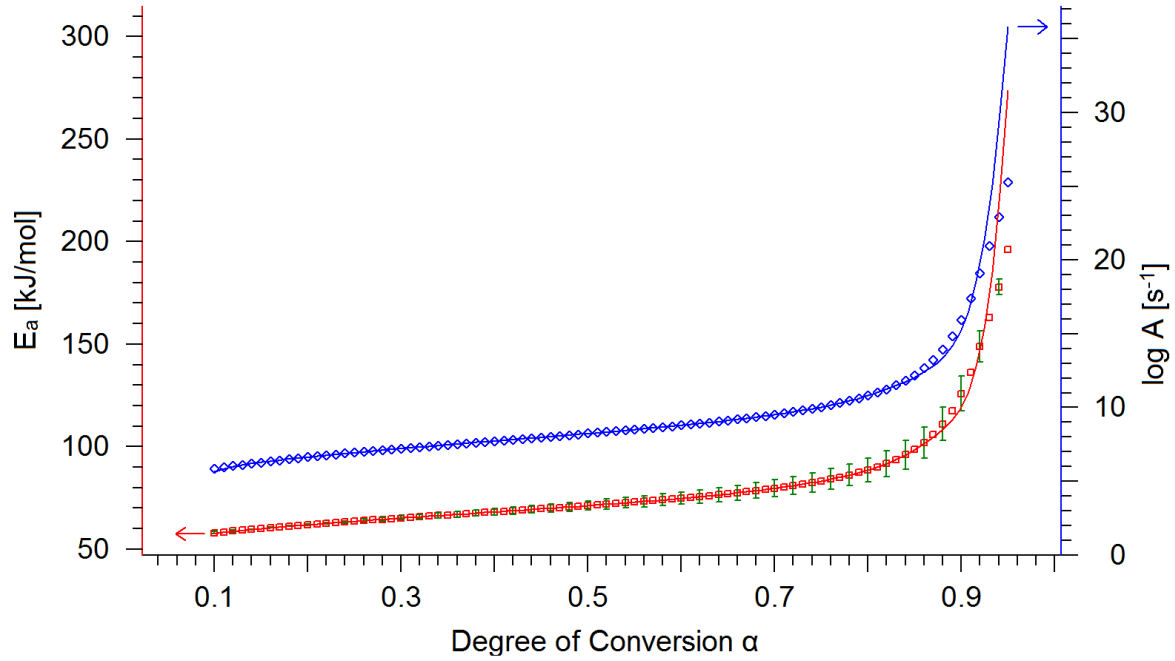

Figure 44: Estimated activation energy E_a and pre-exponential factor A according to the Ozawa-Flynn-Wall analysis.

As a starting point, a single-step reaction model of n^{th} order with autocatalysis was used for a rough estimation. This model yielded an unsatisfying fit, which is in agreement with the Friedman and Ozawa-Flynn-Wall analysis, both indicating a multi-step reaction. The best model fit yielded a two step reaction model of n^{th} order with autocatalysis and diffusion control, shown in Figure 45. A very good correlation coefficient of 0.99942 is obtained. According to Table 5 the reaction model consists of two following reactions of n^{th} order with autocatalysis, indicated by Cn with diffusion control indicated by index d. The code for this reaction model is displayed by Cn,d Cn,d. The catalyst for the first reaction step is intermediate B and for the second reaction step product C. From the mechanistic point of view, product C with its hydroxy groups also catalysis the first reaction step, but this cannot be considered by the underlying differential equations.

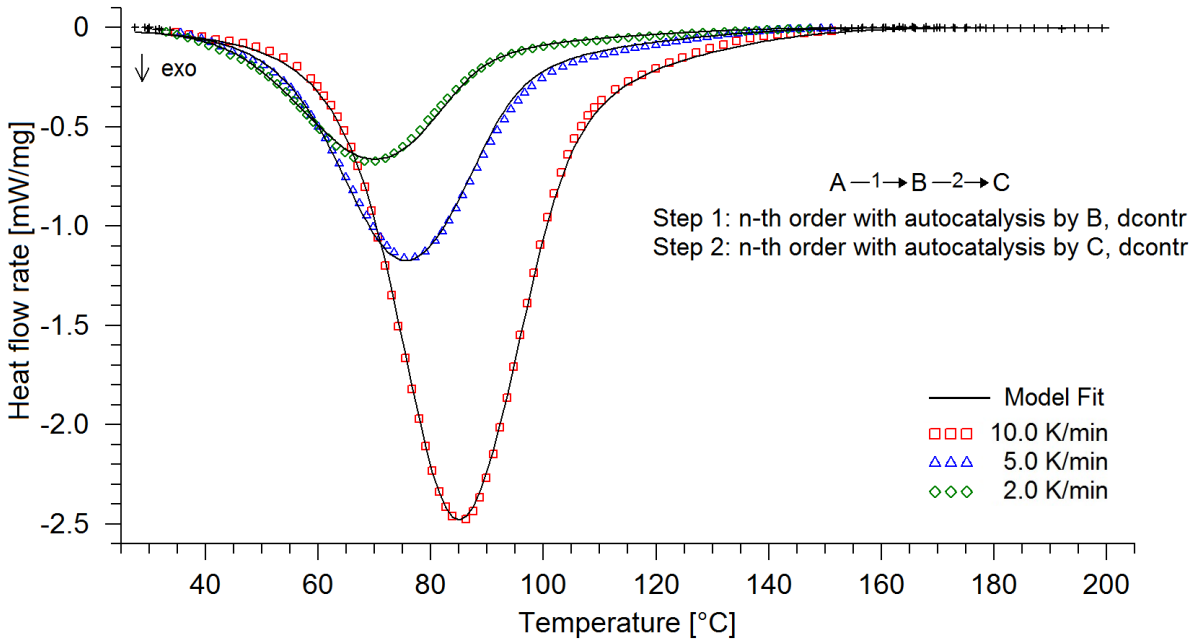

Figure 45: Model fit of a 2-step model, n^{th} order with autocatalysis and diffusion control superimposed by experimental NIR spectroscopy input data.

Table 8 shows the kinetic parameters and the respective standard deviations of the Cn,d Cn,d model. The activation energy E_a and the pre-exponential factor A for the first reaction step are below the estimated values of the Friedman and Ozawa-Flynn-Wall analysis. However, E_a and the A rise for the second reaction step and both values are in the estimated range. The first reaction is describe by a reaction order $n = 0.9$ and for the second reaction $n = 1.8$. The reaction rate constant for the autocatalytic part of the differential equation k_{cat2} is smaller than k_{cat1}, indicating that with higher crosslinking density and therefore decreasing mobility of the molecules and functional groups, the catalytic effect of hydroxy groups decreases.

Table 8: Kinetic parameters and standard deviation of the best fit model based on NIR spectroscopy data.

#	Parameter	Optimum Value	std. Deviation
1	log A_1 [s^{-1}]	4.3828	0.3677
2	E_{a1} [kJ/mol]	45.7062	2.4597
3	React. Order 1	0.8935	$6.4215 \cdot 10^{-2}$
4	log k_{cat1}	0.8102	$8.2675 \cdot 10^{-2}$
5	log k_{diff1} [s^{-1}]	–0.2981	34069.8468
6	log A_2 [s^{-1}]	11.0357	0.6281
7	E_{a2} [kJ/mol]	88.6152	3.9454
8	React. Order 2	1.7491	$8.5038 \cdot 10^{-2}$
9	log k_{cat2}	–0.6760	0.5947
10	log k_{diff2} [s^{-1}]	–1.9127	0.1808
11	C_1	137.8650	4095.8407
12	C_2 [K]	1094.2828	33116.6142
13	Foll. React. 1	0.1537	$2.2256 \cdot 10^{-2}$
14	Area 1 [J/g]	–522.7980	2.5423
15	Area 2 [J/g]	–514.9212	2.7577
16	Area 3 [J/g]	–493.0605	3.2714

5.3.2.2 Temperature Dependent Cure Simulation

The prediction of the progress of the degree of conversion α and the glass transition temperature T_g over the time at a heating rate of 1 K/min is shown in Figure 46. Similar to the findings of the prediction based on the DSC kinetic model, the prediction at 1 K/min heating rate also shows vitrification effects due to approximation of the glass transition temperature T_g to the cure temperature.

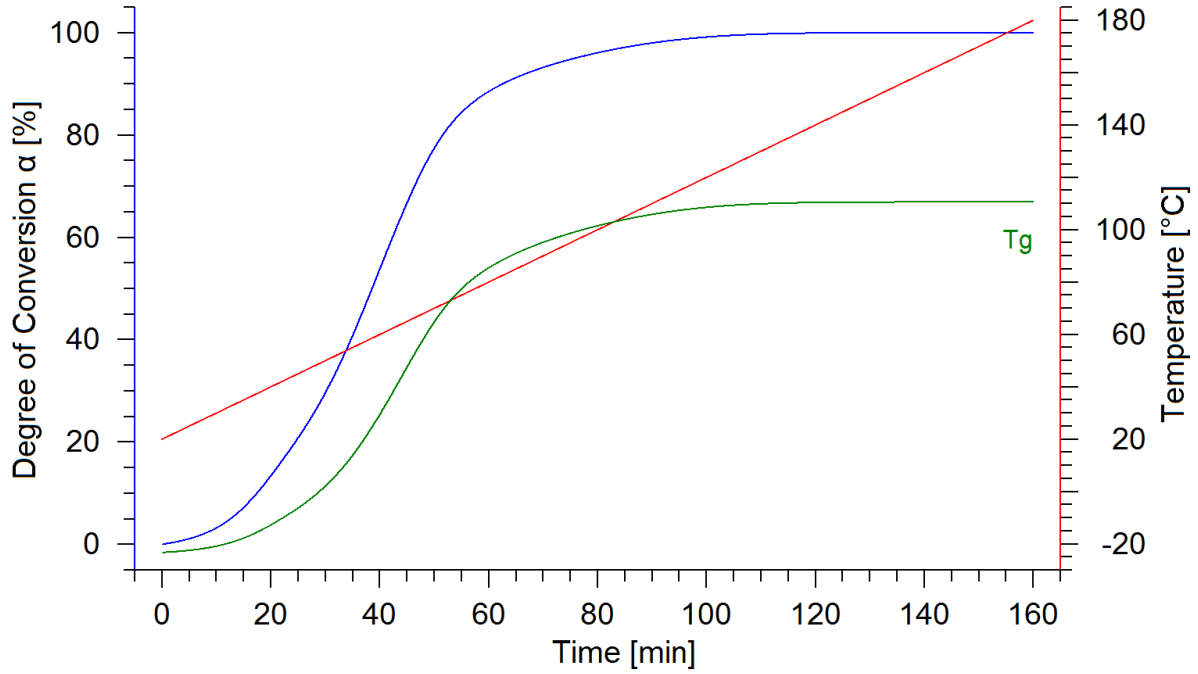

Figure 46: Prediction of degree of conversion α and the progress of the glass transition temperature T_g at 1 K/min heating rate from 20 – 180°C.

The prediction of the progress of the degree of conversion α and the glass transition temperature T_g over the time a heating rate of 10 K/min is shown in Figure 47. Due to the higher heating rate, the cure temperature rises faster than the glass transition temperature T_g and therefore no vitrification occurs.

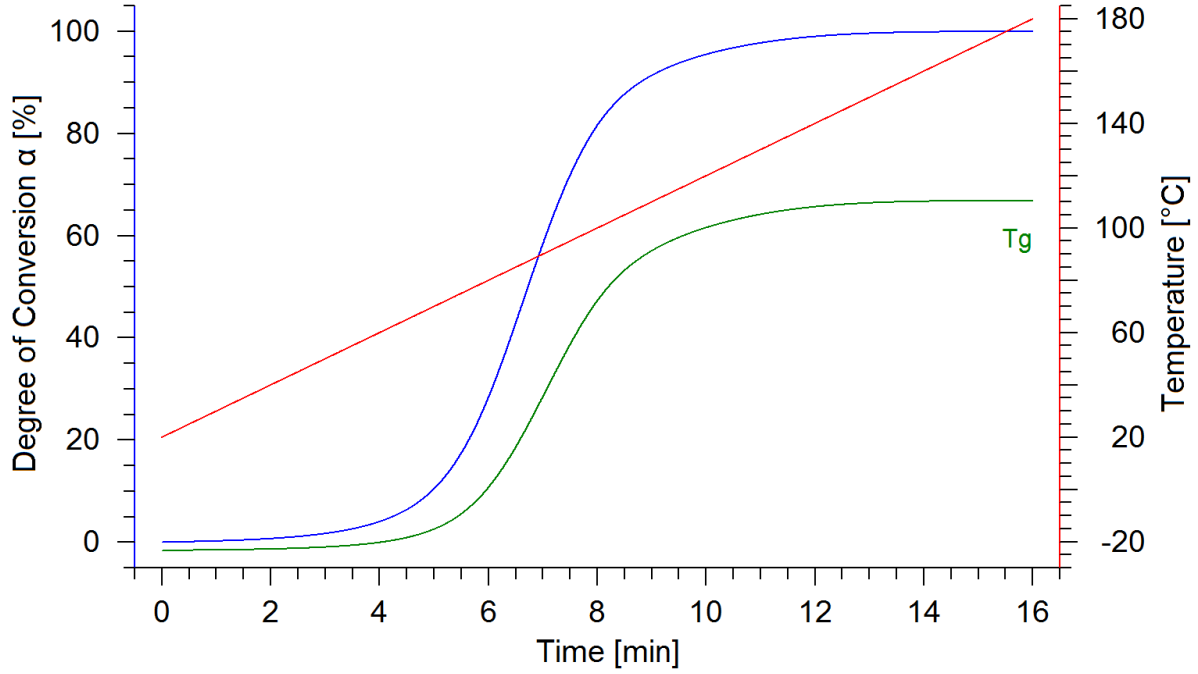

Figure 47: Prediction of degree of conversion α and the progress of the glass transition temperature T_g at 10 K/min heating rate from 20 – 180°C.

The progress of the degree of conversion α and the glass transition temperature T_g at isothermal cure temperatures 70, 80, 90, 100, 110 and 120°C is shown in Figure 48. Similar to the prediction based on the DSC kinetic model, the reaction is not completed for cure temperatures 70 – 100°C due to vitrification.

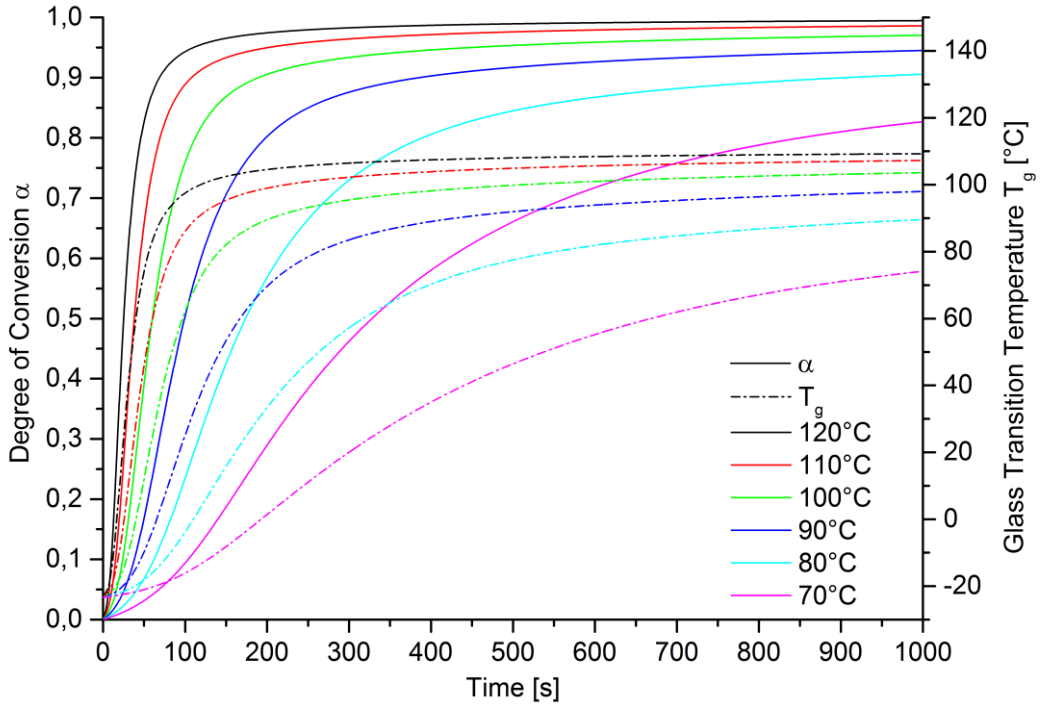

Figure 48: Prediction of degree of conversion α and the progress of the glass transition temperature T_g at isothermal cure temperatures from 70 – 120°C.

The predicted values of the degree of conversion α and the glass transition temperature T_g after 5 min and 35 min are shown in Table 9.

Table 9: Predicted values of degree of conversion α and glass transition temperature T_g after 5 min and 35 min at the respective isothermal cure temperature.

Curing Temp. [°C]	α (5 min)	T_g (5 min)	α (35 min)	T_g (35 min)
70	0.46	20.1	0.89	86.9
80	0.73	57.2	0.94	95.9
90	0.88	83.6	0.96	102.0
100	0.93	94.5	0.98	106.3
110	0.96	102.3	0.99	108.8
120	0.98	106.5	1.00	110.0

5.3.2.3 Time-Temperature-Transformation Analysis

The TTT diagram predicted by the NIR spectroscopy kinetic model is shown in Figure 49. The deceleration of the reaction at cure temperature from 70 – 100°C is display by the flat rise of the glass transition temperature at high degrees of conversion and flat isoconversional lines. For cure temperatures at 110°C and 120°C $T_{g\infty}$ is reached fast and no vitrification is observed.

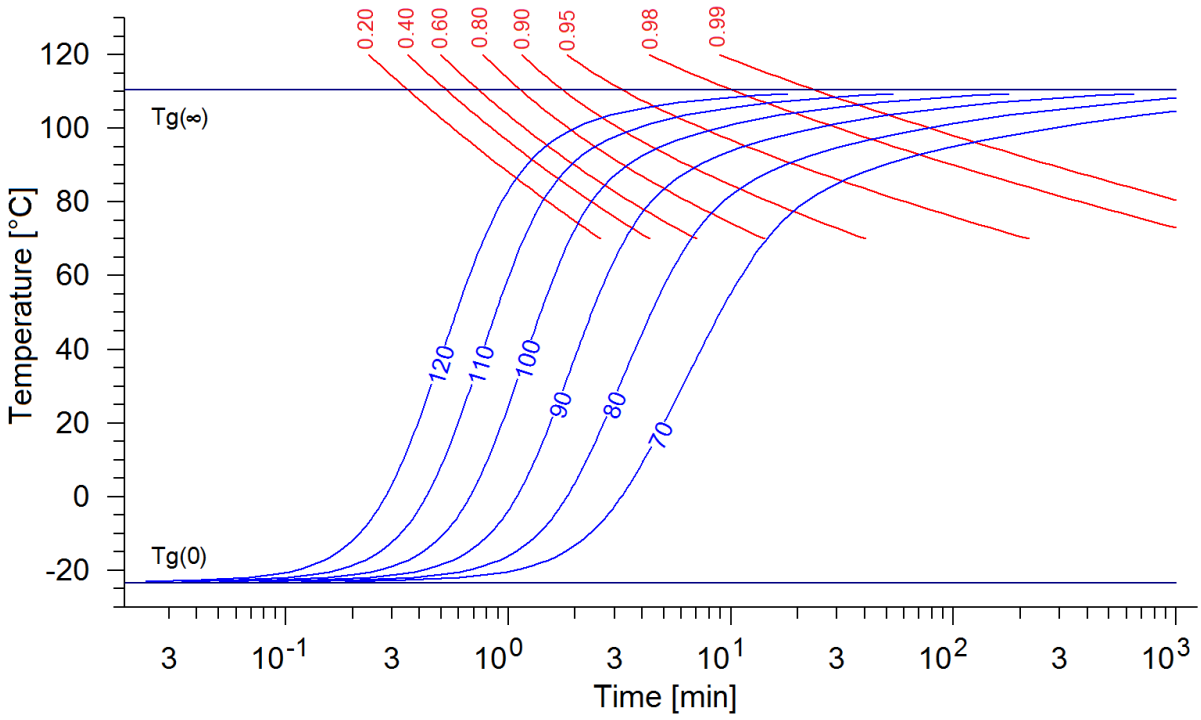

Figure 49: Predicted TTT diagram at isothermal cure temperatures from 70 – 120°C with T_{g0} and $T_{g\infty}$ the progress of the glass transition temperature (blue) and isoconversional lines (red).

5.3.3 Comparison of Kinetic Models based on DSC- and NIR-Data

To compare the kinetic model based on experimental DSC data and experimental NIR spectroscopy data the prediction of the degree of conversion α is used. Figure 50 shows the progress of α at isothermal cure temperatures 70, 80, 90, 100, 110 and 120°C over the time. The predictions of both kinetic models show a good correlation in their principal course at the isothermal cure temperature. The deviation of the predicted degrees of conversion α lies typically in a range of 0.05 and at some sections at 0.1 for a short time. However, the end of the reaction, which is the important information for process control and cure time definition, is shown at similar times for both predictions. This findings show that it is possible to generate a kinetic model by NIR spectroscopy heating rate experiments comparable to DSC measurements.

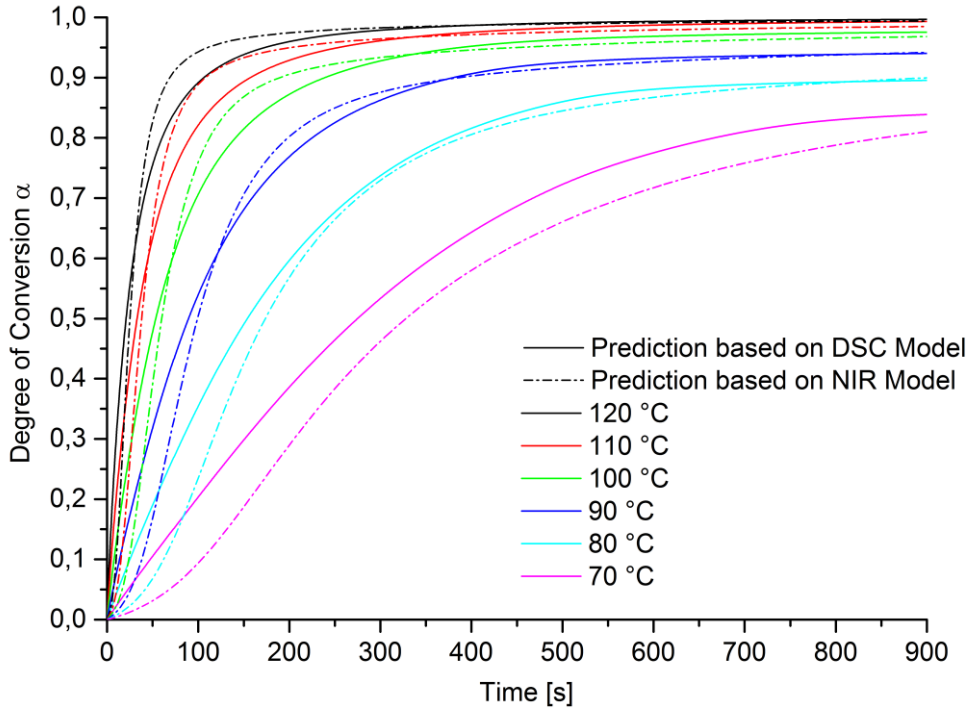

Figure 50: Comparison of the predicted progress of the degree of degree of conversion α over the time at isothermal cure temperatures from 70 – 120°C derived from DSC kinetic model (solid line) and NIR spectroscopy kinetic model (dot dashed line).

However, the following comparisons of experimental data for isothermal cure characterization with kinetic cure simulation are limited to the predictions of the kinetic model based on DSC data. The reason for this is that the DSC kinetic model is considered reliable because of the experimental input data. The sample mass of the NIR experiments is higher and self-heating effects due to the exothermic reaction, which affect the curing progress and falsify the kinetic interpretation, cannot be excluded. Additionally the conversion of the NIR heating rate data of the decrease of the Epoxy 1 signal to DSC like $d\alpha/dt$ referenced to –515.16 J/g is an expedient to provide a suitable form of the kinetic input data and therefore may be an error source.

C. ISOTHERMAL CURE CHARACTERIZATION AND PROCESS ANALYSIS OF EPOXY RESIN SYSTEM A

6 Laboratory Analytical Methods for Characterization of Curing-State and -Progress of Epoxy Resins

6.1 Differential Scanning Calorimetry DSC

In the following the isothermal curing segment 1 of the previously conducted and described combined DSC experiments with a mixed temperature profile, introduced in section 4.1.4, is analyzed.

6.1.1 Interpretation of Isothermal DSC Experiments

The isothermal segment 1 of the DSC experiments with cure temperature of 50°C is shown in Figure 51. The integrated DSC signal provides the information of the progress of the enthalpy of reaction ΔH_R over the time. By setting a linear baseline horizontally extended from the right end of the DSC signal to $t = 0$ s an excessive value of released enthalpy of reaction ΔH_R which does not correspond to the residual enthalpy of reaction ΔH_{res} measured after the isothermal curing to yield ΔH_{tot} = -515.16 J/g. In addition the linear horizontal baseline leads to a steady increase of ΔH_R though the reaction is completed. This leads to the conclusion, that the DSC signal is slightly tilted, which cannot be noticed, as the first part of the reaction and the baseline prior to $t = 0$ s is missing. Therefore a linear baseline in form of a tangent was adapted at the right end of the DSC signal to compensate the inclination of the signal. The uncorrected linear horizontal baseline (red dashed line) and the corrected baseline (blue dashed line) with the according integral curves and obtained values for ΔH_R are shown in Figure 51.

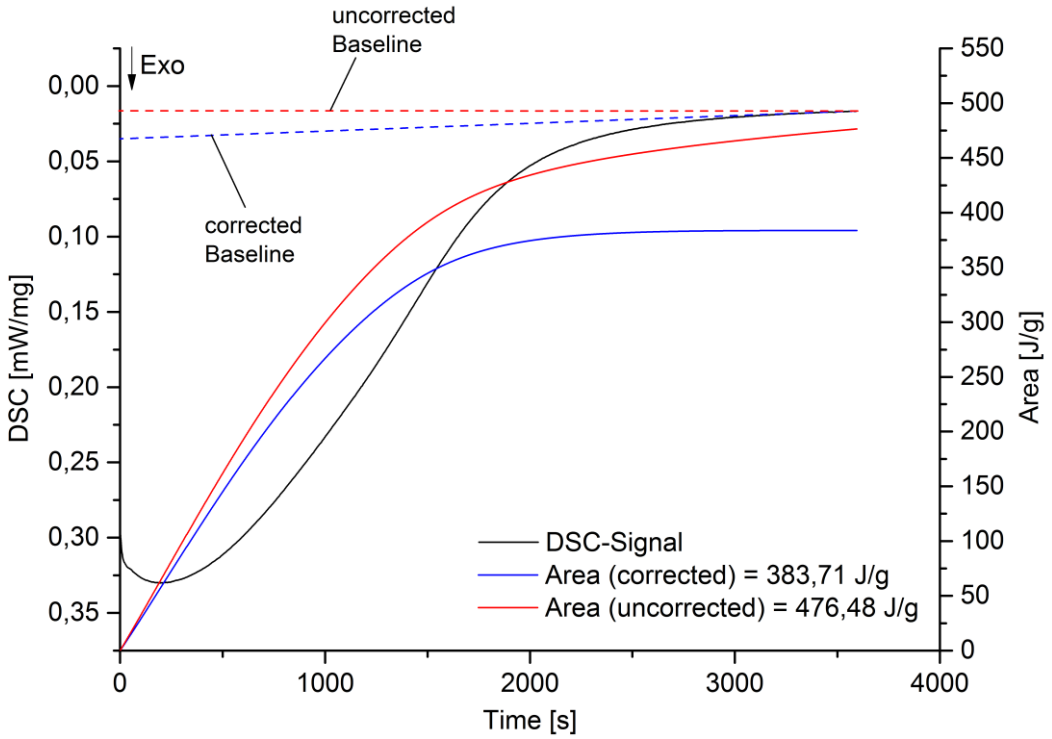

Figure 51: Isothermal DSC experiments at 50°C cure temperature with uncorrected linear horizontal baseline (red dashed line) and the corrected baseline (blue dashed line) and the respective integral curves and ΔH_R values.

Because of the high reactivity of the epoxy resin, the curing progress starts immediately after insertion of the sample into the preheated sample chamber. Due to an initialization period of the DSC prior to the first measurement point, the start of the reaction cannot be detected. Therefore $\Delta H_{tot} = \Delta H_R + \Delta H_{res}$ is not given. The non-detectable enthalpy of reaction ΔH_{loss} at the beginning of the measurement was calculated by equation (23).

$$\Delta H_{loss} = \Delta H_{tot} - \left(\Delta H_{res} + \Delta H_R\right) \qquad (23)$$

The degree of conversion α of the isothermal DSC experiments was calculated by equation (24).

$$\alpha = \frac{\Delta H_{loss} + \Delta H_R}{\Delta H_{tot}} \qquad (24)$$

6.1.2 Results and Discussion of Isothermal DSC Experiments

The isothermal segment 1 of the DSC experiments introduced in introduced in section 4.1.4, are shown in Figure 52 for isothermal cure temperatures 70, 80, 90, 100, 110 and 120°C. The total curing time is 30 min for 70 and 90°C and 20 min for 100, 110 and 120°C to ensure that the curing reaction is completed. The progress of the respective enthalpy of reaction ΔH_R over time is given by integration of the DSC signals by applying a corrected baseline according to Figure 51.

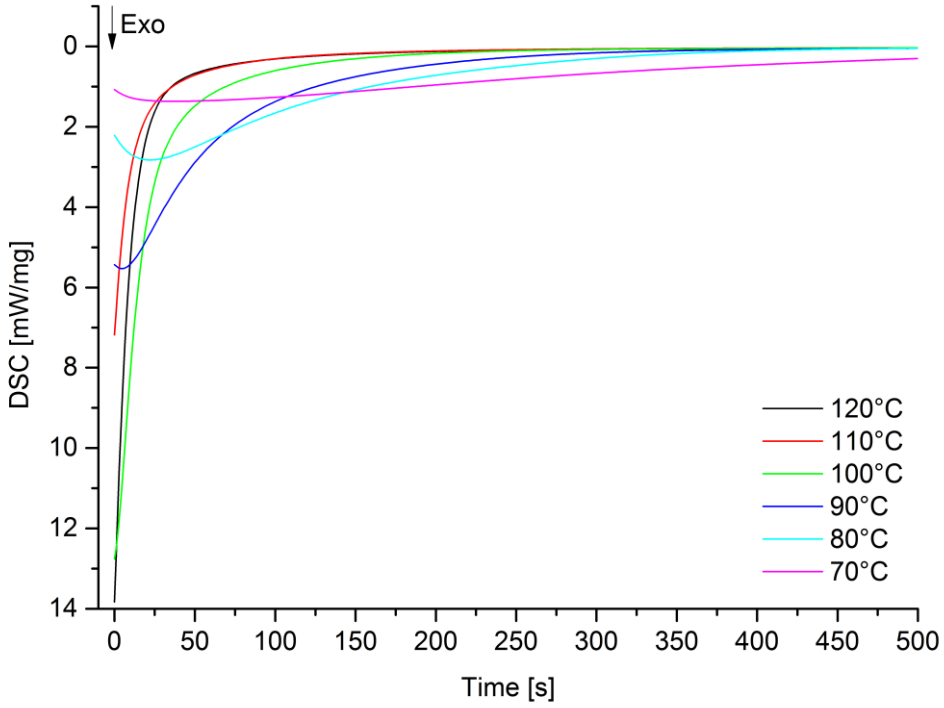

Figure 52: DSC signals at isothermal cure temperatures 70, 80, 90, 100, 110 and 120°C.

Using the values for the residual enthalpy of reaction ΔH_{res}, obtained by an analytical dynamic DSC run after the isothermal segment shown in Table 3, the non-detectable enthalpy of reaction ΔH_{loss} at the beginning of the measurement is calculated according to equation (23) with the total heat of reaction $\Delta H_{tot} = -515.16$ J/g. The respective degrees of conversion α are then calculated according to equation (24).

The measured values of enthalpy of reaction ΔH_R at the isothermal cure temperatures, the residual enthalpy of reaction ΔH_{res} after isothermal curing, the calculated non-detectable enthalpy of reaction ΔH_{loss} and the respective degrees of conversion α are shown in Table 10.

Table 10: Enthalpies of reaction ΔH_R, residual enthalpies of reaction ΔH_{res}, non-detectable enthalpy of reaction ΔH_{loss} and calculated corresponding degrees of conversion α at respective isothermal cure temperatures.

Cure Temp [°C]	ΔH_{loss} **[J/g]**	ΔH_R **[J/g]**	ΔH_{res} **[J/g]**	**Degree of Conv.** α
70	–1.38	–461.57	–52.21	0.90
80	–65.35	–430.24	–19.57	0.96
90	–45.98	–458.57	–10.70	0.98
100	–183.20	–331.37	–0.59	1.00
110	–362.55	–152.61	0	1.00
120	–311.36	–203.80	0	1.00

Curing at 70°C and 90°C does not provide a full reaction of the epoxy resin and leads to a degree of conversion of 0.90 and 0.98. For higher cure temperatures, the polymerization reaction is completed.

Due to the fast reaction the beginnings of the isothermal DSC measurements, especially at high temperatures, were cut off. To provide a comparison of the isothermal DSC experiments with other results, ΔH_{loss} has to be reconstructed by extrapolation, to provide a qualitative curve progression and a uniform starting point $t = 0$. The function for the extrapolation was given by a 7^{th}-order polynomial fit of the experimental data and the new starting point $t = 0$ s was set at $\alpha = 0$ for all curves. The progress of the degree of conversion α for isothermal temperatures from 70 – 120°C is shown in Figure 53.
The curing progress of the epoxy resin system A is extremely slow at 70°C and α increases only in a moderately. At 80 and 90°C cure temperature α increases clearly faster but turns into a plateau at $\alpha \sim 0.85$ due to vitrification and only rises slowly. At higher cure temperatures from 100°C to 120°C the reaction proceeds very fast and the polymerization is finished at around 3.5 min. Above 100°C the reaction speed increases only moderately for higher temperatures. An overview of the curing performance of epoxy resin system A is given by the degrees of conversion α after 2, 5, 20, 35 min curing at the respective isothermal cure temperatures, shown in Table 11.

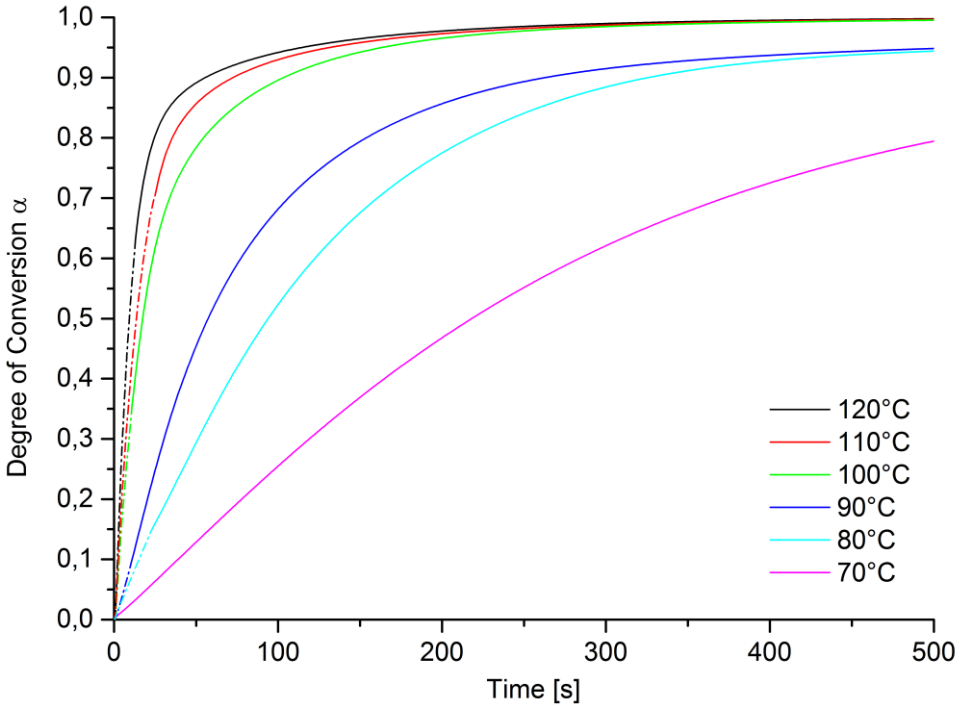

Figure 53: Progress of degree of conversion α for isothermal DSC experiments at temperatures from 70 – 120°C with the experimentally determined enthalpy of reaction ΔH_R (solid lines) and the calculated and reconstructed non-detectable enthalpy of reaction ΔH_{loss} (dot dashed lines).

An overview of the curing performance of epoxy resin system A is given by the degrees of conversion α after 2, 5, 20, 35 min curing at the respective isothermal cure temperatures, shown in Table 11.

Table 11: Degrees of conversion α after 2, 5, 20, 35 min curing time derived from isothermal DSC curing experiments.

Curing Temp. [°C]	α (2 min)	α (5 min)	α (20 min)	α (30 min)
70	0.30	0.62	0.89	0.90
80	0.59	0.88	0.96	0.96
90	0.74	0.92	0.98	0.98
100	0.92	0.99	1.00	1.00
110	0.94	0.99	1.00	1.00
120	0.95	0.99	1.00	1.00

6.1.3 Comparison with DSC Kinetic Model

Figure 54 shows the comparison of the progress of the degree of conversion α of the isothermal DSC experiments, afterwards referred to as α_{exp}, and the prediction of α derived by the DSC kinetic model, afterwards referred to as α_{pred}, at isothermal cure temperatures 70 – 120°C. The progress of α_{pred} at isothermal cure temperatures lags behind the experimentally determined values for each temperature. This applies especially to the higher cure temperatures 100, 110 and 120°C.

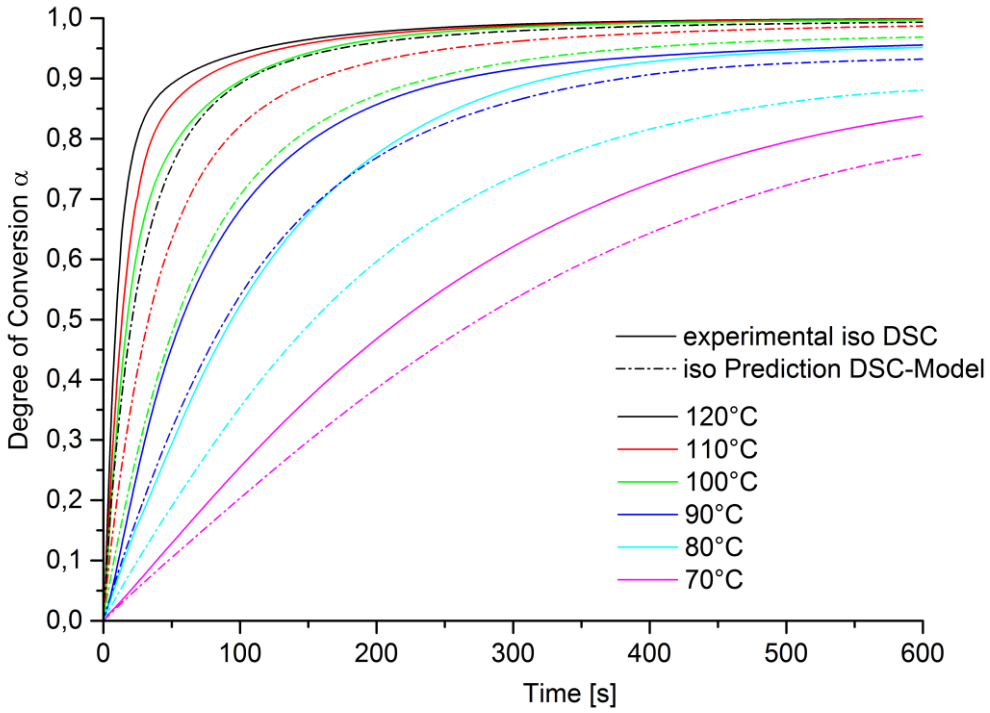

Figure 54: Comparison of degrees of conversion α_{exp} of isothermal DSC experiments (solid lines) and prediction α_{pred} of the DSC kinetic model (dot dashed lines) at isothermal cure temperatures 70 – 120°C.

A comparison of the experimental and predicted degrees of cure at 2, 5, 20 and 30 min at the respective temperatures is shown in Table 12. After 20 min and 30 min curing time and at 70 – 100°C cure temperature the predicted values α_{pred} are 2 – 5% below the experimentally determined values. One explanation for this disparity is that the curing progress and mechanism at isothermal temperatures is not comparable to that taking place in heating rate experiments.

Table 12: Experimentally determined degrees of conversion α_{exp} and predicted degrees of conversion α_{pred} after 2, 5, 20, 30 min curing at isothermal cure temperatures 70 – 120°C.

	2 min		**5 min**		**20 min**		**30 min**	
Temp. [°C]	α_{exp}	α_{pred}	α_{exp}	α_{pred}	α_{exp}	α_{pred}	α_{exp}	α_{pred}
70	0.30	0.24	0.62	0.53	0.89	0.85	0.90	0.86
80	0.59	0.41	0.88	0.74	0.96	0.90	0.96	0.91
90	0.74	0.61	0.92	0.86	0.98	0.94	0.98	0.95
100	0.92	0.76	0.99	0.93	1.00	0.98	1.00	0.98
110	0.94	0.86	0.99	0.96	1.00	1.00	1.00	1.00
120	0.95	0.92	0.99	0.98	1.00	1.00	1.00	1.00

6.2 NIR-Spectroscopy

The isothermal NIR spectroscopy experiments were conducted according to the description in section 4.2.2. The first measurement point is obtained 8 seconds after placing the cuvette into the heated NIR cell. For the quantitative analysis of the curing progress the Epoxy 1 signal was used and a temperature correction of the peak area was conducted according to the description in section 4.2.3

6.2.1 Results and Discussion of Isothermal NIR Spectroscopy Experiments

The curing progress of epoxy resin system A on the basis of the conversion of epoxy groups, according to the reciprocal and normalized signal area of Epoxy 1, at isothermal cure temperatures 80°C and 100°C and 20 minutes curing time, is shown in Figure 55. In addition the sample temperature during the curing reaction was measured via a thermocouple sensor. It can be observed that the initial temperature of the sample is below the cure temperature. The sample heats up immediately after placing the sample container into the preheated sample chamber. However it takes 39 s to reach the isothermal cure temperature at 80°C and 18 s to reach 100°C. Due to the exothermic reaction the sample temperature overshoots the cure temperature to a maximum of 91°C for isothermal curing at 80°C and to a maximum of 118°C for isothermal curing at 100°C. This is due to the sample weight of 0.4 g and the bad thermal conductivity properties of the epoxy resin and the glass cuvette. At the temperature maximum of the sample, the degree of conversion has its steepest slope and the speed of the polymerization reaction reaches its maximum. As expected, the curing reaction is faster at 100°C and is fully cured yielding a degree of conversions $\alpha = 1.00$. The curing reaction is not completed at 80°C cure temperature due to vitrification and a degree of conversions $\alpha = 0.93$ is obtained. These findings are in agreement with the previous results.

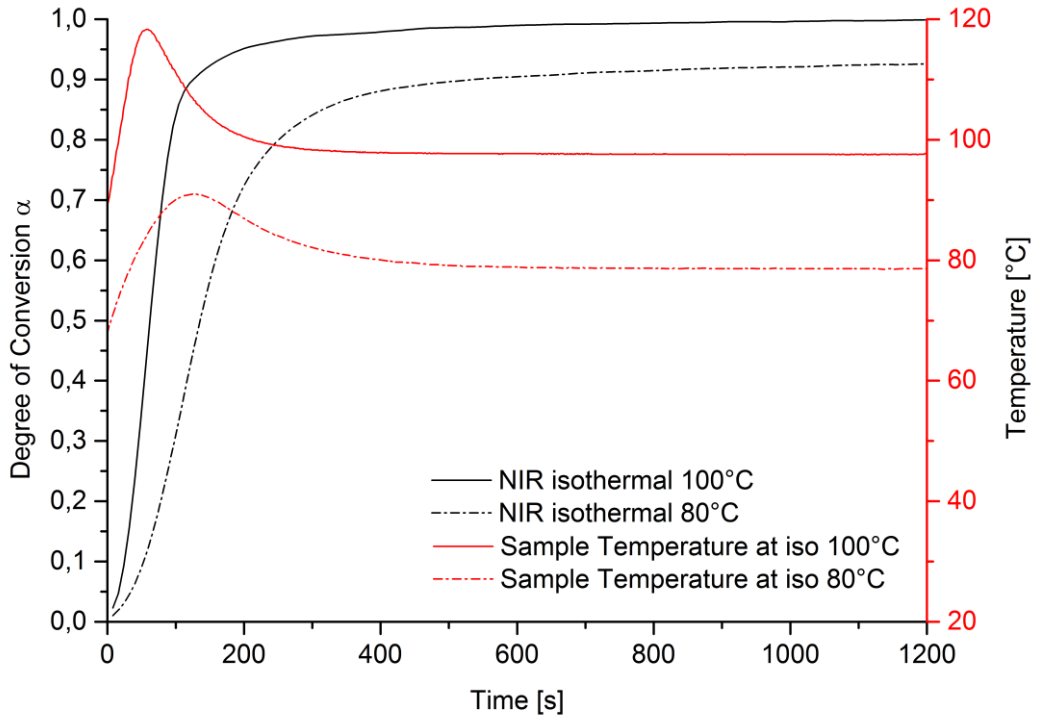

Figure 55: Progress of the degree of conversion α of epoxy resin system A according to the reciprocal, normalized and temperature corrected Epoxy 1 signal at isothermal cure temperatures 80°C and 100°C and the respective measured sample temperature.

6.2.2 Comparison with isothermal DSC Results

The comparison of the isothermal NIR spectroscopy with the isothermal DSC experiment at 80°C and 100°C cure temperature is shown in Figure 56. The degree of conversion α obtained by NIR spectroscopy lags approx. 40s behind the DSC measurement for both temperatures. This can be explained by the different sample temperature course of the NIR spectroscopy measurement, which takes a longer time to heat up to reach the set cure temperature. At 100°C cure temperature the slope of α of the NIR and DSC measurement is almost identical for $0.1 < \alpha$ 0.8. At $\alpha > 0.9$ both curves are almost identical and reach the same final degree of conversion $\alpha = 1.0$. The overshooting sample temperature in the NIR spectroscopy measurement compensates the lag at the beginning of the reaction due to lower sample temperature compared to the cure temperature. At 80°C cure temperature the slope of α of the NIR and DSC measurement is almost identical for $0.1 < \alpha$ 0.5 and almost catches up at $\alpha = 0.7$. The overshooting sample temperature in the NIR spectroscopy measurement compensates the lag but is not able to reach the same degree of conversion at 80°C cure temperature.

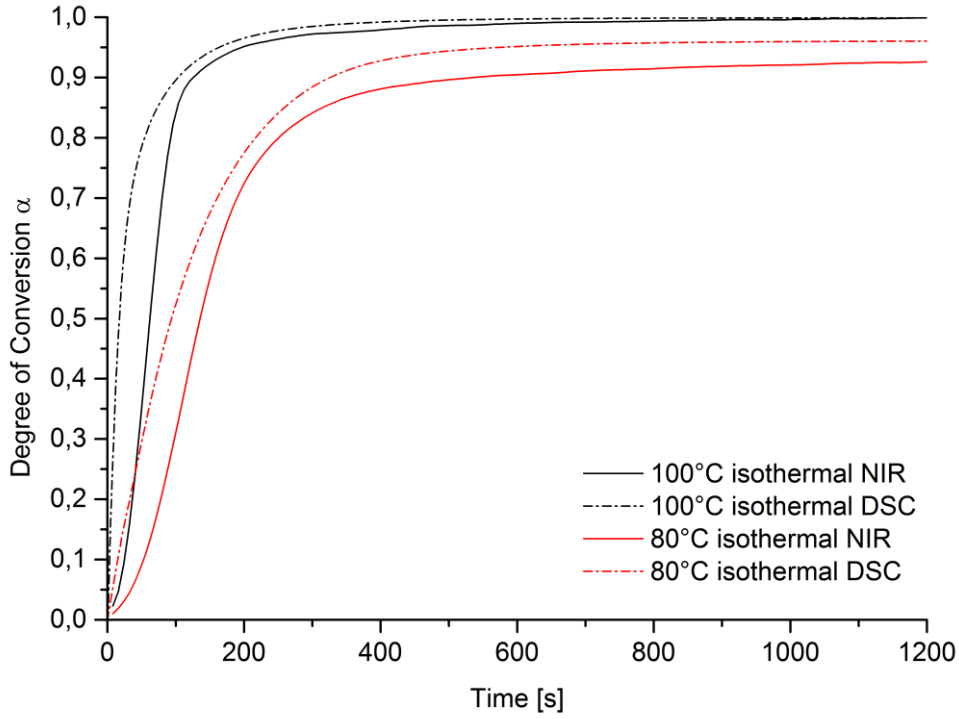

Figure 56: Comparison of the progress of degree of conversion α of epoxy resin system A obtained by isothermal NIR-Spectroscopy and isothermal DSC experiment at 80°C and 100°C cure temperature.

Additionally it has to be kept in mind that DSC measures the polyaddition reaction indirectly via the differential temperature profile and the heat emitted during the reaction, while NIR spectroscopy directly measures the crosslinking reaction by concentration measurement of the epoxy group.

6.2.3 Comparison with DSC Kinetic Model

The comparison of the isothermal NIR spectroscopy at 80°C and 100°C cure temperature with the prediction of the curing process based on the DSC kinetic model is shown in Figure 57. The sample temperature profile, shown in Figure 55, was taken as basis for the prediction. The experimental data and the predicted course show a very good agreement and are similar at both cure temperatures. Only a very small deviation of the degree of conversion of 0.02 at the end of the reaction is observed at both temperatures.

The final degree of conversion reached after 20 minutes at 100°C cure temperature is $\alpha = 1.0$ according to the NIR measurement and $\alpha = 0.98$ according to the prediction. At 80°C the α values are 0.92 and 0.90 respectively. In summary, the consistency of the experimental data with the prediction is very good.

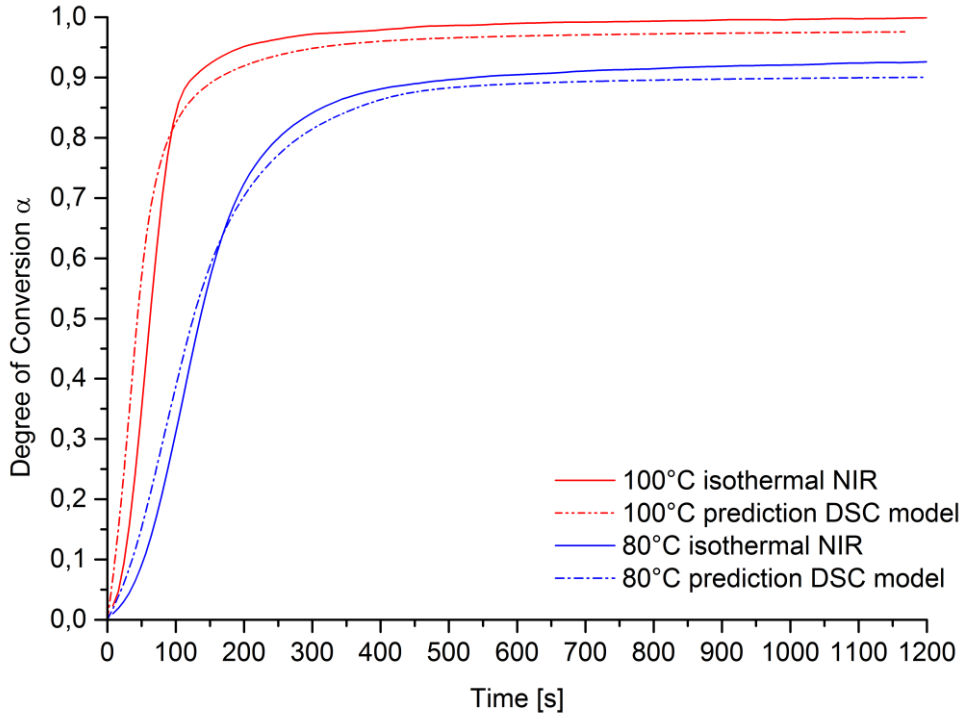

Figure 57: Comparison of the progress of degree of conversion α of epoxy resin system A obtained by isothermal NIR spectroscopy and prediction of the curing process based on the DSC kinetic model and the measured sample temperature determined at 80°C and 100°C cure temperature.

7 Laboratory Analytical Methods for Characterization of Curing-Progress of Epoxy Resins based on Mechanical Parameters

7.1 Rheometric Analysis

7.1.1 Basic Working Principle of a Rheometer

In steady-shear rheology a continuous shearing deformation of the material is induced by rotation of the upper plate of a plate rheometer, shown in Figure 58.

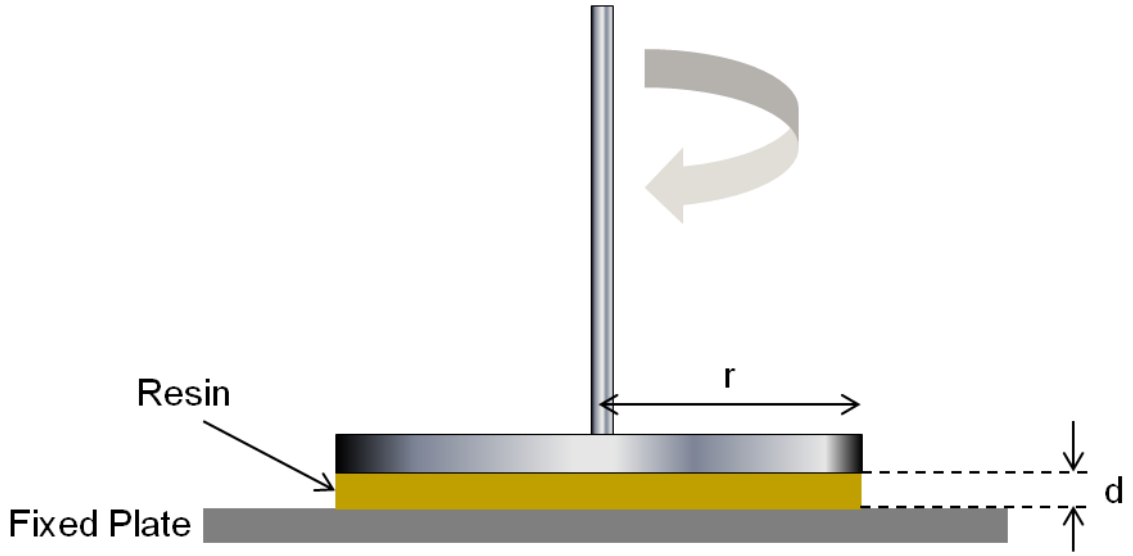

Figure 58: Scheme of rotating plate rheometer.

The shear viscosity η is measured by rheometry in rotation mode and is defined as the ratio of shear stress τ and shear rate $\dot{\gamma}$ as follows.

$$\eta = \frac{\tau}{\dot{\gamma}} \qquad (25)$$

In a parallel plate rheometer the shear stress τ and shear rate $\dot{\gamma}$ are determined as follows

$$\dot{\gamma} = \frac{V}{d} \qquad (26)$$

$$\tau = F_{\tau} \cdot T \qquad (27)$$

where V is the change in fluid velocity with shear gap d, F_{τ} (= $2/\pi r^3$) is the shear stress factor with the torsional force T.

In dynamic-shear rheology an oscillating shearing deformation of the material is induced by oscillation of the upper plate of a plate rheometer.

In the dynamic shear rheology the shear strain γ is described by the strain amplitude γ_0 and the angular frequency ω.

$$\gamma = \gamma_0 \cdot \sin(\omega \cdot t) \qquad (28)$$

In the dynamic shear rheology, the resulting shear stress τ is described by the stress amplitude τ_0 and the phase angle δ.

$$\tau = \tau_0 \cdot \sin(\omega \cdot t + \delta) \qquad (29)$$

For solid material, which is entirely elastic the strain γ is directly related to the stress τ, also called in-phase, and this results in a phase angle $\delta = 0°$.

For Newtonian liquids, which are entirely viscous, the strain γ follows the stress τ at a phase angle $\delta = 90°$, also called out-of-phase, resulting in

$$\tau = \tau_0 \cdot \sin(\omega \cdot t - 90) = \tau_0 \cdot \cos(\omega \cdot t) \qquad (30)$$

For viscoelastic materials, which exhibit both viscous and elastic behavior under deformation, the phase angle is between $0° < \delta < 90°$. This applies for example for epoxy resins during curing.
This behavior takes a contribution of both, in-phase and out-of-phase components into account and stress τ is formed to

$$\tau = \tau_0 \cdot [G' \cdot \sin(\omega \cdot t) + G'' \cdot \cos(\omega \cdot t) \qquad (31)$$

where $G'\sin(\omega t)$ is the in-phase or solid-like stress response and $G''\cos(\omega t)$ is the out-of-plane or liquid-like stress response. G' and G'' are represent the storage modulus and loss modulus respectively.

The dynamic viscosity η' is related to the loss modulus G'' and the out-of-phase viscosity η'' is related to the storage modulus G' as follows:

$$\eta' = \frac{G''}{\omega} \tag{32}$$

$$\eta'' = \frac{G'}{\omega} \tag{33}$$

The Cox-Merz rule is an empirical finding and states that the shear viscosity η as a function of the shear rate $\dot{\gamma}$ and the complex viscosity η^* as a function of frequency ω are equal.

$$\eta(\dot{\gamma}) = \eta^*(\omega) \tag{34}$$

The complex viscosity η^* contains both a real and an imaginary part and is defined by,

$$\eta^* = \eta' - i\frac{G'}{\omega} \tag{35}$$

where η' is the dynamic viscosity, G' is the dynamic shear modulus, $i = \sqrt{-1}$.[70]
For magnitude of the complex viscosity η^* then follows

$$|\eta^*| = \frac{1}{\omega}\sqrt{G'^2 + G''^2} \tag{36}$$

7.1.2 Determinable Parameters

Several important parameters for the processability of epoxy resin systems for the application in the HP-RTM process are obtained by rheometric measurements. The initial viscosity of the mixed epoxy resin system and the change of the viscosity in the early stage of the curing reaction at process temperatures can be obtained by measurements in rotation mode and are important for the injection phase of the HP-RTM process.
At the first major transition during the curing process of the epoxy resin system, i. e. when gelation occurs, the shear viscosity becomes infinite and the elastic modulus becomes measurable, as shown in Figure 59.

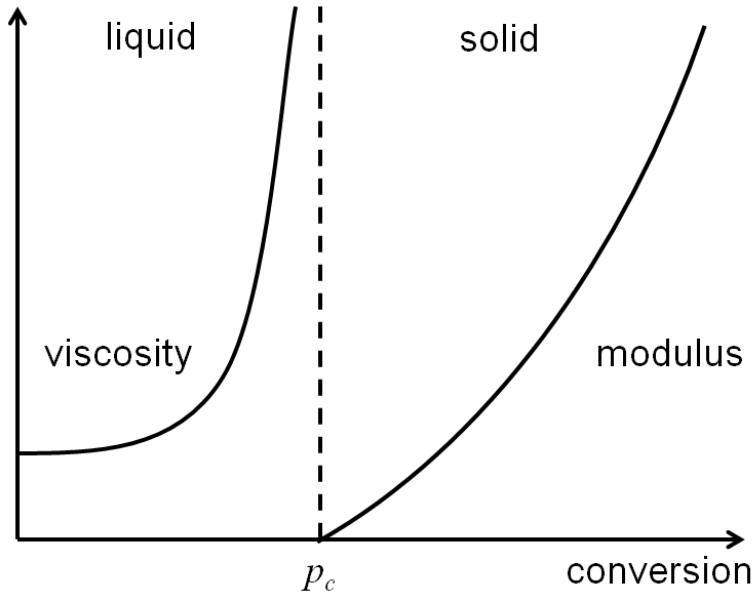

Figure 59: Schematic curing profile of an epoxy resin with the progress of the shear viscosity in the liquid state and the modulus in the solid state.[23]

For further analysis of the rheological properties after the transition of the sample from liquid to solid state, the storage modulus *G*' and the loss modulus *G*" can be obtained by measurements in oscillation mode. According to equation (36) the complex viscosity is calculated at a given the angular frequency ω.

The phenomenon of gelation and the determination of the gel point is a deeply investigated and controversially discussed topic in rheometry. The most established definition and determination of gelation, the rheological gel point, is the crossover of the storage modulus *G*' and the loss modulus *G*" in oscillatory rheometry measurements.[71,72] According to this theory, the determined gelation time should be independent of the measurement frequency. In the following gelation is determined according to the crossover of *G*' and *G*".

Another determinable transformation of a polymer by rheometry is vitrification. This is the transformation from an either liquid-like or a rubber-like behavior to a solid glass-like state and occurs when the glass transition temperature of the resin and the (cure-) temperature are approximately equal. Four different criteria are commonly accepted for the determination of vitrification, which are: the onset of the frequency dependence of the storage modulus *G*', the peak of tan (δ) at 1 Hz, the peak of the loss modulus *G*" at 1 Hz and end of the frequency dependence of the storage modulus *G*'.[73,74] In the following vitrification is determined by using the peak of the loss modulus *G*".

7.1.3 Rheometer Measurement Assembly

All steady-shear rheology measurements were conducted on a Brookfield CAP 2000 of *Brookfield Engineering Laboratories Inc*. The parameters of the dynamic-shear rheology measurements are shown in Table 13.

Table 13: Parameters of steady-shear rheology measurements

Measurement Geometry	cone-plate
Cone Geometry	30 mm diameter, 45° angle
Shear rate	1330 s^{-1}

All dynamic-shear rheology measurements were conducted on a MCR 302 Rheometer of *Anton Paar GmbH*. The parameters of the dynamic-shear rheology measurements are shown in Table 14.

Table 14: Parameters of dynamic-shear rheology measurements

Measurement Geometry	plate-plate, diameter 25 mm
Shear gap	0.5 mm
Deformation	1%
Frequency	1 Hz

For all experiments the components were weighed separately according to the respective mixing ration 100 (epoxy resin) : 19 (hardener) : 2 (IMR) weight equivalents calculated for 2 g batch and subsequently mixed with a spatula for 30 s to provide a homogeneous mixture. Approx. 0.40 g of the mixed epoxy resin system was applied to the lower plate immediately afterwards. A constant sample weight of 0.25 g between the rheometer plates is given by the plate diameter and shear gap.

7.1.4 Interpretation of Rheological Data

An isothermal rheometry measurement in oscillation mode at 70°C of the curing reaction of epoxy resin system A is shown Figure 60. First accurate measured values for the storage modulus *G*' and the loss modulus *G*" are obtained at 205 s and 55 s respectively. The period of time up to the first accurate measured values is typical for this particular rheometry measurement setup which provides a compromise between an appropriate sensitivity over a large modulus magnitude. However, all important information is obtained to give a proper description of the viscoelastic behavior of the curing epoxy resin and to determine the related major transformations gelation and vitrification. As

stated above, the rheological gel point is determined by the crossover of *G*' and *G*", which occurs after 365 s curing time at 70°C. Vitrification is determined by the peak of *G*" and occurs after 524 s. Shortly after vitrification is observed, the storage modulus *G*' reaches a plateau and the crosslinking reaction has come to an end. This is in very good agreement to the previous results which have shown, that the crosslinking reaction dramatically decreases after vitrification.

The calculated complex viscosity η^* rises accordingly with progressing crosslinking reaction and also reaches a plateau shortly after vitrification.

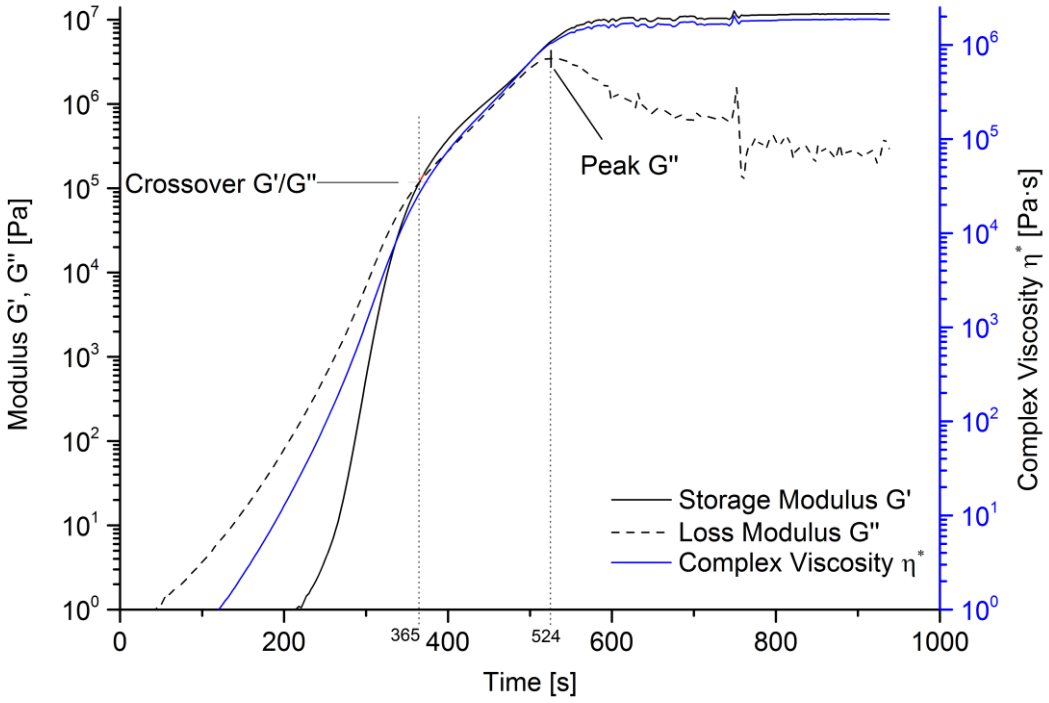

Figure 60: Measurement of storage modulus *G*' and the loss modulus *G*" and the calculated complex viscosity η^* of an isothermal rheometry measurement in oscillation mode at 70°C cure temperature of epoxy resin system A.

7.1.5 Results and Discussion of isothermal Rheometry Measurements

Rotation mode:

The progressing shear viscosities η of the crosslinking reaction of epoxy resins system A at isothermal cure temperatures 70, 80, 90, 100 and 110°C were measured in rotation mode and are shown in Figure 61. At higher cure temperatures the viscosity is increasing faster. The shear viscosity at η = 0.3 Pa·s was defined in an internal *BMW* specification as the maximum viscosity for proper epoxy resin injection in the HP-RTM process. The shear viscosity at η = 1.8 Pa·s is the maximum that can be measured reliably by the Brookfield rheometer and is taken as reference for the oscillatory determined complex viscosity η^*, which yields accurate values > 1.5 Pa·s.

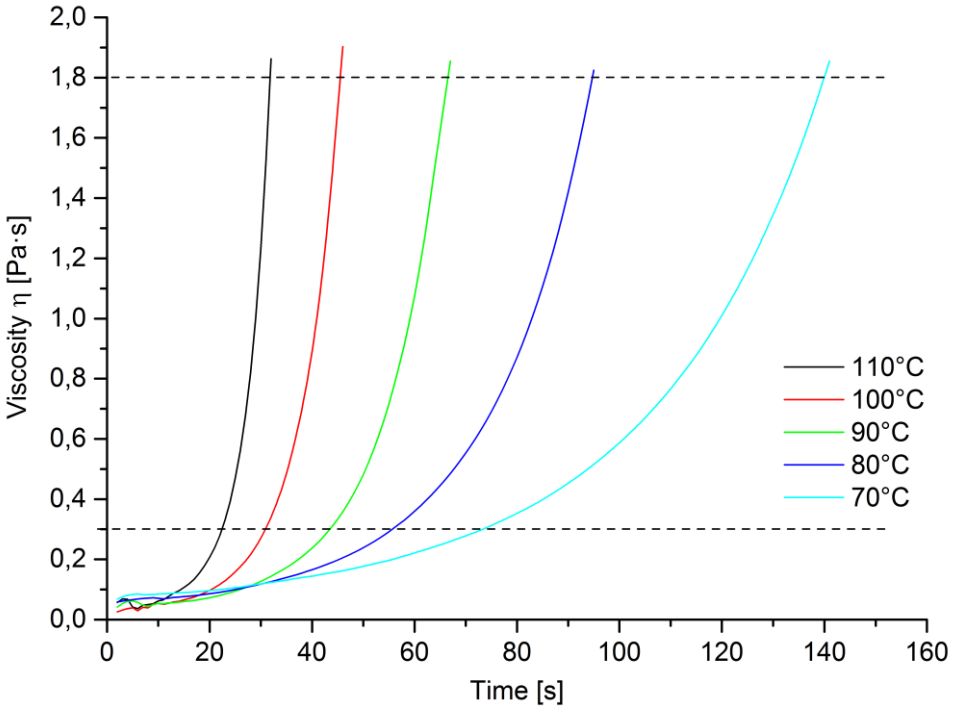

Figure 61: Measurements of the shear viscosity η in rotation mode of the curing reaction of epoxy resins system A at isothermal cure temperatures 70, 80, 90, 100 and 110°C.

The times at which η = 0.3 Pa·s and η = 1.8 Pa·s are reached at the respective isothermal cure temperature are listed in Table 15.

Table 15: Times at which η = 0.3 Pa·s and η = 1.8 Pa·s are reached at the respective isothermal cure temperatures.

Cure Temp.	70°C	80°C	90°C	100°C	110°C
$t_{0.3Pa\cdot s}$ [s]	74	58	45	32	23
$t_{1.8Pa\cdot s}$ [s]	140	95	66	45	31

Oscillation mode:

Because of the delay of the first accurate measurement points, a time-adjustment of the calculated complex viscosity η^* at 1.8 Pa·s was made with the shear viscosities η obtained from the ration mode measurements. With the help of the time-corrected complex viscosity η^*, a time correction of the actual measured storage modulus G' and the loss modulus G'' is achieved. The complex viscosity η^* were not used for further analysis of the curing characterization.

The measured storage modulus G' and the loss modulus G'' for isothermal cure temperatures at 70, 80, 90 and 100°C of epoxy resin system A is shown in Figure 62. At all cure temperatures gelation occurs

well before vitrification. The peak of *G*" is clear to see at all cure temperatures and as expected vitrification is also observed at 100°C cure temperature. This shows that the distance of $T_{g\infty}$ = 113°C is sufficiently high at 100°C cure temperature.

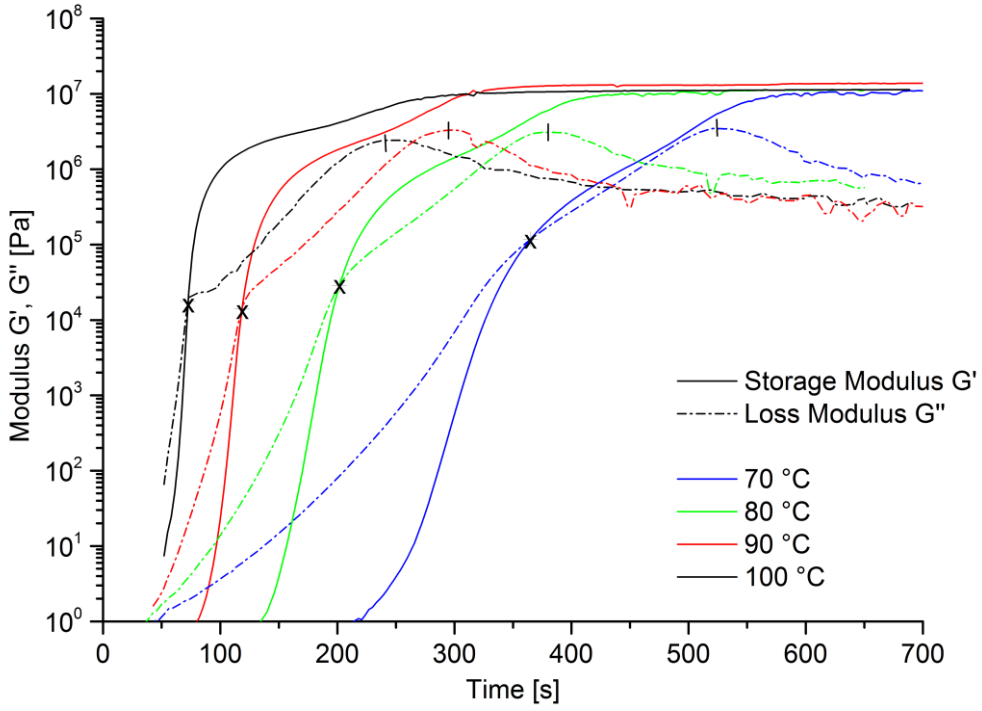

Figure 62: Measurements of storage modulus *G*' and loss modulus *G*" in oscillation mode of the curing reaction of epoxy resins system A at isothermal cure temperatures 70, 80, 90 and 100°C.

The gelation and vitrification times were determined as described above and are summarized in Table 16.

Table 16: Gelation and vitrification times of epoxy resin system A at isothermal cure temperatures.

Cure Temp.	70°C	80°C	90°C	100°C
Gelation (*G*'/*G*") [s]	365	201	118	72
Vitrification (Peak *G*") [s]	524	380	295	241

7.1.6 Comparison of Rheological Data with Kinetic Model Prediction, DSC and NIR-Spectroscopy Results

In the following the gelation and vitrification times determined by rheometry measurements are compared with the degrees of conversion and glass transition temperatures obtained by the prediction based on the DSC kinetic model, of the isothermal DSC experiments and of the isothermal NIR

spectroscopy. The respective degrees of conversion α at gelation times at 70, 80, 90 and 100°C cure temperature are summarized in Table 17.

The degrees of conversion α_{pred} of the prediction are in a range of 0.60 – 0.61 for all cure temperatures. These values are in very good agreement with literature values and the calculated theoretical value of 60% degree of conversion at the gel point, previously discussed in section 2.1.3.

The degrees of conversion at the gel point of the isothermal DSC measurement are higher than the calculated and literature values. The deviation increases with higher cure temperatures up to α_{exp} = 0.85.

The degree of conversion at the gel point obtained by isothermal NIR spectroscopy at 100°C is in good agreement with the calculated theoretical value. However at 80°C the degree of conversion is 12% higher than the calculated value.

Table 17: Gelation times obtained by rheometry measurements at 70, 80, 90 and 100°C cure temperature and the respective degrees of conversion α of the prediction based on the DSC kinetic model, of the isothermal DSC experiments and of the isothermal NIR spectroscopy.

Cure Temperature	70°C	80°C	90°C	100°C
Gelation Time (G'/G'')	365 s	201 s	118 s	72 s
α_{pred} DSC kinetic Model	0.61	0.60	0.60	0.60
α_{exp} isothermal DSC	0.69	0.77	0.73	0.85
α_{exp} isothermal NIR spectroscopy	-	0.72	-	0.61

The large deviation of the degrees of conversion of the isothermal DSC experiment at the gelation time compared to literature values for epoxy resins and the calculated theoretical value of α = 0.60 suggest that the isothermal DSC method is too inaccurate and erroneous for fast curing epoxy resins like those under investigation. The cut-off curves at the beginning of the measurements represent a major source of error. As a result of the cut-off curves, the reference of the baseline for the integration at the beginning of the exothermic signal is missing, which can lead to an incorrect evaluation of the enthalpy of reaction and therefore a wrong curve progression. In addition, the cut-off curves had to be reconstructed by mathematical means to provide the starting point of α = 0 at t = 0. The reconstruction does not necessarily resemble the true progression of the degree of conversion and can result in a temporal shift of the curves which in turn leads to a deviation.

For these reasons the isothermal DSC measurements are not included in the following evaluations and comparisons.

The predicted glass transition temperatures of the DSC kinetic model at the vitrification times obtained by rheometry are shown in Table 18. When vitrification is observed according to rheometry, the predicted glass transition temperature lies approx. 10 K below the cure temperature. This finding

shows that vitrification occurs quite early but it does not lead to an instant freeze of the polymerization reaction. It rather leads to a gradual deceleration of the reaction due to continuous rise of the glass transition temperature until the mobility of the polymer network is reduced to such an extent that the polymerization reaction becomes infinitely slow.

Table 18: Predicted glass transition temperatures of the DSC kinetic model at the vitrification times obtained by rheometry.

Cure Temperature	70°C	80°C	90°C	100°C
Time of Vitrification (G" Peak)	524 s	380 s	295 s	241 s
T_g Prediction DSC kinetic Model	58.6°C	70.0°C	80.4°C	88.7°C
Difference Cure Temp. and T_g	11.4 K	10.0 K	9.6 K	11.3 K

7.2 Online-Cure-Monitoring using Ultrasound at Laboratory Scale

7.2.1 Basic Working Principles of Ultrasonic Measurement System

The potential of ultrasound measurement to track the curing progress of epoxy resins is shown in the literature.[75–78]

For the investigation of the curing progress and curing behavior of epoxy resins, the ultrasonic impulse transmission method was used. The working principle is shown in Figure 63.

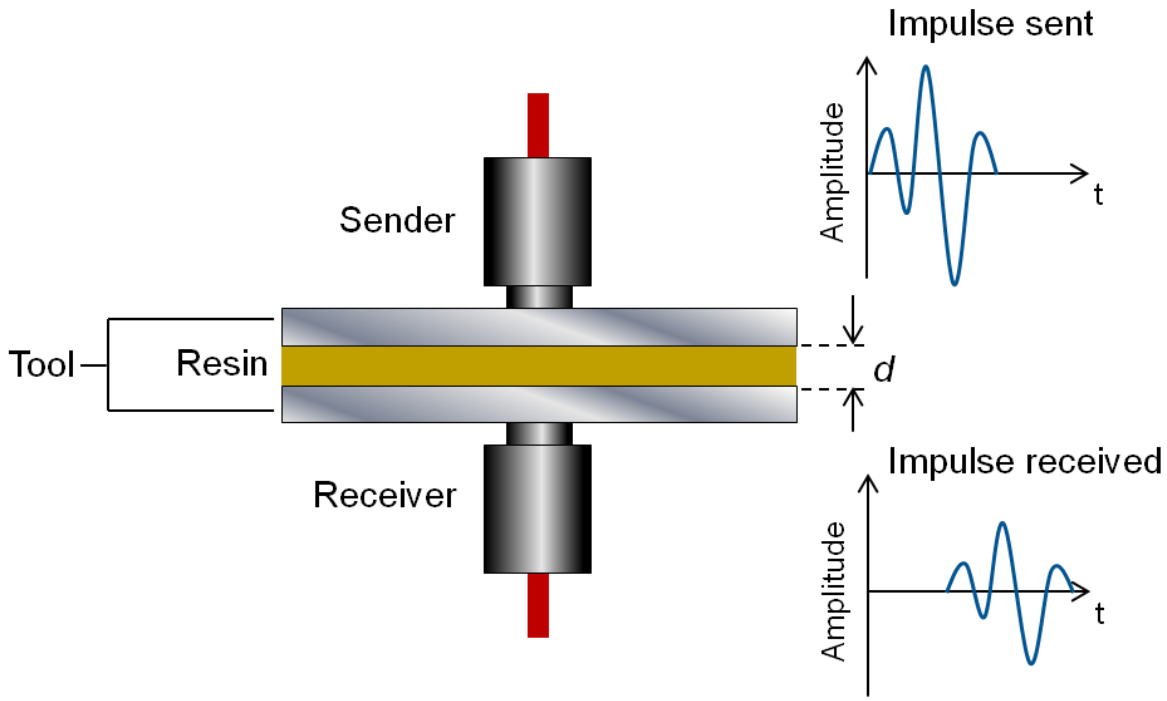

Figure 63: Working principle of the ultrasonic impulse transmission method.

An acoustic signal is transmitted from the sender to the receiver, whereby the transmission time Δt_{trans} and the amplitude are detected. With the known sample thickness d the sound velocity c can be calculated according to equation (37).

$$c = \frac{d}{\Delta t_{trans}} \tag{37}$$

The sound velocity of longitudinal waves in viscoelastic a material can be described by following,

$$c_L = \sqrt{\frac{L'}{\rho}} \tag{38}$$

where L' is the longitudinal modulus and ρ is the density of the material. [77]

The longitudinal modulus can be expressed as follows,

$$L' = K' + \frac{4}{3} G' \qquad (39)$$

where K' is the compression modulus and G' is the shear modulus.[77]

7.2.2 Ultrasonic Measurement Assembly for Laboratory Analysis

All experiments were conducted with the ultrasonic measurement system US-plus® by *Sensor- und Lasertechnik – Dr. Bohmeyer*. A small pneumatic press with a maximum pressure of 4 bar, shown in Figure 64, was used for the investigation of the curing behavior of the epoxy resin by ultrasound in the laboratory scale. The upper and lower plate of the press are heatable and each plate is equipped with an ultrasound sensor.

The employed ultrasound sensors are Type K4V1 sensors by General Electric with a middle frequency of 4.0 MHz and are temperature resistant up to 180°C. For all experiments a measuring interval of 1/s was used.

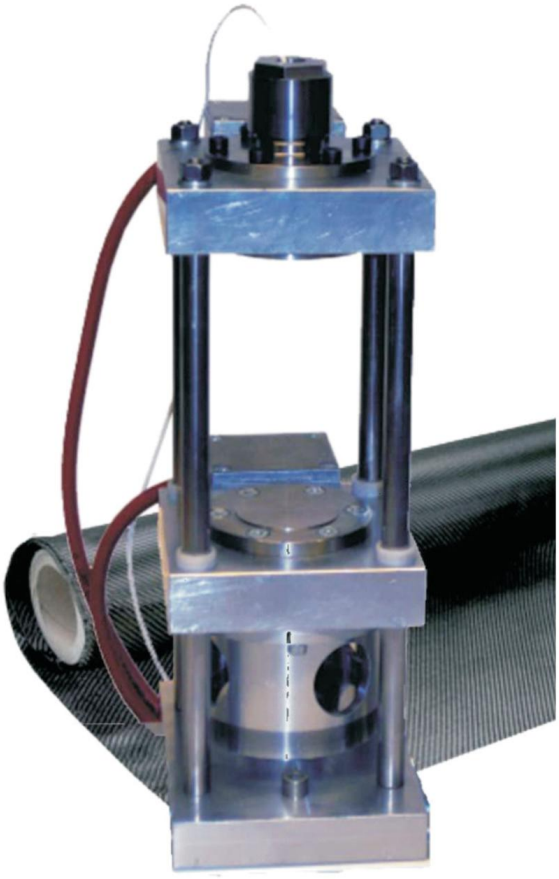

Figure 64: Pneumatic press with a maximum pressure of 4 bar with heatable upper and lower plate each equipped with an ultrasound sensor.

For all experiments the components were weighed separately according to the respective mixing ration 100 (epoxy resin) : 19 (hardener) : 2 (IMR) weight equivalents calculated for 5 g batch and subsequently mixed with a spatula for 30 s at room temperature to provide a homogeneous mixture. Approx. 0.4 g of the mixed epoxy resin system was applied to the lower plate of the preheated press and the press was closed immediately afterwards. The sample height is 1.4 mm and the sample diameter is 20 mm.

7.2.3 Interpretation of Cure Behavior Using Ultrasound

Figure 65 shows the progression of the sound velocity at isothermal curing conditions at 90°C and the according normalized sound velocity. The absolute values of the sound velocity are determined by the mechanical properties of the epoxy resin, i.e. the harder the epoxy resin, the higher the sound velocity. Due to progressing crosslinking reaction a dense network is developed and the modulus of the material increases resulting in a higher mechanical strength. A short drop of the sound velocity is observed at the beginning of the measurement with its minimum at 14 s. This is where the epoxy resin which is initially at room temperature is heated in the preheated press and softens. After that, the progressing crosslinking reaction leads to an increase of the sound velocity due to the increasing modulus. When

the polymerization reaction is done or the reaction comes to halt due to vitrification the sound velocity reaches a plateau. Similar to rheometry the sound velocity measures a mechanical parameter and not the degree of conversion directly, i. e. when the sound velocity reaches a plateau this is not correlated to a fully cured resin but only means that no polymerization reaction can be observed. This either happens due to vitrification or after complete conversion. The absolute sound velocity reached at the plateau is affected by the temperature. In general, a fully cured epoxy resin is softer at higher temperatures and therefore the sound velocity will be lower despite the same crosslinked network. This can also be compared with the transition of an epoxy resin from the vitrified state at which $T < T_g$ to the gel rubber state at which $T > T_g$. The normalization was conducted to eliminate the scattering of the absolute sound velocity due to temperature effects and to provide a better interpretation of the ultrasound data and comparability with other methods. As explained, the normalized values are not identical to the degree of conversion α.

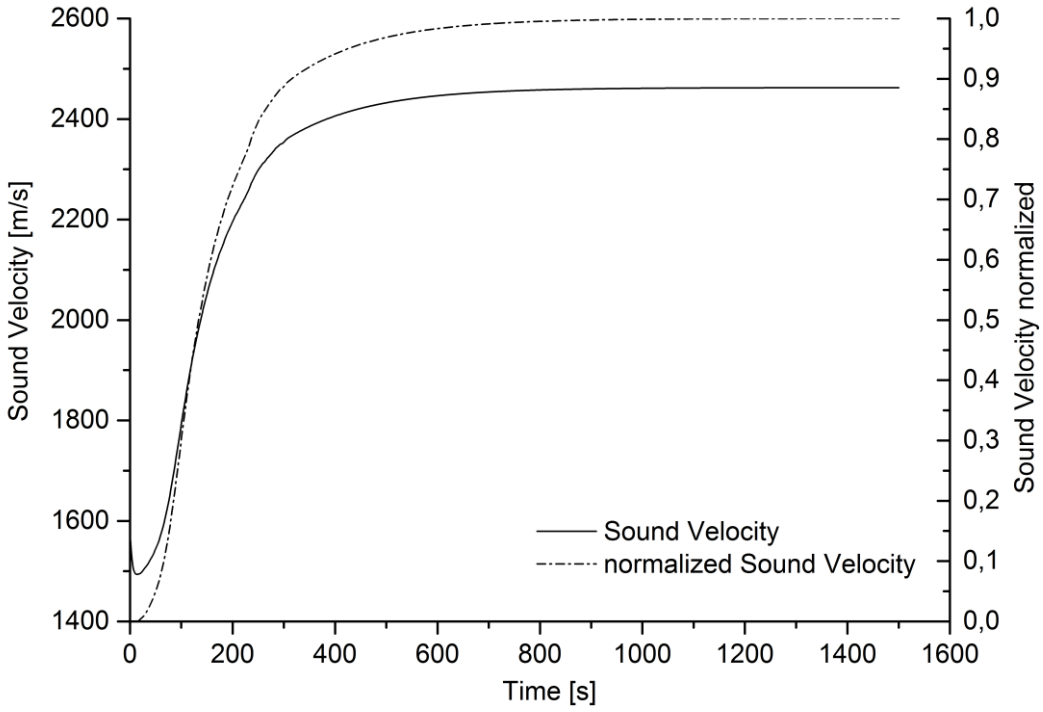

Figure 65: Progression of the sound velocity and normalized sound velocity at 90°C.

7.2.4 Results and Discussion of Ultrasound in Laboratory Analysis

The progressions of the absolute sound velocities of ultrasound laboratory measurements at isothermal cure temperatures 70, 80, 90, 100 and 110°C are shown in Figure 66. The effect of initial softening and the associated decrease of the sound velocity at the beginning is more pronounced at higher

temperatures and no longer observable at 70°C. Due to the immediately starting crosslinking reaction after applying the epoxy resin in the preheated press the modulus directly increases and compensates for the softening of the epoxy resin. At higher temperature the crosslinking reaction is faster which is reflected in a steeper and faster rise of the sound velocity at high temperatures and a later reached plateau at lower temperatures. The different final values of the sound velocity after reaching the plateau, i .e. when no polymerization reaction is observable, can be explained by the respective reached glass transition temperatures and the cure temperature. On the one hand, the reached glass transition temperature is higher at higher cure temperature and correspondingly, the mechanical strength. On the other hand, the epoxy resin is softer at higher temperatures. This leads to the distribution of the final sound velocity values $c_{80°C} > c_{90°C} > c_{100°C} > c_{110°C}$. At 70°C the resulting network formation is significantly lower resulting in a final sound velocity lower than $c_{80°C}$ and $c_{90°C}$.

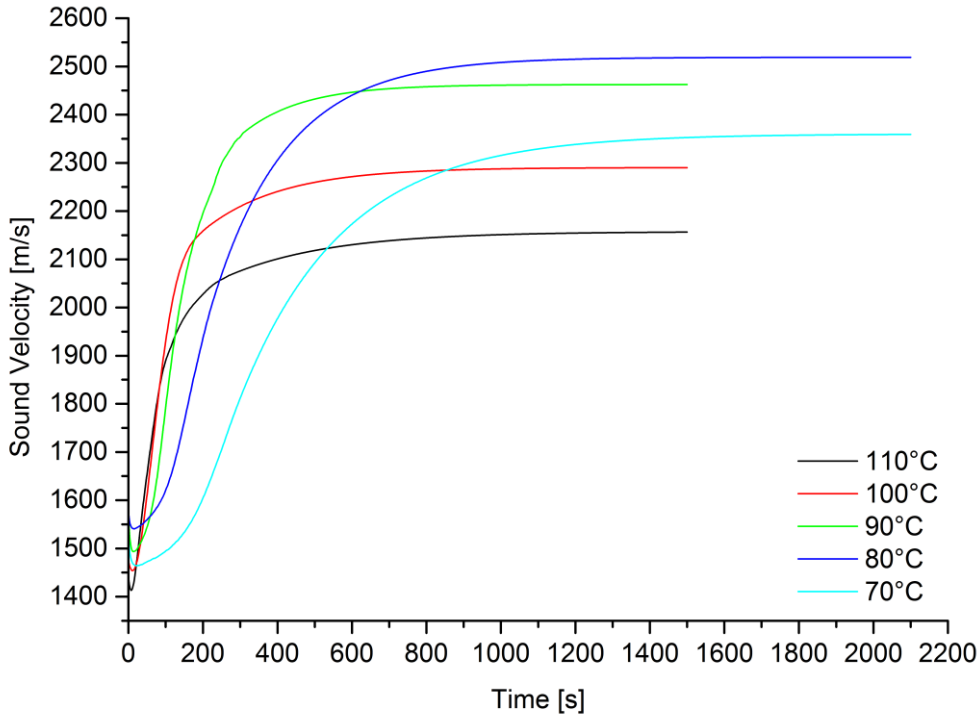

Figure 66: Progressions of the absolute sound velocities of ultrasound laboratory measurements at isothermal cure temperatures 70, 80, 90, 100 and 110°C.

The respective normalized sound velocities of the isothermal curing measurements are shown in Figure 67. The increasing speed of the crosslinking reaction at higher temperatures is also shown by the normalized curves. As could be seen in the previous isothermal DSC measurements and the prediction of the curing progress based on the DSC kinetic model, the acceleration of the reaction speed decreases with higher temperatures, which is shown in the almost identical curves at 100°C and

110°C. Also the curve at 90°C is not much slower. This confirms the findings from previous experiments, that the reaction speed increase is limited at higher temperatures.

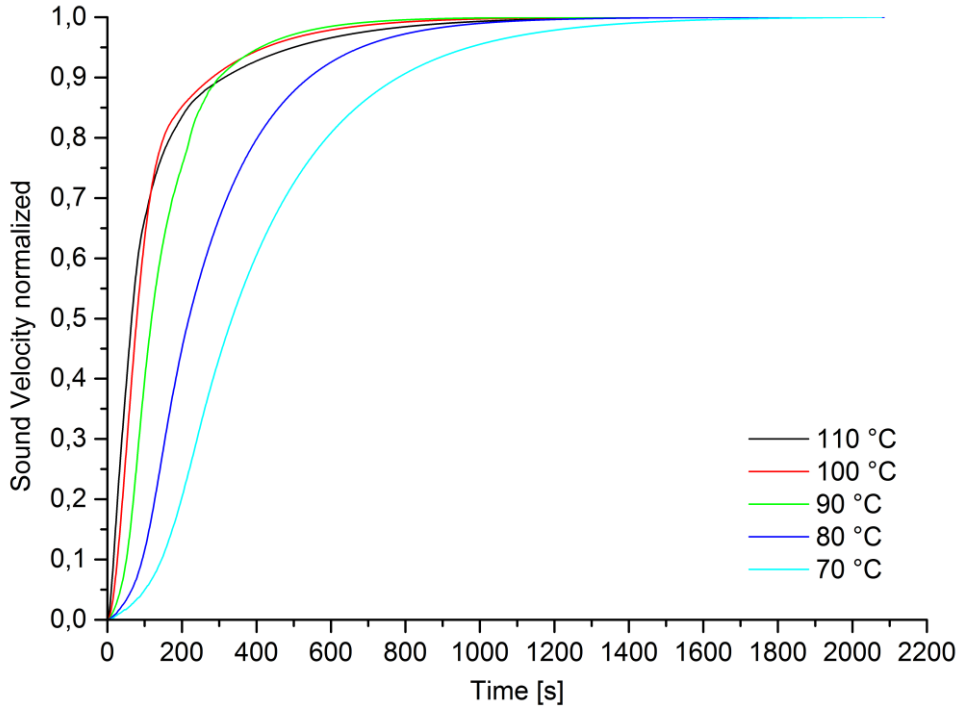

Figure 67: Normalized sound velocities of ultrasound laboratory measurements at isothermal cure temperatures 70, 80, 90, 100 and 110°C.

7.2.5 Interpretation of Sound Velocity using Rheometry and DSC Kinetic Model

The progression of the absolute sound velocities for cure temperatures of 70 – 100°C with the respective marks for the gelation and vitrification times, derived by rheometry measurements, is shown in Figure 68. The respective values of the degree of conversion α and the glass transition temperature T_g are derived by the prediction of the DSC kinetic model. It can be observed that gelation occurs approximately in the middle of the steepest increase of the sound velocity at all cure temperatures. According to this finding, gelation occurs at the highest turnover rate. At the time of vitrification determined by rheometry, the ultrasound measurements show a clear deceleration of the reaction indicated by the slower increase of the sound velocity. As already discussed, vitrification does not lead to an instant freeze of the reaction, which is also demonstrated by the further increase of the sound velocity and the degree of conversion and the glass transition temperature predicted at the end of the measurement. This finding is in agreement with the previous results.

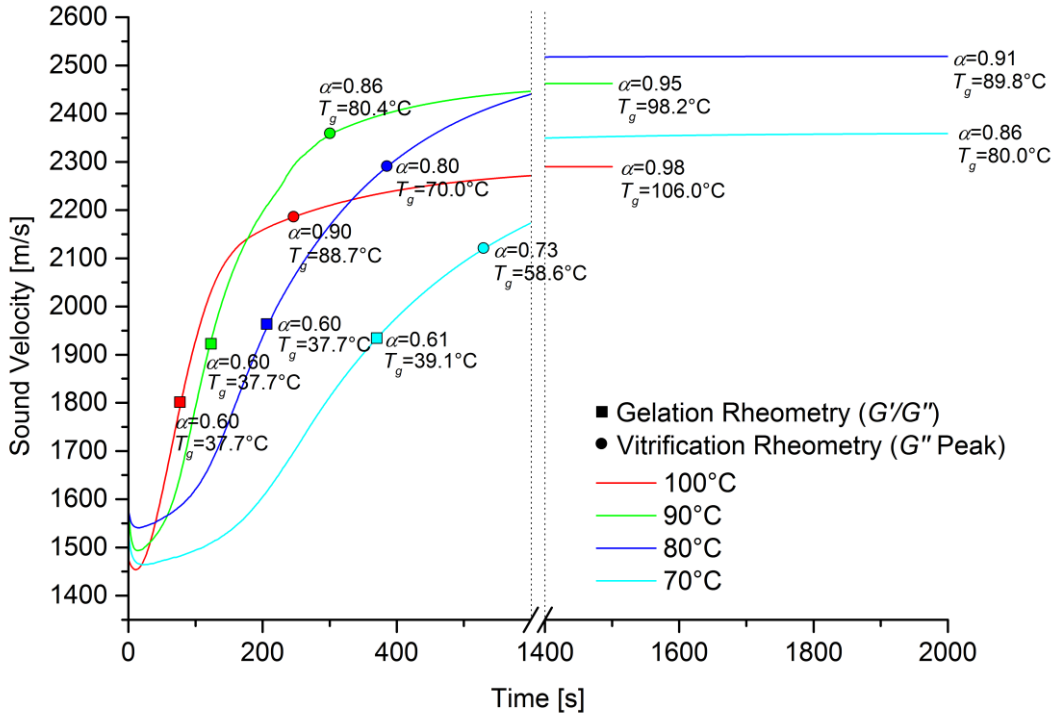

Figure 68: Progression of sound velocities from 70 – 100°C cure temperature with the respective marks for the gelation and vitrification times and the respective degrees of conversion and glass transition temperatures at gelation, vitrification and the end of the ultrasound measurements according to the cure prediction based on the DSC kinetic model.

As explained above, the normalized sound velocities do not represent the degree of conversion automatically. Especially at low temperatures a plateau of the absolute sound also occurs, despite the fact that 100 % conversions cannot be reached at these temperatures. This is because ultrasound is a mechanical analysis technique and only shows the qualitative progress of the crosslinking reaction but not the quantitative conversion. The same applies for rheometry. However, the experimental DSC results show, that the crosslinking reaction at 90°C and 100°C reaches a degree of conversion of $\alpha = 0.98$ and $\alpha = 1.00$ respectively. Based on the assumption, that the crosslinking reaction progresses to the same degrees of conversion in the ultrasound measurements in the laboratory, a direct correlation of the progression of the normalized sound velocity and the degree of conversion is made.

Figure 69 shows the normalized sound velocity obtained by a laboratory ultrasound measurement and the progress of the degree of conversion α according to the prediction of the DSC kinetic model at 90°C cure temperature. The marked gelation and vitrification times are derived by rheometry measurement. It can be observed that the normalized sound velocity starts to rise slowly first and begins to rise much more at $\alpha = 0.2$. This finding can be explained by the behavior of the sound velocity in liquids. As stated in equations (38) and (39) the sound velocity is influence by the compression modulus K' and the shear modulus G'. In liquids $G' = 0$ and only K' is taken into account.

With progressing network formation the liquid character of the epoxy resin decreases and the material tends to a gel like behavior and $G' > 0$. The increase of the shear modulus results in a better transmission of the acoustic signal and a steeper increase of the sound velocity is observable. Gelation occurs at 0.50 of the normalized sound velocity. Vitrification occurs at 0.90 of the normalized sound velocity and the increase of the sound velocity clearly slows down. This is also observed for the predicted degree of conversion. According to the prediction, the reaction is not fully completed and a degree of conversion of 0.94 is reached. The qualitative curve progression of the predicted degree of conversion and the normalized sound velocity shows a good correlation.

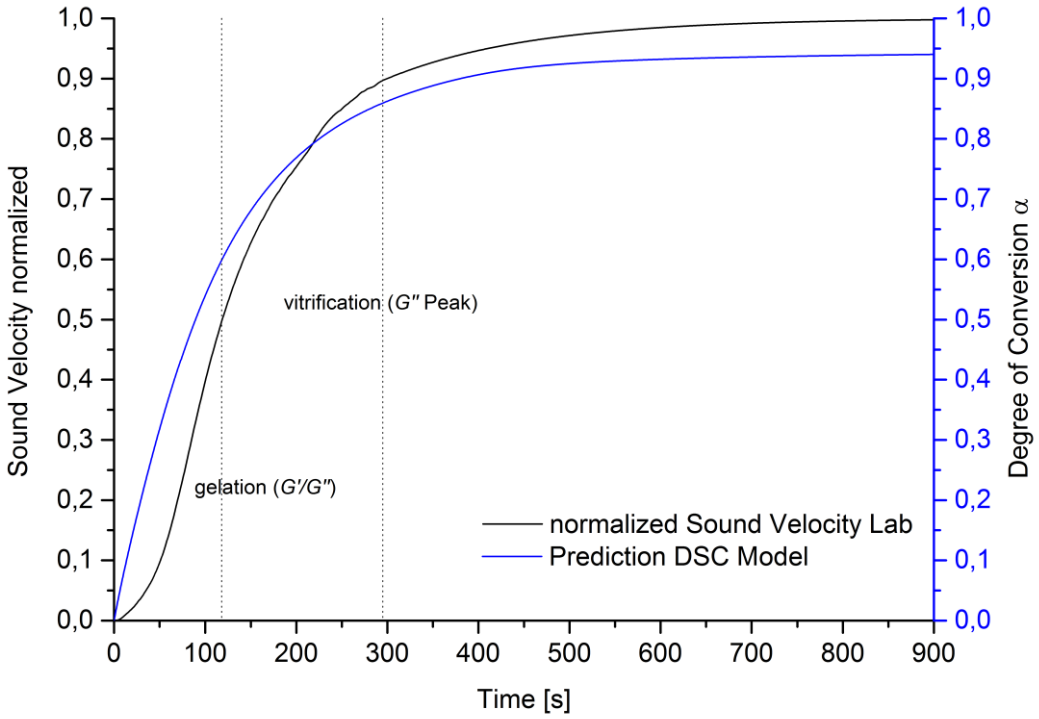

Figure 69: Normalized sound velocity of laboratory ultrasound measurement compared to the degree of conversion α according to the prediction of the DSC kinetic model at 90°C cure temperature. The marked times for gelation and vitrification are derived by rheometry measurements at 90°C cure temperature.

The normalized sound velocity obtained by a laboratory ultrasound measurement and the prediction of the degree of conversion α according to the DSC kinetic model at 100°C cure temperature is shown in Figure 70. The marked gelation and vitrification time are derived by rheometry measurement. The delay of the increase of the normalized sound velocity at the beginning of the measurement is only apparent very small at 100°C, showing that the polymerization reaction proceeds much faster than at 90°C. The progressions of both curves show a very good correlation. Gelation occurs at 0.47 of the normalized sound velocity and vitrification at 0.88 which is comparable to the values obtained at 90°C. After vitrification the increase of the normalized sound velocity is clearly lower again. The lower rise

of the sound velocity after vitrification at 100°C compared to 90°C cure temperature can be explained by less sharp vitrification because the cure temperature is nearer the glass transition temperature of the fully cured resin $T_{g\infty}$ = 113.1°C. This allows a higher rest mobility of the functional groups and therefore a longer curing reaction. The final degree of conversion according to the prediction is 0.98. This is in accordance with the normalized sound velocity which shows a slight increase at the end of the measurement indicating that the reaction is not fully completed.

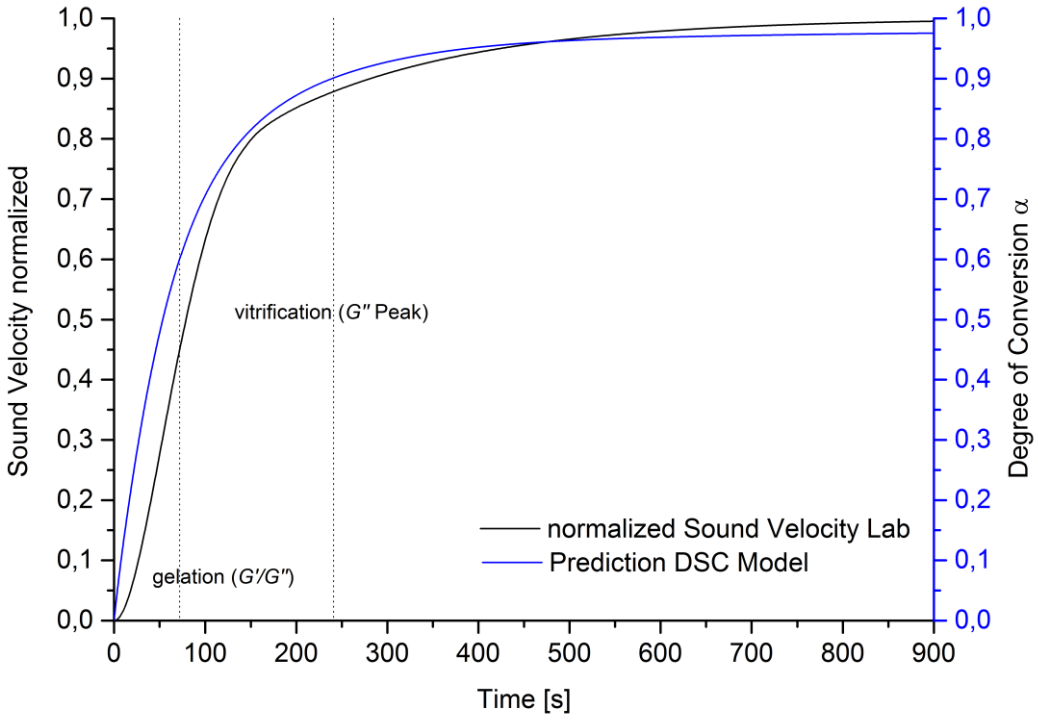

Figure 70: Normalized sound velocity of laboratory ultrasound measurement compared to the degree of conversion α according to the prediction of the DSC kinetic model at 100°C cure temperature. The marked times for gelation and vitrification are derived by rheometry measurements at 100°C cure temperature.

7.3 Online-Cure-Monitoring in RTM-Process using Ultrasound

7.3.1 Ultrasonic Measurement Assembly for Online-Cure-Monitoring in a Large Scale RTM-Mould

The ultrasound measurements for online-cure-monitoring in the HP-RTM process were conducted with a plate tool (PT) with the size 520 x 520 mm shown in Figure 71. Although the used plate tool is not for serial production, the complete processing is similar to it. A two component injection system is used with two separated and heatable tanks. One tank contains the epoxy resin in which the internal mould release agent is added and stored at 65°C. The other tank contains the epoxy resin hardener and is stored at 30°C. These temperature conditions are required to reduce the viscosity of the resin and ensure a proper infiltration of the carbon fiber fabric placed in the mould and sufficient injection time to fill the mould completely. For all ultrasound measurements in the HP-RTM plate tool an injection time of 20 s is realized. Due to structural limitations of the sensor placement in the mould only two ultrasound sensor pairs were placed in the mould at the most diverse positions. One ultrasound sensor pair 1 (channel 1) is placed near the injection port and the second ultrasound sensor pair 2 (channel 2) is placed in the center of the right edge of the plate. The resin flows from the injection port via the distribution channel from the middle of the mould to the outer edges. Due to the distribution channel the resin reaches the front and the back edge much earlier and the left and right edge and the corners are filled at last. Thereby the injected resin is pressed from the middle of the mould to the rim by the constantly injected resin. This has the consequence, that the resin at channel 2 is approx. 15 s longer in the heated mould and fabric and has more time to react than the resin injected at the end.
The used carbon fiber fabric is a unidirectional stack consisting of 6 layers and the final plate thickness is 2.2 mm yielding a fiber volume fraction of approx. 50%.

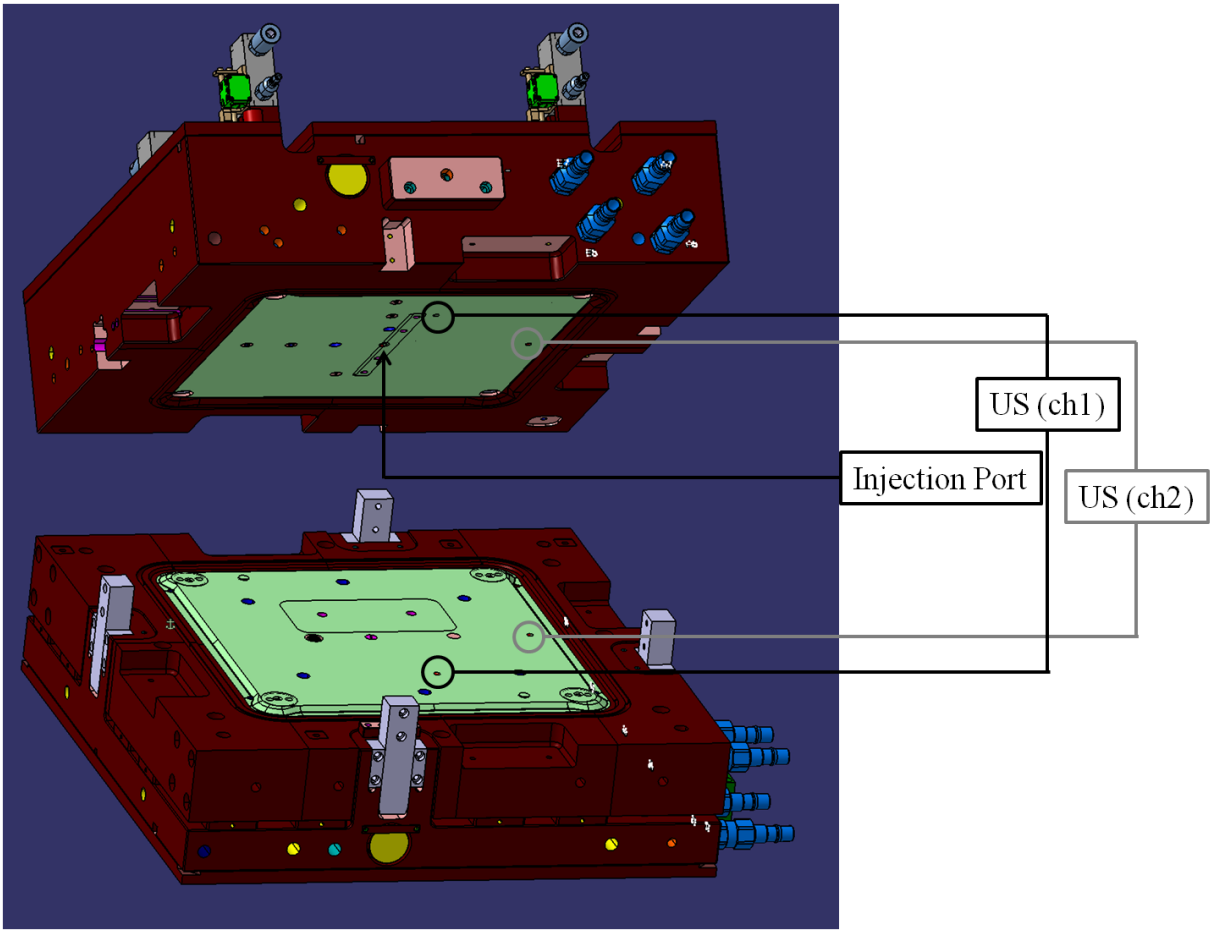

Figure 71: HP-RTM plate tool (PT) (520 x 520 mm) with injection port and distribution channel and the sensor positions of ultrasound sensor pair 1 (channel 1) and ultrasound sensor pair 2 (channel 2).

7.3.2 Results and Discussion of Ultrasound in HP-RTM Process

As was observed in NIR spectroscopy measurements, the temperature of the epoxy resin sample can increase due to the exothermic polymerization reaction. The increase of the temperature depends on the one hand on the cure temperature, and is higher at higher temperatures due to an acceleration of the polymerization reaction and more heat of reaction is released in a shorter time. On the other hand the thermal conductivity properties and the heat capacity of the sample environment play an important role. As in the RTM process the epoxy resin cures in a dense network of carbon fibers which have good thermal conductivity, the self-heating of the epoxy resin is limited due to heat dissipation effects. However, reliable temperature profiles of the curing reaction of the epoxy resin in the RTM process could not be obtained as the introduced thermocouples are constantly being sheared off by the tool sealing. From experience it can be said that the temperature of the investigated epoxy resin systems during curing in the RTM process does not exceed the cure temperature higher than 5 – 10°C.

The progression of the sound velocity measured at channel 1 in the plate tool with unidirectional carbon fiber fabric at 80, 90 and 100°C cure temperature are shown in Figure 72. As explained in the

ultrasound measurements in the laboratory scale, the reached final sound velocity value depends on the cure temperature and is higher for lower temperatures. The speed of the crosslinking reaction indicated by the change of the sound velocity is faster for higher temperatures and can be distinguished well by the normalized sound velocities.

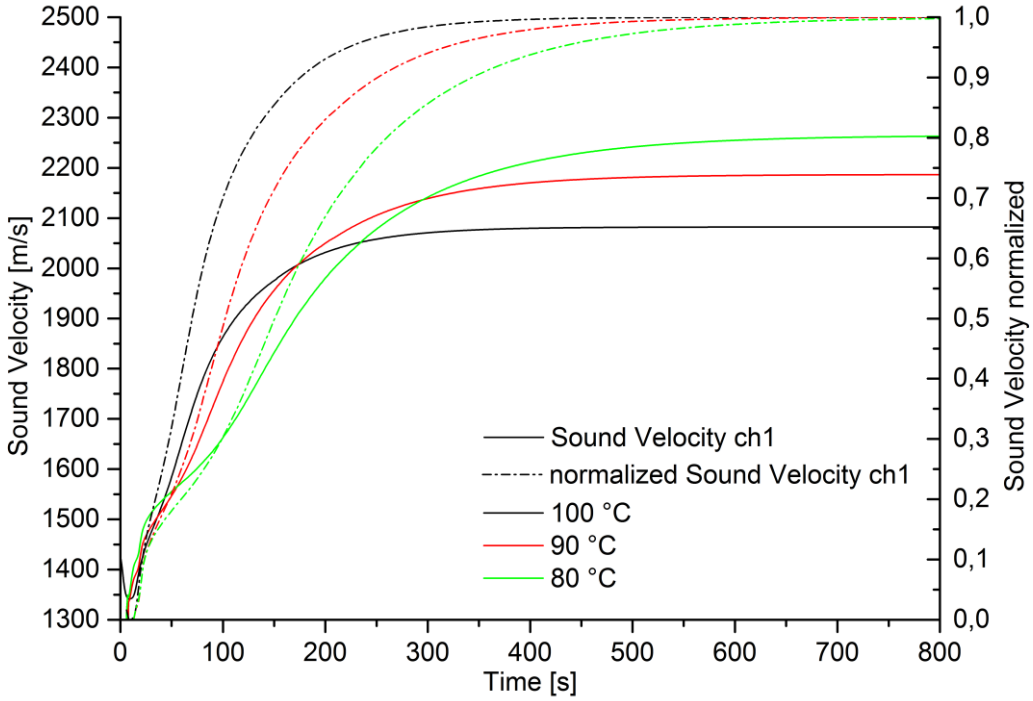

Figure 72: Measured sound velocity at channel 1 and the associated normalized sound velocity during the curing of epoxy resin system A at 80, 90 and 100°C cure temperature.

The progression of the sound velocity of the second ultrasound sensor (channel 2), placed at the edge of the plate tool, is shown in Figure 73. The distribution of the absolute sound velocities is identical to channel 1 and higher at lower cure temperatures. The different of the absolute sound velocities can of channel 2 compared to channel 1 can be explained by the great difficulty of an exact sensor placement in the tool, and small deviations lead to a falsification of the sensor calibration. However, this is a systematical error and has no influence on the qualitative sound velocity measurement. Also, this deviation is erased by normalizing the sound velocities. The crosslinking reaction according to the normalized sound velocities progresses almost similar to the measurements of channel 1.

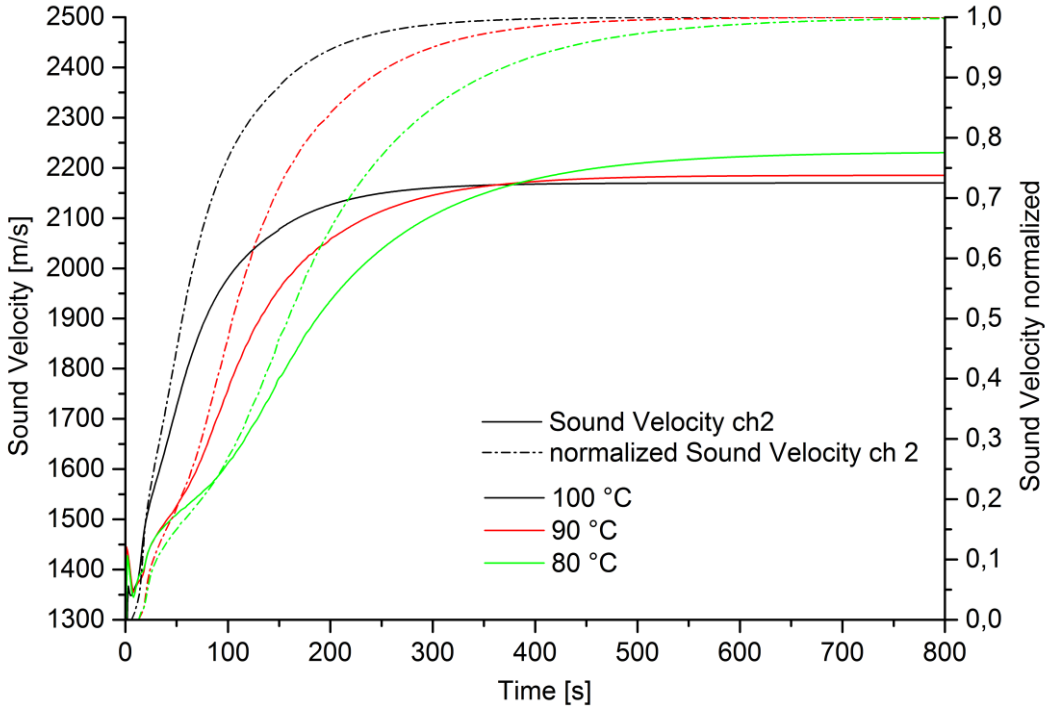

Figure 73: Measured sound velocity at channel 2 and the associated normalized sound velocity during the curing of epoxy resin system A at 80, 90 and 100°C cure temperature.

The comparison of the progression of the measured sound velocities of channel 1 and channel 2 and the associated normalized sound velocities at 100°C cure temperature is shown in Figure 74. It can be observed that the sound velocity at channel 2 rises earlier than measured at channel 1. Also the end of the curing reaction, indicated by the reached plateau, is detected earlier at channel 2. This is very apparent from the normalized sound velocity. This finding is in agreement with the sensor positions. As described above, the injected epoxy resin is pushed through the mould and has time to react during infiltration. As channel 2 is at the edge of the mould, the approaching epoxy resin has time to heat up in the mould with the carbon fiber fabric as good heat conductor and the crosslinking reaction starts immediately. The resin which is injected at the end of the injection time has 20 s less time to for conditioning and reacting. The part of the injected epoxy resin which is measured at channel 1 has approx. 15 s less time than the resin measured at channel 2, which explains the difference in the progression of the sound velocity.

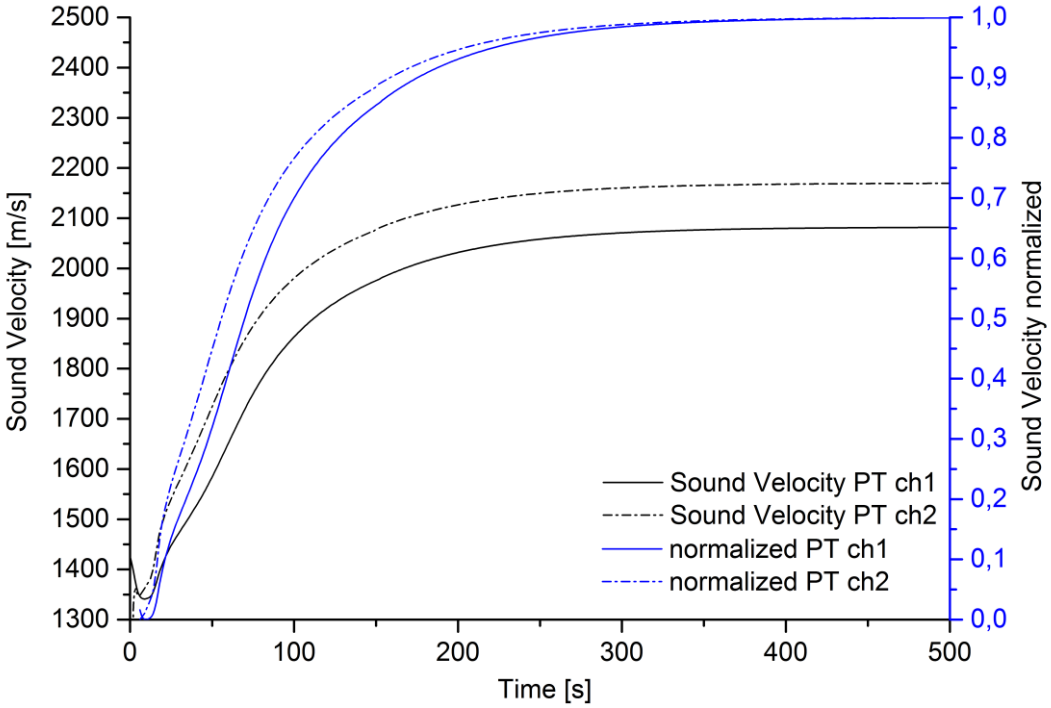

Figure 74: Comparison of measured sound velocities at channel 1 and channel 2 and the associated normalized sound velocity during the curing of epoxy resin system A at 100°C cure temperature.

7.3.3 Comparison with Laboratory Ultrasound Measurements

The comparison of the progression of the normalized sound velocities measured in the laboratory and in the HP-RTM process at 80, 90 and 100°C cure temperature is shown in Figure 75. The discrepancy of the progression of the normalized sound velocities measured in the plate tool (PT) in the HP-RTM process is due to the sensor position as explained above. The change of the sound velocity occurs faster in the HP-RTM process for all temperatures compared to the laboratory measurements. Also the plateau of the sound velocity is reached earlier.

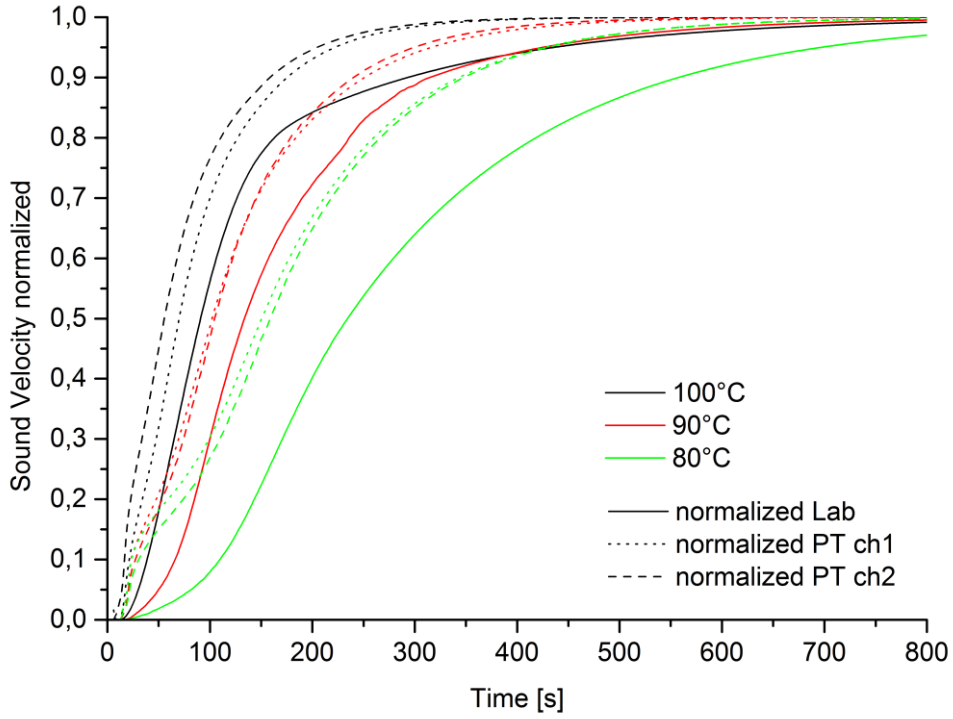

Figure 75: Comparison of normalized sound velocities measured in the laboratory (Lab) and in HP-RTM process (ch 1 and ch2) at 80, 90 and 100°C cure temperatures.

Several effects may be the cause for this different progression of the normalized sound velocities in the laboratory and the HP-RTM process. One influencing factor is the different initial temperature of the epoxy resin. In the HP-RTM process the epoxy resin component and the amine hardener are preheated at 65°C and 30°C to reduce the resin viscosity and provide a better infusion. The epoxy resin used for laboratory ultrasound measurements was mixed at room temperature and afterwards put in the laboratory press. Another influence is the different sample heating. In the process a carbon fiber fabric is inserted in the mould and heated 1 min prior to injection. At the time of injection, the fabric has the same temperature as the mould. Through the huge surface of the dense carbon fiber network and the good thermal conductivity of the carbon fiber fabric a very good and fast heat transfer to the injected epoxy resin is provided. The epoxy resin in the laboratory press is only heated by the upper and lower plate. Also the homogeneity of the mixed epoxy resin is a critical factor for the speed of the crosslinking reaction. A homogenous mixture provides a stoichiometric distribution of resin and hardener molecules which facilitates the crosslinking reaction and creates an optimal polymer. In a non-homogenous mixture, areas with an excess of the epoxy resin component or the hardener are present resulting in a non-optimal crosslinking reaction, and diffusion effects of the monomers delay the reaction. In the HP-RTM process the epoxy resin components are injected in a mixing head with high pressure to provide a homogenous mixture. During the injection in the mould, the epoxy resin is additionally mixed by pushing it through the dense carbon fiber fabric. In the laboratory measurements

the epoxy resin system was mixed by hand with a spatula for 30 s. Even when the mixing time is longer, the mixing quality of the HP-RTM process cannot be reached.
It is also unclear whether the carbon fiber itself has an influence on the crosslinking reaction in terms of catalytic or inhibiting effects.

7.3.4 Comparison with DSC Kinetic Model and Rheometry

The comparison of the normalized sound velocities of channel 1 and channel 2 and the degree of conversion α according to the prediction based on the DSC kinetic model at 90°C cure temperature is shown in Figure 76. The marked times for gelation and vitrification are derived by the results of the rheometry measurements. The progression of the normalized sound velocity of channel 1 and channel 2 and predicted degree of conversion show a very good correlation. Gelation occurs at 0.65 of the normalized sound velocity of channel 1 and channel 2, which is close to the prediction and the theoretical and calculated value of the gel point α = 0.60. Vitrification occurs at 0.95 of the normalized sound velocity for both ultrasound channels.

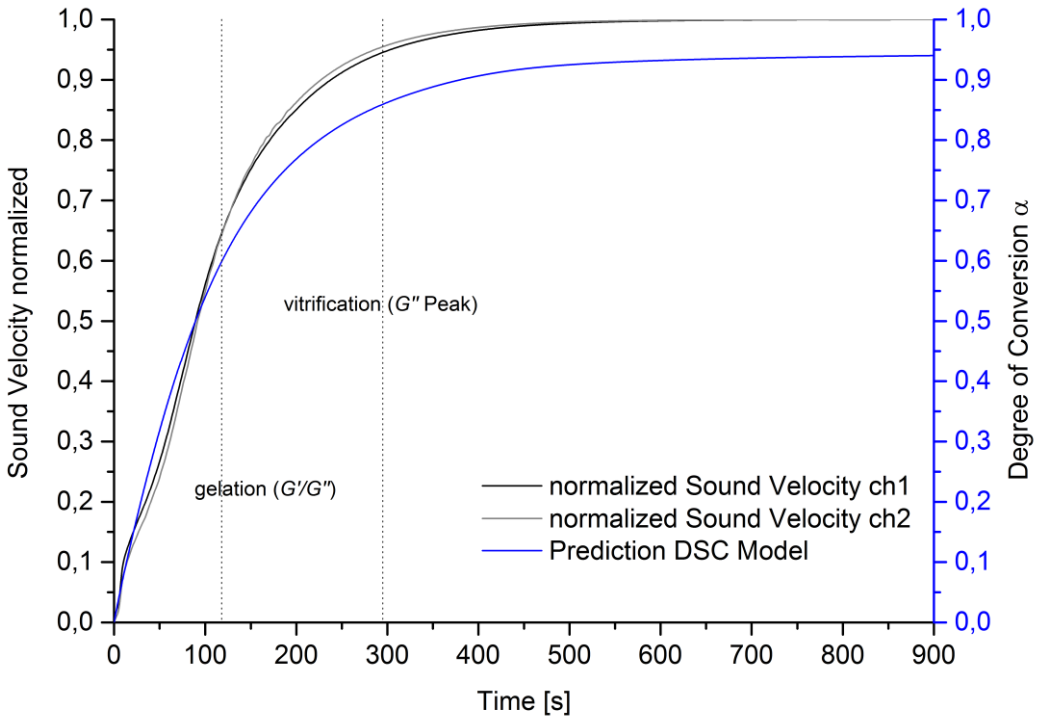

Figure 76: Normalized sound velocities of channel 1 and channel 2 compared to the degree of conversion α according to prediction based on the DSC kinetic model at 90°C cure temperature. The marked times for gelation and vitrification are derived by rheometry measurements at 90°C cure temperature.

It should here be pointed out again that 1.0 of the normalized sound velocity does not automatically resemble a degree of conversion α of 1.0. This means that the normalized sound velocity has to be

calibrated to the respective degree of conversion by appropriate means. The calibration of the normalized sound velocity value 1.0 of channel 1 and channel 2 of the HP-RTM measurement at 90°C with the final value of the predicted degree of conversion $\alpha = 0.94$ was conducted and shown in Figure 77. The calibration of the final value alpha with the normalized sound velocity value 1.0 shows even more the very good correlation of the progress of the sound velocity and the prediction.

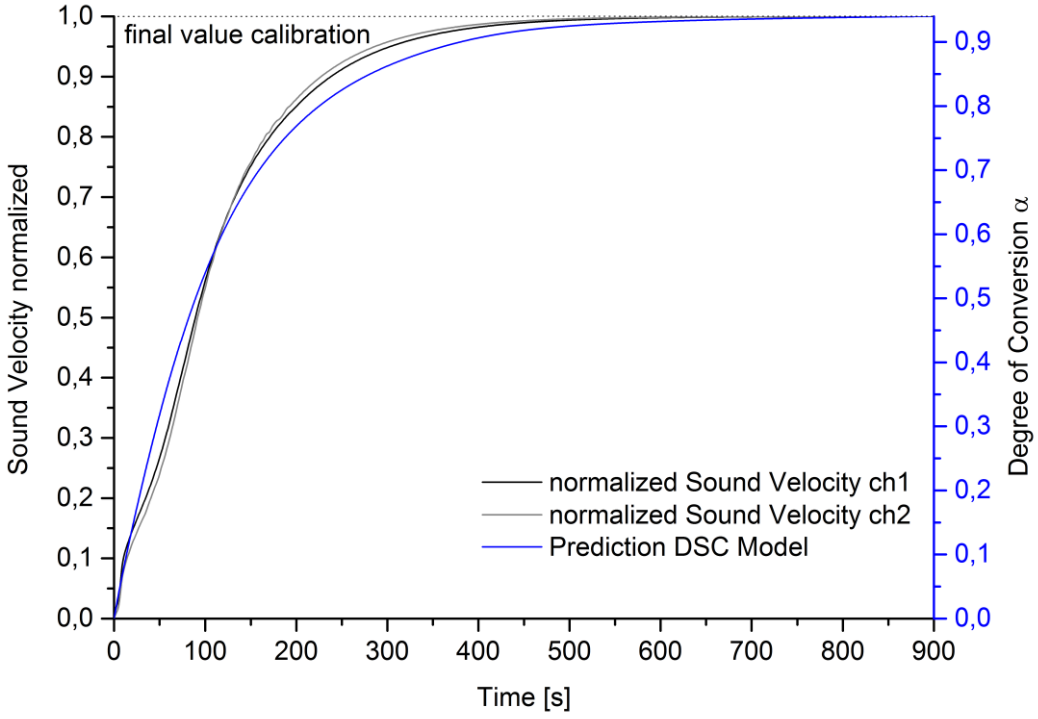

Figure 77: Calibration of the normalized sound velocity value 1.0 of channel 1 and channel 2 to the final degree of conversion degree of conversion α according to the prediction of the DSC kinetic model at 90°C cure temperature.

The comparison of the normalized sound velocities of channel 1 and channel 2 and the degree of conversion α according to the prediction based on the DSC kinetic model at 100°C cure temperature is shown in Figure 78. The marked gelation and vitrification times are derived by rheometry measurement. A very good correlation of the predicted progress of the degree of conversion and of the normalized sound velocities of channel 1 and channel 2 is observable. Gelation occurs at 0.55 of the normalized sound velocity for channel 1 and at 0.65 for channel 2, which is close to the prediction and the theoretical and calculated value of the gel point $\alpha = 0.60$. Vitrification occurs at 0.95 of the normalized sound velocity for both ultrasound channels, which is identical to the value at 90°C cure temperature.

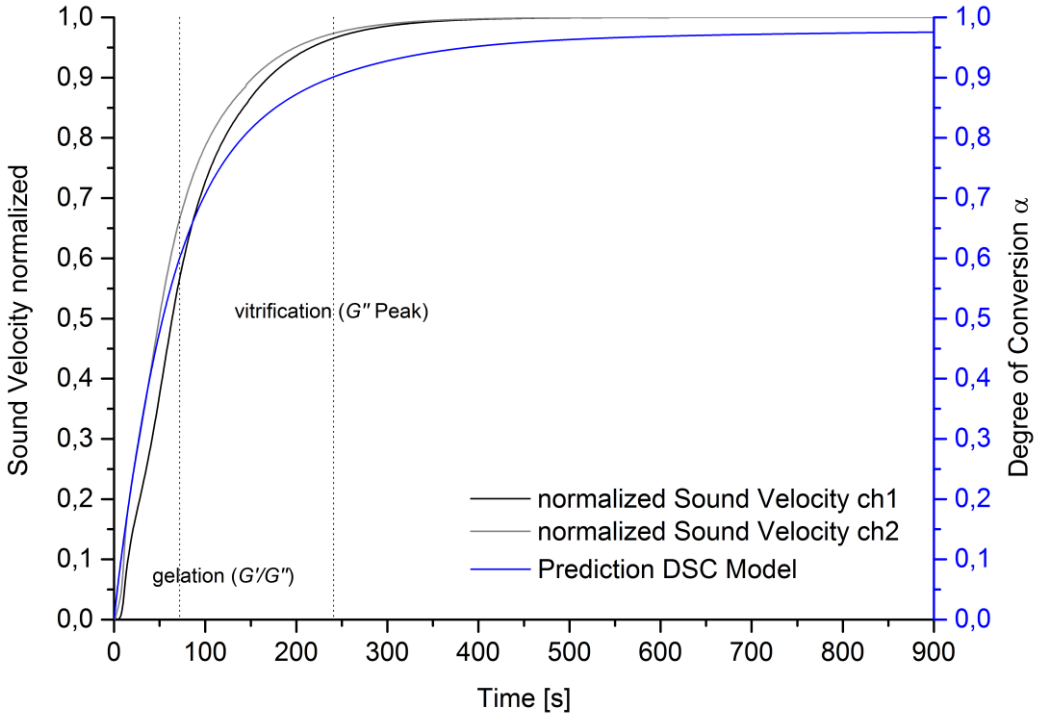

Figure 78: The normalized sound velocities of channel 1 and channel 2 compared to the degree of conversion α according to isothermal DSC measurement, prediction based on the DSC kinetic model and isothermal NIR spectroscopy at 100°C cure temperature. The marked times for gelation and vitrification are derived by rheometry measurements at 100°C cure temperature.

The calibration of the normalized sound velocity value 1.0 of channel 1 and channel 2 of the HP-RTM measurement at 100°C with the final value of the predicted degree of conversion $\alpha = 0.98$ was conducted and is shown in Figure 79. Again, the calibration shows a very good agreement of the curves.

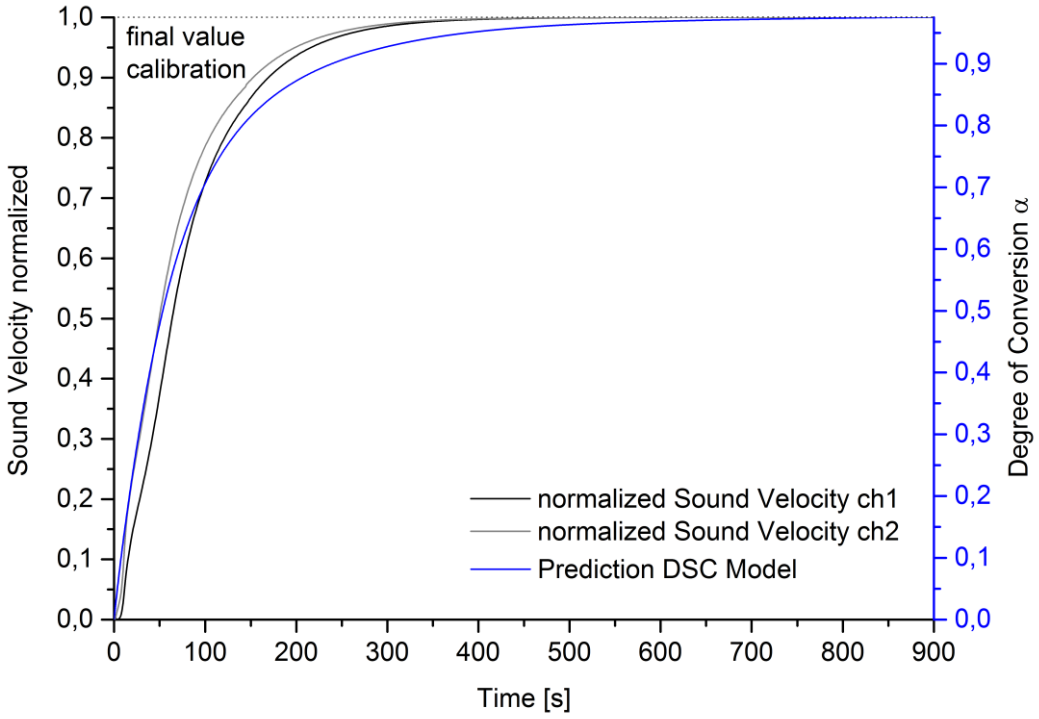

Figure 79: Calibration of the normalized sound velocity value 1.0 of channel 1 and channel 2 to the final degree of conversion degree of conversion α according to the prediction of the DSC kinetic model at 100°C cure temperature.

An important piece of data, when thinking about process strategies, is the time at which the part is cured to an extent where it is dimensionally stable and can be removed from the mould. This property is reached when vitrification occurs. Therefore a correlation of the values of the normalized sound velocities was made with the obtained times for vitrification derived by the rheometry measurements. The values of the normalized sound velocities of channel 1 and channel 2 at which vitrification occurs at 80, 90 and 100°C cure temperatures are shown in Table 19. For all temperatures and both channels, vitrification is observed at normalized sound velocity values 0.94 and 0.95. As both methods rheometry and ultrasound measure a mechanical parameter, the modulus, a very good correlation is found in the similar values at which vitrification occurs.

Table 19: Values of normalized sound velocities of channel 1 and channel 2 at which vitrification according to rheometry measurements is observed at 80, 90 and 100°C cure temperature.

	80°C	90°C	100°C
Vitrification normalized ch1	0.94	0.95	0.94
Vitrification normalized ch2	0.94	0.95	0.95

D. DEVELOPMENT OF A KINETIC MODEL AND SIMULATION OF EPOXY RESIN SYSTEM B

8 Analytical Methods to derive a Kinetic Model

8.1 Results and Discussion of Heating Rate DSC Experiments

First the correlation of the glass transition temperature T_g and the degree of conversion α was determined according to the experiments conducted for epoxy resin system A and described in section 4.1.4. The curing times and the isothermal cure temperatures are shown in Table 20.

Table 20: Isothermal curing conditions of the first segment of combined DSC experiments

Curing Temp. [°C]	10	25	50	70	80	90	100	110	120
Curing Time [min]	800	600	120	45	40	30	20	20	20

Table 21 shows the values residual enthalpy of reaction ΔH_{res}, degree of conversion α and the glass transition temperature T_g of the uncured, the partially cured (isothermal cure temperatures 10 – 110°C) and fully cured (isothermal cure temperature 120°C) of the epoxy resin system B. The total enthalpy of reaction of epoxy resins system B was determined to ΔH_{tot} = –547.86 J/g, the glass transition temperature of the uncured resin was determined to T_{g0} = –36.0°C and the glass transition temperature of the fully cured resin was determined to $T_{g\infty}$ = 124.2°C

Table 21: States of the uncured, partially and fully cured epoxy resin system B.

Isothermal Cure Temp [°C]	Residual enthalpy ΔH_{res} [J/g]	Degree of Conv. α	Glass transition Temp. T_g [°C]
--	–547.86	0	–36.0
10	–345.96	0.37	7.1
25	–182.06	0.67	44.1
50	–127.18	0.77	66.8
70	–76.28	0.86	84.5
80	–53.82	0.90	95.1
90	–32.12	0.94	105.1
100	–16.35	0.97	112.8
110	–8.48	0.99	120.2
120	–0.22	1.00	124.2

Additionally to the experimentally determined values of the correlation of the glass transition temperature T_g and the degree of conversion α the fitting curves were determined according to equation (4) derived by Hesekamp and equation (5) derived by DiBenedetto. For equation (4) following fit parameter were determined:

$T_g(0)$ = –33.9°C

g_1 = 1.0196

g_2 = 3.0222

The best fit for equation (5) was derived with the fit parameter λ = 0.54.

The experimentally determined values of correlation of the glass transition temperature T_g and the degree of conversion α and both fitting curves are shown in Figure 80. Both equations provide a very good fit to the experimentally determined values. Similar to epoxy resin system A, a strong increase of the glass transition temperature is observed for high degree of conversion $\alpha > 0.80$.

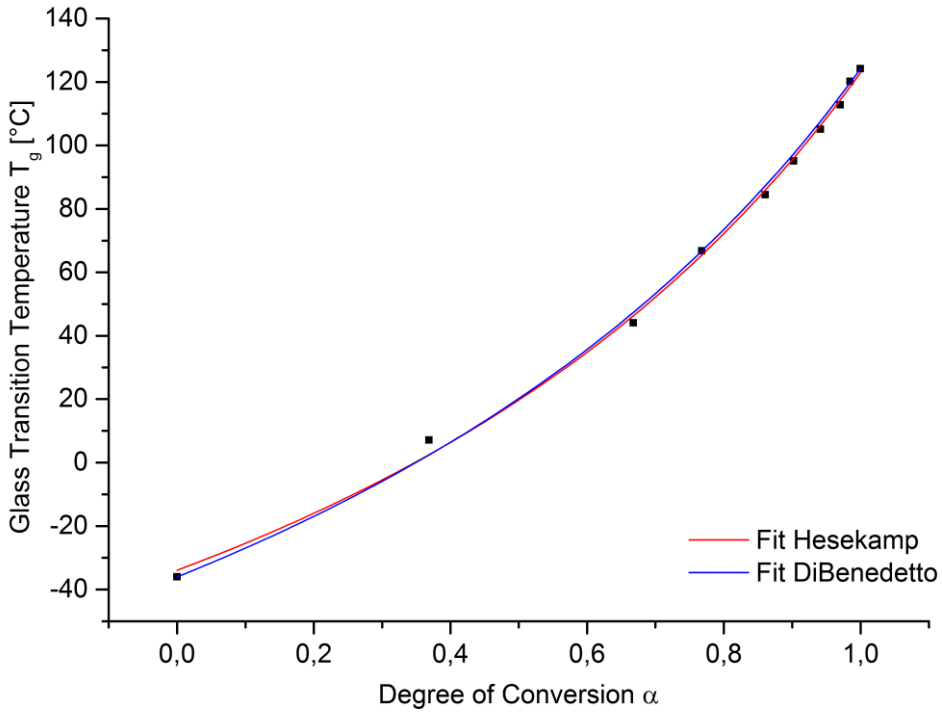

Figure 80: Correlation of glass transition temperature T_g and degree of conversion α of epoxy resin system B.

The measurement of the complete curing progress of epoxy resin system B by dynamic DSC experiments at heating rates of 1, 2, 5, 10 and 20 K/min plotted over the is shown Figure 81. The DSC signals show similar behavior as those for epoxy resin system A, discussed in section 4.1.4. The DSC heating rate experiments are again used for reaction kinetic modeling.

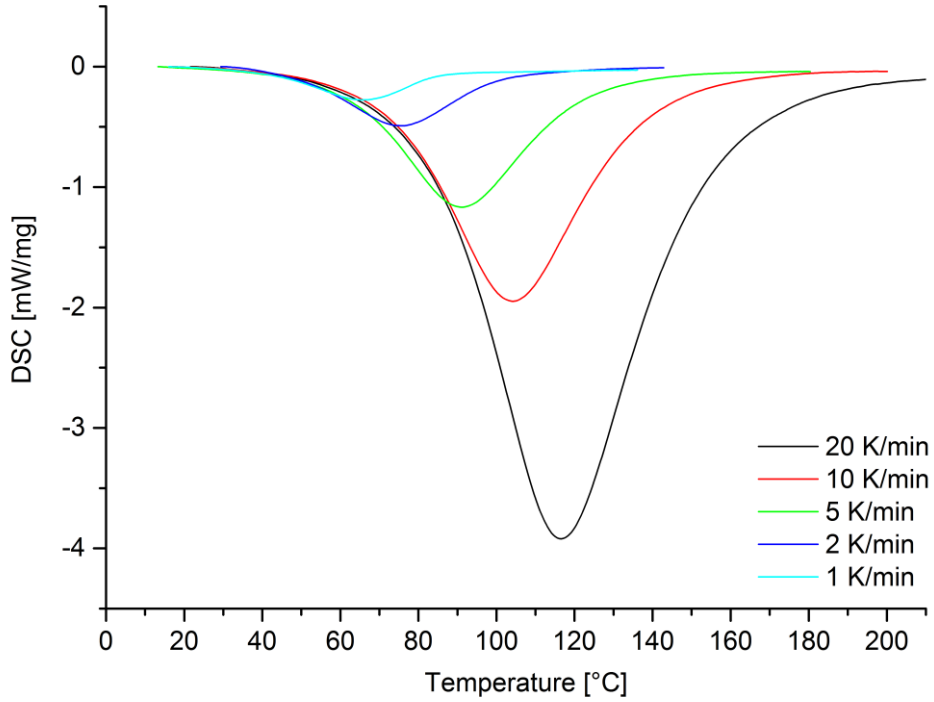

Figure 81: DSC experiments of epoxy resin system B at heating rates of 1 K/min, 2 K/min, 5 K/min, 10 K/min and 20 K/min.

9 Kinetic Modeling and Simulation

9.1 Reaction Kinetic Model based on Experimental DSC Data

9.1.1 Development of Reaction Kinetic Model

The dynamic DSC measurements of epoxy resin system B at heating rates of 1, 2, 5, 10 and 20 K/min in temperature ranges from 10°C up to 200°C shown in Figure 81 are used as input data for the reaction kinetic model.

The Friedman plot with isoconversional lines for all heating rates of DSC input data is shown in Figure 82. The slopes of the isoconversional lines and experimental are identical in the low temperature range which indicates a non-catalytic reaction. The change of the slopes of the isoconversional lines towards higher degrees of conversion α indicates a multi-step reaction.

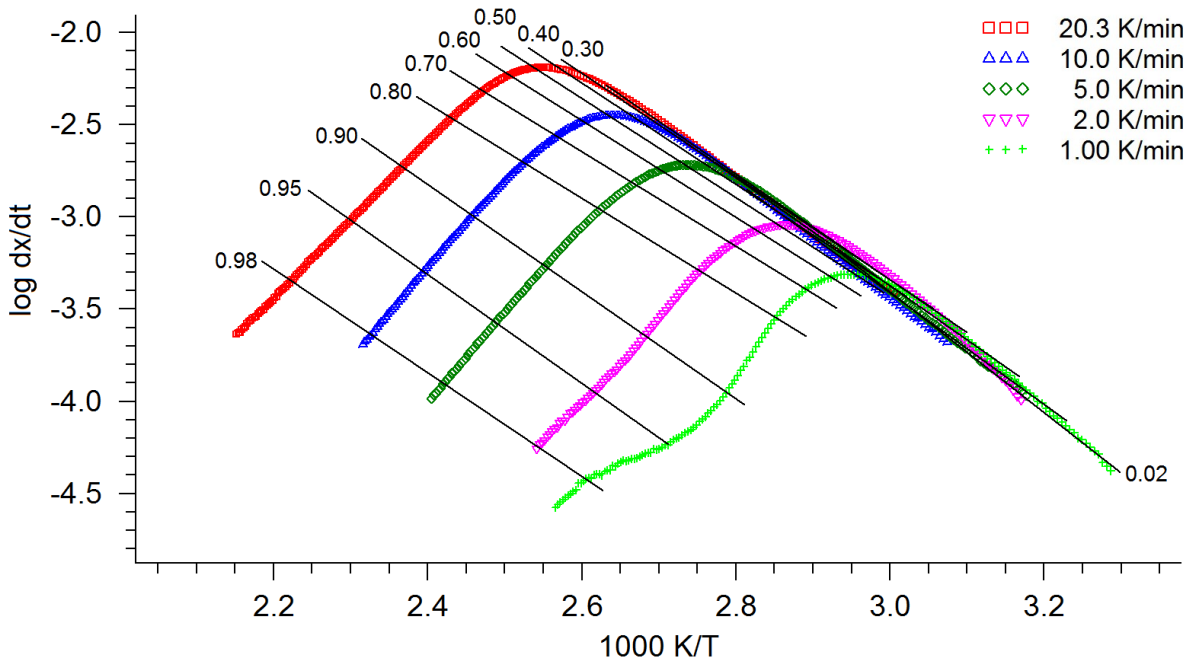

Figure 82: Friedman plot of the dynamic DSC heating rate experiments at 1, 2, 5, 10 and 20 K/min with isoconversional lines.

The estimated activation energy E_a and pre-exponential factor A derived from the Friedman analysis depending on the degree of conversion α is shown in Figure 83. The activation energy decreases from 56 kJ/mol to 49 kJ/mol for a degree of conversion $\alpha < 0.8$. For $\alpha > 0.8$ the activation energy seems to increase, but also the error bars spread which is an indication for vitrification. The same can be observed for the pre-exponential factor A which decreases from 5.5 s^{-1} to 4.4 s^{-1} for a degree of conversion $\alpha < 0.8$ and increases for $\alpha > 0.8$. Because the determination of the pre-exponential factor A derived by the activation energy, the increase of A at $\alpha > 0.8$ can therefore be attributed to the

uncertain E_a values. The change of the activation energy with progressing degree of conversion also indicates a multi-step reaction.

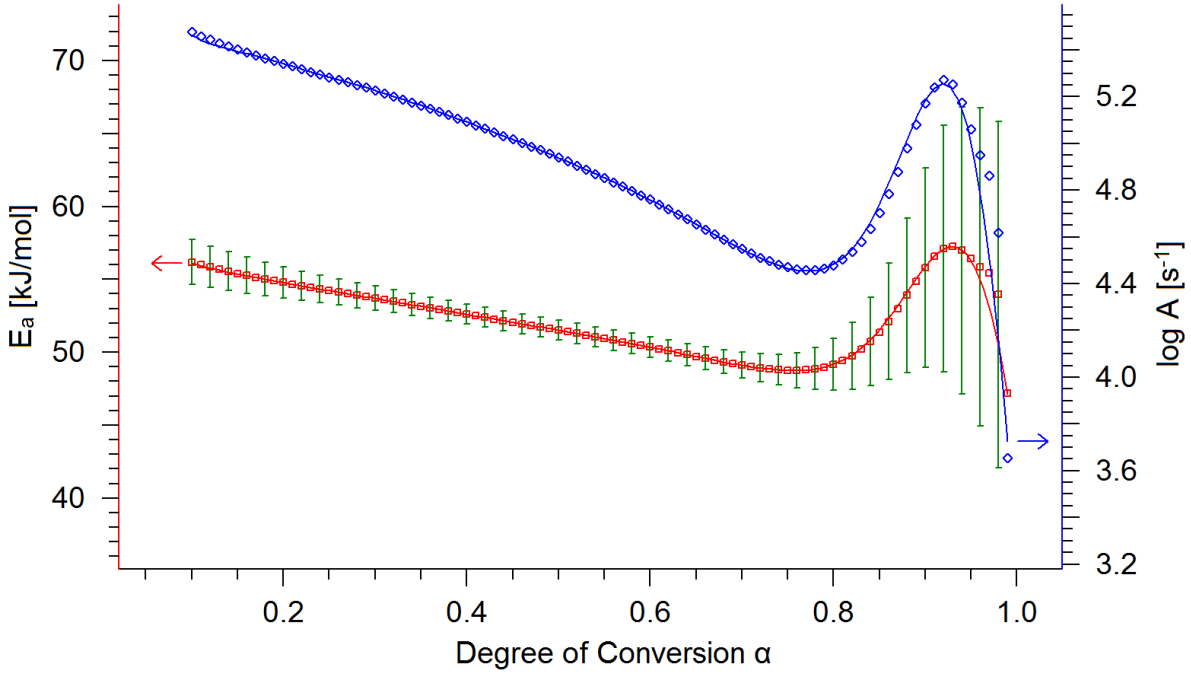

Figure 83: Estimated activation energy E_a and pre-exponential factor A according to the Friedman analysis.

The Ozawa-Flynn-Wall plot with isoconversional lines for all heating rates of DSC input data is shown in Figure 84. Similar to the Friedman plot, the change of the slopes of the isoconversional lines towards higher degrees of conversion α is also observed and indicates a multi-step reaction.

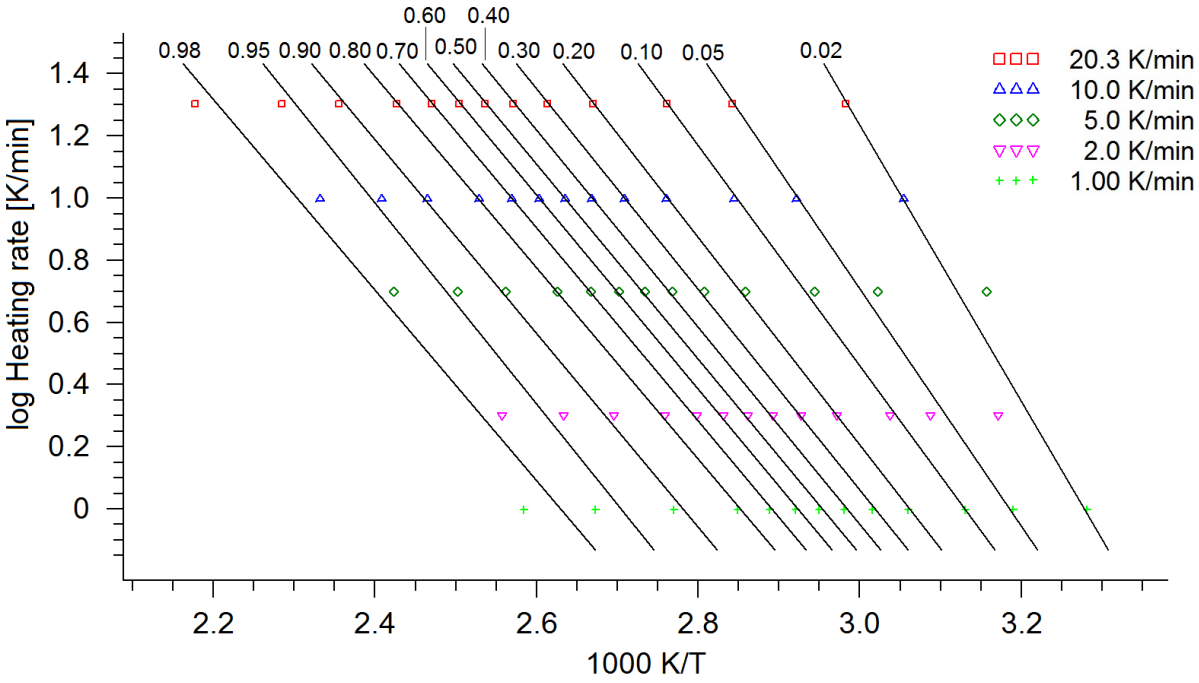

Figure 84: Ozawa-Flynn-Wall plot of the dynamic DSC heating rate experiments at 1, 2, 5, 10 and 20 K/min with isoconversional lines.

The Ozawa-Flynn-Wall plot of estimated activation energy E_a and pre-exponential factor A depending on the degree of conversion α is shown in Figure 85. The activation energy decreases from 58 kJ/mol to 54 kJ/mol for a degree of conversion $\alpha < 0.8$. For $\alpha > 0.8$ the activation energy seems to increase, but also the error bars spread which is an indication for vitrification. The same can be observed for the pre-exponential factor A which decreases from 5.8 s^{-1} to 5.1 s^{-1} for a degree of conversion $\alpha < 0.8$ and increases for $\alpha > 0.8$. The values are in the same range as the estimated activation energy E_a and pre-exponential factor A according to the Friedman analysis. The change of the activation energy with progressing degree of conversion also indicates a multi-step reaction.

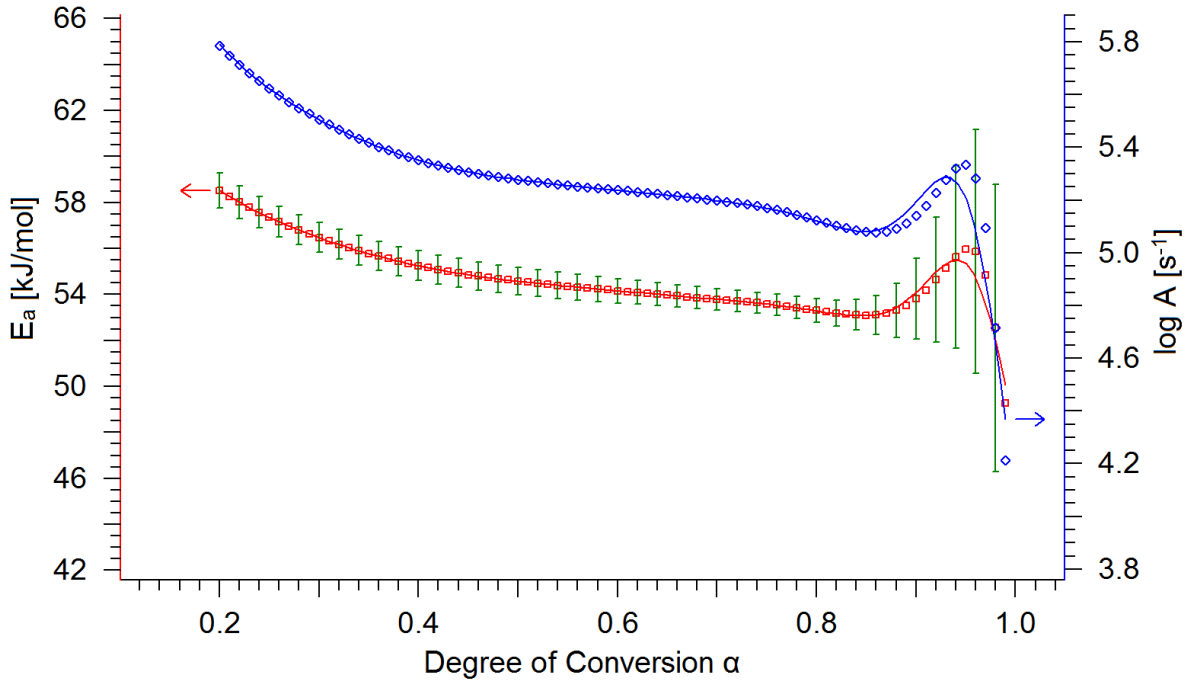

Figure 85: Estimated activation energy E_a and pre-exponential factor A according to the Ozawa-Flynn-Wall analysis.

After the estimation of the energy E_a and pre-exponential factor A, which are needed as initial parameters, the best fitting model was determined. The best fit provided a kinetic model with two following steps of n^{th} order of reaction and diffusion control for the second step (reaction type according to Table 5: Fn Fn,d), which is shown in Figure 86. This is in total agreement with the indication of Friedman and Ozawa-Flynn-Wall analysis. The correlation coefficient, which indicates the fit quality of the model to the experimental data, is 0.9998.

Also for epoxy resin system B a 2-step reaction model is reasonable in the sense of the crosslinking reaction of an epoxy resin with amine hardener, though it is only a formal kinetic evaluation. As it is an epoxy resin with amine components in the hardener only, the first reaction step can be attributed to the reaction of an epoxy group with a primary amine, yielding intermediate B in form of a secondary amine, according to reaction (i) of Scheme 2. The second reaction step displays the reaction of an epoxy group with a secondary amine, yielding a non-reactive tertiary amine, according to reaction (ii) of Scheme 2.

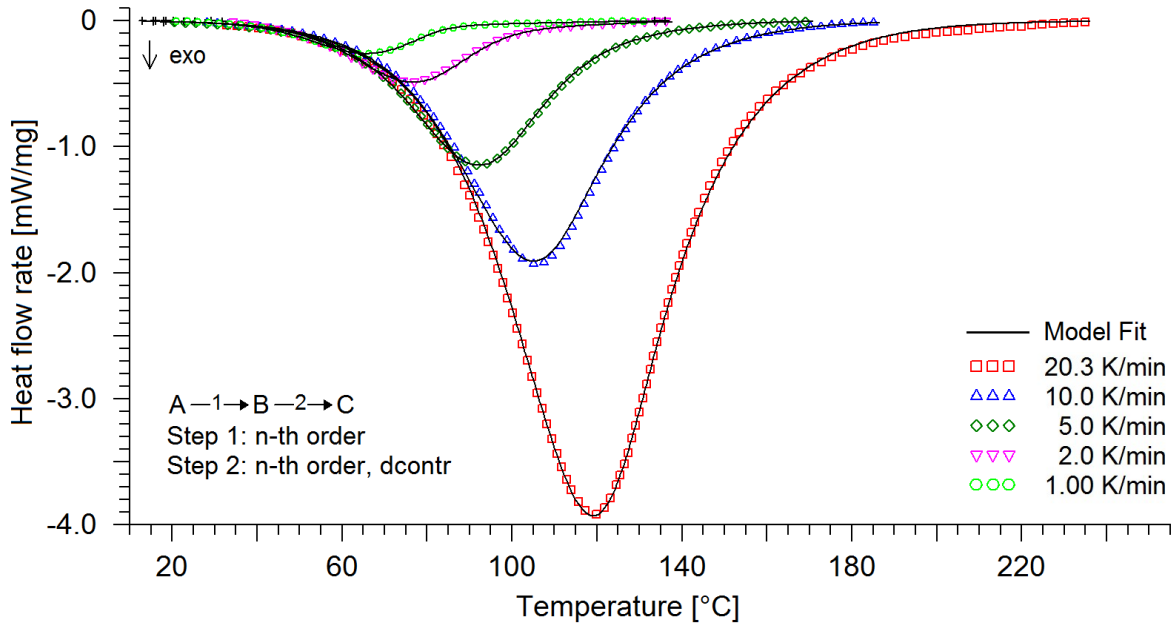

Figure 86: Model fit of a 2-step model, n^{th} order and diffusion control in the second step, superimposed by experimental DSC input data.

The optimum values of the kinetic parameters and the respective standard deviation of the Fn,d Fn,d model are shown in Table 22. The values of the activation energy E_{a1} and the pre-exponential A_1 of the first step are in good agreement with the Friedman and Ozawa-Flynn-Wall analysis and the literature values discussed in section 5.3.1.1. The decrease of activation energy E_{a2} and the pre-exponential A_2 do also match with the Friedman and Ozawa-Flynn-Wall analysis. The decrease of the activation energy during the crosslinking reaction can be explained by the increase of the hydroxy group concentration, which facilitate the polyaddition of epoxy and amine groups like shown in Scheme 3. The first reaction step is describe by a reaction order $n = 1$, the second reaction step by $n = 1.4$.

Table 22: Kinetic parameters and standard deviation of the best fit model Fn Fn,d based on DSC data.

#	Parameter	Optimum Value	std. Deviation
1	log A_1 [s^{-1}]	6.8598	$5.7231 \cdot 10^{-2}$
2	E_{a1} [kJ/mol]	61.4445	0.3838
3	React. Order 1	0.9429	$1.6331 \cdot 10^{-2}$
4	log A_2 [s^{-1}]	4.6414	0.1130
5	E_{a2} [kJ/mol]	48.4961	0.8242
6	React. Order 2	1.3736	$3.4475 \cdot 10^{-2}$
7	log k_{diff2} [s^{-1}]	–1.8603	$7.2068 \cdot 10^{-2}$
8	C_1	5.2541	2.0771
9	C_2 [K]	36.7762	15.1901
10	Foll. React. 1	0.2024	$8.1982 \cdot 10^{-3}$
11	Area 1 [J/g]	–598.3328	2.4047
12	Area 2 [J/g]	–542.8603	1.8706
13	Area 3 [J/g]	–595.6843	1.9576
14	Area 4 [J/g]	–550.5384	1.7282
15	Area 5 [J/g]	–546.2116	1.9325

9.1.2 Temperature Dependent Cure Simulation

The prediction of the progress of the degree of conversion α and the glass transition temperature T_g over the time at a heating rate of 1 K/min is shown in Figure 87. It can be observed that at 1 K/min heating rate the increasing glass transition T_g reaches the cure temperature and the reaction is dramatically slowed down by vitrification at which the crosslinking reaction gets diffusion controlled. This finding was also observed for the curing progress of epoxy resin system A and shows again the importance of diffusion control considerations in the reaction kinetic model.

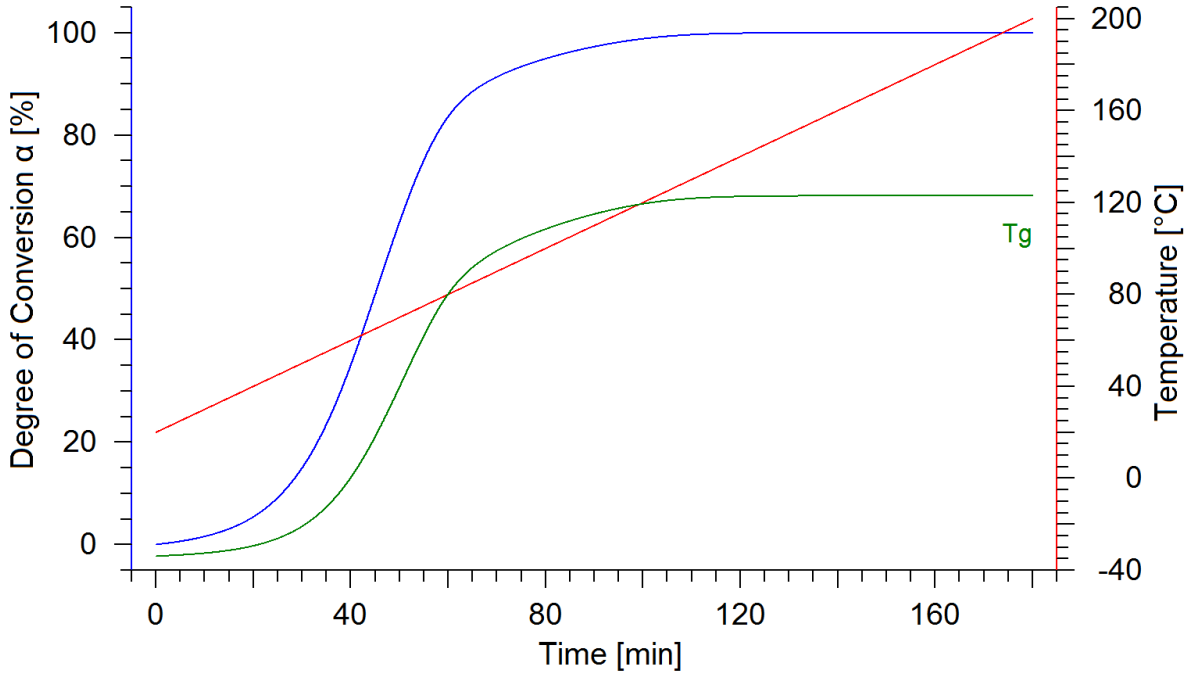

Figure 87: Prediction of degree of conversion α and the progress of the glass transition temperature T_g at 1 K/min heating rate from 20 – 200°C.

The prediction of the progress of the degree of conversion α and the glass transition temperature T_g at a heating rate of 10 K/min, shown in Figure 88, shows that the cure temperature is increasing faster than the glass transition temperature T_g and the reaction does not vitrify.

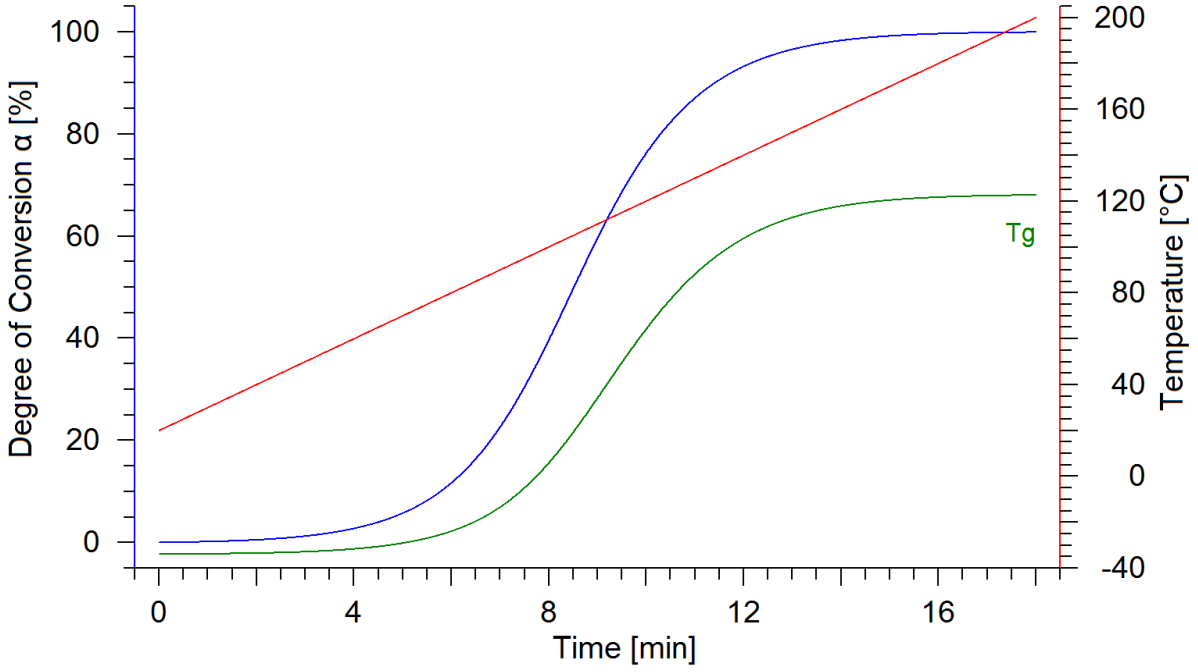

Figure 88: Prediction of degree of conversion α and the progress of the glass transition temperature T_g at 10 K/min heating rate from 20 – 200°C.

The prediction of the progress of the degree of conversion α and the increase of the corresponding glass transition temperature T_g over the time at isothermal cure temperatures 70, 80, 90, 100, 110 and 120°C is shown in Figure 89. As expected, and similar to epoxy resin system A the curing reaction is faster at higher cure temperatures.

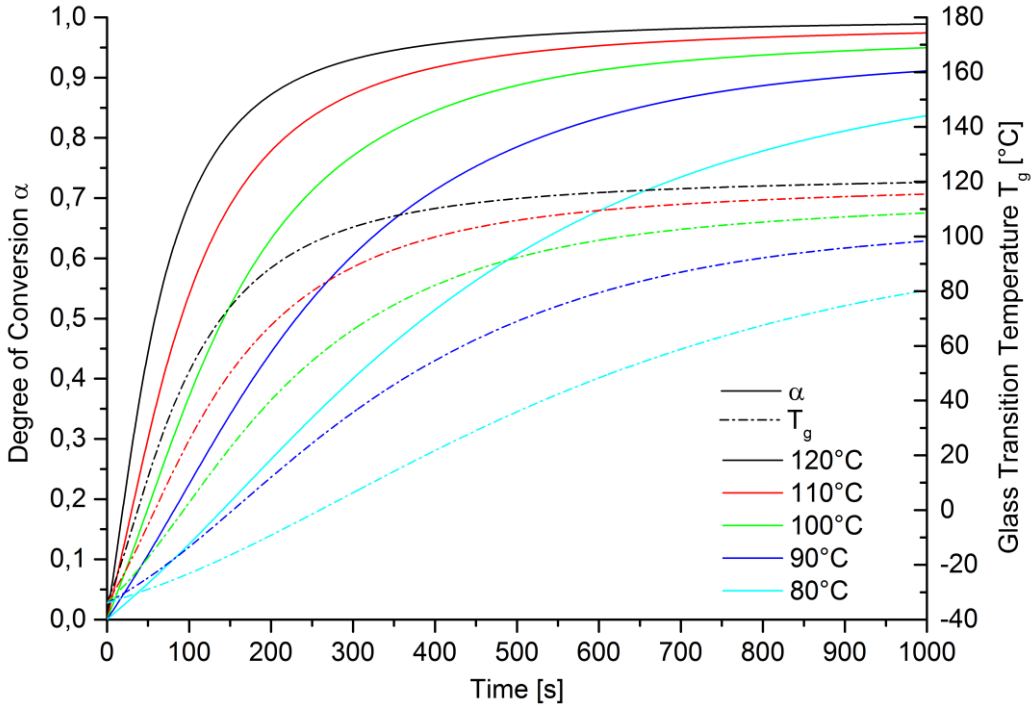

Figure 89: Prediction of degree of conversion α and the progress of the glass transition temperature T_g at isothermal cure temperatures from 80 – 120°C.

The predicted values of the degree of conversion α and the glass transition temperature T_g after 5 min and 35 min are shown in Table 23. Only at 120°C cure temperature, a complete curing is achieved after 35 min. At 110°C complete curing is almost reached after 35 min. At cure temperatures 80, 90 and 100°C the curing reaction is not completed due to vitrification. The resulting T_g at these temperatures is 19°C, 18°C and 15°C above the cure temperature. Compared to epoxy resin system A, the final glass transition temperature of a vitrified and not fully cured sample is even higher.

Table 23: Predicted values of degree of conversion α and glass transition temperature T_g after 5 min and 35 min at the respective isothermal cure temperature.

Curing Temp. [°C]	α (5 min)	T_g (5 min)	α (35 min)	T_g (35 min)
80	0.40	6.4	0.91	99.2
90	0.61	35.7	0.95	108.1
100	0.77	66.0	0.97	114.9
110	0.88	88.8	0.99	119.6
120	0.93	103.4	1.00	122.0

9.1.3 Time-Temperature-Transformation Analysis

Figure 90 shows the predicted TTT diagram of epoxy resin system B at isothermal cure temperatures from 80 – 130°C. A clear deceleration of the curing reaction due to vitrification can be observed for cure temperatures from 80 – 100°C. This graphical representation of the relation of curing time, cure temperature, degree of conversion and progress of the glass transition temperatures provides very good and quick overview of the curing performance of epoxy resin system B and is especially helpful for practitioners.

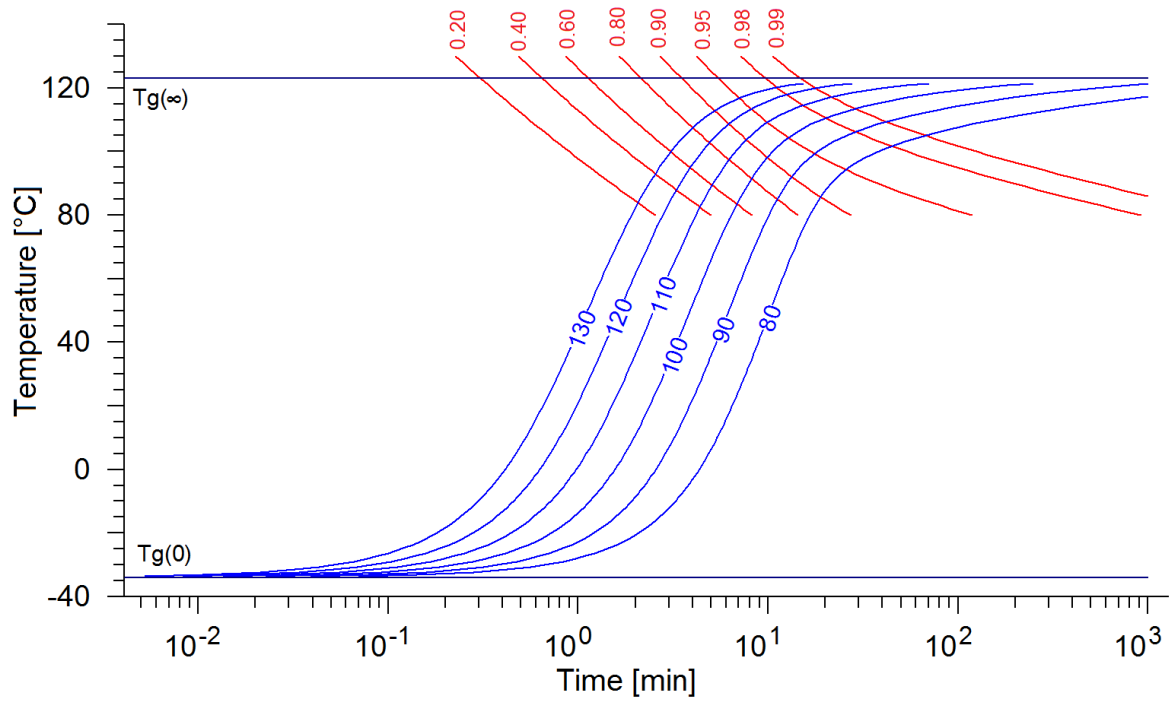

Figure 90: Predicted TTT diagram at isothermal cure temperatures from 80 – 130°C with T_{g0} and $T_{g\infty}$ the progress of the glass transition temperature (blue) and isoconversional lines (red).

E. ISOTHERMAL CURE CHARACTERIZATION AND PROCESS ANALYSIS OF EPOXY RESIN SYSTEM B

10 Laboratory Analytical Methods for Characterization of Curing-State and -Progress of Epoxy Resins

10.1 Isothermal DSC Experiments

10.1.1 Results and Discussion of isothermal DSC Experiments

The isothermal DSC experiments at 80, 90, 100, 110 and 120°C cure temperature are shown in Figure 91. At 80°C the total curing time is 40 min, at 90°C the total curing time is 30 min and at 100, 110 and 120°C the total curing time is 20 min to ensure that the curing reaction is completed. The progress of the respective enthalpy of reaction ΔH_R over time is given by integration of the DSC signals. A baseline correction for the integration of the DSC signals, as discussed in section 6.1.1, was also conducted.

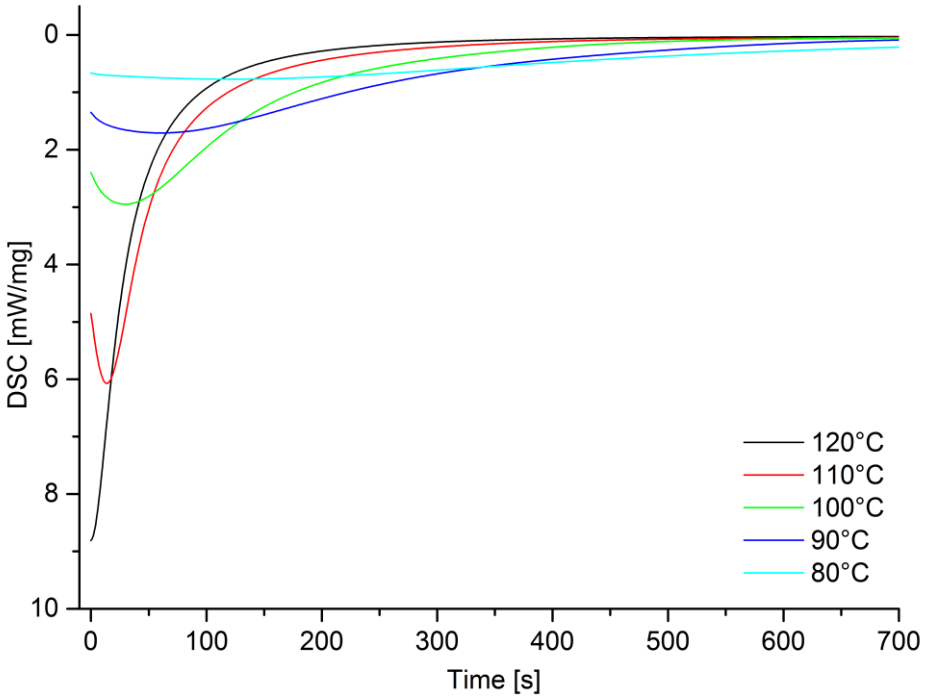

Figure 91: DSC signals at isothermal cure temperatures 70, 80, 90, 100, 110 and 120°C.

Using the values of the residual enthalpy of reaction ΔH_{res}, obtained by an analytical dynamic DSC run after the isothermal segment shown in Table 21, the non-detectable enthalpy of reaction ΔH_{loss} at the beginning of the measurement is calculated according to equation (23) with the total heat of reaction ΔH_{tot} = –547.86 J/g. The respective degrees of conversion α are then calculated according to equation (24).

The measured values of enthalpy of reaction ΔH_R at the isothermal cure temperatures, the residual enthalpy of reaction ΔH_{res} after isothermal curing, the calculated non-detectable enthalpy of reaction ΔH_{loss} and the respective degrees of conversion α are shown in Table 24.

Table 24: Enthalpies of reaction ΔH_R, residual enthalpies of reaction ΔH_{res}, non-detectable enthalpy of reaction ΔH_{loss} and calculated corresponding degrees of conversion α at respective isothermal cure temperatures.

Cure Temp [°C]	ΔH_{loss} **[J/g]**	ΔH_R **[J/g]**	ΔH_{res} **[J/g]**	**Degree of Conv.** α
80	–109.01	–430.24	–53.82	0.90
90	–24.93	–458.57	–32.12	0.94
100	–59.46	–331.37	–16.35	0.97
110	–83.99	–152.61	–8.48	0.99
120	–143.14	–203.80	–0.22	1.00

Similar to epoxy resin system A the beginning of the polymerization reaction cannot be detected by isothermal DSC measurements due to the initialization time needed. ΔH_{loss} is also reconstructed by extrapolation, to provide a qualitative curve progression and a uniform starting point $t = 0$. The function for the extrapolation was given by a 7^{th}-order polynomial fit of the experimental data and the new starting point $t = 0$ s was set at $\alpha = 0$ for all curves. The progress of the degree of conversion α for isothermal temperatures from 80 – 120°C is shown in Figure 92.

The curing progress of the epoxy resin system B is extremely slow at 80°C and α increases only moderately. At 90°C cure temperature α increases clearly faster but turns into a plateau at $\alpha \sim 0.93$ due to vitrification and only rises slowly. At 100°C and 110°C a deceleration of the reaction due to vitrification is observed at $\alpha \sim 0.96$ and $\alpha \sim 0.97$. Only at 120°C full conversion of the polymerization reaction is obtained.

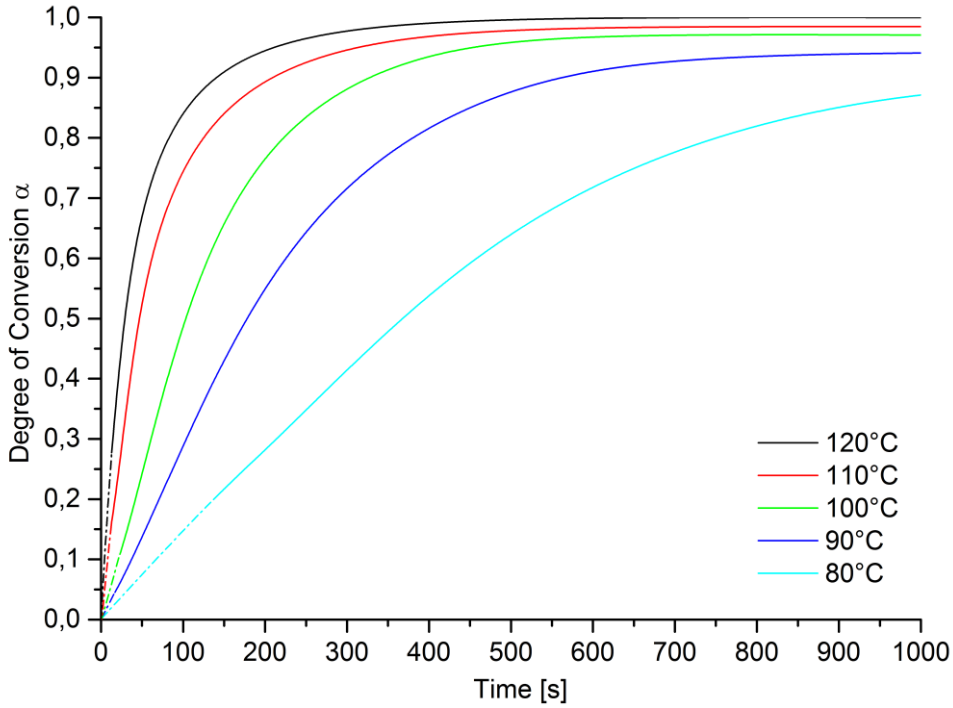

Figure 92: Progress of degree of conversion α for isothermal DSC experiments at temperatures from 80 – 120°C with the experimentally determined enthalpy of reaction ΔH_R (solid lines) and the calculated and reconstructed non-detectable enthalpy of reaction ΔH_{loss} (dotdashed lines).

An overview of the curing performance of epoxy resin system B is given by the degrees of conversion α after 2, 5, 20, 30 min curing at the respective isothermal cure temperatures, shown in Table 25.

Table 25: Degrees of conversion α after 2, 5, 20, 30 min curing time derived from isothermal DSC curing experiments.

Curing Temp. [°C]	α (2 min)	α (5 min)	α (20 min)	α (30 min)
80	0.18	0.41	0.89	0.90
90	0.35	0.72	0.94	0.94
100	0.56	0.88	0.97	0.97
110	0.79	0.95	0.99	0.99
120	0.87	0.98	1.00	1.00

10.1.2 Comparison with DSC Kinetic Model

The comparison of the degree of conversion α_{exp} of the isothermal DSC experiments and the prediction α_{pred} of the DSC kinetic model at isothermal cure temperatures 80 – 120°C is shown in Figure 93. The progress of α_{exp} and α_{pred} at 80°C cure temperature shows a good correlation. At higher cure temperatures the predicted value α_{pred} lags behind the experimentally determined values. These

findings are similar to the observations from the comparison of experimental isothermal DSC measurements and the prediction of the DSC kinetic model of epoxy resin system A. Also the possible sources of errors of the experimental isothermal DSC data were discussed in section 7.1.6.

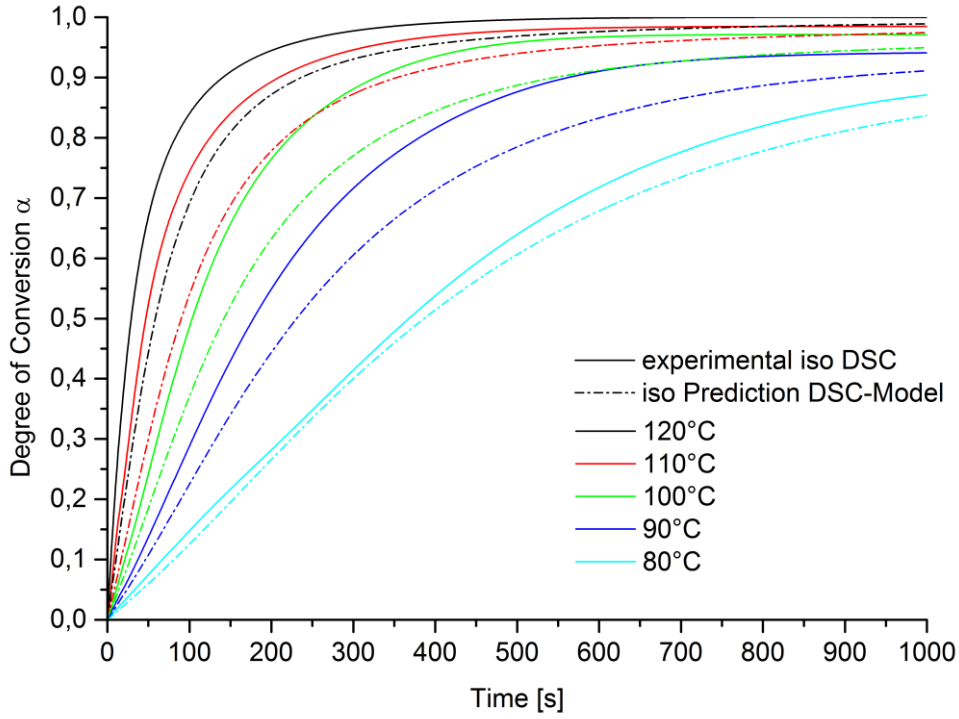

Figure 93: Comparison of degrees of conversion α_{exp} of isothermal DSC experiments (solid lines) and prediction α_{pred} of the DSC kinetic model (dotdashed lines) at isothermal cure temperatures 80 – 120°C.

A comparison of the experimental and predicted degrees of cure at 2, 5, 20 and 30 min at the respective temperatures is shown in Table 26. After 20 min curing time only a minor deviation of the degrees of conversion of 1 – 2% is observable for all cure temperatures. After 30 min curing time the predicted values α_{pred} and the experimentally determined values α_{exp} are identical for all cure temperatures.

Table 26: Experimentally determined degrees of conversion α_{exp} and predicted degrees of conversion α_{pred} after 2, 5, 20, 30 min curing at isothermal cure temperatures 80 – 120°C.

	2 min		**5 min**		**20 min**		**30 min**	
Temp. [°C]	α_{exp}	α_{pred}	α_{exp}	α_{pred}	α_{exp}	α_{pred}	α_{exp}	α_{pred}
80	0.18	0.15	0.41	0.40	0.89	0.87	0.90	0.90
90	0.35	0.27	0.72	0.61	0.94	0.92	0.94	0.94
100	0.56	0.44	0.88	0.77	0.97	0.96	0.97	0.97
110	0.79	0.61	0.95	0.88	0.99	0.98	0.99	0.99
120	0.87	0.75	0.98	0.93	1.00	0.99	1.00	1.00

10.2 Isothermal NIR Spectroscopy

10.2.1 Results and Discussion of isothermal NIR Spectroscopy Experiments

For the evaluation of the curing progress of epoxy resin system B by NIR spectroscopy the Epoxy 1 signal was used as described in section 4.2.3. A temperature correction of the signal area was conducted with the Phenol 2 signal.

The degree of conversion of epoxy resin system B based on the conversion of epoxy groups, according to the reciprocal and normalized signal area of Epoxy 1, at isothermal cure temperatures 100°C and 120°C and 20 minutes curing time is shown in Figure 94. In addition the sample temperature during the curing reaction was measured via a thermocouple sensor. It can be observed, that the initial temperature of the sample is below the cure temperature. The sample heats up immediately after placing the sample container into the preheated sample chamber. At 100°C cure temperature it takes 64 s for the sample to reach the cure temperature and at 120°C the cure temperatures is reached after 29 s. This time which is needed to bring the sample to the actual cure temperature is responsible for the slight delay of the increase of the degree of conversion and the observed acceleration in the reaction at $\alpha < 0.1$ at 100°C. Also for epoxy resin system B the sample temperature overshoots the cure temperature due to the exothermic reaction and reaches a maximum of 106°C and 135°C respectively. The position of the peak maximum and the steepest slope of the increasing degree of conversion correlate. This finding is in agreement with the expectation that the polymerization reaction proceeds fastest at the highest temperature. As expected and confirmed by the NIR spectroscopy measurement, the curing reaction is completed at 120°C cure temperature yielding a degree of conversions $\alpha = 1.00$. The curing reaction is not completed at 100°C cure temperature due to vitrification and a degree of conversions $\alpha = 0.93$ is obtained. These findings are in agreement with the previous results.

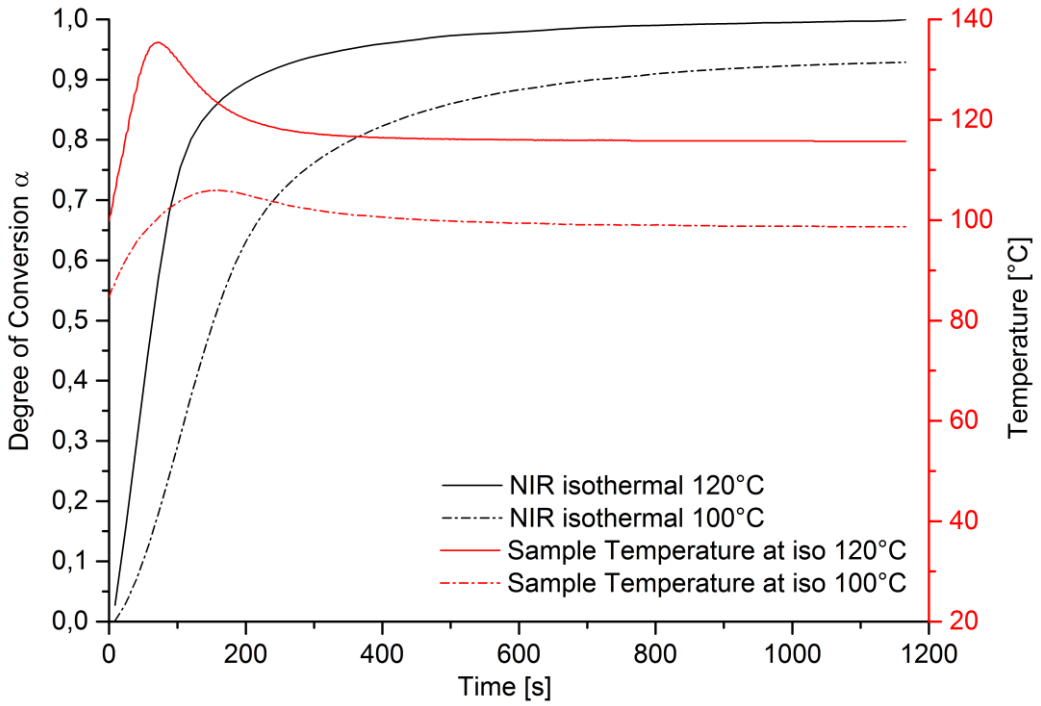

Figure 94: Progress of the degree of conversion α of epoxy resin system B according to the reciprocal, normalized and temperature corrected Epoxy 1 signal at isothermal cure temperatures 100°C and 120°C and the respective measured sample temperature.

10.2.2 Comparison with isothermal DSC Results

The comparison of the isothermal NIR spectroscopy with the isothermal DSC experiment at 100°C and 120°C cure temperature is shown in Figure 95. The degree of conversion α obtained by NIR spectroscopy lags approx. 25 s behind the DSC measurement at 120°C cure temperature and approx. 35 s at 100°C cure temperature. This can be explained by the sample temperature of the NIR spectroscopy measurement, which first has to heat up to the isothermal cure temperature.

At 120°C cure temperature the slope of α of the NIR and DSC measurement is almost identical for $0.2 < \alpha$ 0.8. After 170 s the increase α of both curves flattens to end in a plateau for the DSC measurement, while the curve of the NIR spectroscopy still rises slightly until $\alpha = 1.0$ is reached. One reason for this long rise is that vitrification effects are more prominent due to the sample shape and geometry in NIR spectroscopy compared to DSC measurements.

At 80°C cure temperature the slope of α of the NIR and DSC measurement is almost identical for $0.15 < \alpha$ 0.65. At $\alpha > 0.65$ the curve of the NIR spectroscopy begins to flatten while α according to the DSC measurement keeps rising up to approx. $\alpha = 0.85$ until it turns into a plateau. After 20 min curing

a degree of conversion α = 0.93 is reached according to the NIR spectroscopy measurement and α = 0.97 according to the isothermal DSC measurement.

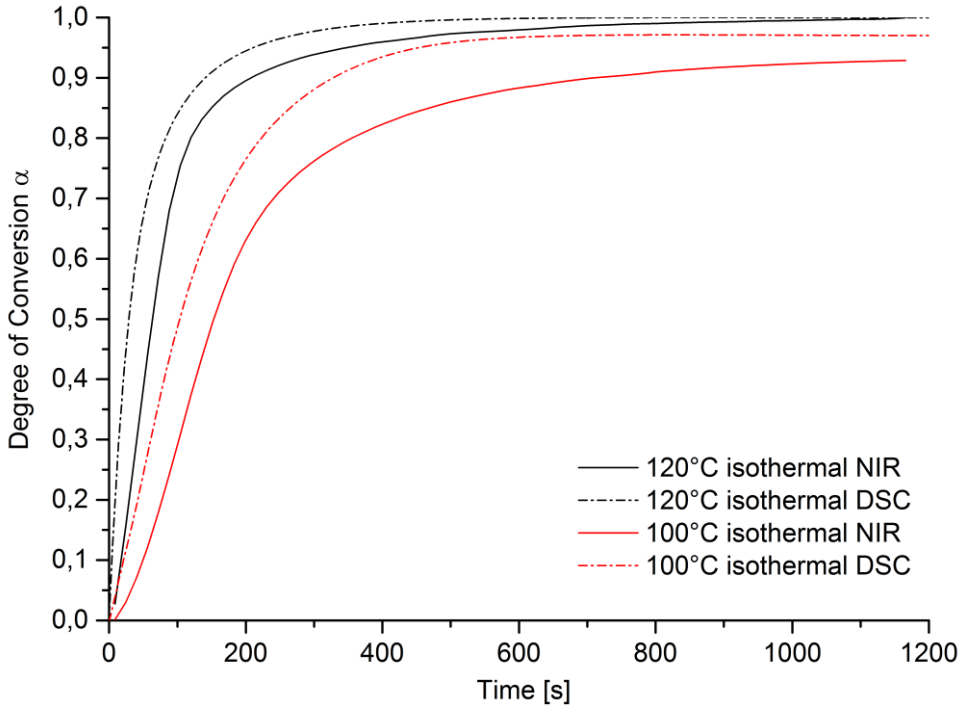

Figure 95: Comparison of the progress of degree of conversion α of epoxy resin system B obtained by isothermal NIR spectroscopy and isothermal DSC measurements at 100°C and 120°C cure temperature.

10.2.3 Comparison with DSC Kinetic Model

The comparison of the isothermal NIR spectroscopy at 100°C and 120°C cure temperature with the prediction of the curing process based on the DSC kinetic model is shown in Figure 96. The sample temperature profile, shown in Figure 94, was taken as basis for the prediction. The curves of the predicted degree of conversion and the NIR spectroscopy measurement fit perfectly at 120° cure temperature. The progression of the degree of conversion is identical at 100°C up to α = 0.65. For α > 0.65 the progression according to the NIR spectroscopy flattens earlier but resumes parallel to the prediction. After 20 min curing at 100°C a degree of conversion α = 0.93 is reached according to the NIR spectroscopy measurement and α = 0.96 according to the prediction.

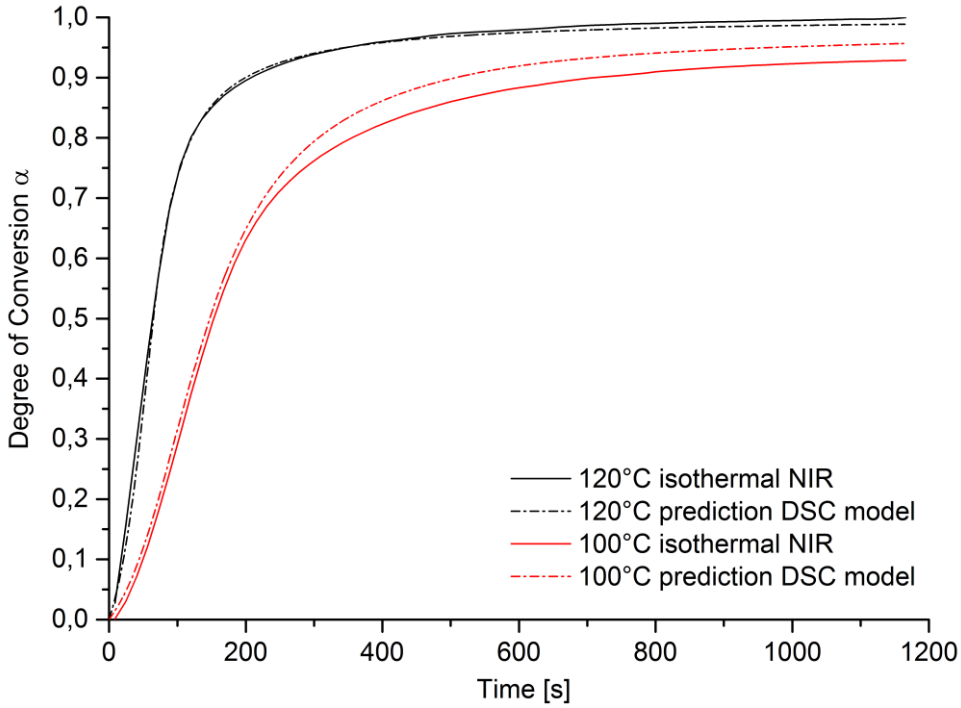

Figure 96: Comparison of the progress of degree of conversion α of epoxy resin system B obtained by isothermal NIR spectroscopy and prediction of the curing process based on the DSC kinetic model and the measured sample temperature determined at 100°C and 120°C cure temperature.

11 Laboratory Analytical Methods for Characterization of Curing-Progress of Epoxy Resins based on Mechanical Parameters

11.1 Rheometric Analysis

11.1.1 Results and Discussion of isothermal Rheometry Measurements

Rotation mode:

The progressing shear viscosities η of the crosslinking reaction of epoxy resins system B at isothermal cure temperatures 90, 100, 110 and 120°C were measured in rotation mode and are shown in Figure 97. At higher curing temperatures the viscosity is increasing faster. As already mentioned in section 7.1.5, the shear viscosity at η = 0.3 Pa·s is defined as the maximum viscosity for proper epoxy resin injection in the HP-RTM process. The shear viscosity at η = 1.8 Pa·s is again taken as reference for the oscillatory determined complex viscosity η^*, which yields accurate values > 1.5 Pa·s.

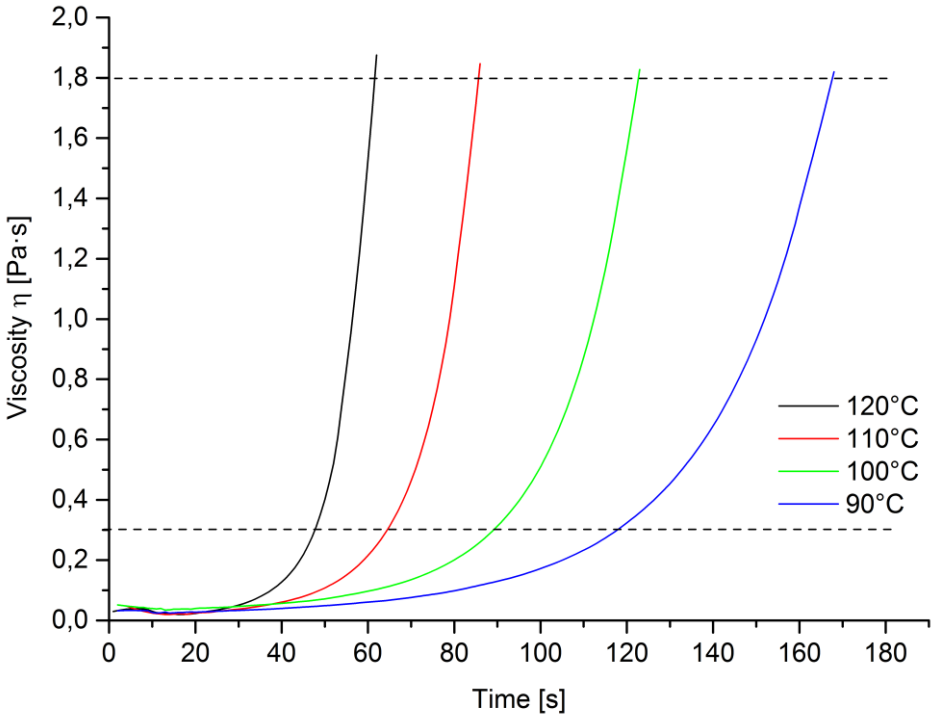

Figure 97: Measurements of the shear viscosity η in rotation mode of the curing reaction of epoxy resins system B at isothermal cure temperatures 90, 100, 110 and 120°C.

The times at which η = 0.3 Pa·s and η = 1.8 Pa·s are reached at the respective isothermal curing temperature are listed in Table 27.

Table 27: Times at which η = 0.3 Pa·s and η = 1.8 Pa·s are reached at the respective isothermal cure temperatures.

Cure Temp.	90°C	100°C	110°C	120°C
$t_{0.3Pa\cdot s}$ [s]	118	89	65	48
$t_{1.8Pa\cdot s}$ [s]	168	123	86	62

Oscillation mode:

A time-adjustment of the calculated complex viscosity η^* at 1.8 Pa·s was made with the shear viscosities η obtained from the ration mode measurements as discussed in section 7.1.5.

The measured storage modulus *G*' and the loss modulus *G*" for isothermal cure temperatures at 80, 90, 100, 110 and 120°C of epoxy resin system B is shown in Figure 98. At all cure temperatures gelation occurs well before vitrification. The peak of *G*" is clear to see at all curing temperatures but gets wider at higher temperatures. This shows that the distance of $T_{g\infty}$ = 124°C is rather small at 120°C cure temperature and no sharp vitrification occurs.

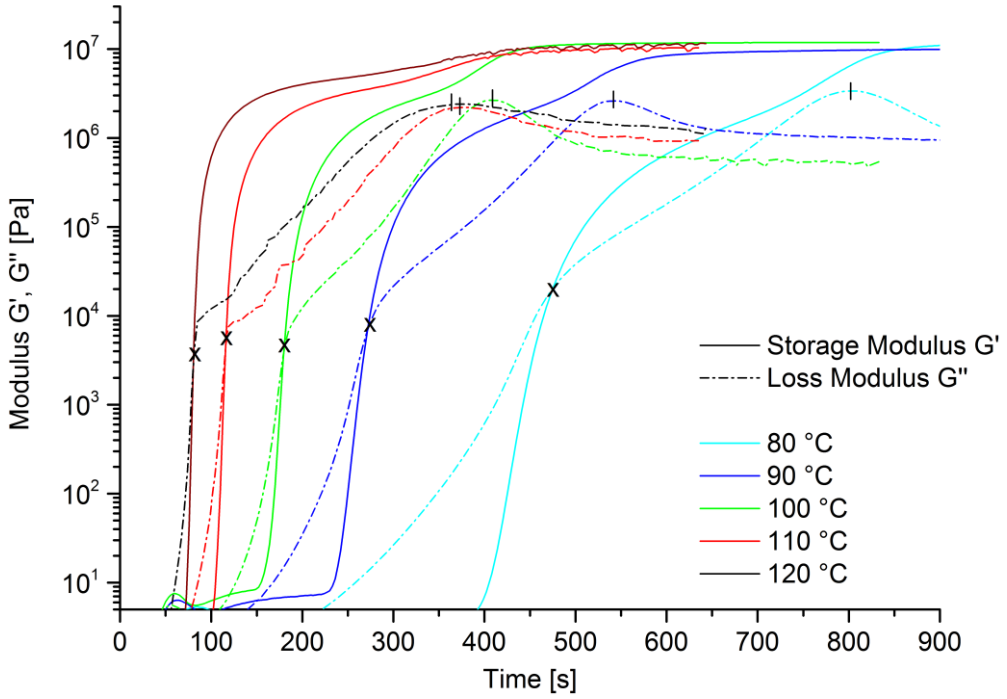

Figure 98: Measurements of storage modulus *G*' and loss modulus *G*" in oscillation mode of the curing reaction reaction of epoxy resins system B at isothermal cure temperatures 80, 90, 100, 110 and 120°C.

The gelation and vitrification times are determined as described in section 7.1.4 and are summarized in Table 28.

Table 28: Gelation and vitrification times of epoxy resin system B at the respective isothermal cure temperatures.

Cure Temp.	80°C	90°C	100°C	110°C	120°C
Gelation (*G'/G"*) [s]	475	271	180	116	80
Vitrification (Peak *G"*) [s]	804	539	407	371	358

11.1.2 Comparison of Rheological Data with Kinetic Model Prediction, DSC and NIR-Spectroscopy Results

The gelation and vitrification times determined by rheometry measurements are compared with the degrees of conversion and glass transition temperatures obtained by the prediction based on the DSC kinetic model, of the isothermal DSC experiments and of the isothermal NIR spectroscopy. The respective degrees of conversion α at gelation times at 80, 90, 100, 110 and 120°C cure temperature are summarized in in Table 29.

The degrees of conversion α_{pred} of the prediction are in a range of 0.57 – 0.61 for all cure temperatures. These values are in very good agreement with literature values and the calculated theoretical value of 60% degree of conversion at the gel point, previously discussed in section 2.1.3.

The degrees of conversion at the gel point of the isothermal DSC measurement are higher than the calculated and literature values. The deviation increases with higher cure temperatures up to α_{exp} = 0.79.

The obtained degrees of conversion α_{exp} isothermal NIR spectroscopy at gelation times are 0.59 and 0.62 which are also in good agreement with literature values and the calculated theoretical value of 60% degree of conversion.

Table 29: Gelation times obtained by rheometry measurements at 80, 90, 100, 110 and 120°C cure temperature and the respective degrees of conversion α of the prediction based on the DSC kinetic model, of the isothermal DSC experiments and of the isothermal NIR spectroscopy..

Cure Temperature	80°C	90°C	100°C	110°C	120°C
Gelation Time (*G'/G"*)	475	271	180	116	80
α_{pred} DSC kinetic Model	0.59	0.57	0.59	0.60	0.61
α_{exp} isothermal DSC	0.62	0.68	0.73	0.78	0.79
α_{exp} isothermal NIR spectroscopy	-	-	0.59	-	0.62

The large deviation of the degrees of conversion of the isothermal DSC experiment at the gelation time compared to literature values for epoxy resins and the calculated theoretical value of α = 0.60 has already been observed for epoxy resin system A. The error sources of experimental isothermal DSC data of fast curing epoxy resins were already discussed in section 7.1.6.

The predicted glass transition temperatures of the DSC kinetic model at the vitrification times obtained by rheometry are shown in Table 30. When vitrification is observed according to rheometry, the predicted glass transition temperature lies below the cure temperature in a range of 11.3 – 16.4 K. This finding confirms the results of epoxy resin system A and shows that vitrification occurs quite early but it does not lead to an instant freeze of the polymerization reaction.

Table 30: Predicted glass transition temperatures of the DSC kinetic model at the vitrification times obtained by rheometry

Cure Temp.	80°C	90°C	100°C	110°C	120°C
Time of Vitrification (*G*" Peak)	804	539	407	371	358
T_g Prediction DSC kinetic Model	68.0°C	74.4°C	83.4°C	98.0°C	108.7°C
Difference Cure Temp. and T_g	12.0 K	15.6 K	16.4 K	12.0 K	11.3 K

11.2 Online-Cure-Monitoring using Ultrasound at Laboratory Scale

11.2.1 Results and Discussion of Ultrasound in Laboratory Analysis

The progressions of the absolute sound velocities of ultrasound laboratory measurements at isothermal cure temperatures 80, 90, 100, 110 and 120°C are shown in Figure 99. The effect of initial softening of the epoxy resin and the associated decrease of the sound velocity at the beginning of the measurement is not observable at 80°C and only slightly at 90°C. At higher temperature the crosslinking reaction is faster which is reflected in a steeper and faster rise of the sound velocity at high temperatures and a later reached plateau at lower temperatures. The difference of the final sound velocity values is also observed for epoxy resin system A and was already explained in section 7.2.4.

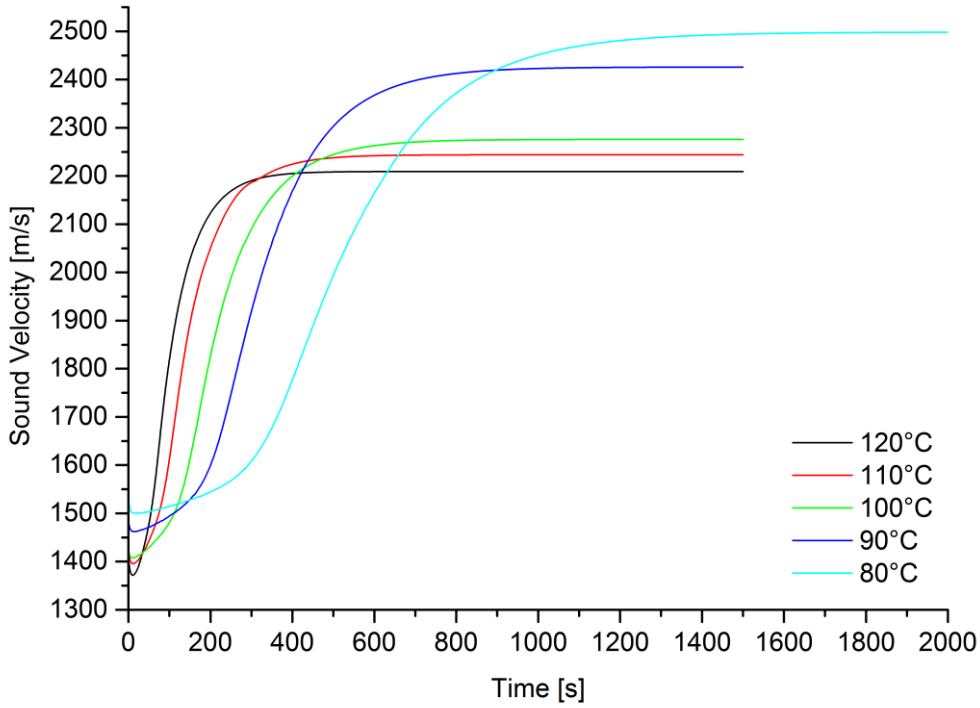

Figure 99: Progress of the absolute sound velocities of ultrasound laboratory measurements at cure temperatures 80, 90, 100, 110 and 120°C.

The respective normalized sound velocities of the isothermal curing measurements are shown in Figure 100. The increasing speed of the crosslinking reaction of epoxy resin system B at higher temperatures is also shown by the normalized curves. At higher cure temperatures only a minor speed increases is observed. This confirms the finding from previous experiments, that the reaction speed increase is limited at higher temperatures.

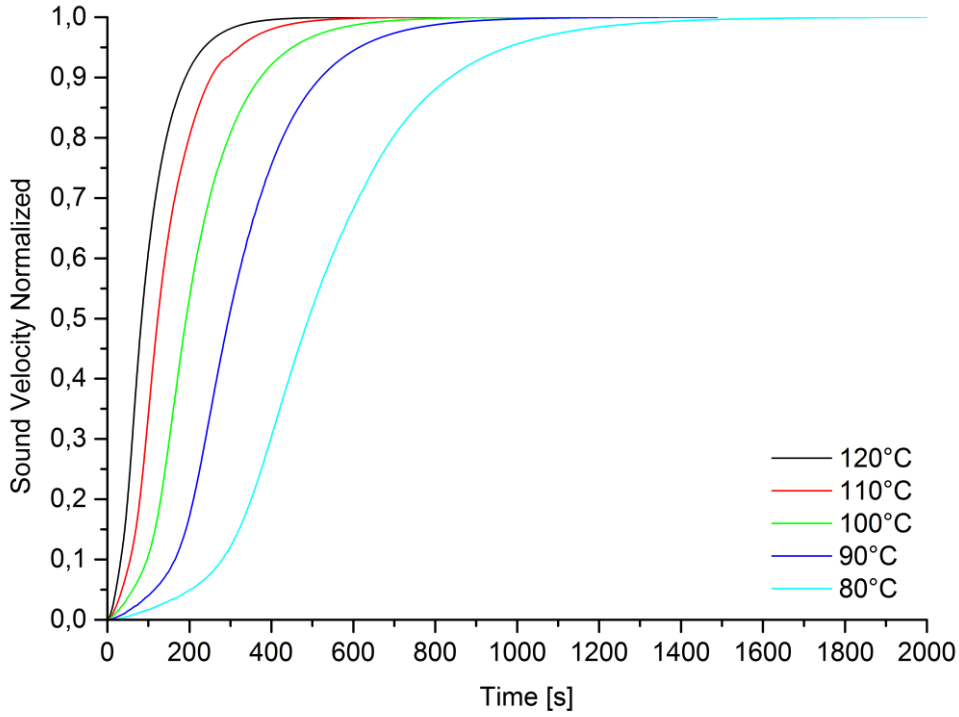

Figure 100: Normalized sound velocities of ultrasound laboratory measurements at cure temperatures 80, 90, 100, 110 and 120°C.

11.2.2 Interpretation of Sound Velocity using Rheometry and DSC Kinetic Model

The progression of the absolute sound velocities for cure temperatures of 80 – 120°C with the respective marks for the gelation and vitrification times, derived by rheometry measurements, is shown in Figure 101. The respective values of the degree of conversion α and the glass transition temperature T_g are derived by the prediction of the DSC kinetic model. It can be observed that gelation occurs approximately in the middle of the steepest increase of the sound velocity at all cure temperatures. According to this finding, gelation occurs at the highest turnover rate. This confirms the results for epoxy resin system A.

At the time of vitrification determined by rheometry, the ultrasound measurements show a clear deceleration of the reaction indicated by the slower increase of the sound velocity. At 110°C and 120°C cure temperature vitrification occurs when the sound velocity has almost reached the plateau. This rather late vitrification can be explained by the high cure temperatures compared to the glass transition temperature of the fully cured resin $T_\infty = 124$°C. This leads to an unsharp vitrification indicated by the broad peak of G'' in the rheometry measurements. As already discussed and confirmed as well for epoxy resin system B, vitrification does not lead to an instant freeze of the reaction, which is also demonstrated by the further increase of the sound velocity and the degree of conversion and the glass transition temperature predicted at the end of the measurement.

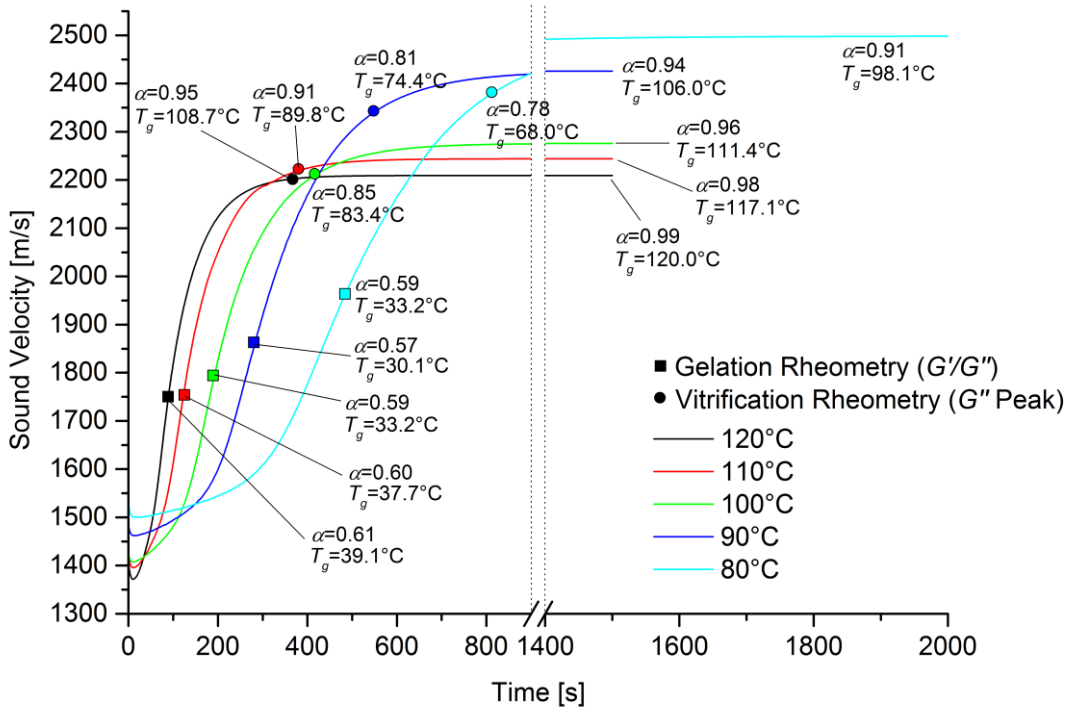

Figure 101: Progress of sound velocities from 80 – 120°C cure temperature with the respective marks for the gelation and vitrification times and the respective degrees of conversion and glass transition temperatures at gelation, vitrification and the end of the ultrasound measurements according to the cure prediction based on the DSC kinetic model.

The comparison of the normalized sound velocity of laboratory ultrasound measurements and the predicted degree of conversion according to the DSC kinetic model at 120°C cure temperature is shown in Figure 102. The marked gelation and vitrification time is derived by rheometry measurement. The progress of the predicted degree of conversion and the normalized sound velocity show a good correlation. The short delay of the normalized sound velocity was also observed for epoxy resin system A and previously discussed in section 7.2.5. Gelation occurs at 0.50 of the normalized sound velocity. Vitrification occurs at 0.99 of the normalized sound velocity, which is due to the unsharp vitrification due to the high cure temperature compared to T_∞ = 124°C. Compared to the prediction, the normalized sound velocity is reached earlier. After 500 s the normalized value 1.0 is reached. Due to less pronounced vitrification, the reaction can still proceed at an adequate speed and the end of the reaction is reached earlier. The predicted degree of conversion at vitrification time is $\alpha = 0.95$. However, the effect of vitrification is better taken into account by the DSC kinetic model and the residual crosslinking reaction proceeds at slow speed.

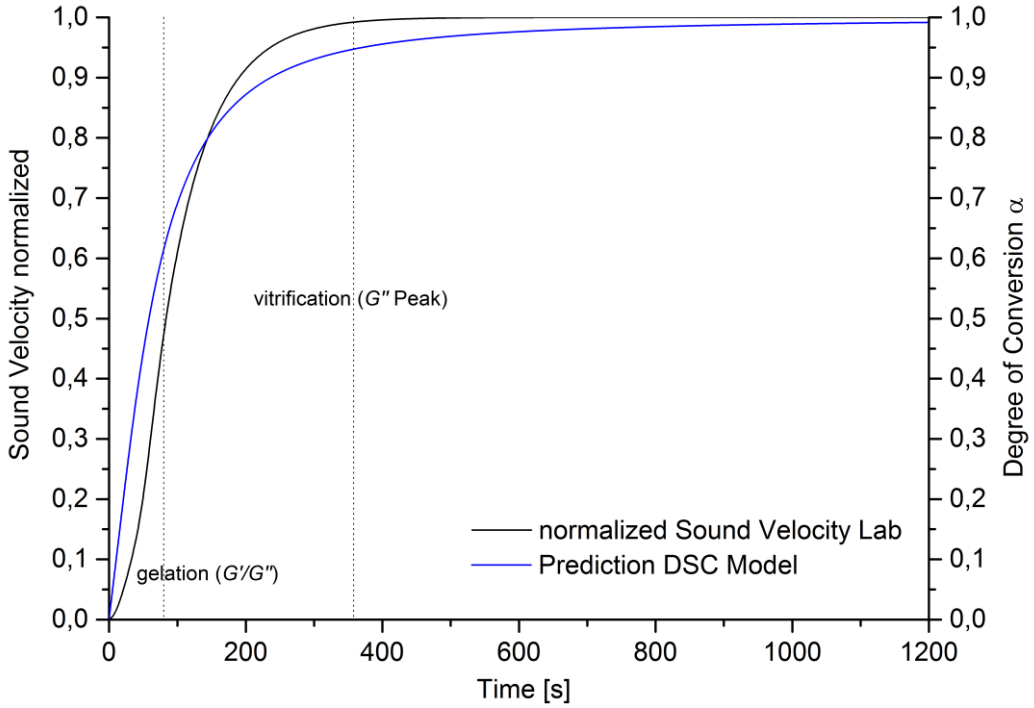

Figure 102: Normalized sound velocity of laboratory ultrasound measurement compared to the degree of conversion α according to the prediction of the DSC kinetic model at 120°C cure temperature. The marked times for gelation and vitrification are derived by rheometry measurements at 120°C cure temperature.

11.3 Online-Cure-Monitoring in RTM-Process using Ultrasound

11.3.1 Results and Discussion of Ultrasound in HP-RTM Process

The progress of the sound velocity measured at channel 1 in the plate tool with unidirectional carbon fiber fabric at 100, 110 and 120°C cure temperature is shown in Figure 103. The distribution of the absolute sound velocities is as expected higher at lower cure temperatures. The different speed of the crosslinking reaction is clearly shown by the normalized sound velocities.

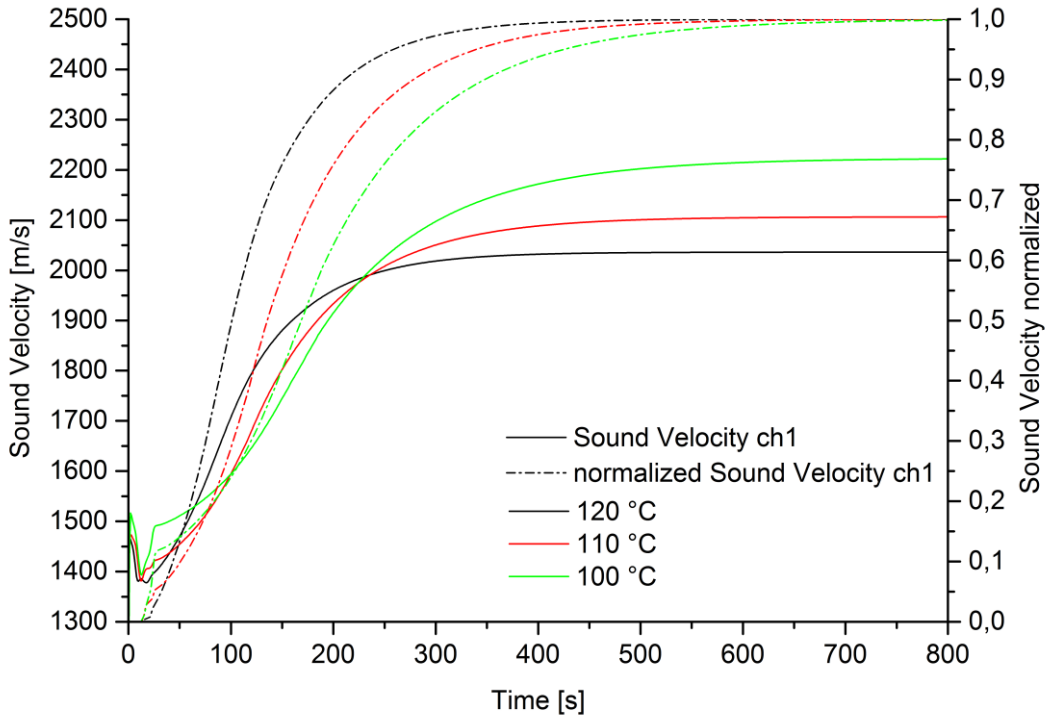

Figure 103: Measured sound velocity at channel 1 and the respective normalized sound velocity of the curing reaction of epoxy resin system B at 100, 110 and 120°C cure temperature.

The progress of the sound velocity of the second ultrasound sensor (channel 2), placed at the edge of the plate tool, is shown in Figure 104. The distribution of the absolute sound velocities is identical to channel 1 and higher at lower cure temperatures. The crosslinking reaction according to the normalized sound velocities progresses almost identical to the measurements of channel 1.

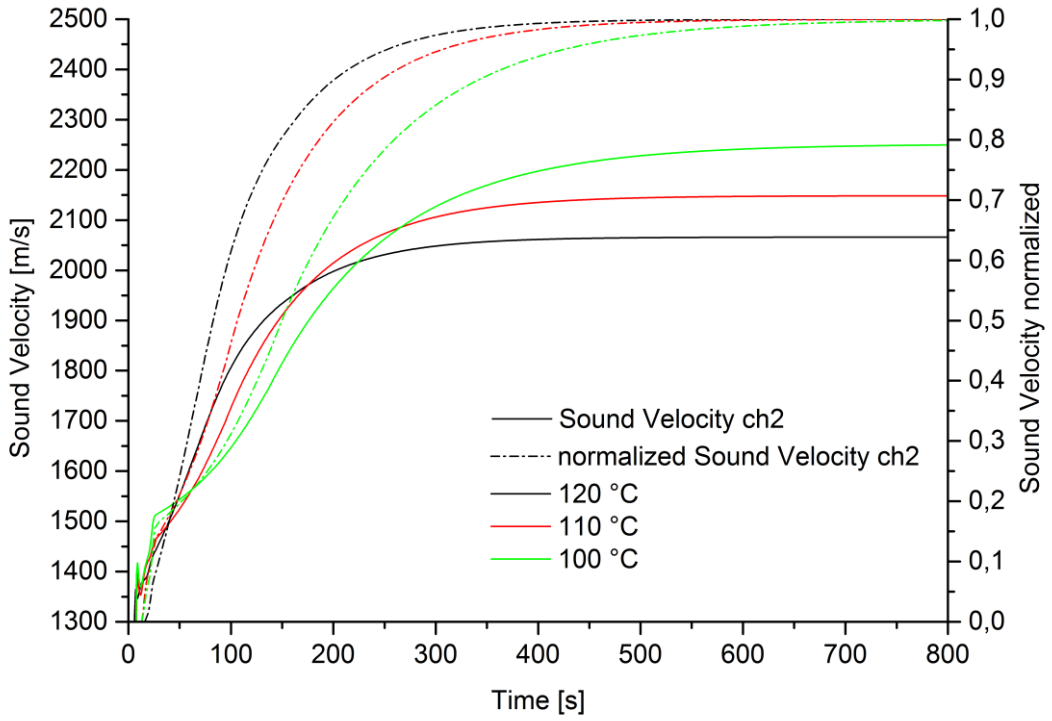

Figure 104: Measured sound velocity at channel 2 and the respective normalized sound velocity of the curing reaction of epoxy resin system B at 100, 110 and 120°C cure temperature

The comparison of the progression of the measured sound velocities of channel 1 and channel 2 and the associated normalized sound velocities at 120°C cure temperature is shown in Figure 105. It can be observed that the sound velocity at channel 2 rises earlier than measured at channel 1. This was also observed for epoxy resin system A and is related to the sensor placement in the plate tool as discussed in section 7.3.2.

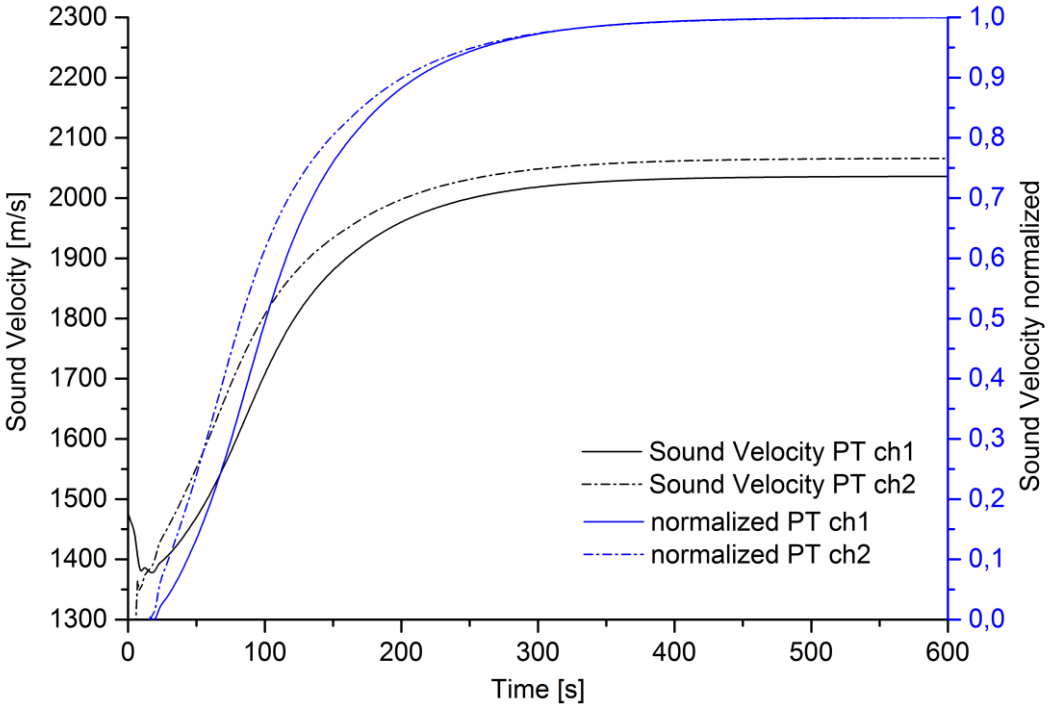

Figure 105: Comparison of measured sound velocities at channel 1 and channel 2 and the associated normalized sound velocity during the curing of epoxy resin system A at 120°C cure temperature

11.3.2 Comparison with Laboratory Ultrasound

The comparison of the progression of the normalized sound velocities measured in the laboratory and in the HP-RTM process at 100, 110 and 120°C cure temperature is shown in Figure 106. The discrepancy of the progression of the normalized sound velocities measured in the plate tool (PT) in the HP-RTM process is due to the sensor position as explained above. At 110°C and 120°C cure temperature a good correlation of the normalized sound velocity measured in the laboratory and the normalized sound velocity measured at channel 2 in the HP-RTM process is observable. At 100°C the normalized sound velocity increases faster in the HP-RTM process. Due to the better heat distribution in the HP-RTM process provided by the carbon fiber fabric, the reaction can proceed faster at lower temperatures. However, at each cure temperature the plateau of the normalized sound velocity is reached at the same time for both the laboratory and the process measurement.

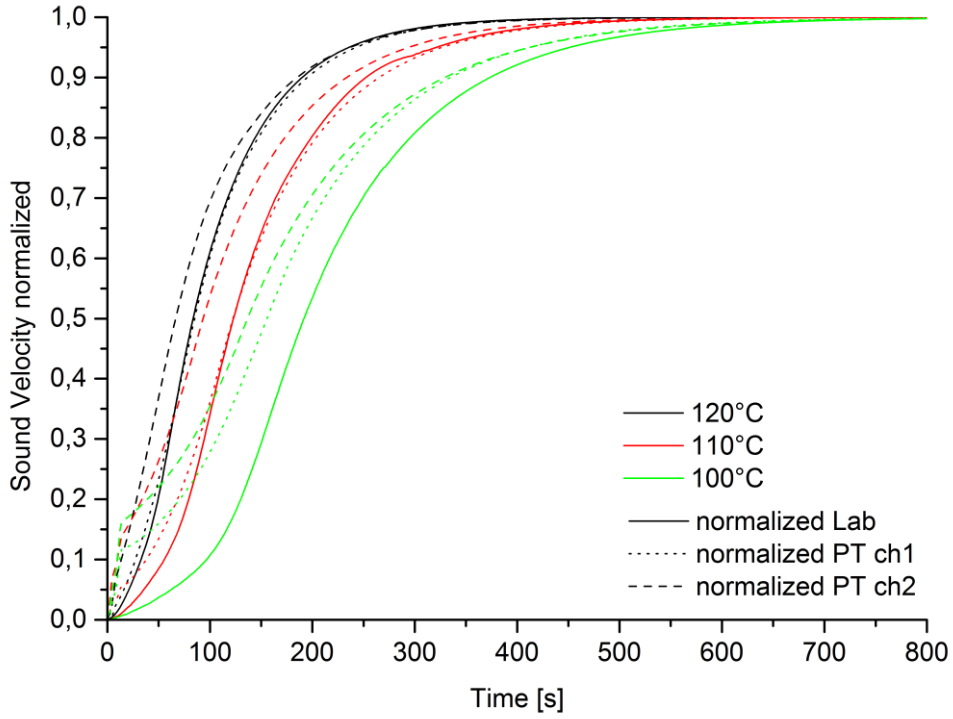

Figure 106: Comparison of normalized sound velocities measured in the laboratory (Lab) and in HP-RTM process (PT ch 1 and PT ch2) at 100, 110 and 120°C cure temperatures.

11.3.3 Comparison with DSC Kinetic Model and Rheometry

The comparison of the normalized sound velocities of channel 1 and channel 2 and the degree of conversion α according to the prediction based on the DSC kinetic model at 90°C cure temperature is shown in Figure 107. The marked times for gelation and vitrification are derived by the results of the rheometry measurements. The progression of the normalized sound velocity of channel 1 and channel 2 and predicted degree of conversion show a very good correlation. Gelation occurs at 0.60 of the normalized sound velocity of channel 2, which is in perfect agreement with the prediction and the theoretical and calculated value of the gel point $\alpha = 0.60$. At channel 1 gelation occurs at 0.49. Vitrification occurs at 0.99 of the normalized sound velocity for both ultrasound channels. This was also found for the ultrasound measurements in the laboratory and can be explained by the unsharp vitrification at 120°C cure temperature.

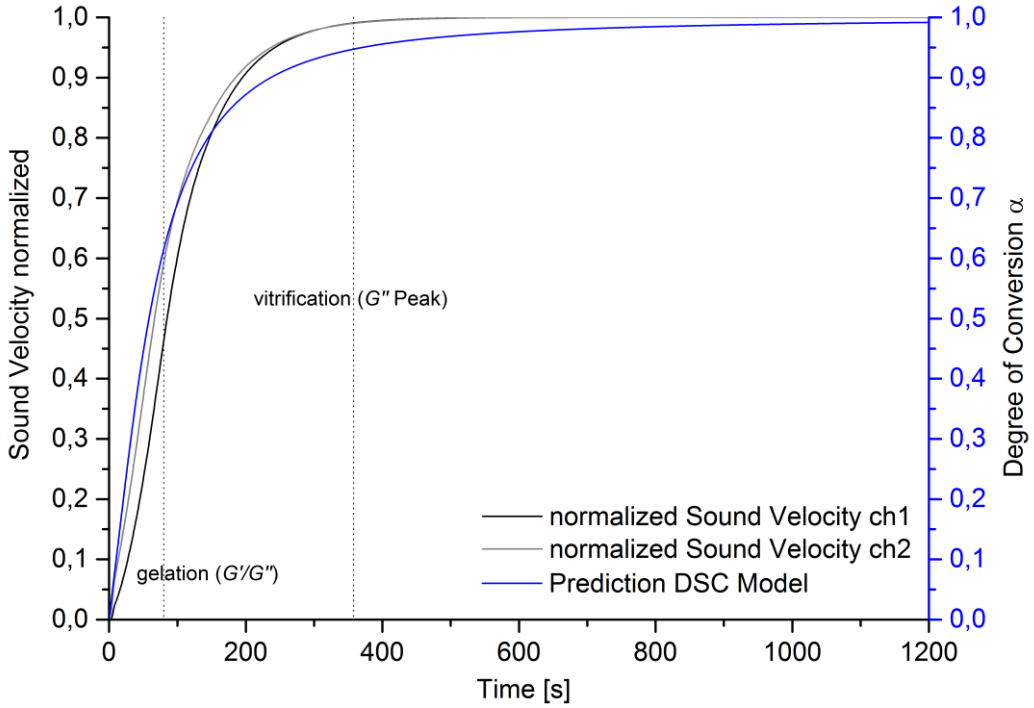

Figure 107: Normalized sound velocities of channel 1 and channel 2 compared to the degree of conversion α according to prediction based on the DSC kinetic model at 120°C cure temperature. The marked times for gelation and vitrification are derived by rheometry measurements at 120°C cure temperature.

F. SUMMARY

12 Benchmark Method to Compare the Curing Performance of Epoxy Resins

A goal of the developed methodology is to provide benchmark methods in order to compare the cure performance of resin systems for the HP-RTM process. In the following, this is shown exemplary for epoxy resin system A and B. The comparison of the times at which the viscosity η reaches 0.3 and 1.8 Pa·s and when gelation (*G′/G″*) occurs according to rheometry measurements for epoxy resin system A and B is shown in Figure 108 for different cure temperatures. This shows that epoxy resin system A reacts faster at lower temperatures compared to epoxy resin system B. Therefore, different process temperatures must be applied. It is also shown, that for a slight extension of the injection time (η = 0.3 Pa·s) by reduction of the cure temperature, the curing time increases disproportionally which is represented by the times of gelation (*G′/G″*) which indicates a degree of conversion α = 0.60 as was shown in the previous experiments for both epoxy resin systems.

In this way it is possible to compare injection times at different temperatures and thus the related curing performance of present epoxy resin systems with future potential matrix systems for CFRP parts. The ideal resin system has long latency to provide long injection times and after mould filling the full cure should take place immediately.

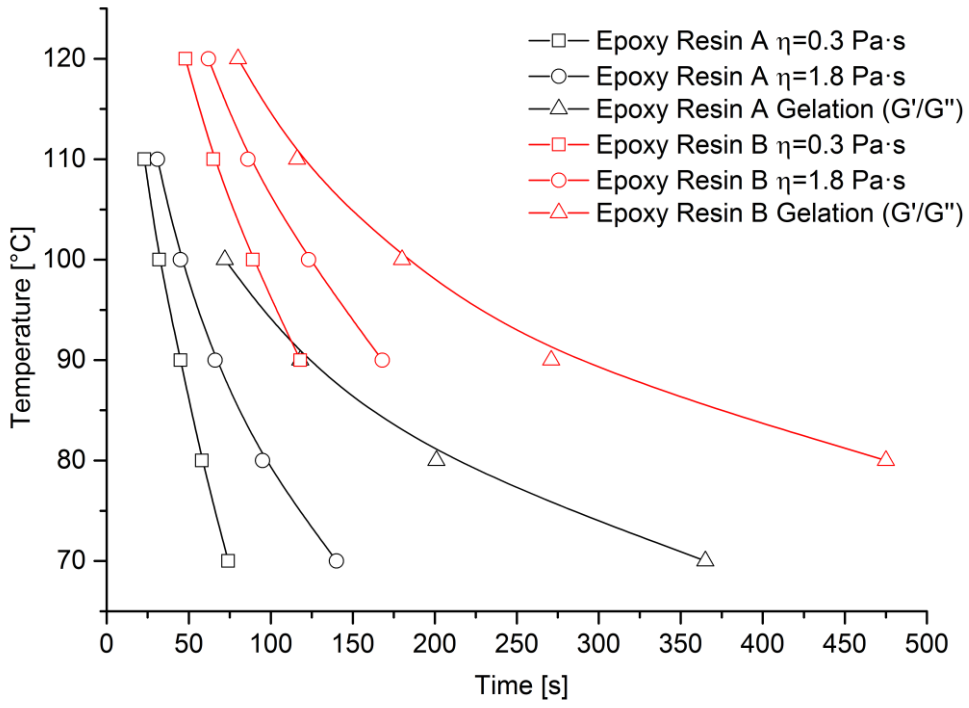

Figure 108: Comparison of the times at which the viscosity η reaches0.3 and 1.8 Pa·s and when gelation (*G′/G″*) occurs according to rheometry measurements for epoxy resin system A and B at different cure temperatures.

To provide a reasonable compromise between a long injection time and a short curing time a cure temperature of 100°C is proposed for epoxy resin system A (injection time 32 s) and 120°C for epoxy

resin system B (injection time 48 s). After the assessment of the cure temperature based on a suitable injection time the progress of the degree of conversion can be predicted based on the DSC kinetic model to provide a continuous comparison of the curing performance until the end of cure. The comparison of the predicted the degree of conversion based on the DSC kinetic models of epoxy resin system A at 100°C cure temperature and epoxy resin system B at 120°C cure temperature is shown in Figure 109. It can be observed that the curing performance of both epoxy resin systems at the respective cure temperature is almost identical.

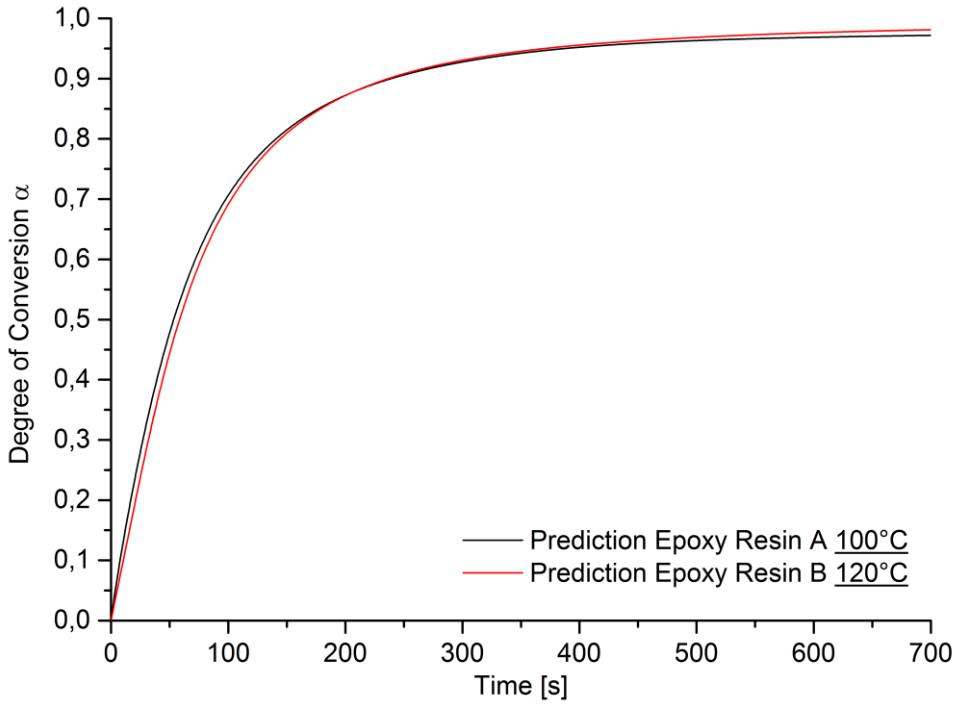

Figure 109: Comparison of the predicted the degree of conversion based on the DSC kinetic models of epoxy resin system A at 100°C cure temperature and epoxy resin system B at 120°C cure temperature.

Based on the evaluation of the injection behavior depending on the temperature and the predicted progression of the degree of conversion α, it can be concluded that epoxy resin system B shows a better performance at the chosen cure temperatures because it has a longer injection time at the same curing time. Thus, epoxy resin system B should be preferred for the use in the HP-RTM process.

13 Conclusions

A comprehensive characterization of the curing progress for two epoxy resin systems A and B, which are suitable for mass production of CFRP parts for the vehicle body structure, was conducted using differential scanning calorimetry, rheometry, NIR spectroscopy and ultrasound technique. Furthermore, an overall correlation was established with the cure simulation derived by a reaction kinetic model.

Based on DSC and NIR spectroscopy heating rate experiments a reaction kinetic model of epoxy resin system A was developed for each method and a good correlation to the experimental data was achieved. Though it is only a formal kinetic model which does not necessarily resemble the crosslinking mechanism, the derived two-step reaction model for both experimental input data sets is reasonable in terms of the principle reaction mechanism of the polymerization. The kinetic parameters of all derived kinetic models were also in good agreement with literature values for typical epoxy resins with amine hardeners. Due to possible sources of error of the NIR spectroscopy heating rate input data the following comparisons were conducted with the predictions based on the DSC kinetic model. For epoxy resin system B only a reaction kinetic model was developed based on DSC heating rate experiments. Also, this developed reaction kinetic model provided a good correlation with the experimental data and the values reported in literature.

The basis of the correlation of the degree of conversion α and the glass transition temperature T_g was provided by partially cured epoxy resin samples by a set of different isothermal DSC measurements and subsequent assessment of the reached cure state. The fit equations proposed by Hesekamp and DiBenedetto showed a good agreement with the experimental data and provided a consistent correlation over the entire curing range.

The isothermal DSC measurements showed that for fast curing epoxy resins at high curing temperatures a measurement of the entire curing reaction is not possible and the beginning of the reaction is cut-off due to the required device initialization time. An attempt was made to reconstruct the beginning of the reaction course based on the measurable part of the reaction. Neither the prediction of the curing reaction nor the experimental data obtained by rheometry and NIR spectroscopy showed a consistent agreement with the isothermal DSC measurements.

It could be shown that NIR spectroscopy provides a better and more reliable assessment of the curing reaction of epoxy resin systems compared to mid-infrared spectroscopy. Consistent measurement results were obtained by isothermal NIR spectroscopy for both epoxy resin systems which were in good agreement with the cure prediction of the DSC kinetic model.

The progression of the viscosity at the beginning of the curing reaction could be determined well with rheometry measurements in rotation mode. According to the defined maximum of viscosity for injection in the HP-RTM process of 0.3 Pa·s, the injection times for various cure temperatures could be provided. The times for gelation and vitrification were determined by rheometry measurements in oscillation mode. The correlation of the gelation times at different cure temperatures with degrees of conversion derived by the prediction of the DSC kinetic model and the isothermal NIR spectroscopy measurements showed a good agreement with the calculated theoretical value of $\alpha = 0.60$ and the reported values in the literature for typical epoxy resin systems with amine hardeners of $\alpha = 0.58 – 0.60$. It could be shown that at the times when vitrification is observable according to rheometry measurements (Peak G'') also a decrease of the curing reaction occurs according to the curing prediction of the DSC kinetic model and the ultrasound measurements.

Ultrasound technique provided a good method for the cure characterization of fast curing epoxy resins. In addition, it is a suitable method for online-cure-monitoring in a real production process. Different results of the curing behavior were determined for ultrasound measurements in the laboratory and in the HP-RTM process. These deviations could be attributed to several causes. The clarification of the exact impact of the influencing factors was not within the scope of this work. However, the ultrasound measurements in the HP-RTM process showed a good correlation to the prediction of the DSC kinetic model, which in turn was in very good agreement with NIR spectroscopy. The gelation times determined by rheometry were also in good correlation to the prediction and NIR spectroscopy.

Furthermore, it could be shown that the developed methodology provides a suitable method for process analysis and the matching of applied epoxy resins with process requirements. In addition benchmark methods are provided for the comparison of prior art epoxy resins systems and future CFRP matrix systems.

Finally it can be said that the developed methodology provides a comprehensive and consistent characterization of the curing behavior of fast curing epoxy resin systems both in the laboratory and in the HP-RTM production process and a confident prediction of the curing progress depending on the applied cure temperatures is possible.

14 Outlook

As was discussed in this work, the experimental cure characterization of fast curing epoxy resin systems is difficult due to the limitations of the analytical methods, because of difficult sample handling and error sources by inadequate acquisition times. This applies especially for high cure temperatures. Here, the cure simulation is advantageous. The input data of the reaction kinetic model is obtained by a reasonable experimental measurement series. After an appropriate kinetic model is generated the curing progress of the resin can be predicted at significantly higher temperatures compared to the achievable experimental curing conditions. The predicted progress of the degree of conversion α of epoxy resin system B at 120, 130, 140, 150, and 160°C is shown in Figure 110. It can be seen that the prediction yields reasonable progressions of the degree of conversion α even at very high cure temperatures up to 160°C. For comparison, the cure temperature at which reliable experimental measurements are possible is around 120°C. This opens the possibility to assess the curing progress and performance of epoxy resins beyond experimental accessible cure temperatures and therefore to evaluate the potential of cycle time reduction as indicated in the figure.

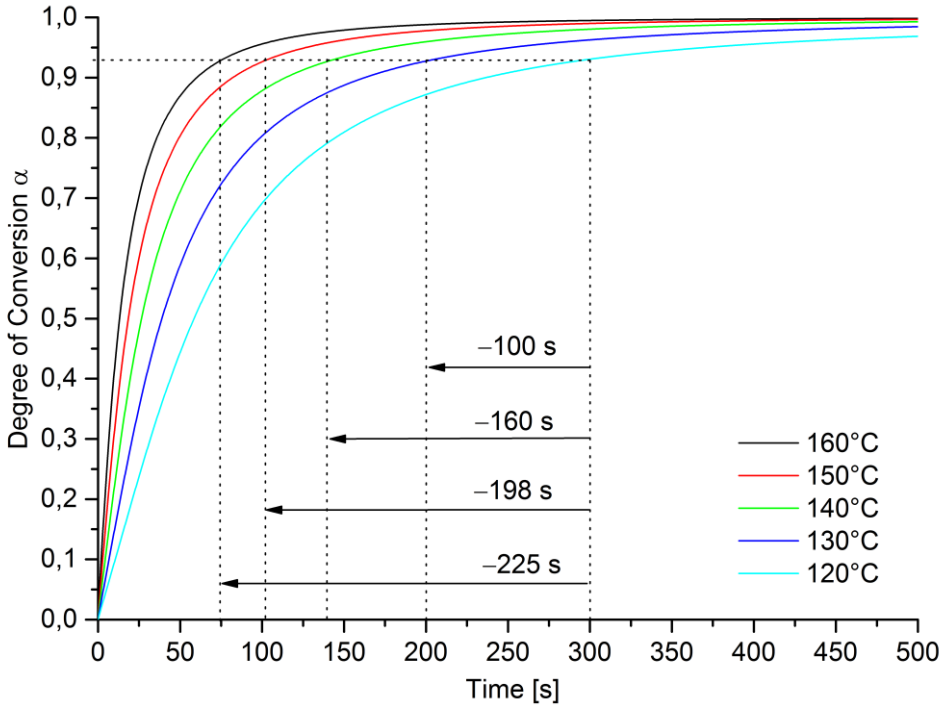

Figure 110: Prediction of degree of conversion *α* of epoxy resin system B at isothermal cure temperatures from 120 – 160°C.

The kinetic model provides another opportunity regarding future process strategies. In contrast to experimental analytic methods the cure simulation allows the prediction of the curing progress according to any temperature profiles desired. This is displayed exemplary for the predicted curing

progress of epoxy resin system B at an isothermal cure temperature of 120°C and the prediction according to a temperature profile consisting of an isothermal segment at 120°C during the injection phase and subsequent heating to 130°C cure temperature, shown in Figure 111. After 5 min curing with the applied temperature profile, the same degree of conversion α is reached 75 s earlier than at isothermal curing conditions. This shows the potential of optimized processes by dynamic heating, which can be realized by induction heated tools for example.

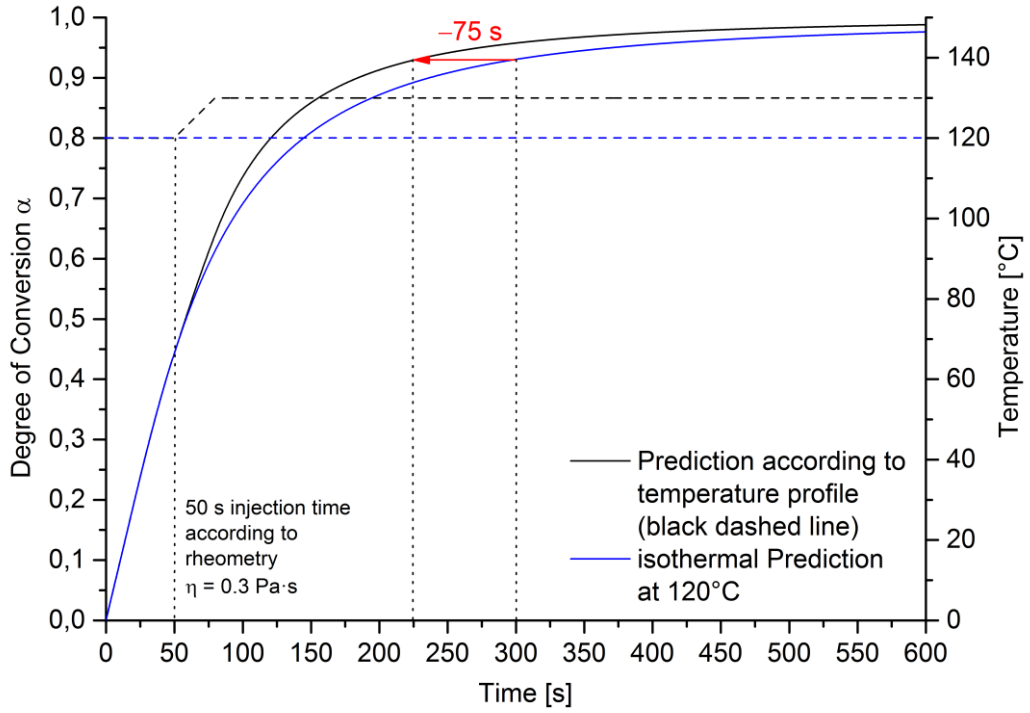

Figure 111: Comparison the isothermal cure prediction at 120°C cure temperature (blue solid and dashed line) and the prediction of the curing progress according to the given temperature profile (black solid and dashed line).

For further optimizations of the prediction by the kinetic model for future investigations it is recommended to provide a suitable method to measure the temperature of the epoxy resin in the HP-RTM reliably and exactly to generate a temperature profile which can be taken as basis for cure simulations.

It was shown that ultrasound technique is a suitable method for online-cure-monitoring in the HP-RTM process. This can be used not only for investigative purposes but also for process control. By correlation of the desired state of cure with the normalized sound velocity an ultrasound dependent cure control is feasible. This can then, in turn, directly be connected to the control unit of the RTM press which opens as soon the adjusted normalized sound velocity is reached. This allows an individual process control for each CFRP part and ensures continuous quality control regarding the curing state of the matrix system.

G. APPENDIX

References

[1] United Nations, *Kyoto Protocol to the United Nations Framework Convention on Climate Change*, **1998**.

[2] N. Metz (Ed.) *Fachbuch / Haus der Technik, Vol. 72*, expert-Verl., Renningen, **2007**.

[3] in *Amtsblatt der Europäischen Union*, **2009**.

[4] *Die EU-Verordnung zur Verminderung der CO2 - Emissionen von Personenkraftwagen*, **2009**.

[5] *BMW AG*, "Die Zukunft der urbanen Mobilität", can be found under http://www.bmw.de/de/neufahrzeuge/bmw-i/bmw-i/konzept.html#lifedrive.

[6] K.D. Potter, *Composites Part A: Applied Science and Manufacturing* **1999**, *30*, 619–621.

[7] R.F.J. McCarthy, G.H. Haines, R.A. Newley, *Composites Manufacturing* **1994**, *5*, 83–93.

[8] P. Beardmore, C.F. Johnson, *Composites Science and Technology* **1986**, *26*, 251–281.

[9] Erica R.H. Fuchs, Frank R. Field, Richard Roth, Randolph E. Kirchain, *Composites Science and Technology* **2008**, *68*, 1989–2002.

[10] Ahmad Mayyas, Ala Qattawi, Mohammed Omar, Dongri Shan, *Renewable and Sustainable Energy Reviews* **2012**, *16*, 1845–1862.

[11] D. Braun, D. W. Lee, *Die Angewandte Makromolekulare Chemie* **1975**, *48*, 161–173.

[12] J.-P. Pascault, R. J. J. Williams, *Epoxy polymers. New materials and innovations*, Wiley-VCH, Weinheim, **2010**.

[13] C. A. May, *Epoxy resins. Chemistry and technology*, M. Dekker, New York, **©1988**.

[14] K. Horie, H. Hiura, M. Sawada, I. Mita, H. Kambe, *Journal of Polymer Science Part A-1: Polymer Chemistry* **1970**, *8*, 1357–1372.

[15] J. Mijovic, J. Wijaya, *Macromolecules* **1994**, *27*, 7589–7600.

[16] S. Luňák, K. Dušek, *Journal of Polymer Science: Polymer Symposia* **1975**, *53*, 45–55.

[17] D. Verchere, H. Sautereau, J. P. Pascault, C. C. Riccardi, S. M. Moschiar, R. J. J. Williams, *Macromolecules* **1990**, *23*, 725–731.

[18] Nigel A. St John, Graeme A. George, *Polymer* **1992**, *33*, 2679–2688.

[19] L. Shechter, J. Wynstra, R. P. Kurkjy, *Industrial & Engineering Chemistry* **1956**, *48*, 94–97.

[20] Ieuan T. Smith, *Polymer* **1961**, *2*, 95–108.

[21] L. Shechter, J. Wynstra, *Industrial & Engineering Chemistry* **1956**, *48*, 86–93.

[22] T. F. Saunders, M. F. Levy, J. F. Serino, *Journal of Polymer Science Part A-1: Polymer Chemistry* **1967**, *5*, 1609–1617.

[23] J.-P. Pascault, *Thermosetting polymers*, Marcel Dekker, New York, **2002**.

[24] B. Sedláček, J. Kahovec, *Crosslinked epoxies. Proceedings of the 9th discussion conference, Prague, Czechoslovakia, July 14-17, 1986*, W. de Gruyter, Berlin, New York, **1987**.

[25] H. H. Winter, *The critical gel - The universal material state between liquid and solid*, ScholarWorks@UMass Amherst, Massachusetts, **2002**.

[26] P. J. Flory, *Journal of the American Chemical Society* **1941**, *63*, 3083–3090.

[27] P. J. Flory, *The Journal of Physical Chemistry* **1942**, *46*, 132–140.

[28] W. H. Stockmayer, *The Journal of Chemical Physics* **1943**, *11*, 45–55.

[29] P. J. Flory, *Principles of polymer chemistry*, Cornell University Press, Ithaca, **1953**.

[30] M. Nič, J. Jirát, B. Košata, A. Jenkins, A. McNaught, *IUPAC Compendium of Chemical Terminology*, IUPAC, Research Triagle Park, NC, **2009**.

[31] D. Stauffer, A. Coniglio, M. Adam in *Advances in Polymer Science* (Ed.: K. Dušek), Springer Berlin Heidelberg, **1982**.

[32] J. K. Gillham, *Polymer Engineering & Science* **1986**, *26*, 1429–1433.

[33] G. Höhne, W. Hemminger, H.-J. Flammersheim, *Differential scanning calorimetry. An introduction for practitioners*, Springer, Berlin, New York, **2003**.

[34] D. Hesekamp, H. C. Broecker, M. H. Pahl, *Chemical Engineering & Technology* **1998**, *21*, 149–153.

[35] A. T. DiBenedetto, *Journal of Polymer Science Part B: Polymer Physics* **1987**, *25*, 1949–1969.

[36] J. P. Pascault, R. J. J. Williams, *Journal of Polymer Science Part B: Polymer Physics* **1990**, *28*, 85–95.

[37] Hideki Yamasaki, Shigeaki Morita, *Journal of Molecular Structure* **2014**, *1069*, 164–170.

[38] G. A. George, G. A. Cash, L. Rintoul, *Polymer International* **1996**, *41*, 169–182.

[39] G. Nikolic, S. Zlatkovic, M. Cakic, S. Cakic, C. Lacnjevac, Z. Rajic, *Sensors* **2010**, *10*, 684–696.

[40] F. Carrasco, P. Pagès, T. Lacorte, K. Briceño, *Journal of Applied Polymer Science* **2005**, *98*, 1524–1535.

[41] U. Braun, K. Brademann-Jock, W. Stark, *Journal of Applied Polymer Science* **2014**, *131*.

[42] Andrés Rigail-Cedeño, Chong Sook Paik Sung, *Polymer* **2005**, *46*, 9378–9384.

[43] Gilbert Lachenal, Alain Pierre, Nicolas Poisson, *Micron* **1996**, *27*, 329–334.

[44] N. Poisson, G. Lachenal, H. Sautereau, *Vibrational Spectroscopy* **1996**, *12*, 237–247.

[45] S. T. Cholake, M. R. Mada, R. K. S. Raman, Y. Bai, X. Zhao, S. Rizkalla, S. Bandyopadhyay, *Defence Science Journal; Vol 64, No 3: Polymer Science and Technology* **2014**.

[46] L. Bokobza, *Journal of Near Infrared Spectroscopy* **1998**, *6*, 3–17.

[47] D. A. Burns, E. W. Ciurczak, *Handbook of near-infrared analysis*, CRC Press, Boca Raton, **2008**.

[48] G. A. George, P. Cole-Clarke, N. St. John, G. Friend, *Journal of Applied Polymer Science* **1991**, *42*, 643–657.

[49] R. F. Goddu, D. A. Delker, *Analytical Chemistry* **1958**, *30*, 2013–2016.

[50] S. A. Arrhenius, *Zeitschrift für Physikalische Chemie* **1889**, *4*, 226–248.

[51] S. Vyazovkin, N. Sbirrazzuoli, *Macromolecules* **1996**, *29*, 1867–1873.

[52] H. Flammersheim, J. Opfermann, *Thermochimica Acta* **1999**, *337*, 141–148.

[53] H.-J. Flammersheim, J. R. Opfermann, *Macromolecular Materials and Engineering* **2001**, *286*, 143–150.

[54] S. Sourour, M. Kamal, *Thermochimica Acta* **1976**, *14*, 41–59.

[55] M. R. Kamal, S. Sourour, *Polymer Engineering & Science* **1973**, *13*, 59–64.

[56] H. Flammersheim, *Thermochimica Acta* **1998**, *310*, 153–159.

[57] J.R. Opfermann, *Journal of Thermal Analysis and Calorimetry* **2000**, *60*, 641–658.

[58] E. Rabinowitch, *Trans. Faraday Soc.* **1937**, *33*, 283–293.

[59] Christopher W. Wise, Wayne D. Cook, Andy A. Goodwin, *Polymer* **1997**, *38*, 3251–3261.

[60] Takeo Ozawa, *Thermochimica Acta* **1992**, *203*, 159–165.

[61] H. L. Friedman, *Journal of Polymer Science Part C: Polymer Symposia* **1964**, *6*, 183–195.

[62] I. V. Arkhangel'skii, *Non-isothermal kinetic methods*. *Workbook and laboratory manual*, Ed. Open Acess, Berlin, **2013**.

[63] J. Opfermann, *Software Handbuch - NETZSCH Thermokinetics*, NETZSCH-Gerätebau GmbH, Selb.

[64] J. H. Flynn, L. A. Wall, *Journal of Polymer Science Part B: Polymer Letters* **1966**, *4*, 323–328.

[65] Takeo Ozawa, *Bulletin of the Chemical Society of Japan* **1965**, *38*, 1881–1886.

[66] J. B. Enns, J. K. Gillham, *Journal of Applied Polymer Science* **1983**, *28*, 2567–2591.

[67] M.E. Ryan, A. Dutta, *Polymer* **1979**, *20*, 203–206.

[68] Y. Deng, G. C. Martin, *Macromolecules* **1994**, *27*, 5147–5153.

[69] F. G. A. E. Huguenin, M. T. Klein, *Industrial & Engineering Chemistry Product Research and Development* **1985**, *24*, 166–171.

[70] W. P. Cox, E. H. Merz, *Journal of Polymer Science* **1958**, *28*, 619–622.

[71] H. H. Winter, *Polymer Engineering & Science* **1987**, *27*, 1698–1702.

[72] H. H. Winter, M. Mours in *Advances in Polymer Science*, Springer Berlin Heidelberg, **1997**.

[73] J Lange, N Altmann, C.T Kelly, P.J Halley, *Polymer* **2000**, *41*, 5949–5955.

[74] H. Teil, S. A. Page, V. Michaud, J.-A. E. Månson, *Journal of Applied Polymer Science* **2004**, *93*, 1774–1787.

[75] M Rath, J Döring, W Stark, G Hinrichsen, *5NDT6 & E International* **2000**, *33*, 123–130.

[76] J. H. Töpker, *Ultraschallmesstechnik zur Online-Erfassung und Analyse des Injektions- und Härtungsablaufs beim Resin transfer moulding*. *Ultrasonic measurement technique for online control and analysis of the impregnation and curing process by Resin transfer moulding*, Mainz, Aachen, **2003**.

[77] J. McHugh, *Ultrasound technique for the dynamic mechanical analysis (DMA) of polymers*, Bundesanstalt für Materialforschung und -prüfung (BAM), Berlin, **2008**.

[78] W. Stark, W. Bohmeyer in *Woodhead Publishing Series in Composites Science and Engineering* (Ed.: V. M. Karbhari), Woodhead Publishing, **2013**.